



UNIVERSITÀ Technical University of Denmark
DEGLI STUDI
DI PADOVA



*DESIGN AND OPTIMIZATION OF
HEAT EXCHANGERS FOR
ORGANIC RANKINE CYCLES*

Student:

Luca Barbazza

Supervisors:

Fredrik Haglind
Leonardo Pierobon
Jorrit Wronsky
Alberto Mirandola

Preface

The present work has been developed at Denmark Technical University under the supervision of Professor Fredrik Haglind (department of mechanical engineering, Lyngby, Denmark) and Professor Alberto Mirandola (dipartimento di Ingegneria Industriale, Padova, Italia). I am grateful to Leonardo Pierobon and Jorri Wronky for the support and the help they gave me.

I thank my parents and my family for allowing me to study and live this awesome experience. I thank especially my girlfriend, Sara, for the support during this period. I hope to help her live something similar.

Kogens Lyngby , 20th Januray 2013

Luca Barbazza

Abstract

The exploitation of low and medium grade heat is receiving growing interest due to the increased concern about energy storage and global warming. There are a number of new solutions proposed to generate electricity from the low temperature heat source. Among them, organic Rankine cycle is one of the promising technologies aimed at converting low grade heat into electricity and is used in practical industry applications exploiting biomass, solar power, ocean thermal energy, geothermal energy and waste heat. In fact, industrial plants continuously reject large amounts of thermal energy through warm liquid or gaseous effluents directly into the atmosphere due to the lack of effective methods for its recovery and utilization during their normal operation. Recovering energy from waste flue gas, converting it to electricity, can reduce fossil fuel consumption and environmental problems. Therefore, greater and greater attention has been paid to these technologies in recent years and many researches mainly focused on working fluid selection and optimization of organic Rankine cycles.

Heat exchangers are one of the main source of entropy generation that reduce the performance of the cycle. The optimization of heat exchangers can help enhance the exploitation of the heat source.

In this work, I employ the multi-objective genetic algorithm to optimize the performances of the organic Rankine cycle and the design of the heat exchangers. I consider two levels of optimization. The first level aims to define the operating conditions of the cycle in order to maximize the net power output and to minimize the entropy generation rate. The second levels of optimization aims to model the heat exchangers in order to minimize simultaneously volume, pressure drop and total annual cost.

I consider the evaporating pressure and the working fluids as optimization variables for the first level of optimization. Moreover, I select the working fluids based on environmental impact, safety and availability.

The design parameters of the second level of optimization are the geometric characteristics of the heat exchangers. Flat plate heat exchangers with herringbone corrugations are selected for low-grade heat source and six design parameters are used to model the pre-heater and the evaporator: plate width, plate length, channel spacing, Chevron angle, number of channels per pass and number of passes.

Shell and tube heat exchangers are considered for higher heat transfer rate such as the heat recovered from gas turbine in off-shore applications. The design variables considered are: shell diameter, tube outer diameter, baffle spacing at the center, baffle spacing at the inlet and outlet, baffle cut, tube pitch, layout of the tubes and fluid arrangement.

The results of the first level of optimization indicate that the working fluid, the evaporating pressure and the pinch point have the major impact on the performance of the cycle. Among the fluids considered, R245fa, R236ea and R245ca are the most promising. The environmental impact, the safety and the performances of these fluids represent the best trade-off for medium-grade heat source.

In the second level, the results of the multi-objective optimization clearly reveal the antagonism between the two objective functions. Namely, the lower the compactness, the higher the pressure drop of the heat exchangers. Total annual cost can be used to find the minimum between initial costs and operating cost. Initial cost is related to the volume whereas operating cost depends on the pumping power and on the pressure drop.

Nomenclature

A	Area	$[m^2]$
b	Channel spacing	$[m]$
c_p	Heat capacity	$[J/kg \cdot K]$
C_{in}	Initial cost	$[\$]$
C_{op}	Operating cost	$[\$/year]$
C_{tot}	Total annual cost	$[\$/year]$
d	Diameter	$[m]$
d_h	Hydraulic diameter	$[m]$
D_{ctl}	Diameter of the circle through the centers of the outermost tubes	$[m]$
D_{otl}	Diameter of the circle through the outermost tubes	$[m]$
D_s	Shell diameter	$[m]$
ec	Electricity cost	$[\$/kWh]$
E_s	Pumping power – shell side	$[W]$
E_t	Pumping power – tube side	$[W]$
f	Friction factor	$[-]$
F_t	Correction factor	$[-]$
g	Gravitational acceleration	$[m/s^2]$
G	Mass velocity	$[kg/m^2s]$
h	Specific enthalpy	$[J/kg]$
i_{fg}	Latent heat	$[J/kg]$
\dot{I}	Irreversibility rate	$[J/s]$
k	Thermal conductivity	$[W/mK]$
l_c	Baffle cut	$[m]$
L	Length	$[m]$
$L_{b,c}$	Baffle spacing	$[m]$
$L_{b,i}$	Baffle spacing at inlet/outlet	$[m]$
L_w	Plate width	$[m]$
L_v	Plate length	$[m]$
\dot{m}	Mass flow rate	$[kg s^{-1}]$
n	lifetime	$[years]$
$N_{chxPass}$	Number of channels per pass	$[-]$
N_{pass}	Number of pass	$[-]$
$N_{s,\Delta T}$	Entropy generation number – temperature contribution	$[-]$
$N_{s,\Delta P}$	Entropy generation number – pressure drop contribution	$[-]$
N_t	Number of tubes	$[-]$
Nu	Nusselt number	$[-]$
op	Operating hours	$[hours/year]$
p_c	Corrugation pitch	$[m]$
p_t	Tube pitch	$[m]$
P	Pressure	$[kPa]$
Pr	Prandtl number	$[-]$

q_h	Heat flow rate hot side	[W]
q_c	Heat flow rate cold side	[W]
\dot{Q}	Heat flow rate	[W]
Re	Reynolds number	[-]
R_t	Fouling factor tube side	[km^2/W]
R_s	Fouling factor shell side	[km^2/W]
s	Specific entropy	[J/kg]
\dot{S}	Entropy generation rate	[J/sK], [W/K]
t	Plate thickness	[m]
T_0	Dead temperature	[K]
T	Temperature	[K]
u	Internal energy	[J]
u	Velocity	[m/s]
U	Overall heat transfer coefficient	[W/m^2K]
V	Volume	[m^3]
v	Specific volume	[m^3/kg]
x	Quality	[-]
X	Channel aspect ratio	[-]
\dot{W}	Power	[W]
\dot{W}_{rev}	Reversible power	[W]

Greek symbols

α	Heat transfer coefficient	[W/m^2K]
β	Chevron angle	[°]
ΔP	Pressure drop	[kPa]
ε	Effectiveness	[-]
ε	Void fraction	[-]
η_{ORC}	Efficiency of ORC	[-]
η_{exp}	Isentropic efficiency of expander	[-]
η_{pump}	Isentropic efficiency of pump	[-]
θ_{ctl}	Angle between the baffle cut and two radii of a circle through the centers of the outermost tubes	[rad]
θ_b	Angle in radians between two radii intersected at the inside shell wall with the baffle cut	[rad]
λ	Thermal conductivity	[W/mK]
μ	Dynamic viscosity	[Pa · s]
μ_p	Dynamic viscosity at wall	[Pa · s]
ρ	Density	[kg/m^3]
φ	Irreversibility ratio	[-]
ϕ	Enlargement factor	[-]

Subscript

s	Shell side
t	Tube side
h	Hot side
c	Cold side
eva	Evaporator
eco	Economizer

exp	Expander
cond	Condenser
p	Pump
l	Liquid
g	Vapor
i	inner
o	outer

Table of Contents

	Page
1. Organic Rankine Cycle	1
1.1. Organic Rankine cycle	
1.2. Selection of the working fluid	
1.3. Applications of the ORC technology according to the energy source	
1.4. Mathematical model	
1.5. Fluid candidates and their properties	
2. Heat Exchanger Design Methodology	12
2.1. Heat Exchanger Design Methodology	
2.2. Problem specification	
2.3. Exchanger Specifications	
2.4. Thermal and Hydraulic Design	
2.5. Mechanical Design	
2.6. Manufacturing Considerations and Cost Estimates	
2.7. Trade-off factors and optimization	
2.8. General method for the optimum design of ORC heat exchangers	
3. Thermal Design	18
3.1. Thermal Design Theory	
4. Plate heat exchanger	22
4.1. Plate Heat Exchangers	
4.2. Geometry	
4.3. Flow arrangement	
4.4. Single-phase heat transfer and pressure drop	
4.5. Two-phase heat transfer	
4.6. Pressure drop for single phase flow	
4.7. Pressure drop for two - phase flow	
5. Shell and tube heat exchangers	31
5.1. Shell and tube heat exchangers	
5.2. Allocation of streams in a shell and tube Exchanger	
5.3. Geometrical characteristics	
5.4. Heat transfer and pressure drop calculation	
5.4.1. Heat transfer on shell side	

5.4.2.	Pressure drop on shell side	
5.4.3.	Heat transfer on tube side	
5.4.4.	Pressure drop on tube side	
6.	Entropy Generation Minimization	45
6.1.	Entropy Generation Minimization	
6.2.	Energy and Exergy	
6.3.	Entropy Generation and Exergy Destruction	
6.4.	Heat exchanger Design by Entropy Generation Minimization	
6.5.	Minimization of the total entropy generation rate	
7.	Genetic algorithms	50
7.1.	Genetic algorithm	
7.2.	Characteristics of GAs	
7.3.	Reproduction	
7.4.	Crossover	
7.5.	Mutation	
7.6.	Multi-objective genetic algorithm	
8.	Optimization of organic Rankine cycle	54
8.1.	Organic Rankine Cycle Optimization	
8.2.	ORC analysis with fixed heat source	
8.3.	ORC analysis with variable heat source	
8.4.	Fluid selection	
9.	Optimization of STHes for ORC	78
9.1.	Multi-Objective Optimization of Shell and tube Heat Exchanger	
9.2.	Design problem formulation	
9.3.	Test case and validation	
9.3.1.	Optimal solutions	
9.4.	Multi objective optimization of economizers for organic Rankine cycle	
9.4.1.	Volume and pressure drop minimization	
9.4.2.	Volume, pressure drop and cost minimization	
10.	Optimization of shell and tube heat exchanger for ORC cycle	102
10.1.	Multi-objective optimization of plate heat exchangers	
10.2.	Plate heat exchanger design	
10.3.	Test case and validation	
10.4.	Sensitivity analysis	
10.4.1.	Width of the plate, Channel spacing and number of plates	
10.4.2.	Chevron angle	
10.4.3.	Channel aspect ratio	
10.5.	Optimization	
10.6.	Optimization of plate heat exchangers for organic Rankine cycles	
10.7.	Optimization of economizer	
10.8.	Optimization of evaporator	

10.9. Techno-economic optimization

11. Conclusions

126

Appendix I

Appendix II

Appendix III

Appendix IV

References

1.1. Organic Rankine Cycle

The operating principle of ORC is the same as the conventional Rankine cycle with the difference that the working fluid is an organic compound instead of water. The simplest cycle consists of a pump, an evaporator, an expander and a condenser. The pump pressurizes the liquid fluid which is injected into an evaporator to produce a vapor that is expanded in a turbine connected to a generator. The evaporator is the device that allows the heat transfer between the heat source and the working fluid. Finally, the vapor discharged from the turbine is condensed and sucked up by the pump to start a new cycle (*Fig.1.1*). In order to enhance the performance of the cycle, it is possible to include a heat exchanger at the outlet of the turbine to preheat the pumped fluid that will enter the evaporator as shown in *Fig.1.2*.

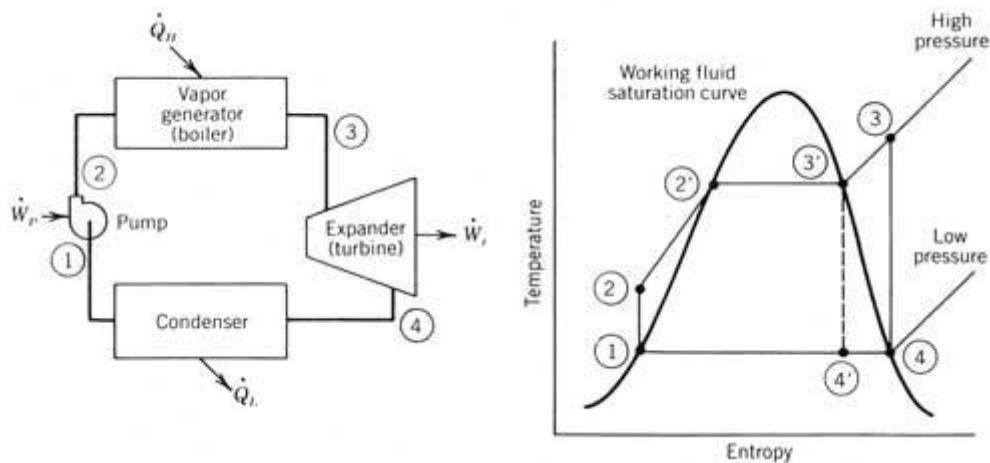


Figure 1.1. Rankine cycle with ideal transformations

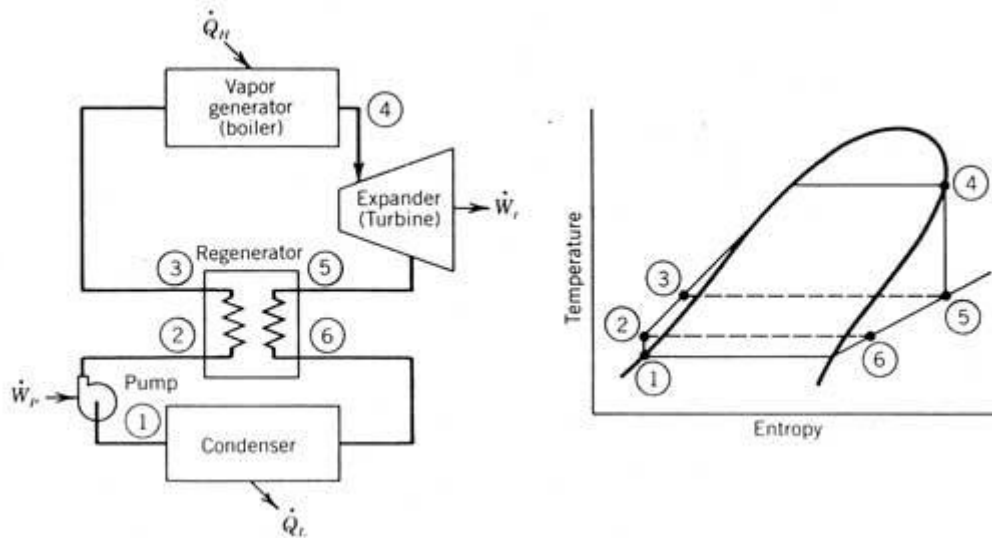


Figure 1.2. Organic Rankine cycle with regenerator

An ideal Rankine cycle is composed by four processes as shown in *fig. 1.2*. The segment 1-2 is represents an isentropic compression of the saturated liquid from the condensing pressure to the evaporating pressure. Along the ideal isobaric line 2-3, heat is extracted from the heat source and transferred to the working fluid. Afterwards, the fluid is expanded through an isentropic process and finally an isobaric heat transfer occurs in order to return at the initial condition. More realistic cycle is represented by an increase of entropy in the compression and expansion process. Furthermore, heat exchangers are characterized by pressure drops.

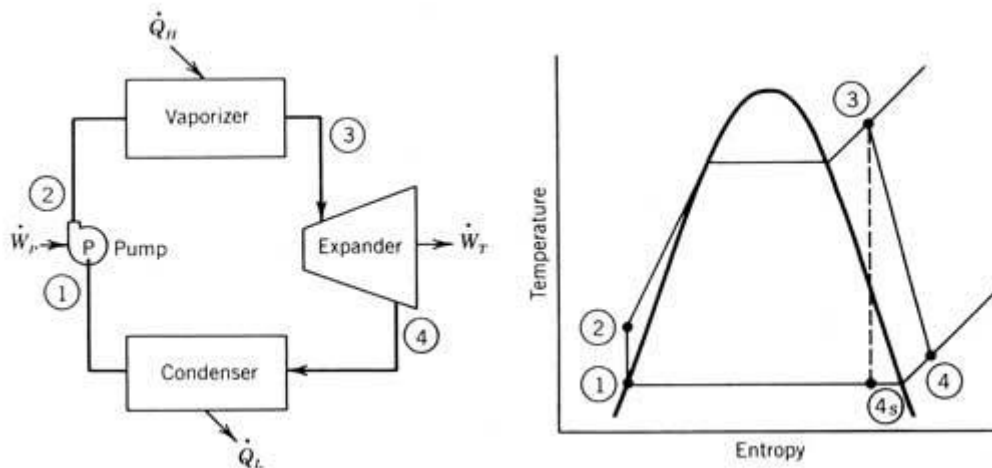


Figure 1.3. Rankine cycle with real transformations

The turbine is connected to a generator so that the net power output is the difference between the output work and the input work in the pump.

1.2. Selection of the working fluid

One of the most interesting aspects of ORC is the selection of the fluids that could be used in the cycle. Nowadays, there are several organic fluids and the designer must take into consideration different aspects

to choose the best one. Working fluid selection for ORC has been studied in a number of previous works [1,2,3] and several criteria are defined such as having optimal thermodynamic properties at the lowest temperatures and pressures and being economical, nontoxic and nonflammable. Furthermore, the growing attention to environmental impact limits the list to just few fluids.

The aspects to take in consideration are:

- a. Environmental: Montreal and Kyoto protocol define the guideline to evaluate the environmental impact. Ozone Depleting Potential (ODP) and Greenhouse Warming Potential (GWP) are indexes which intend to prevent the destruction of the ozone layer and emission of gases causing the greenhouse effect. Due to environmental concerns, some working fluids have been phased out, such as R-11, R-12, R-113, R-114 and R-114 while some others are being phased out by 2020 or 2030 (such as R-21, R-22, R-123, R-124, R-141b, R-142b and R-134a)
- b. Safety: the fluid should be non-toxic, non-corrosive and non-flammable. The security classification of the ASHRAE is used as an indicator of the fluids' degree of danger.
- c. Stability: chemical stability is an important characteristic of the fluid which can reduce the operating condition of the plant. Too high operating temperature could break down the fluid and produce toxic and irritating compounds that could induce health problems if leaks occur.
- d. Pressure: The higher the pressure, the higher the equipment cost necessary to the plant in order to ensure high levels of resistance.
- e. Availability and low cost: High availability and/or low cost are preferred.
- f. Latent heat and molecular weight: The greater the molecular weight and latent heat of the fluid, the more energy can be absorbed from the heat source in the evaporator and, therefore, the size of the installation and the consumption of the pump can be smaller, due to decrease of the flow rate required.
- g. Curve of saturation: The thermodynamic properties of the fluid could have a great influence on the characteristic of the ORC. The slope of the saturation curve can be negative, vertical or positive as shown in *Fig.1.4*. The saturation curves are called wet, isentropic and dry respectively. ORC are designed to operate at low and medium temperature so the superheating of the vapor, as in the traditional steam Rankine cycle, is not suitable. Moreover, when an expansion of a wet fluid without superheating happens, it falls into the liquid/vapor area, causing damage to the turbine and inefficiencies in the cycle because of the phase change. Isentropic and dry fluids can expand and fall into the saturated vapor zone or in the superheated zone without causing problems.

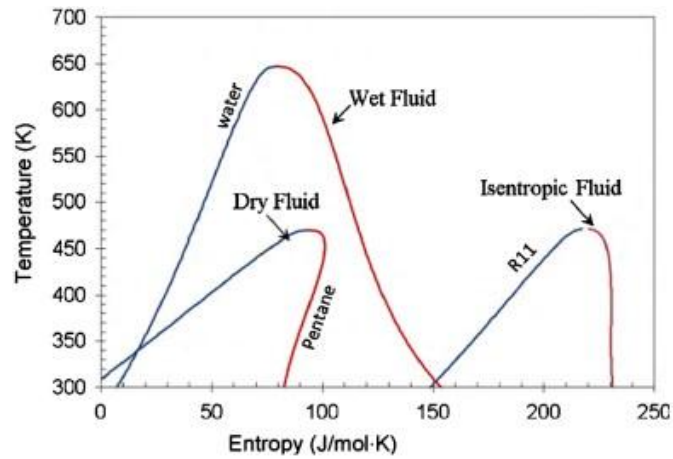


Figure 1.4. Typical saturation curves for dry, wet and isentropic fluid

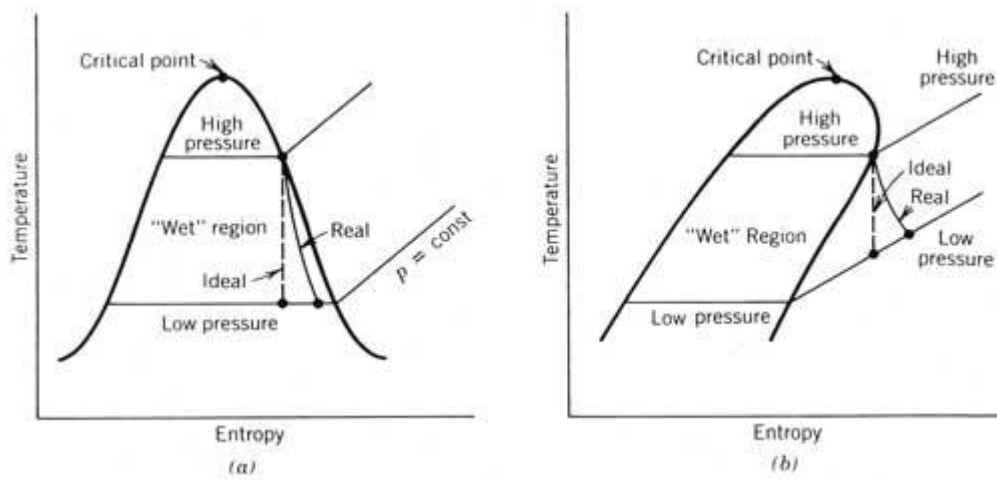


Figure 1.5. Fluid state at the outlet of the turbine.

From the previous considerations the influence of fluid selection on the cycle performance is clear. One of the most important factors which influence the choice of the fluid is the temperature of the heat source. A rough screening is based on the heat source temperature as shown in Fig. 1.6.

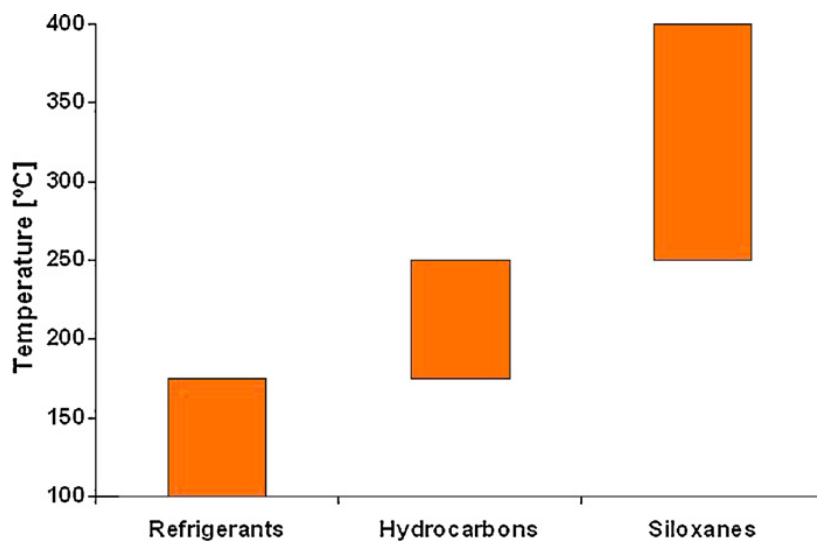


Figure 1.6. Range of use of typical organic fluids.

1.3. Applications of the ORC technology according to the energy source

Modularity, versatility and the possibility of using different temperature ranges are some of the most interesting characteristics of ORCs. This technology can be used in different ways in order to achieve different goals. One of the most attracting uses is the matching of topping and bottoming cycles, producing heat and power.

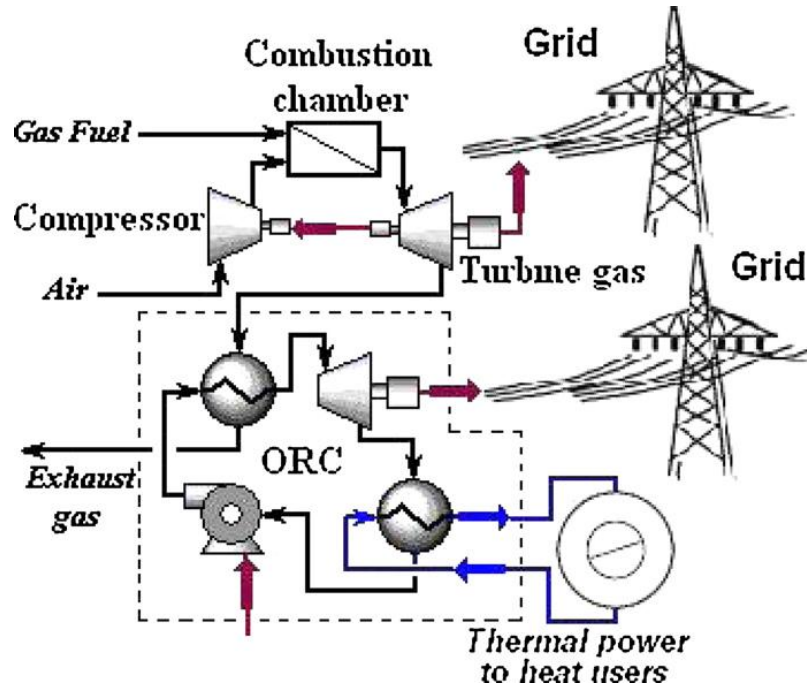


Figure 1.7. Waste heat recovery system.

A review on the possible configurations that can be done with the ORC is reported below.

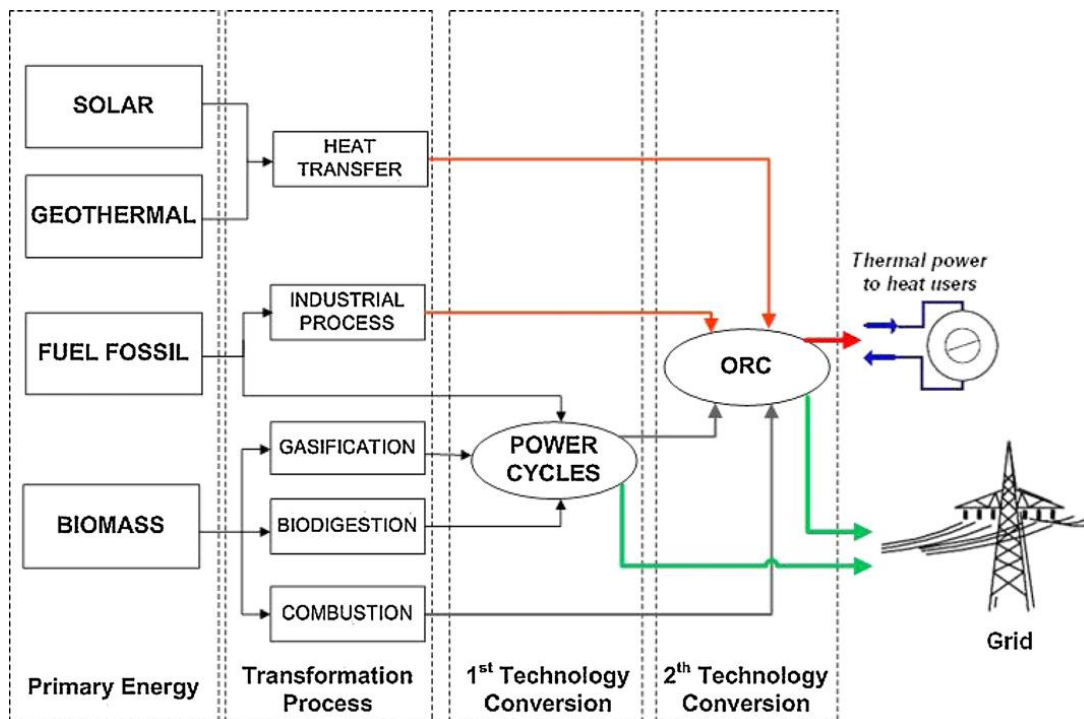


Figure 1.8. ORC applications.

1.4. Mathematical model

According to the first and second law of thermodynamics, the following equations can be applied to calculate the performance indexes of organic Rankine cycle. In order to simplify calculations some assumption are necessary. The cycle operates at steady state and pressure drops are not considered in connecting pipes and heat exchangers. Moreover, heat losses in each component are ignored and the isentropic efficiency of pump and expander are fixed.

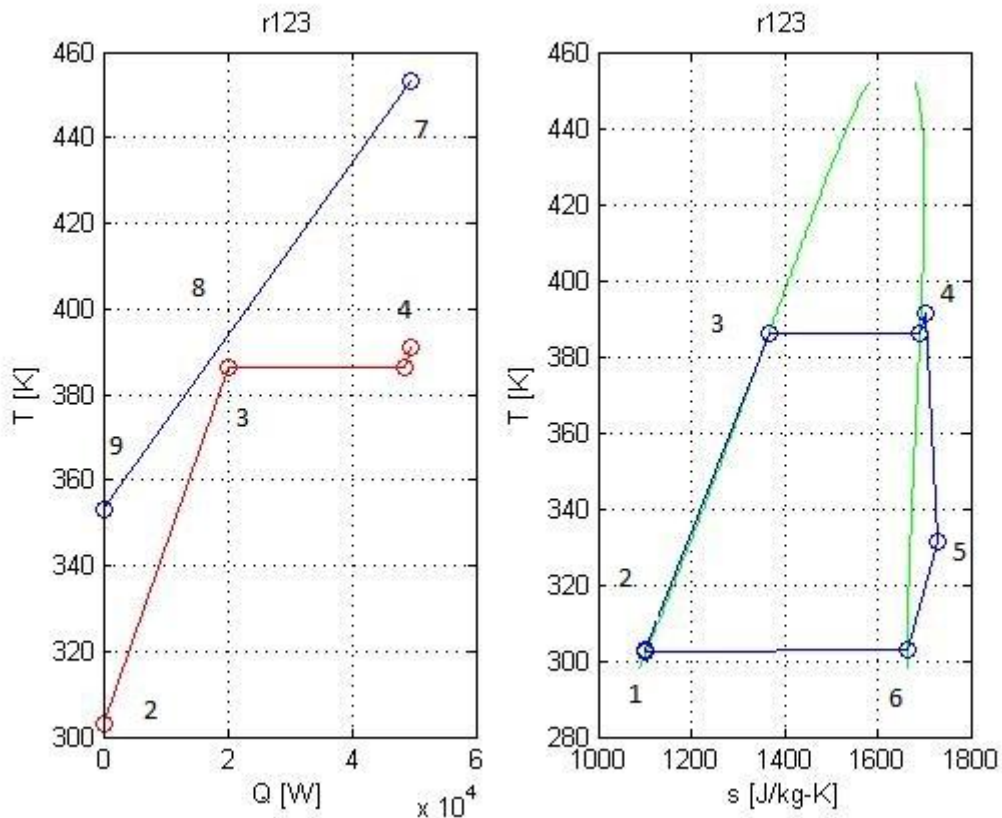


Figure 1.9. (a) T-Q diagram of pre-heater and evaporator; (b) Organic Rankine cycle for r123. The most important state points are displayed.

The available energy that can be extracted from the heat source can be calculated as

$$\dot{Q}_{hs} = \dot{m}_{hs} (h_{hs,in} - h_{hs,out}) = \dot{m}_{hs} (h_7 - h_9) \quad (1.1)$$

The power necessary to the pump is:

$$\dot{W}_p = \dot{m}_{wf} (h_{p,out} - h_{p,in}) = \dot{m}_{wf} (h_2 - h_1) = \dot{m}_{wf} (h_{2,is} - h_1) / \eta_p \quad (1.2)$$

The heat exchange in the evaporator is obtained by:

$$\dot{Q}_{wf} = \dot{m}_{wf} (h_{eva,out} - h_{eva,in}) = \dot{m}_{wf} (h_4 - h_2) \quad (1.3)$$

Along the isobaric process, sensible and latent heat transfer are expressed as:

$$\dot{Q}_{wf,sens} = \dot{m}_{wf} (h_3 - h_2) \quad (1.4)$$

$$\dot{Q}_{wf,lat} = \dot{m}_{wf} (\Delta h_{lat}) = \dot{m}_{wf} (h_{3r} - h_3) \quad (1.5)$$

$$\dot{Q}_{wf,suph} = \dot{m}_{wf} (h_4 - h_{3r}) \quad (1.6)$$

The power extracted by the expander can be calculated by the expression:

$$\dot{W}_t = \dot{m}_{wf} (h_{t,in} - h_{t,out}) = \dot{m}_{wf} (h_4 - h_5) = \dot{m}_{wf} (h_4 - h_{5,is}) \eta_t \quad (1.7)$$

The heat exchange in the condenser is:

$$\dot{Q}_{wf} = \dot{m}_{wf} (h_{cond,in} - h_{cond,out}) = \dot{m}_{wf} (h_5 - h_1) \quad (1.8)$$

This heat is transferred to the cooling fluid (water):

$$\dot{Q}_{wtr} = \dot{m}_{wtr} (h_{wtr,out} - h_{wtr,in}) = \dot{m}_{wtr} (h_{12} - h_{10}) \quad (1.9)$$

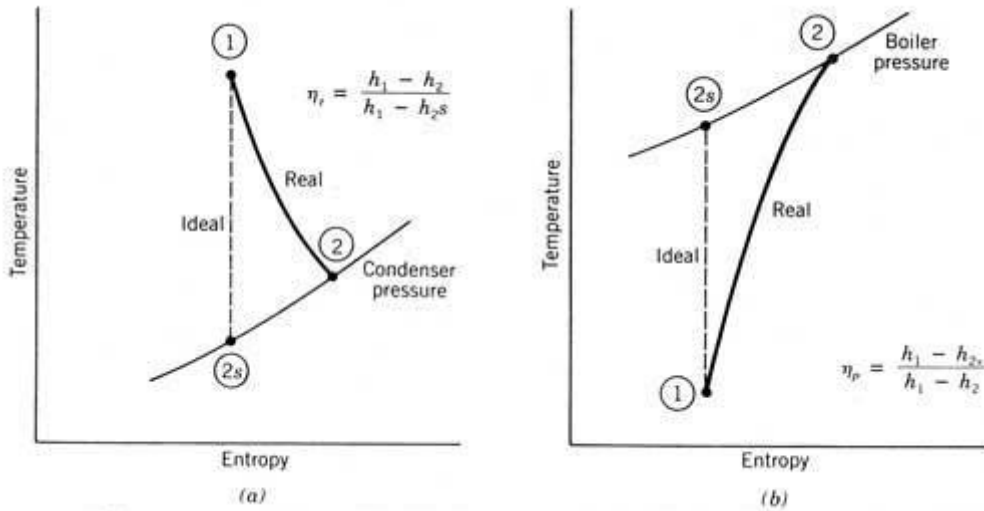


Figure 1.10. (a) Isentropic expansion; (b) Isentropic compression.

It is clear that the lower condensation temperature is, the more power will be generated by ORC unit. However, condensation temperature is strongly limited by the cooling source. Furthermore, a lower condensation temperature will inevitably lead to a larger cooling heat transfer surface and more complex sealing devices. Hence, a low condensation temperature implies high investment cost.

The thermal efficiency of ORC is defined as:

$$\eta_{ORC} = \frac{\dot{W}_{net}}{\dot{Q}_{hs}} = \frac{\dot{W}_t - \dot{W}_p}{\dot{Q}_{hs}} \quad (1.10)$$

The performance of evaporator is expressed by the effectiveness:

$$\varepsilon = \frac{q}{q_{max}} = \frac{\dot{m}c_p(T_i - T_o)}{(\dot{m}c_p)_{min}(T_i - t_i)} = \frac{\dot{m}c_p(t_o - t_i)}{(\dot{m}c_p)_{min}(T_i - t_i)} \quad (1.11)$$

Finally, the system efficiency can be calculated as the product of thermal efficiency and effectiveness.

$$\eta_{system} = \eta_{ORC} \cdot \varepsilon \quad (1.12)$$

Besides first law analysis, it is important to consider the irreversibility rate in various processes of the system in order to carry out an exergy (or entropy) analysis of the ORC. In a real process, the total entropy generation is caused by external and internal factors. The internal entropy generation mainly occurs due to pressure drop caused by friction, losses in the turbine and internal transfer of energy over a finite temperature difference in the components. The external entropy generation can be caused by the mechanical transfer of work and heat transfer over a finite temperature difference.

The irreversibility rate can be calculated for each component of ORC defining an appropriate control volume:

$$\dot{i} = T_0 \frac{ds_{total}}{dt} \quad (1.13)$$

$$\dot{i} = \dot{m}T_0 \left[\sum s_{outlet} - \sum s_{inlet} + \frac{ds_{system}}{dt} + \sum_k \frac{q_k}{T_k} \right] \quad (1.14)$$

Where T_k is the thermodynamic temperature of each heat source and q_k is the heat transferred across the control volume. T_0 is the ambient temperature. The assumption that the system works at the steady state implies that $\frac{ds_{total}}{dt} = 0$.

Based on the cycle description above, the irreversibility rates for each component can be expressed as:

$$\dot{i}_{eva} = \dot{m}_{wf}T_0 \left[(s_4 - s_2) - \frac{(h_4 - h_2)}{T_H} \right] = \dot{m}_{wf}T_0 [(s_4 - s_2) + (s_9 - s_7)] \quad (1.15)$$

$$\dot{i}_t = \dot{m}_{wf}T_0 (s_5 - s_4) \quad (1.16)$$

$$\dot{i}_{cond} = \dot{m}_{wf}T_0 \left[(s_5 - s_1) + \frac{(h_5 - h_1)}{T_L} \right] = \dot{m}_{wf}T_0 [(s_5 - s_1) + (s_{12} - s_{10})] \quad (1.17)$$

$$\dot{i}_p = \dot{m}_{wf}T_0 (s_2 - s_1) \quad (1.18)$$

If the control volume is defined around the ORC

$$\dot{i}_{cycle} = \dot{m}_{wf}T_0 \left[-\frac{(h_4 - h_2)}{T_H} + \frac{(h_5 - h_1)}{T_L} \right] \quad (1.19)$$

From the previous expressions, it is possible to calculate the entropy generation simply dividing by T_0 .

$$\dot{S}_{eva} = \dot{m}_{wf} \left[(s_4 - s_2) - \frac{(h_4 - h_2)}{T_H} \right] = \dot{m}_{wf} [(s_4 - s_2) + (s_9 - s_7)] \quad (1.20)$$

$$\dot{S}_{exp} = \dot{m}_{wf} (s_5 - s_4) \quad (1.21)$$

$$\dot{S}_{cond} = \dot{m}_{wf} \left[(s_5 - s_1) + \frac{(h_5 - h_1)}{T_L} \right] = \dot{m}_{wf} [(s_5 - s_1) + (s_{12} - s_{10})] \quad (1.22)$$

$$\dot{S}_{pump} = \dot{m}_{wf} (s_2 - s_1) \quad (1.23)$$

$$\dot{S}_{cycle} = \dot{m}_{wf} \left[-\frac{(h_4 - h_2)}{T_H} + \frac{(h_5 - h_1)}{T_L} \right] \quad (1.24)$$

The Irreversibility ratio is defined as the ratio between the total irreversibility rate of the system and the total energy supplied by the thermal source:

$$\varphi = \frac{\dot{I}_{cycle}}{\dot{Q}_{hs}} \quad (1.25)$$

Based on exergy destruction in the system, it is possible to calculate the second law efficiency. It is defined as the ration between the turbine output and the maximum work obtainable by the system:

$$\eta_{II} = \frac{\dot{W}}{\dot{W} + \dot{I}_{cycle}} \quad (1.26)$$

The cycle considered is a simple cycle where the working fluid is saturated liquid at the exit of the condenser. A sub-cooling of 5°C can be taken in consideration. As explained before, no superheating is necessary. However, 5°C of superheating could be imposed. Minimum approach temperature of 10°C in the evaporator and 10 °C in the condenser is assumed when comparison of working fluid on the basis of the maximum power output is carried out. This imposition will be removed when comparison will be carried out with a fixed heat flux. The pinch point in the evaporator could be be either at the point where evaporation starts or at the inlet of working fluid as shown in *Fig.1.11*. It is possible to forecast the position of pinch point considering working fluid and boundary conditions, however, a check is necessary.

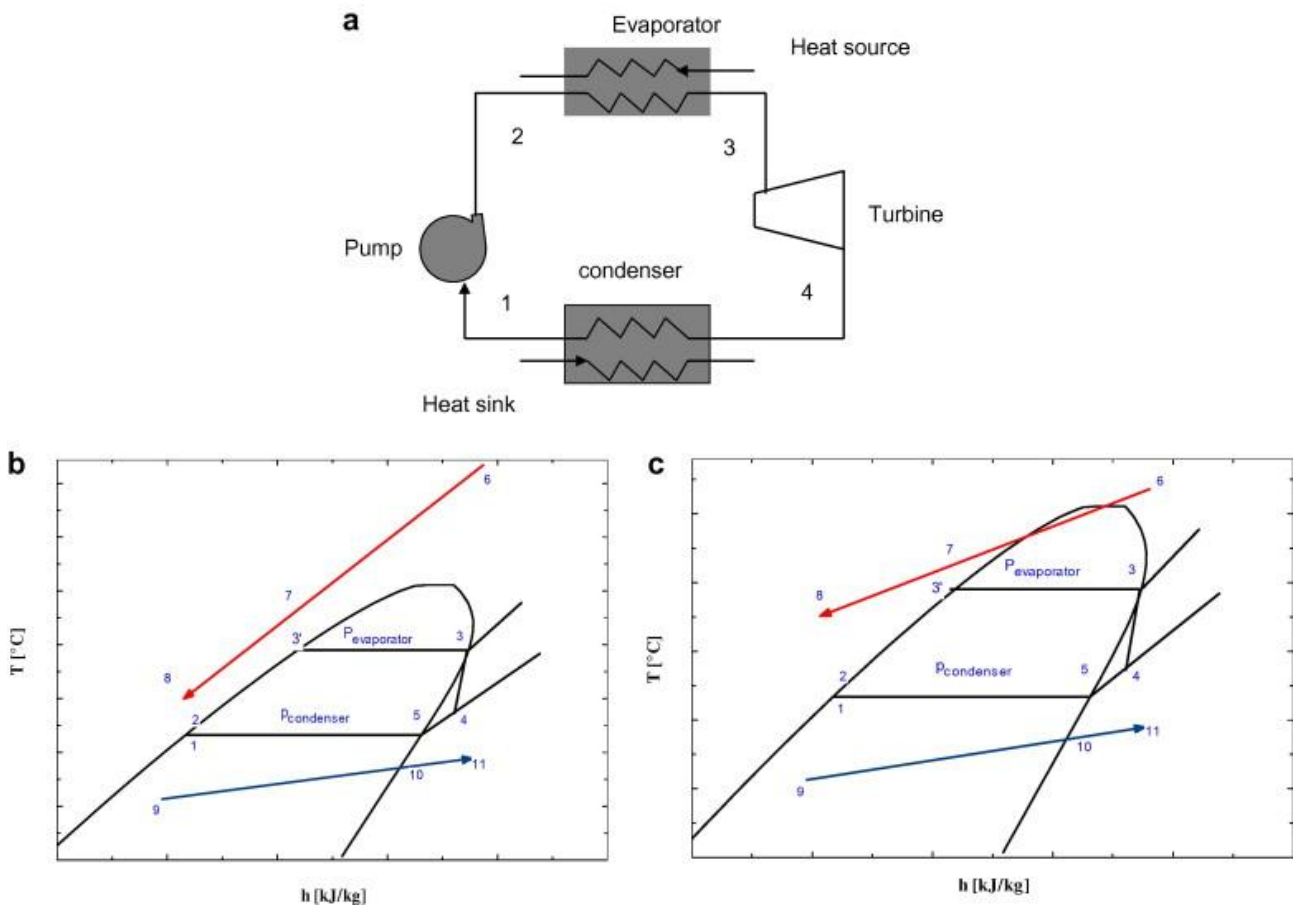


Figure 1.11.(a) Rankine cycle(b) Pinch point position. Inlet of pre-heater or inlet of evaporator.

Pinch point plays a key role in influencing the heat transfer performance. This is the smallest heat transfer temperature difference in the vapor generator which determines the performance limit (heat transfer and entropy generation) of evaporator and economizer.

1.5. Fluid candidates and their properties

The screening of more than 20 working fluids has been carried out based on thermodynamic and physical properties, stability and compatibility, environmental impacts, safety, availability and cost. Some of the most important saturation curves of the fluid are shown in the following figure:

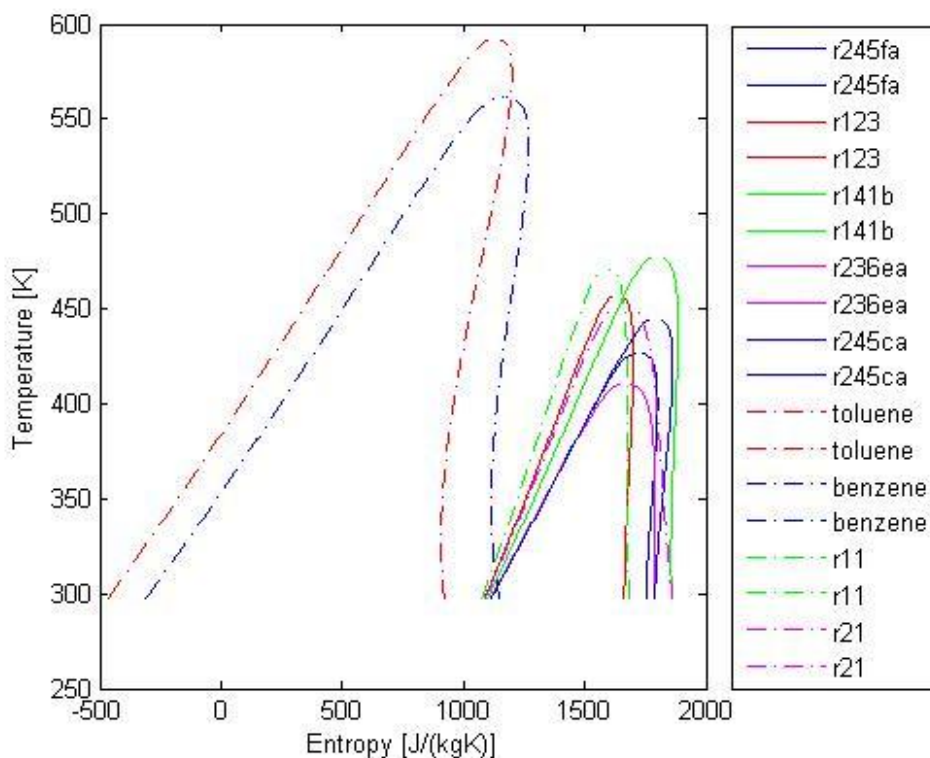


Figure 1.12. Saturation curve of typical organic fluids.

Thermodynamic and physical properties are the first characteristics to take into consideration. The molecular weight is related to the density of the fluid whereas the critical point suggests the possible operating temperature and pressure range. Parameter ξ , is related to the type of the fluid (wet, isentropic or dry) thus influences the effectiveness of superheating.

As described by Chen et al. [3], there are five groups of fluids that are similar characteristics.

- *Benzene and toluene.* They are considered as isentropic fluids with relatively high critical temperatures. They are used for medium-high operating temperature.
- *Fluids R-170, R7-44, R-41, R-23, R-116, R-32, R-125 and R143a.* This group of fluids can be considered as wet fluids with low critical temperatures and reasonable critical pressure. These characteristics are desirable for supercritical ORC.

- Fluids propyne , HC-270,R-152a, R-22 and R-1270. They are wet fluids with relatively high critical temperatures. Superheating is usually needed when they are applied in organic Rankine cycles.
- Fluids R-21,R142b,R-134a,R-1234yf,R-290,R-141b,R-123,R-245ca,R-245fa,R-236ea,R-124,R-227ea and R-218. They are considered isentropic fluids and are widely used for low grade heat recovery.
- Fluids R-601,R-600,R-600a,FC-4-1-12,RC318,R-3-1-10. These fluids are considered dry fluids and can be used in supercritical Rankine cycles and organic Rankine cycles.

Fluid	Tcrit[K]	Pcrit[bar]	Molar mass[g/mol]	Density[kg/m ³]
r245fa	427.16	36.51	134.05	516.08
r123	456.83	36.62	152.93	550.00
r141b	477.50	42.12	116.95	458.56
r142b	410.26	40.55	100.50	446.00
r236ea	412.44	35.02	152.04	563.00
r245ca	447.57	39.25	134.05	523.59
toluene	591.75	41.26	92.14	291.99
benzene	562.02	49.06	78.11	304.79
r11	471.11	44.08	137.37	554.00
r21	451.48	51.81	102.92	526.00
r134a	374.21	40.59	102.03	511.90
r227ea	374.90	29.25	170.03	594.25
r1234yf	367.85	33.82	114.04	475.55
cycloopen	511.69	45.15	70.13	267.91
cyclohex	553.64	40.75	84.16	273.00

Table 1.1. Properties of typical organic fluids

The decision on which fluids could be used may be based on how the operating temperature is tailored to cope with the heat source temperature profile. The parameters that can be used to evaluate the performance of different working fluids are the net power output (or the system efficiency) and the irreversibility ratio.

2.1. Heat Exchanger Design Methodology

The methodology of heat exchanger design is complicated because several quantitative and qualitative design aspects must be taken into account to get to an optimal solution. An overview of heat exchanger design approach is presented below but a more detailed description is shown in [8,9,10] .

A methodology for designing a new heat exchanger is illustrated in *figure 2.1*; it is based on experience and presented by Kays and London (1998), Taborek (1988), and Shah (1982) for compact and shell-and-tube exchangers. Major design considerations include:

- Process and design specifications
- Thermal and hydraulic design
- Mechanical design
- Manufacturing considerations and cost
- Trade-off factors and system-based optimization

The design considerations are usually not sequential and there is a strong relation between several aspects. This implies a number of iterations to achieve the optimal solution.

Multi-objective optimization can reduce iterations to find the optimal solution, hence less time is required.

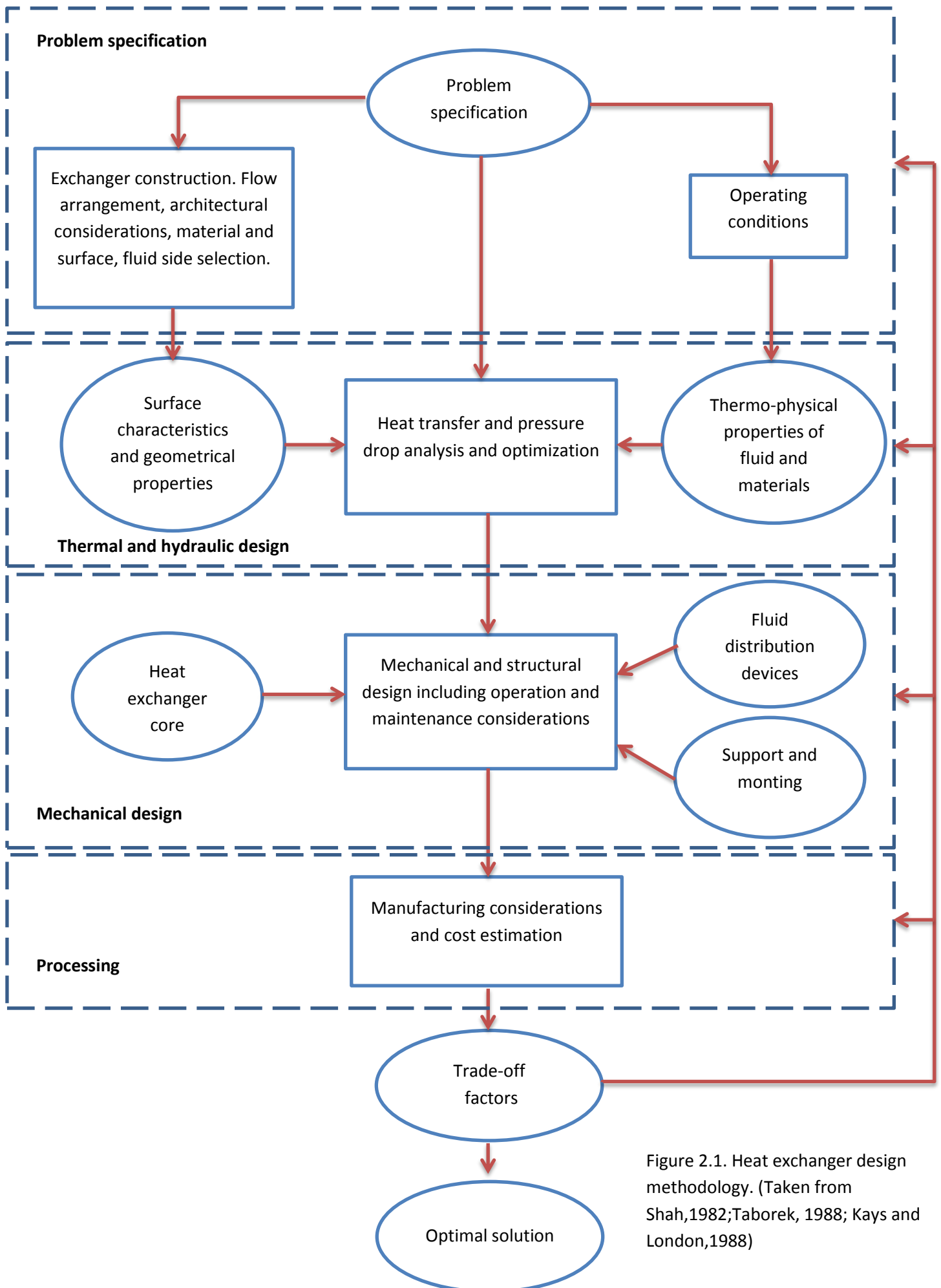


Figure 2.1. Heat exchanger design methodology. (Taken from Shah,1982;Taborek, 1988; Kays and London,1988)

2.2. Problem Specifications

First of all it is necessary to define the design basis (i.e. design conditions). Design requires the specification of operating and the environmental conditions upon which the heat exchanger is going to be operated. It is important to analyze heat exchanger performance at the design point and off-design conditions.

In a ORC the operating conditions could be:

- Fluids and their thermo-physical properties
- Inlet temperatures of both fluid streams
- Inlet pressure of both fluid streams
- Required heat duty
- Maximum allowed pressure drop on both fluid sides
- Maximum allowed space and weight occupied by HE
- Corrosive and fouling characteristics of the fluids
- Costs
- Material

In an organic Rankine cycle there are several aspects that influence the design of heat exchangers. A previous cycle optimization is important in order to select the right fluid and operating conditions.

2.3. Exchanger Specifications

Based on the problem specifications, the exchanger construction type and flow arrangement are first selected. Selection of the construction type depends on several aspects:

- Fluid (gas, liquid, evaporation/condensation)
- Operating pressures
- Operating temperatures
- Mass flow rate
- Fouling and cleanability
- Fluids and material compatibility
- Corrosiveness of the fluids
- Costs

In an ORC, typically, are used plate heat exchangers or shell and tube heat exchangers. Afterwards, it is necessary to select the core or surface geometry and material. The core geometry for a shell and tube exchanger includes shell type, number of passes, baffle geometry. The surface geometry is chosen for a plate heat exchanger. The criteria for core and surface geometry are desired heat transfer performance within specified pressure drop, operating pressure and temperature, thermal/pressure stresses, leaks and corrosion characteristics of the fluids.

2.4. Thermal and Hydraulic Design

Heat exchanger thermal and hydraulic design procedures involve exchanger rating and/or sizing and this is the core of the procedure. There are two main relations that constitute the entire thermal design procedure:

I. Enthalpy rate equations

$$q_h = \dot{m}_h \Delta h_h = \dot{m}_h (T_{h,in} - T_{h,out}) \quad (2.1)$$

$$q_c = \dot{m}_c \Delta h_c = \dot{m}_c (T_{c,out} - T_{c,in}) \quad (2.2)$$

$$q_h = q_c \quad (2.3)$$

II. Heat transfer rate equation

$$q = UA\Delta T_m \quad (2.4)$$

The first equation relates the heat transfer rate with the enthalpy rate change for an open non-adiabatic system. The second equation reveals a convection-conduction heat transfer phenomena in a two fluid heat exchanger. It is possible to note the influence of the area (A) and the overall heat transfer coefficient (U) on heat transfer rate. The heat transfer rate is also proportional to the mean temperature difference (ΔT_m). This mean temperature difference is a log-mean temperature difference and takes into account the arrangement (countercurrent or parallel flow).

2.5. Mechanical Design

Mechanical design is fundamental to ensure the mechanical integrity of the heat exchanger under steady-state, transient, startup, shutdown, upset and part load operating conditions. The heat exchanger core is designed for the desired structural strength based on the operating pressures, temperatures, and corrosiveness or chemical reaction of fluids with materials. Pressure/thermal stress calculations are performed to determine the thicknesses of critical parts in the exchangers, such as the fin, plate, tube, shell, and tube sheet. In addition to the heat exchanger core, the proper design of flow distribution devices (headers, tanks, manifolds, nozzles, or inlet–outlet pipes) is made to ensure that there is uniform flow distribution through the exchanger flow passages, and that neither erosion nor fatigue will be a problem during the design life of the exchanger.

2.6. Manufacturing Considerations and Cost Estimates

The overall cost, also called lifetime costs, associated with a heat exchanger may be categorized as the capital, installation, operating and sometimes also disposal cost. The capital (total installed) cost includes the costs associated with design, materials, manufacturing (machinery, labor, and overhead), testing, shipping, installation, and depreciation. Installation of the exchanger on the site can be as high as the capital cost for some shell-and-tube and plate heat exchangers. The operating cost consists of the costs associated with fluid pumping power, warranty, insurance, maintenance, repair, cleaning, lost production/downtime due to failure, energy cost associated with the utility (steam, fuel, water) in conjunction with the exchanger in the network, and decommissioning costs. Some of the cost estimates are difficult to obtain and best estimates are made at the design stage.

2.7. Trade-off factors and optimization

As mention before, several factors influence in different way the performance of heat exchangers. The complex procedure shown in *figure 2.1* leads the designer to make a trade-off among different possible choices.

In fact, heat exchangers are designed for many different applications, and hence may involve many different optimization criteria. These criteria for heat exchanger design may be:

- Minimum initial and operating costs
- Minimum weight
- Minimum value of heat transfer surface area
- Minimum pressure drop
- Minimum entropy generation

When a performance measure has been defined quantitatively it can be minimized or maximized and it is called an objective function in a design optimization. A particular application can also be subjected to certain requirements, such as required heat transfer, allowable pressure drop, weight or area limitations and so on. These limitations are called constraints in the design optimization. All the variables that can be changed are called design variables associated with a heat exchanger design.

Nowadays, the possibility to use optimization algorithm to obtain optimal solution plays a key role in the thermo-economical design. Using multi-objective algorithm it is possible to evaluate the influence of a great number of variables on performance indexes of a system and obtain a set of solutions that have the best trade-off between several fitness functions.

2.8. General method for the optimum design of waste heat recovery heat exchangers

A key component in waste heat recovery is the heat exchanger. The profitability of an investment in waste heat recovery depends heavily on the efficiency of heat exchangers and their associated life cycle costs (purchase, maintenance, etc). The optimizations of pre-heater, evaporator, super-heater and condenser play an important role in the entire cycle design. According to the current technical practice, it can be organized at different levels of complexity with objectives sequentially defined: operating parameters, geometrical details and technological elements.

According to A. Franco and N. Giannini [21] the optimization can be organized at two levels: the first one enables to obtain the main operating parameters of the heat exchangers, while the second involves the detailed designed of the component concerning the geometric variables of the heat transfer sections. The output of the first-level optimization is the input of the second level.

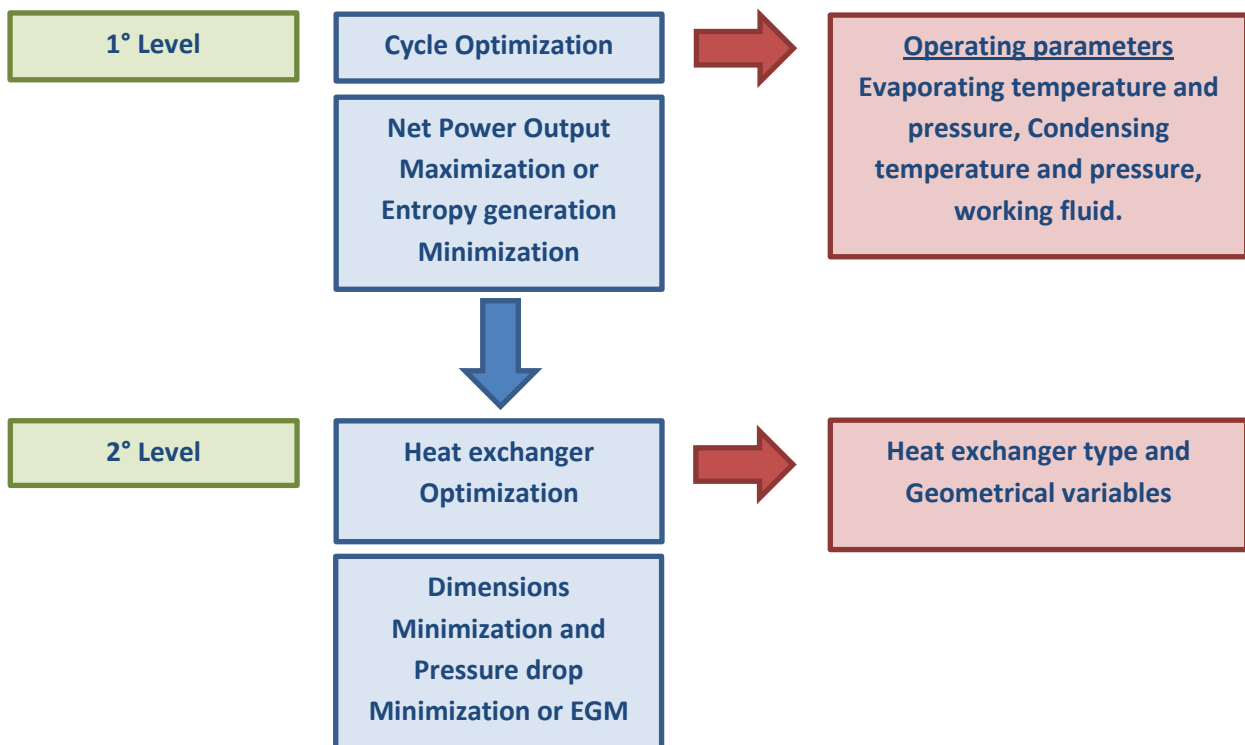


Figure 2.2. Two levels optimization

Once that the optimization at the higher level is carried out, the emerged optimum results will become the boundary condition for the following optimization level. This means that the results coming from the higher optimization level represent the input data for the detailed design of the economizer and evaporator. The same approach can be implemented in order to optimize all the systems of the plant such as condenser, expander and pump.

The first optimization aims to assess the operating parameters as pressures, mass flow rates and temperature profile in the evaporator. Those operating variables can be determined with thermodynamic, thermo-economic or economic optimization, minimizing a suitable objective function as the thermal exergy losses, the total cost per unit power installed or an alternative objective function.

The second-level optimization involves the detailed design of the evaporator basing on a thermal and fluid-dynamic model. In this case, the objective function can be the minimization of the evaporator dimensions (volume, weight etc.), or the minimization of the pressure losses, for the heat flow rate defined at the previous level. The entropy generation minimization proposed by Bejan is another possible approach. This approach will be treated in the following chapters.

3.1. Thermal Design Theory

In a heat exchanger two fluids are separated by a heat transfer surface and they ideally do not mix. Each fluid has an inlet temperature and an outlet temperature. If the temperature of inlet and outlet are equal means that the fluid is changing in phase. This is what happens in evaporator and condenser. The temperature difference along the heat exchanger is the driving force for overall heat transfer. Along the heat exchanger the fluids change their enthalpy following the first law of thermodynamics:

$$\frac{dE_{cv}}{dt} = \dot{Q}_{cv} - \dot{W}_{cv} + \dot{m}_i \left(u_i + p_i v_i + \frac{V_i^2}{2} + gz \right) + \dot{m}_o \left(u_o + p_o v_o + \frac{V_o^2}{2} + gz \right) \quad (3.1)$$

Defining the enthalpy as:

$$h = u + pv \quad (3.2)$$

the expression becomes:

$$\frac{dE_{cv}}{dt} = \dot{Q}_{cv} - \dot{W}_{cv} + \dot{m}_i \left(h_i + \frac{V_i^2}{2} + gz \right) + \dot{m}_o \left(h_o + \frac{V_o^2}{2} + gz \right) \quad (3.3)$$

Considering a control volume around heat exchanger at the steady state, the condition of the mass within the control volume and at the boundary does not vary with time. The mass flow rates and the rates of energy transfer by heat and work are also constant with time. There can be no accumulation of mass within the control volume so the mass rate balance takes the form:

$$\sum_i \dot{m}_i = \sum_o \dot{m}_o \quad (3.4)$$

Furthermore, at the steady state $\frac{dE_{cv}}{dt} = 0$ and the equation can be rewritten as:

$$\dot{Q}_{cv} - \dot{W}_{cv} + \dot{m}_i \left(h_i + \frac{V_i^2}{2} + gz \right) + \dot{m}_o \left(h_o + \frac{V_o^2}{2} + gz \right) = 0 \quad (3.5)$$

Considering zero the terms $\dot{W}_{cv}, \frac{V_i^2}{2}, gz$:

$$\dot{Q}_{cv} = \dot{m}(h_o - h_i) \quad (3.6)$$

Defining as control volume each side of the heat exchanger:

$$\dot{Q}_h = \dot{m}_h(h_{h,o} - h_{i,in}) \quad (3.7)$$

$$\dot{Q}_c = \dot{m}_c(h_{c,o} - h_{c,in}) \quad (3.8)$$

With the assumption of adiabatic system:

$$\dot{Q}_h + \dot{Q}_c = 0 \quad (3.9)$$

The subscript h and c denote hot and cold fluid, respectively. As shown in Fig. 3.1, the previous equation can be expressed for the differential element of area dA .

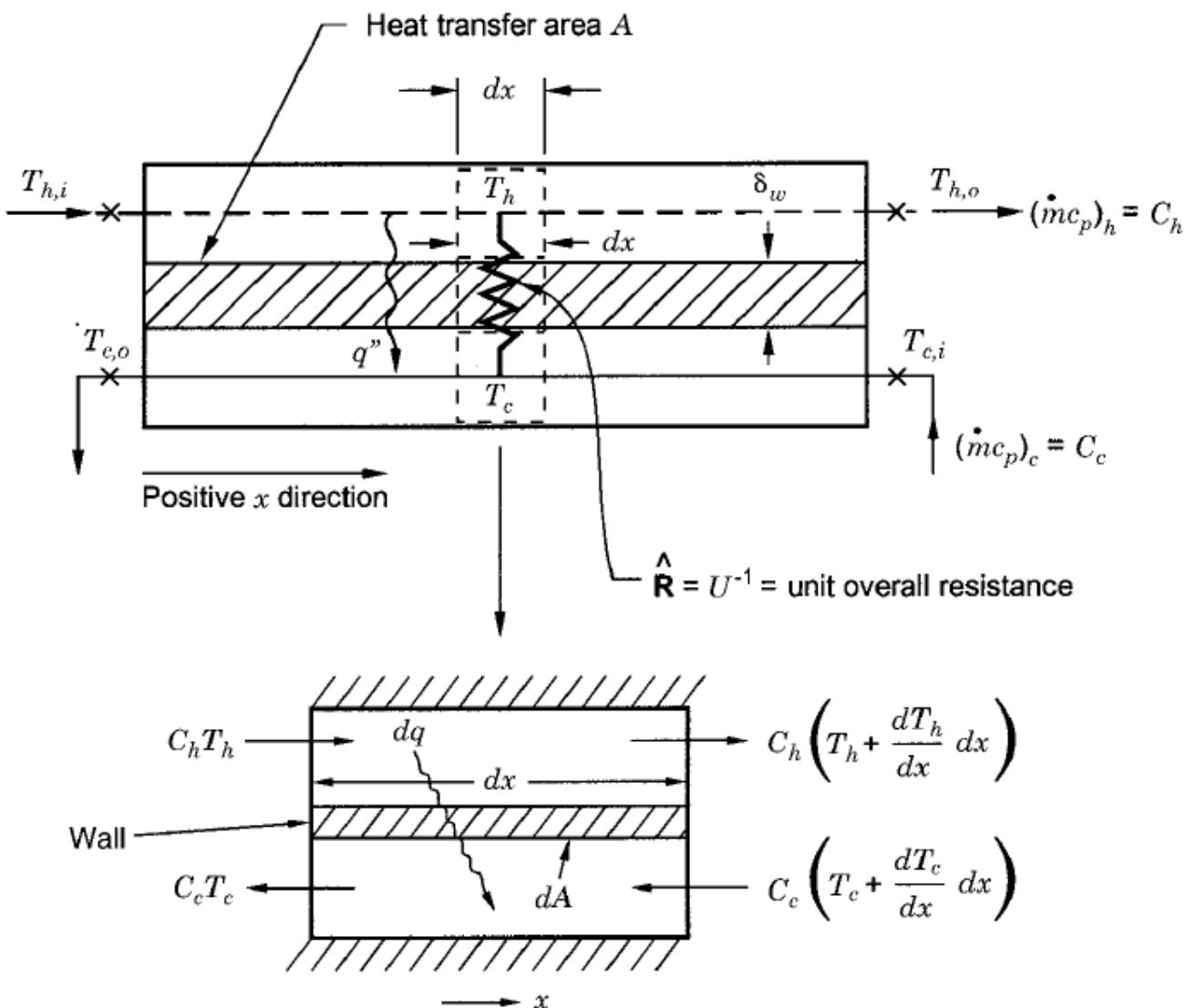


Figure 3.1. Heat transfer through a surface with conduction and convection. Radiation is neglected. (From Shah, 1983)

To perform the heat transfer analysis, it is necessary another equation that relate heat transfer rate \dot{Q} , heat transfer area A and overall heat transfer coefficient U :

$$d\dot{Q} = U\Delta T dA \quad (3.10)$$

Where U is the local overall heat transfer coefficient and is a parameter related to the overall differential thermal resistance dR_o . As shown in Fig.3.2., the overall thermal resistance consists of component resistances in series:

$$\frac{1}{UdA} = dR_o = dR_h + dR_{h,f} + dR_w + dR_{c,f} + dR_c \quad (3.11)$$

$$\frac{1}{UdA} = \frac{1}{(\eta_o\alpha dA)_h} + \frac{1}{(\eta_o\alpha_f dA)_h} + dR_w + \frac{1}{(\eta_o\alpha dA)_c} + \frac{1}{(\eta_o\alpha_f dA)_c} \quad (3.12)$$

Considering finite areas, one can obtain:

$$\frac{1}{UA} = \frac{1}{(\eta_o\alpha A)_h} + \frac{1}{(\eta_o\alpha_f A)_h} + dR_w + \frac{1}{(\eta_o\alpha A)_c} + \frac{1}{(\eta_o\alpha_f A)_c} \quad (3.13)$$

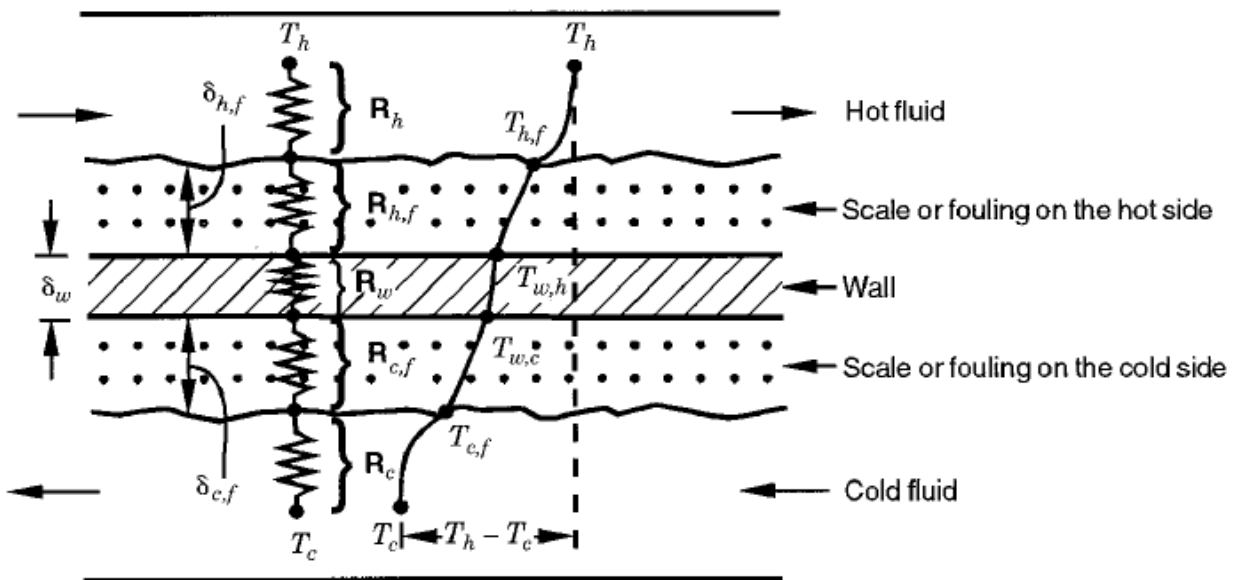


Figure 3.2. Thermal resistances (From Shah, 1983).

The values of U and α are assumed to be local and the final value will be a mean value. As shown in the figure below, there are several resistances that influence the overall heat transfer coefficient:

$$R_h = \frac{1}{(\eta_o\alpha A)_h} \text{ hot fluid side convection resistance} \quad (3.14)$$

$$R_{h,f} = \frac{1}{(\eta_o\alpha_f A)_h} \text{ hot fluid side fouling resistance} \quad (3.15)$$

$$R_w = \begin{cases} \frac{\delta_w}{k_w A_w} & \text{wall thermal resistance for flat walls} \\ \frac{\ln(d_o/d_i)}{2\pi k_w L N_t} & \text{wall thermal resistance for } N_t \text{ circular tubes} \end{cases} \quad (3.16)$$

$$R_{c,f} = \frac{1}{(\eta_o \alpha A)_c} \text{ cold fluid side convection resistance} \quad (3.17)$$

$$R_c = \frac{1}{(\eta_o \alpha_f A)_c} \text{ cold fluid side fouling resistance} \quad (3.18)$$

The previous expressions are easy to manage but they do not take into considerations thermophysical properties changing with the temperature. In order to solve this problem it is possible to split up the heat transfer area in small portions where the heat is transferred. In this way, one can define thermophysical properties in each interval with better approximation.

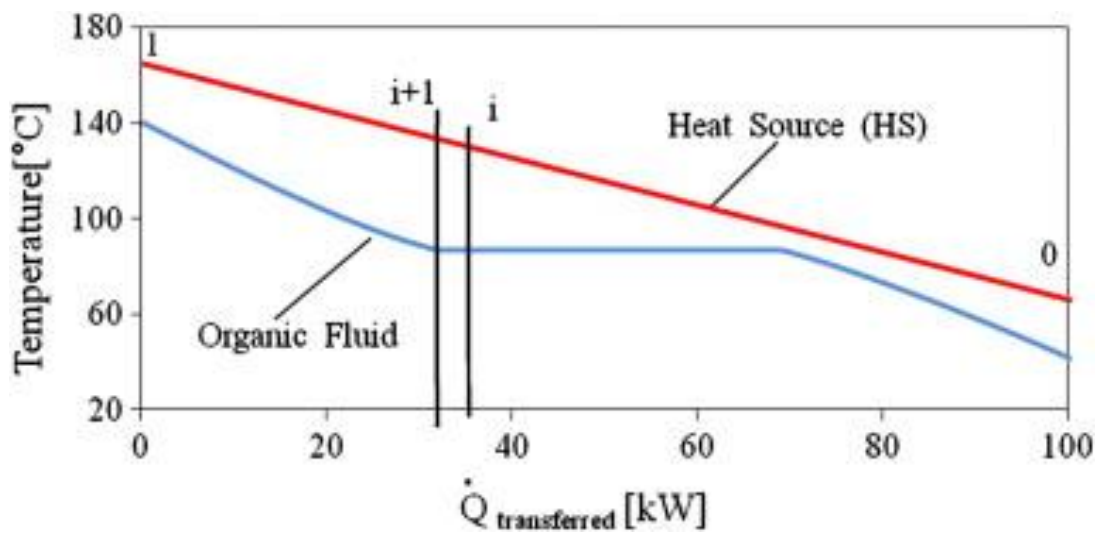


Figure 3.3. heat transfer surface divided in small intervals.

4

Plate Heat Exchangers

4.1. Plate Heat Exchangers

Plate heat exchangers (*PHE*) consist of a stack of parallel thin plates that lie between end plates. Each fluid stream passes alternately between adjoining plates in the stack, exchanging heat through the plates. The plates are corrugated for strength and to enhance heat transfer by directing the flow and increasing turbulence. These exchangers have high heat-transfer coefficients and area, the pressure drop is also typically low, and they often provide very high effectiveness. However, they have relatively low pressure capability.

The fluids are directed into their proper chambers either by a suitable gasket or a weld, depending on the chosen type of exchanger. Traditionally, plate and frame exchangers have been used almost exclusively for liquid to liquid heat transfer. The best example is in the dairy industry. Today, many variations of the plate technology have proven useful in applications where a phase change occurs as well. This includes condensing duties as well as vaporization duties. Plate heat exchangers are best known for having overall heat transfer coefficients (*U*-values) in excess of 3–5 times the *U*-value in a shell and tube designed for the same service.

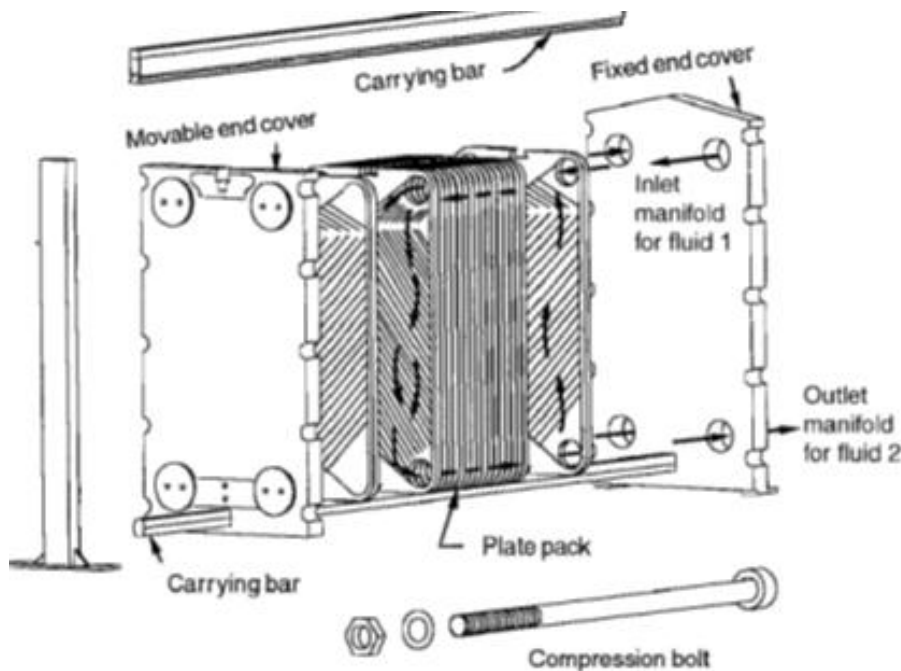


Figure 4.1. Plate heat exchanger

Plate heat exchanger is an attractive option when more expensive materials of construction can be used. The significantly higher *U*-value results in far less area for a given application. The higher *U*-values are

obtained by inducing turbulence between the plate surfaces. Owing to this they are also known to minimize the fouling.

Some inherent limitations of the plate heat exchangers are caused by plates and gaskets as follows. The plate exchanger is capable of handling up to a maximum pressure of about 3 MPa gauge but is usually operated below 1.0 MPa gauge.

The gasket materials restrict the use of PHEs in highly corrosive applications; they also limit the maximum operating temperature to 260°C but are usually operated below 150°C to avoid the use of expensive gasket materials. Gasket life is sometimes limited. Frequent gasket replacement may be needed in some applications. For equivalent flow velocities, pressure drop in a plate exchanger is very high compared to that of a shell-and tube exchanger. However, the flow velocities are usually low and plate lengths are “short,” so the resulting pressure drops are generally acceptable.

Recently, the development of brazing techniques has allowed the use of PHEs as evaporators and condensers. Brazed plate heat exchangers can manage high pressures (up to 40 bar) and temperatures (up to 200°C). Since the advent of the brazed plate heat exchangers (BPHE) in the 1990s, the studies on the condensation and/or evaporation heat transfer have been started for its application in refrigeration and power system application. The disadvantage of such a design is the loss of disassembling flexibility on the fluid sides where the welding is done.

Table 4.1.

Unit	
Maximum surface area	2500 m ²
Number of plates	3 to 700
Port size	Up to 400 mm
Operation	
Pressure	0.1 to 3.0 MPa
Temperature	-40 to 260°C
Maximum port velocity	6 m/s (for liquids)
Channel flow rates	0.05 to 12.5 m ³ /h
Maximum unit flow rate	2500 m ³ /h
Plates	
Thickness	0.5 to 1.2 mm
Size	0.03 to 3.6 m ²
Channel spacing	1.5 to 7 mm
Width	70 to 1200 mm
Length	0.4 to 5 m
Hydraulic diameter	2 to 10 mm
Surface area per plate	0.02 to 5 m ²
Performance	
Temperature approach	As low as 1°C
Heat exchanger efficiency	Up to 93%
Heat transfer coefficients for water-water duties	3000 to 8000 W/ m ² K

4.2. Geometry

The corrugated grooves on the right and left outer plates have a 'V' shape but those in the middle plate have a contrary 'V' shape on both sides. This arrangement allows the flow to be divided into two different flow directions along the plates. Due to the contrary 'V' shapes between two neighbor plates the flow streams near the two plates cross each other in each channel. This cross flow results in significant flow unsteadiness and randomness. In this way, the flow is highly turbulent even when the Reynolds Number is low.

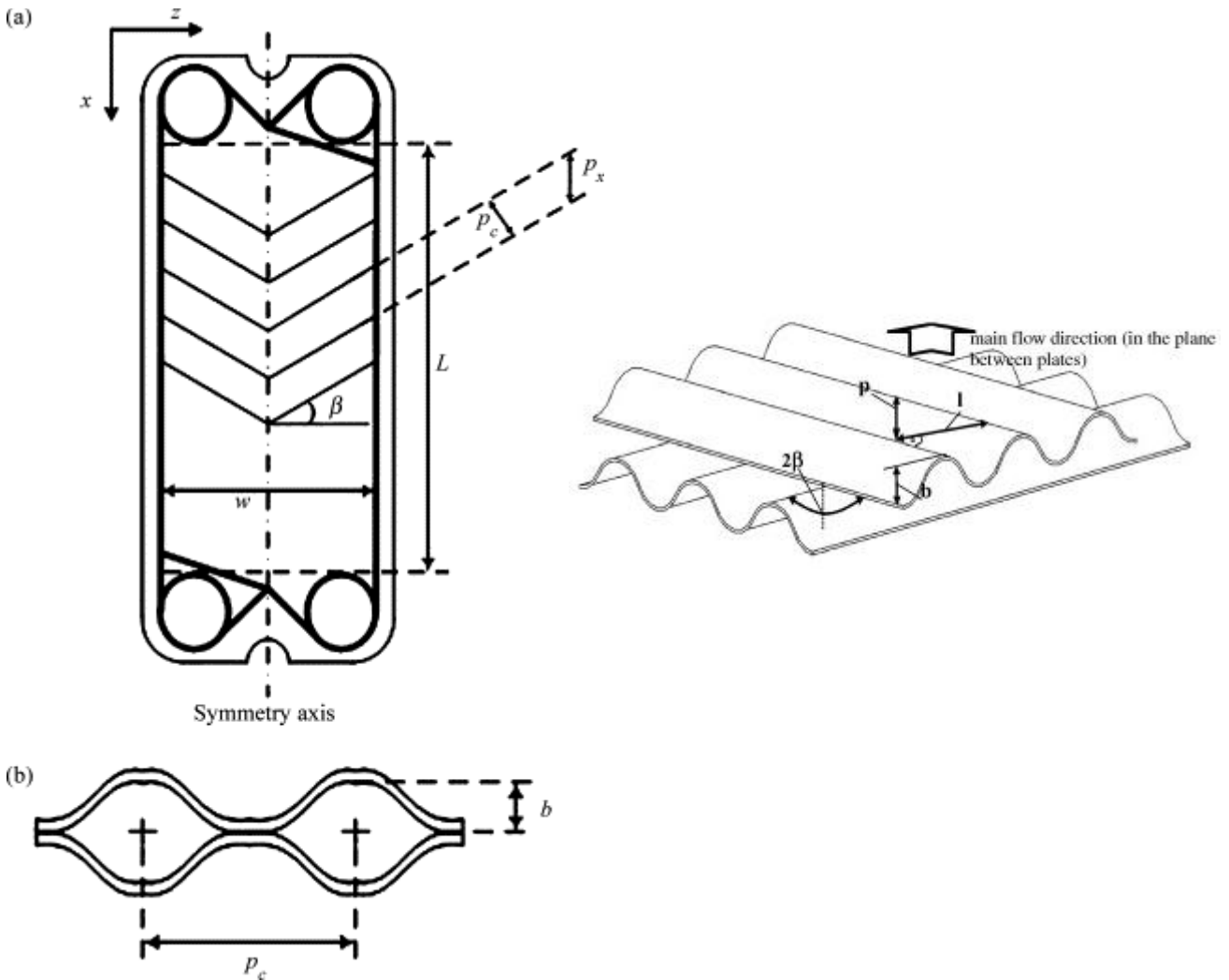


Figure 4.2. (a) Geometric characteristics of chevron pattern; (b) flow inside a channel.

Different geometric parameters of PHE are defined as follows:

1. Chevron angle

The angle of the herringbone β , generally varies between 25° and 65° . This angle has a great influence on heat transfer coefficient and pressure drop.

2. Mean channel spacing

This is defined as the actual gap available for the flow. The depth of the corrugations generally varies between 3 and 5 mm:

$$b = (p - t) \quad (4.1)$$

3. Enlargement factor

The factor ϕ is the ration between the developed length and the projected length. The value of ϕ is related to the mean channel spacing b and the corrugation pitch p_c :

$$X = \frac{2b}{p_c} \quad (4.2)$$

$$\phi = \frac{1}{6} \left(1 + \sqrt{1 + X^2} + 4 \sqrt{1 + \frac{X^2}{2}} \right) \quad (4.3)$$

4. Channel flow area

Channel flow area is the value of the cross flow section area between two plates:

$$A_x = b \cdot W \quad (4.4)$$

5. Channel equivalent diameter

The behavior of the corrugation path can be evaluated using the hydraulic diameter:

$$d_h = \frac{4 \cdot \text{channel flow area}}{\text{wetted surface}} = \frac{4bW}{2W\phi} = \frac{2b}{\phi} = \frac{2(p - t)}{\phi} \quad (4.5)$$

6. Heat transfer area

The heat transfer area can be the effective area of the plate including the corrugations or the projected area of the plate on a plane.

$$A_{\text{projected}} = L \cdot W \quad (4.6)$$

$$A = \phi \cdot L \cdot W \quad (4.7)$$

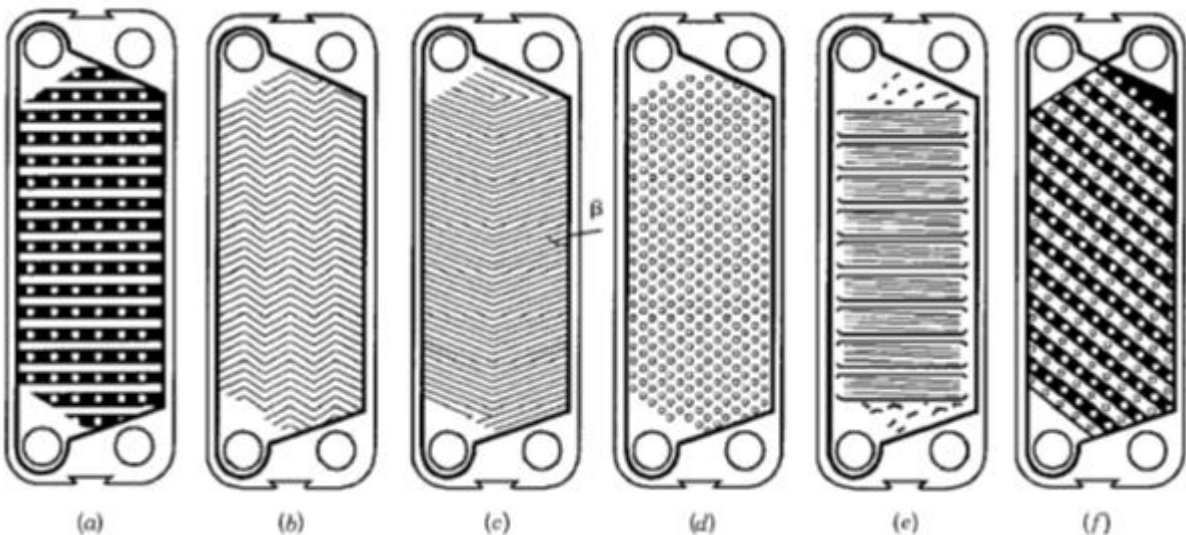


Fig. 4.3. Plate patterns: (a) washboard, (b) zig-zag, (c) chevron or herringbone, (d) protrusions and depressions, (e) washboard with secondary corrugations, (f) oblique washboard.

When the plates are assembled in a stack, the corrugations on the adjoining plates form interrupted flow passages, and these inter-corrugation flow paths promote enhanced convective heat transfer coefficients and decreased fouling characteristics. The corrugations also increase the effective surface area for heat

transfer as well as plate rigidity, and the multiple metal-to-metal contact points between adjacent plates lend greater mechanical support to the stack.

4.3. Flow arrangement

A large number of flow arrangements are possible in a plate heat exchanger depending on the required heat transfer duty, available pressure drops, minimum and maximum velocities allowed, and the flow rate ratio of the two fluid streams. In each pass there can be an equal or unequal number of thermal plates.

There are three main ways to arrange the plates:

- 4.3.1. 1/1 arrangement: one passage for cold fluid and one passage for hot fluid. Both fluid flow counter-current.
- 4.3.2. n/n arrangement: multi-pass arrangements are used when NTU values greater than those given by single plate are required.
- 4.3.3. m/n arrangement. This arrangement can be used when there is a great difference between the mass flow rates or a low value of pressure drop is required for one of the fluids.

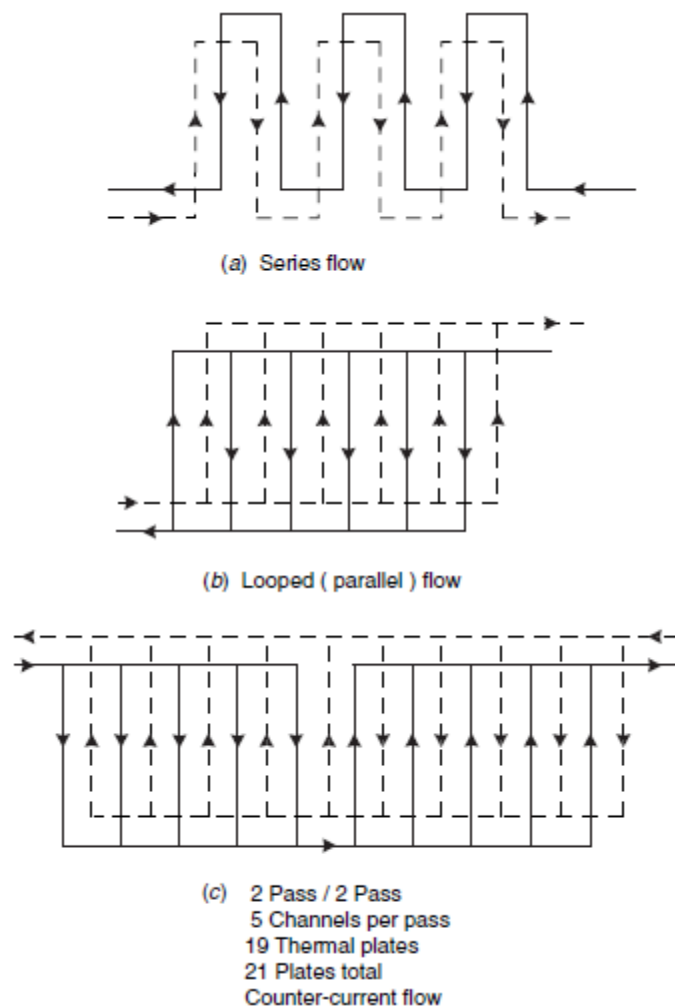


Fig. 4.4. Plate heat exchanger arrangements.

4.4. Single-phase heat transfer and pressure drop

There are over thirty correlations in literature [4] that could be considered. The base formulation is:

$$Nu = \frac{\alpha d_h}{\lambda} = C Re^n Pr^m \left(\frac{\mu}{\mu_p} \right)^x \quad \text{turbulent flows} \quad (4.8)$$

$$Nu = \frac{\alpha d_h}{\lambda} = C \left(Re Pr \frac{d_h}{L} \right)^n \left(\frac{\mu}{\mu_p} \right)^x \quad \text{laminar flows} \quad (4.9)$$

Where

$$Re = \frac{d_h G}{\mu} \quad (4.10)$$

$$Pr = \frac{c_p \mu}{\lambda} \quad (4.11)$$

$$G = \frac{\dot{m}}{b L_w N_{chxPass}} \quad (4.12)$$

$\alpha, \rho, c_p, \mu, \lambda$ are respectively heat transfer coefficient, density, heat capacity, viscosity and thermal conductivity. $N_{chxPass}$ is the number of channel per pass. The values of constant C and exponents m, n, x are obtained for different plate configurations and fluid flows. Generally the values of these parameters are:

$$\begin{aligned} C &= 0.15 - 0.4 \\ n &= 0.65 - 0.85 \\ m &= 0.3 - 0.45 \\ x &= 0.05 - 0.2 \end{aligned}$$

Following, it is reported Martin's equation for the calculation of heat transfer coefficient of liquids that flow on herringbone plates. The correlation is valid for turbulent and laminar flow and takes into consideration chevron angle β :

$$Nu = \frac{\alpha d_h}{\lambda} = 0.205 Pr^{1/3} \left(\frac{\mu}{\mu_p} \right)^{1/6} (f Re^2 \sin 2\beta)^{0.374} \quad (4.13)$$

$$\frac{1}{\sqrt{f}} = \frac{\cos \beta}{(0.045 \tan \beta + 0.09 \sin \beta + f_0 / \cos \beta)^{0.5}} + \frac{1 - \cos \beta}{\sqrt{3.8 f_1}} \quad (4.14)$$

If $Re < 2000$

$$f_0 = \frac{16}{Re} \quad (4.15)$$

$$f_1 = \frac{149.25}{Re} + 0.9625 \quad (4.16)$$

If $Re > 2000$

$$f_0 = (1.56 \ln Re - 3)^{-2} \quad (4.17)$$

$$f_1 = \frac{9.75}{Re^{0.289}} \quad (4.18)$$

The influence of β on heat transfer coefficient and pressure drop is evident. With a fixed specific mass flow rate, the higher β , the higher the heat transfer coefficient since more turbulence is created. On the other hand, the higher β , the higher the pressure drop.

4.5. Two-phase heat transfer

For two-phase applications, such as evaporators and condenser, the correlations available are less and the studies in this field are growing. Contrary to single-phase heat transfer, two-phase flow is strictly correlated with a lot of parameters such as quality, heat flux, surface characteristic, film thickness and mass flow rate.

Recently, Yan and Lin [5] carried out experimental study on compact brazed heat exchangers with R-134a as a refrigerant. Their survey revealed interesting characteristics about flow evaporation in plate heat exchanger. They observed higher heat transfer coefficient as compared to circular tubes, especially at high vapor quality convective regimes. Furthermore, they noted a weak effect of heat flux on the overall heat transfer whereas mass flux played a key role.

Further experimental studies have been conducted by Hsieh-Lin[6] and Han-Lee-Kim[7]. They carried out several experimental investigations and they observed that both, evaporation heat transfer coefficient and pressure drop increase with increasing mass flux and vapor quality and with decreasing evaporation temperature and chevron angle.

They suggested empirical correlations of Nusselt number and friction factor including geometric factors for the tested brazed plate heat exchangers. The correlations are shown below:

$$Nu = G_1 Re_{eq}^{G_2} Bo_{eq}^{0.3} Pr^{0.4} \quad (4.19)$$

$$f = G_3 Re_{eq}^{G_4} \quad (4.20)$$

$$G_1 = 2.81 \left(\frac{p_{co}}{D_h} \right)^{-0.041} \left(\frac{\pi}{2} - \beta \right)^{-2.83} \quad (4.21)$$

$$G_2 = 0.746 \left(\frac{p_c}{D_h} \right)^{-0.082} \left(\frac{\pi}{2} - \beta \right)^{-0.61} \quad (4.22)$$

$$G_3 = 64710 \left(\frac{p_c}{D_h} \right)^{-5.27} \left(\frac{\pi}{2} - \beta \right)^{-3.03} \quad (4.23)$$

$$G_4 = -1.314 \left(\frac{p_c}{D_h} \right)^{-0.62} \left(\frac{\pi}{2} - \beta \right)^{-0.47} \quad (4.24)$$

$$Re_{eq} = \frac{G_{eq} D_h}{\mu_f} \quad (4.25)$$

$$Bo_{eq} = \frac{q''}{G_{eq} i_{fg}} \quad (4.26)$$

$$G_{eq} = G_c \left[1 - x + x \left(\frac{\rho_f}{\rho_g} \right)^{0.5} \right] \quad (4.27)$$

$$G_c = \frac{\dot{m}}{N_{chxPass} b L_w} \quad (4.28)$$

One can observe that G_1, G_2, G_3, G_4 are non-dimensional geometric parameters that involve corrugation pitch (p_c), hydraulic diameter (D_h) and chevron angle (β). Re_{eq} and Bo_{eq} are respectively an equivalent Reynolds number and an equivalent boiling number. The deviation between correlations and experimental data are within $\pm 20\%$ for Nusselt number and $\pm 15\%$ for friction factor.

4.6. Pressure drop for single phase flow

The pressure drop of each fluid is given by the sum:

$$\Delta P = \Delta P_{in-out} + \Delta P_{channels} + \Delta P_m + \Delta P_g \quad (4.29)$$

Where:

- $\Delta P_{in-out} = 1.5N_{pass}\rho_{in}u_{in}^2/2$ is the pressure drop at the inlet and outlet channels. It is caused by the contraction and expansion losses through the ports. N_{pass} is the number of passages of each fluid through the heat exchanger.
- $\Delta P_{channels}$ is the pressure drop due to the friction loss of the stream along one channel. It can be estimated with the following expression:

$$\Delta P_{channels} = \frac{4fL_vN_{pass}G^2}{2D_h\rho} = 2fL_vN_{pass}\rho\frac{u^2}{D_h} \quad (4.30)$$

- $\Delta P_m = G^2\left(\frac{1}{\rho_{out}} - \frac{1}{\rho_{in}}\right)$ is the contribute due to the variation of the momentum of the fluid.
- $\Delta P_g = \rho g L_v \sin \beta$ is the contribute due to the variation of altitude.

4.7. Pressure drop for two - phase flow

The homogeneous flow model provides the simplest technique for analyzing two phase flow. In the homogeneous model, both liquid and vapor phases move at the same velocity:

$$u_l = u_g \quad (4.31)$$

The homogeneous model considers the two-phase flow as a single-phase flow having average fluid properties, which depend upon mixture quality. The void fraction ε based on the homogeneous model can be expressed as follows:

$$u_g = \frac{G \cdot x}{\varepsilon \rho_g} = u_l = \frac{G \cdot (1-x)}{(1-\varepsilon)\rho_l} \quad (4.32)$$

$$\varepsilon = \frac{\rho_g}{\frac{x}{\rho_g} + \frac{1-x}{\rho_l}} = \frac{1}{1 + \frac{(1-x)\rho_g}{x\rho_l}} \quad (4.33)$$

The void fraction ε is defined as the ratio between the volume occupied by the vapor and the total volume. The quality x is the ratio between mass of vapor and liquid. Density and specific volume can be expressed as follows:

$$\rho_m = \varepsilon \rho_g + (1-\varepsilon)\rho_l = \left[\frac{x}{\rho_g} + \frac{1-x}{\rho_l} \right]^{-1} \quad (4.34)$$

$$v_m = xv_g + (1-x)v_l \quad (4.35)$$

In the homogeneous flow model two phase stream is considered as single phase stream having mean velocity $u = u_l = u_g$ and mean density ρ_m .

For a straight channel of flow area A , wetted perimeter P , hydraulic diameter $D_h = 4P/A$, inclination angle θ , and length L , connected to inlet and outlet, the total pressure can be obtained from the steady-state momentum equation:

$$\Delta P = \Delta P_{in-out} + \Delta P_{channels} + \Delta P_m + \Delta P_g \quad (4.36)$$

Where

$$\Delta P_m = G^2 \left(\frac{1}{\rho_l} - \frac{1}{\rho_v} \right) \quad (4.37)$$

$$\Delta P_{channels} = \int_0^L f \frac{1}{D_h} \frac{G^2}{2\rho_m} dz \quad (4.38)$$

$$\Delta P_g = \int_0^L g \rho_m \sin \theta dz \quad (4.39)$$

Note that the above equations are formally identical to the single-phase case with the mixture density, ρ_m used instead of the single-phase density. The friction factor can be evaluated with the Kim's correlation reported in paragraph 4.5.

5

Shell and Tube Heat Exchangers

5.1. Shell and tube heat exchangers

Shell and tube heat exchangers are probably the most widespread and commonly used basic heat exchanger configuration in the process industries. This statement is based on several reasons. The shell and tube heat exchanger provides a comparatively large ratio of heat transfer area to volume and weight. It provides this surface in a form which is relatively easy to construct in a wide range of size and which is mechanically rugged enough to withstand stresses during fabrication and normal operating conditions. Furthermore, there are many modifications of the basis configuration, which can be used to solve special problems. The shell and tube heat exchanger can be easily cleaned, and those components most subject to failure, such as gaskets and tubes, can be easily replaced.

Although several modification of the basis configuration can be perform, typical shell and tube heat exchanger is composed by a bundle of tubes encased in a shell. The tubes provide the heat transfer surface between one fluid flowing inside the tube and the other fluid flowing inside across the outside of the tubes. The tubes may be bare or with extended or enhanced surfaces on the outside. Extended surfaces are used when one fluid has substantially lower heat transfer coefficient than the other fluid.

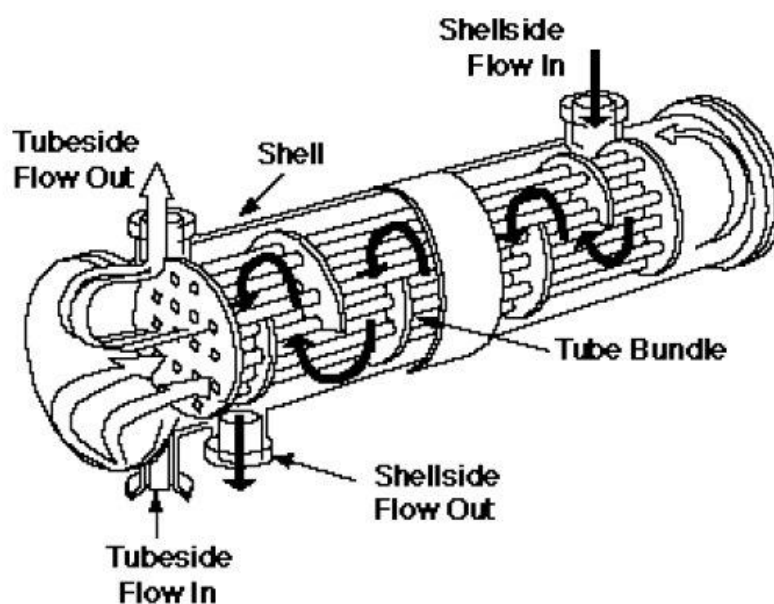


Figure 5.1. Shell and tube heat exchanger

Whereas one fluid flows inside the tubes, the other one flows inside the shell and it is driven by the baffles that increase the velocity and the heat transfer coefficient. Furthermore, baffles support the tubes in the proper position during assembly and operation and prevent vibration of the tubes caused by flow induced eddies. The most common baffle shape is the single segmental with a baffle cut of 20 to 45 percent of the diameter. Other typical baffle segmental are shown in literature [8,9].

The baffle spacing should be correspondingly chosen to make the free flow areas through the “window” (the area between the baffle edge and shell) and cross the tube bank roughly equal.

5.2. Allocation of streams in a shell and tube Exchanger

In principle, either stream entering a shell and tube exchanger may be put on either side tube or shell side. However there are some considerations which can lead to a choice that could be the most economical:

5.2.1. High pressure

The higher pressure stream should be allocated to the tube side. In fact, high pressure tube are cheaper than high pressure shell.

5.2.2. Corrosion

Corrosion generally dictates the choice of material of construction, rather than exchanger design. The corrosive fluid will ordinarily be placed in the tubes so that at least the shell need not be made of corrosion-resistant material.

5.2.3. Fouling

Fouling enters into the design of almost every process exchanger to a measurable extent, but certain streams foul so badly that the entire design is dominated by features which seek:

- To minimize fouling (high velocity, avoided of dead or eddy flow regions)
- To facilitate cleaning (fouling fluid on tube-side, wide pitch and rotate square layout)
- To extend operational life by multiple units.

5.2.4. Low heat transfer coefficient

If one stream has an inherently low heat transfer coefficient (such as low pressure gasses or viscous liquids), this stream is preferentially put on the shell-side so that extended surface may be used to reduce the total cost of the heat exchanger.

5.2.5. Maximum allowable pressure drop

The choice of tube side or shell side stream is influenced by the maximum allowable pressure drop. If the fluid that has the greater influence on the heat transfer has also a low pressure drop, that stream is put on tube side.

5.3. Geometrical characteristics

5.3.1. Tube diameter

Tubes have inside diameter d_i , outside diameter d_o , length L and total number of tubes N_t . Total heat transfer area is:

$$A_i = L\pi d_i N_t \quad (5.1)$$

Similarly, the total heat transfer area outside tube is:

$$A_o = L\pi d_o N_t \quad (5.2)$$

Tubes dimensions are reported in *Table 5.1* whereas in *Table 5.2* are reported the thermal conductivity of the most common materials used.

Table 5.1. Tube dimensions. Taken from Heat Exchanger Design Handbook, T. Kuppan

Outside diameter [in]	Outside diameter [mm]	Wall thickness[mm]
0.25	6.35	0.559 – 0.711
0.375	9.525	0.711 – 0.889 – 1.245
0.5	12.7	0.889 – 1.245
0.625	15.875	0.889 – 1.245 – 1.651
0.75	19.05	0.889 – 1.245 – 1.651 – 2.108 – 2.769
0.875	22.225	0.889 – 1.245 – 1.651 – 2.108
1.0	25.4	1.245 – 1.651 – 2.108 – 2.769
1.25	31.75	1.651 – 2.108 – 2.769 – 3.404
2.0	50.08	2.108 – 2.769

Table 5.2. Thermal conductivity of the most common material used for tubes and shell.

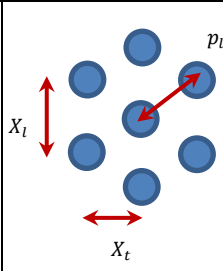
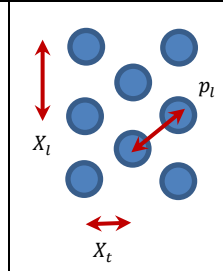
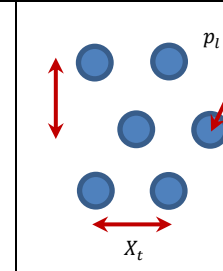
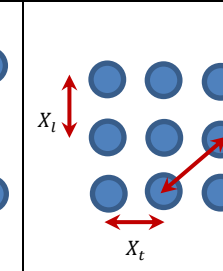
Material	Cu	Al	Cu-Ni 90-10	Cu-Ni 70-30	Carbon steel	stainless steel	Titanium
$\lambda \left[\frac{W}{mK} \right]$	310	180	65	40	38	18	18

5.3.2. Tube layout

Tubes of the bundle are arranged with four different layouts. 30° Triangular staggered array is the most compact and it provides the highest heat transfer area and coefficient as well as the highest pressure drop. 45° Triangular staggered array has lower heat transfer coefficient than the previous but it has also lower pressure drop. 90° Triangular staggered array should be avoided with laminar flow whereas with turbulent

flow provides the lowest pressure drop. In the table below are defined the various arrangements, the longitudinal and transverse pitch.

Table 5.3. Tubes arrangements.

	30° Triangular staggered array	45° Rotated square Triangular staggered array	60° Rotated Triangular staggered array	90° Square Inline array
Layout				
Transverse tube pitch X_t	p_t	$\sqrt{3}p_t$	p_t	$\sqrt{2}p_t$
Longitudinal tube pitch X_l	$\left(\frac{\sqrt{3}}{2}\right)p_t$	$\frac{p_t}{2}$	p_t	$\frac{p_t}{\sqrt{2}}$

5.3.3. Tube count

The total number of tubes in a shell and tube heat exchanger depends on many geometric variables:

- Tube diameter d_o
- Tube pitch p_t
- Layout
- Number of tube passes
- Type of floating head
- The thickness and position of pass dividers
- The omission of tubes due to no tubes in windows design or impingement plates.

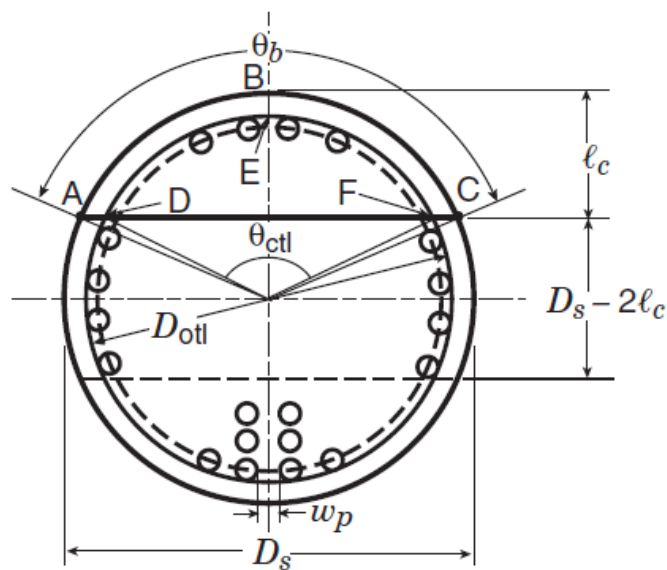


Fig.5.2. Nomenclature for basic baffle geometry relations for a single segmental exchanger. Shah and Sekulic [8]

The exactly tubes number is difficult to determine because the high number of variables involved. Although, only a direct count can define exactly the total number of tubes, some correlations are provided in order to estimate it. For a specified diameter of the circle through the centers of the outermost tubes, D_{ctl} , the effect of the tube bundle type on the total number of tubes N_t is eliminated. Taborek (1988) suggests an approximate expression for the tube count based on D_{ctl} :

$$N_t = \begin{cases} \frac{(\pi/4)D_{ctl}^2}{C_t p_t^2} (1 - \psi_c) & \text{single tube pass} \\ \frac{(\pi/4)D_{ctl}^2}{C_t p_t^2} (1 - \psi_n) & \text{multiple tube pass} \end{cases} \quad (5.3)$$

Where

$$\psi_c = \begin{cases} 0 & \text{no impingement plate} \\ \frac{\theta_{ctl}}{2\pi} - \frac{\sin \theta_{ctl}}{2\pi} & \text{impingement plate on a side} \\ 2 \left(\frac{\theta_{ctl}}{2\pi} - \frac{\sin \theta_{ctl}}{2\pi} \right) & \text{tube field removed on both side} \end{cases} \quad (5.4)$$

And

$$C_t = \begin{cases} 0.866 & \text{layout } 30^\circ \text{ and } 60^\circ \\ 1 & \text{layout } 45^\circ \text{ and } 90^\circ \end{cases} \quad (5.5)$$

The angle θ_{ctl} is in radians and it is given in the following section whereas the value of ψ_n is obtained from figure 5.4.

It is important to remember that the accuracy of these expressions is approximately 5-10% thus they can be used only in the first stage of designing.

5.1.1. Window and crossflow section geometry

In order to apply the Bell-Delaware method, it is necessary to define some geometrical characteristics of the single segmental E shell and tube heat exchanger. *Figure 5.4* show the three sections in which can be divided shell and tube heat exchanger: internal crossflow, window, entrance and exit sections.

As shown in *Fig. 5.4*, the window area is obtained by the expression:

$$A_{fr,w} = \frac{\pi}{4} D_s^2 \left(\frac{\theta_b}{2\pi} - \frac{\sin \theta_b}{2\pi} \right) = \frac{D_s^2}{4} \left[\frac{\theta_b}{2} - \left(1 - \frac{2l_c}{D_s} \right) \sin \theta_b \right] \quad (5.6)$$

Where θ_b is the angle in radians between two radii intersected at the inside shell wall with the baffle cut and is given by:

$$\theta_b = 2 \cos^{-1} \left(1 - \frac{2l_c}{D_s} \right) \quad (5.7)$$

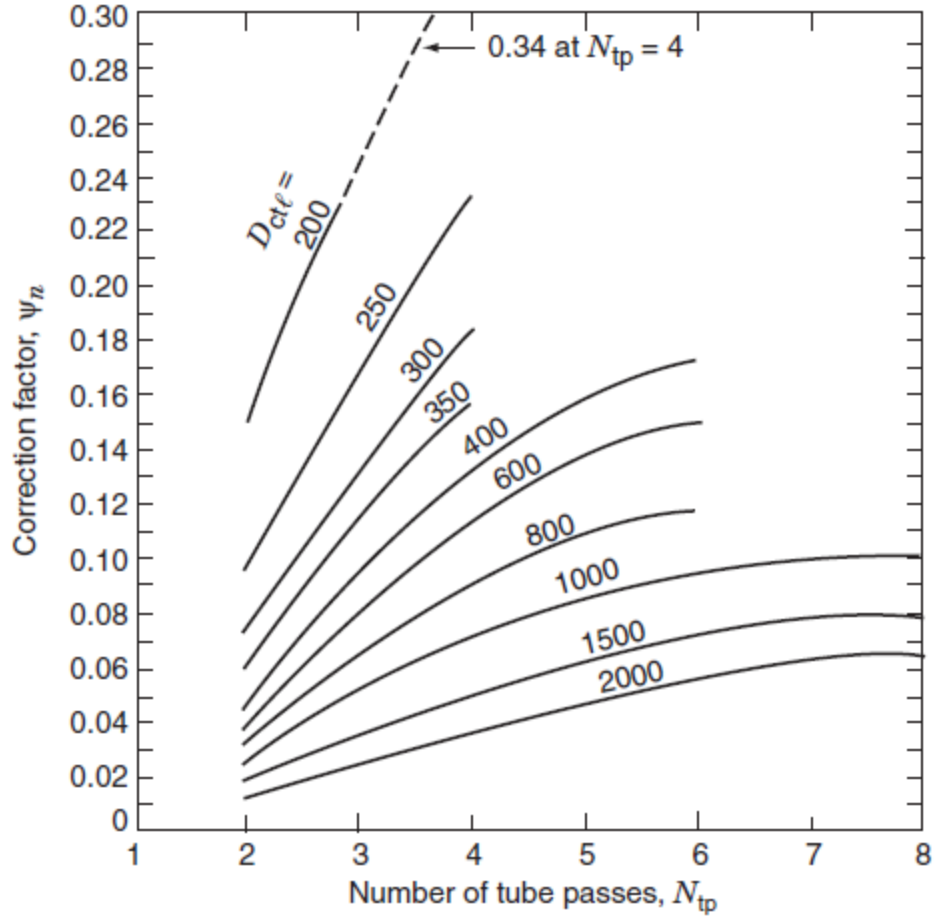


Figure 5.3. Correction factor for tube count with multi-pass. Shah and Sekulic [8].

Sometimes could be necessary to calculate the fraction F_w of the number of tubes in one window section encircled by the centerline of the outer tube row:

$$F_w = \frac{\theta_{ctl}}{2\pi} - \frac{\sin \theta_{ctl}}{2\pi} \quad (5.8)$$

Where the angle θ_{ctl} is expressed in radians and it represents the angle between the baffle cut and two radii of a circle through the centers of the outermost tubes as follows:

$$\theta_{ctl} = 2 \cos^{-1} \left(\frac{D_s - 2l_c}{D_{ctl}} \right) \quad (5.9)$$

Where $D_{ctl} = D_{otl} - d_o$. The number of tubes in the window section is computed as follows:

$$N_{t,w} = F_w N_t \quad (5.10)$$

And the area occupied by the tubes in the window section becomes:

$$A_{fr,t} = \frac{\pi}{4} d_o^2 N_{t,w} = \frac{\pi}{4} d_o^2 F_w N_t \quad (5.11)$$

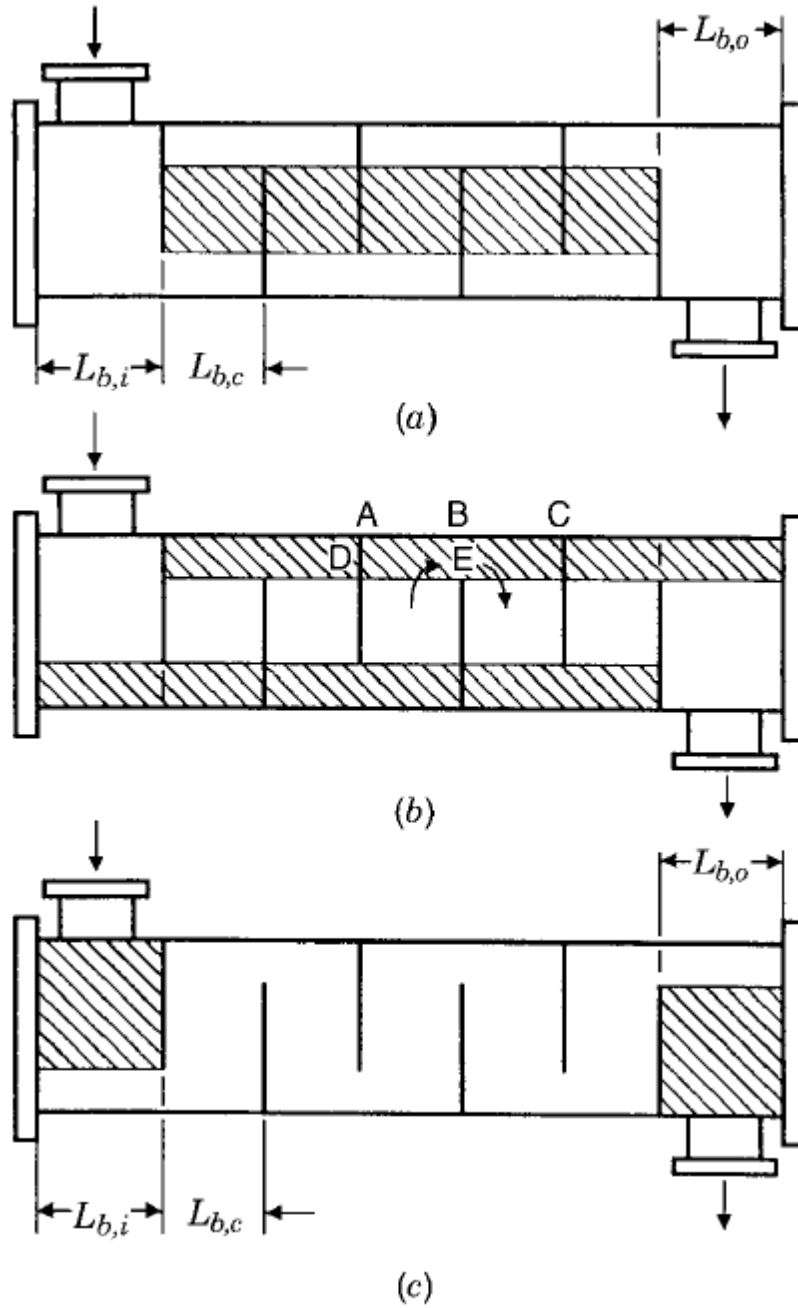


Figure 5.4. (a) internal cross flow section, (b) window section, (c) entrance and exit section. Shah and Sekulic [8].

The net flow area in one window is then:

$$A_{o,w} = A_{fr,w} - A_{fr,t} \quad (5.12)$$

By application of the conventional definition, the hydraulic diameter of the window section of a segmental baffle can be expressed as the ratio between four times the area and the wetted perimeter:

$$D_{h,w} = \frac{4A_{o,w}}{P} = \frac{4A_{o,w}}{\pi d_o N_{t,w} + \pi D_s (\theta_b / 2\pi)} \quad (5.13)$$

The final geometrical input required for the window section is the effective number of tube rows in crossflow needed for the heat transfer and pressure drop correlations:

$$N_{r,cw} = \frac{0.8}{X_l} \left[l_c - \frac{1}{2} (D_s - D_{ctl}) \right] \quad (5.14)$$

As far as the cross flow section, the first parameter to take into account is the fraction F_c of the total number of tubes in the cross-flow section:

$$F_c = 1 - 2F_w = 1 - \left(\frac{\theta_{ctl}}{\pi} - \frac{\sin \theta_{ctl}}{\pi} \right) \quad (5.15)$$

The number of tubes rows $N_{r,cc}$ crossed during flow through one crossflow section between baffle tips may be estimated in the following way:

$$N_{r,cc} = \frac{D_s - 2l_c}{X_l} \quad (5.16)$$

The previous is only an approximation and a better value can be obtained from drawing and direct count.

Another important parameter is the crossflow area at or near the shell centerline for one crossflow section. It may be estimated by:

$$A_{o,cr} = \left[D_s - D_{otl} + \frac{D_{ctl}}{X_t} (X_t - d_o) \right] L_{b,c} \quad (5.17)$$

The previous expression is valid for 30° and 90° tube layout bundles. This equation is also valid for a 45° tube bundle layout having $p_t/d_o \geq 1.707$ and for a 60° tube bundle having $p_t/d_o \geq 3.732$. For 45° and 60° tube bundle having p_t/d_o lower than those indicated in the preceding lines, the expression becomes:

$$A_{o,cr} = \left[D_s - D_{otl} + 2 \frac{D_{ctl}}{X_t} (p_t - d_o) \right] L_{b,c} \quad (5.18)$$

Finally, the number of baffles N_b is calculated on the basis of the geometrical parameters: $L_{b,c}$, $L_{b,o}$, $L_{b,i}$ and L . They are respectively the central baffle spacing, the inlet and outlet baffle spacing and the total length.

$$N_b = \frac{L - L_{b,o} - L_{b,i}}{L_{b,c}} + 1 \quad (5.19)$$

5.1.2. Bypass and leakage flow areas

In order to compute correctly the heat transfer and the pressure drop with the Bell-Delaware method it is necessary to consider the bypass and leakage flow areas. The flow bypass area of one baffle $A_{o,bp}$ is:

$$A_{o,bp} = (D_s - D_{otl} + 0.5N_p w_p) L_{b,c} \quad (5.20)$$

where N_p is the number of pass divider lanes through the tube field that are parallel to the crossflow stream(B) and w_p is the width of the pass divider pass lane.

The tube to baffle leakage area for one baffle is:

$$A_{o,tb} = \frac{\pi}{4} [(d_o + \delta_{tb})^2 - d_o^2] N_t (1 - F_w) \approx \frac{\pi d_o \delta_{tb} N_t (1 - F_w)}{2} \quad (5.21)$$

The shell to baffle leakage area for one baffle is associated with the gap between the shell inside diameter and the baffle and it is estimated as:

$$A_{o,sb} = \pi D_s \frac{\delta_{sb}}{2} (1 - \theta_b/2\pi) \quad (5.22)$$

Where $\delta_{sb} = D_s - D_{baffle}$ as shown below.

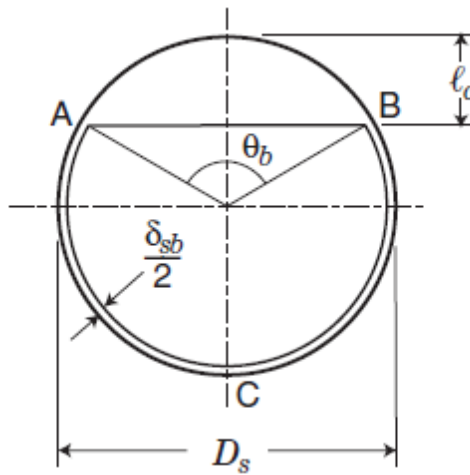


Figure 5.5. Single segmental baffle geometry showing shell-to-baffle diameter clearance δ_{sb} . Shah and Sekulic [8]

5.2. Heat transfer and pressure drop calculation

As described in chapter 3, the relations used to compute heat transfer and are:

$$\dot{Q}_h = \dot{m}_h (h_{h,in} - h_{h,o}) \quad (5.23)$$

$$\dot{Q}_c = \dot{m}_c (h_{c,o} - h_{c,in}) \quad (5.24)$$

Considering the heat capacity constant:

$$\dot{Q}_h = \dot{m}_h c_{p,h} (T_{h,in} - T_{h,o}) \quad (5.25)$$

$$\dot{Q}_c = \dot{m}_c c_{p,c} (T_{c,o} - T_{c,in}) \quad (5.26)$$

The heat transfer surface can be estimated by the following expression:

$$A = \frac{\dot{Q}}{U \Delta T_{lm} F_t} \quad (5.27)$$

Where U is the overall heat transfer coefficient and ΔT_{lm} is the logarithmic mean temperature difference and is the correction factor:

$$\Delta T_{lm} = \frac{(T_{h,in} - T_{c,o}) - (T_{h,o} - T_{c,in})}{\ln\left(\frac{T_{h,in} - T_{c,o}}{T_{h,o} - T_{c,in}}\right)} \quad (5.28)$$

According to A. Fakhri [46], F_t is calculated as follows:

$$P = \frac{T_{c,out} - T_{c,in}}{T_{h,in} - T_{c,in}} \quad (5.29)$$

$$R = \frac{T_{h,in} - T_{h,out}}{T_{c,out} - T_{c,in}} \quad (5.30)$$

$$W = \left(\frac{1 - PR}{1 - P}\right)^{1/N_{ShellPass}} \quad (5.31)$$

$$S = \frac{\sqrt{R^2 + 1}}{R - 1} \quad (5.32)$$

$$F_t = \frac{S \ln W}{\ln\left(\frac{1 + W - S + SW}{1 + W + S - SW}\right)} \quad (5.33)$$

$$U = \left[\frac{1}{\alpha_s} + R_s + \frac{d_o \ln(d_o/d_i)}{2k_w} + R_s \frac{d_o}{d_i} + \frac{1}{\alpha_t} \frac{d_o}{d_i} \right]^{-1} \quad (5.34)$$

Where α_s and α_t are respectively the heat transfer coefficient on the shell side and tube side, R_s and R_t are fouling resistance and k_w is the thermal conductivity of the tube material. The correction factor F takes into consideration the reduction of the effective temperature difference due to the different arrangement (counter-flow/parallel-flow) of the tube when the number of passes is greater than one.

5.2.1. Heat transfer on shell side

Heat transfer analysis is the most important part of the design of an heat exchanger. The method that is applied for the calculation of the heat transfer coefficient is the Bell-Delaware method. It takes into account the effect of various leakage streams and bypass streams in addition to the main crossflow stream to the bundle.

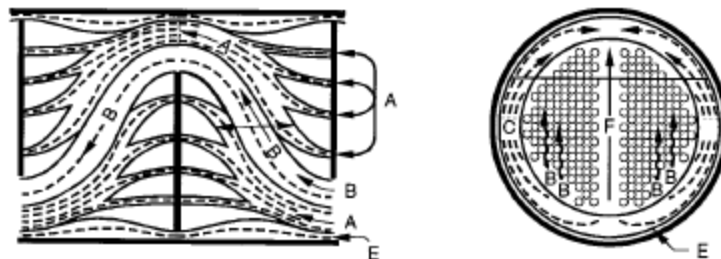


Figure 5.6. Leakage streams (A and E), bypass streams (C), crossflow stream (B). Shah and Sekulic [8]

In this method an ideal heat transfer coefficient α_{id} is calculated and is subsequently corrected by five correction factor that take into consideration the shell geometry and the effect of the above mentioned streams:

$$\alpha_s = \alpha_{id} J_c J_b J_s J_r \quad (5.35)$$

There are several correlations used to compute α_{id} . One of these is:

$$\alpha_{id} = \frac{Nu_s k}{d_o} \left(\frac{\mu_w}{\mu_m} \right)^{-0.14} \quad (5.36)$$

$$Nu_s = 1.04 Re_s^{0.4} Pr_s^{0.36} \left(\frac{Pr_s}{Pr_w} \right)^{-0.14} \quad (5.37)$$

Shell-side mass velocity G_s and shell-side Reynolds number are calculated with the relations:

$$G_s = \frac{\dot{m}}{A_{o,cr}} \quad (5.38)$$

$$Re_s = \frac{G_s d_o}{\mu_s} \quad (5.39)$$

Another correlation for evaluating α_{id} is the following:

$$\alpha_{id} = j \frac{C_{ps} Pr^{-2/3}}{A_{o,cr}} \quad (5.40)$$

Where j is the Colburn factor expressed in ref. [8].

The first correction factor in the calculation of the heat transfer coefficient on the shell-side, J_c , takes into account the baffle configuration:

$$J_c = 0.55 + 0.72 F_c \quad (5.41)$$

The value of F_c represents the total number of tubes in the cross-flow section and it is calculated with *Equation 10.15*.

The second factor in *Equation 10.30* considers both tube-to-baffle and tube-to-shell leakages and it is calculated by:

$$J_l = 0.44(1 - r_s) + [1 - 0.44(1 - r_s)] e^{-2.2/r_{lm}} \quad (5.42)$$

Where

$$r_s = \frac{A_{o,sb}}{A_{o,sb} + A_{o,tb}} \quad (5.43)$$

$$r_{lm} = \frac{A_{o,sb} + A_{o,tb}}{A_{o,cr}} \quad (5.44)$$

The expression of $A_{o,sb}$, $A_{o,tb}$ and $A_{o,cr}$ are given by Equations (10.22), (10.21) and (10.18) respectively.

J_b is the correction factor that takes into account bundle and pass partition bypass stream:

$$J_b = \begin{cases} 1 & \text{for } N_{ss}^+ \geq 1/2 \\ e^{-Cr_b [1 - (2N_{ss}^+)^{1/3}]} & \text{for } N_{ss}^+ \leq 1/2 \end{cases} \quad (5.45)$$

Where

$$r_b = \frac{A_{o,bp}}{A_{o,cr}} \quad N_{ss}^+ = \frac{N_{ss}}{N_{r,cc}} \quad (5.46)$$

$$C = \begin{cases} 1.35 & \text{for } Re_s \leq 100 \\ 1.25 & \text{for } Re_s > 100 \end{cases} \quad (5.47)$$

N_{ss} represents the number of sealing strip pairs whereas $N_{r,cc}$ is the number of tube rows crossed during flow through one cross flow section baffle tips.

The fourth correction factor J_s considers the variation of the baffle spacing at inlet and outlet. Usually, the baffles in the central sections of the heat exchanger are closer together than those at the inlet and outlet. The following expression estimates this influence:

$$J_s = \frac{N_b - 1 + (L_i^+)^{1-n} + (L_o^+)^{1-n}}{N_b - 1 + L_i^+ + L_o^+} \quad (5.48)$$

Considering:

$$n = \begin{cases} 0.6 & \text{for turbulent flow} \\ 1/3 & \text{for laminar flow} \end{cases} \quad (5.49)$$

$$L_i^+ = \frac{L_{b,i}}{L_{bc}} \quad L_o^+ = \frac{L_{b,o}}{L_{bc}} \quad (5.50)$$

Finally J_r is a correction factor for any adverse temperature gradient buildup in laminar flows:

$$J_r = \begin{cases} 1 & Re_s \geq 100 \\ (10/N_{r,c})^{0.18} & Re_s \leq 20 \end{cases} \quad (5.51)$$

Where

$$N_{r,c} = N_{r,cc} + N_{r,cw} \quad (5.52)$$

For $20 < Re_s < 100$ one can linearly interpolate J_r from the two formulas presented.

5.2.2. Pressure drop on shell side

Similar to the shell-side heat transfer calculation, the shell-side pressure drop is estimated using the Bell-Delaware method. The expression to calculate the pressure drop considers an ideal term and some correction factors:

$$\Delta p_s = [(N_b - 1)\Delta p_{b,id}\zeta_b + N_b\Delta p_{w,id}]\zeta_l + 2\Delta p_{b,id} \left(1 + \frac{N_{r,cw}}{N_{r,cc}}\right) \zeta_b \zeta_s \quad (5.53)$$

Where $\Delta p_{b,id}$ is the ideal pressure drop in the central section and is given by

$$\Delta p_{b,id} = \frac{4f_{id}G_s^2 N_{r,cc}}{2\rho_s} \left(\frac{\mu_{sw}}{\mu_s}\right)^{0.25} \quad (5.54)$$

With the ideal friction factor

$$f_{id} = 3.5 \left(1.33 \frac{d_o}{p_t} \right)^b Re_s^{-0.476} \quad (5.55)$$

$$b = \frac{6.59}{1 + 0.14 Re_c^{0.52}} \quad (5.56)$$

The pressure drop associated with an ideal one-window section $\Delta p_{w,id}$ may be estimated with the correlation

$$\Delta p_{w,id} = \frac{\dot{m}_s^2 (2 + 0.6 N_{r,cw})}{2 \rho_s A_{0,cr} A_{o,w}} \quad (5.57)$$

Where, as described in the previous paragraphs, $A_{o,w}$ is net flow area in one window section and $N_{r,cw}$ is the number of effective tube rows crossed during flow through one window zone. The correction factors $\zeta_b, \zeta_l, \zeta_s$ have the same role of J_b, J_l, J_s and are estimated with the following expressions:

$$\zeta_b = \begin{cases} 1 & \text{for } N_{ss}^+ < 1/2 \\ e^{-3.7 r_b [1 - (2 N_{ss}^+)^{1/3}]} & \text{for } N_{ss}^+ \geq 1/2 \end{cases} \quad (5.58)$$

$$\zeta_l = e^{-1.33(1+r_s)r_{lm}^p} \quad (5.59)$$

$$\zeta_s = \left(\frac{L_{b,c}}{L_{b,o}} \right)^{1.8} + \left(\frac{L_{b,c}}{L_{b,i}} \right)^{1.8} \quad (5.60)$$

The value of p is obtained with the formula:

$$p = -[0.15(1 + r_s) + 0.8] \quad (5.61)$$

One can note the opposite behavior of $\zeta_b, \zeta_l, \zeta_s$ and J_b, J_l, J_s . In fact, in order to reduce the total pressure drop should be necessary to have the lowest possible values of $\zeta_b, \zeta_l, \zeta_s$. On the other hand J_b, J_l, J_s have to be as high as possible. The optimal geometry will be the result of a trade-off between the heat transfer and the pressure drop features and a multi-objective optimization can treat this problem.

5.2.3. Heat transfer on tube side

The tube side heat transfer coefficient is straightforward determined with the following correlation [8]:

$$\alpha_t = \frac{Nu_t k_t}{d_i} \quad (10.62)$$

$$Nu_t = 0.023 Pr_t^{1/3} Re_t^{0.8} \left(\frac{\mu_t}{\mu_{tw}} \right)^{0.14} \quad (10.63)$$

Where the Reynolds number and the mass velocity G_t are

$$Re_t = \frac{G_t d_i}{\mu_t} \quad (5.64)$$

$$G_t = \frac{\dot{m}_t}{A_{o,t}} \quad (5.65)$$

Tube-side flow area per pass $A_{o,t}$ and the number of tube per pass are defined as

$$A_{o,t} = \frac{\pi}{4} d_i^2 N_{t,p} \quad (5.66)$$

$$N_{t,p} = \frac{N_t}{N_{pass}} \quad (5.67)$$

5.2.4. Pressure drop on tube side

The tube-side pressure drop is simply:

$$f = 0.046 Re_t^{-0.2} \quad (5.68)$$

$$\Delta p_t = \frac{G_t^2}{2g_c \rho_t} \left[\frac{4fL}{d_i} + (1 - \sigma^2 + K_c) - (1 - \sigma^2 + K_e) \right] N_{pass} \quad (5.69)$$

Where

$$K_c = 0.3 \quad K_e = 0.4 \quad (5.70)$$

$$\sigma = \frac{2(p_t - d_i)}{\sqrt{2} p_t} \quad (5.71)$$

Detailed expressions are described in ref. [8].

6

Entropy Generation Minimization

6.1. Entropy Generation Minimization

Energy generation minimization is a new methodology of thermodynamic optimization based on exergy analysis. Inspired by the minimum production principle advanced by Prigogine [11], Bejan [12,13] developed the entropy generation minimization (EGM) approach to the thermal system optimization. This new approach is based on the simultaneous application of the first law and the second law in analysis and design.

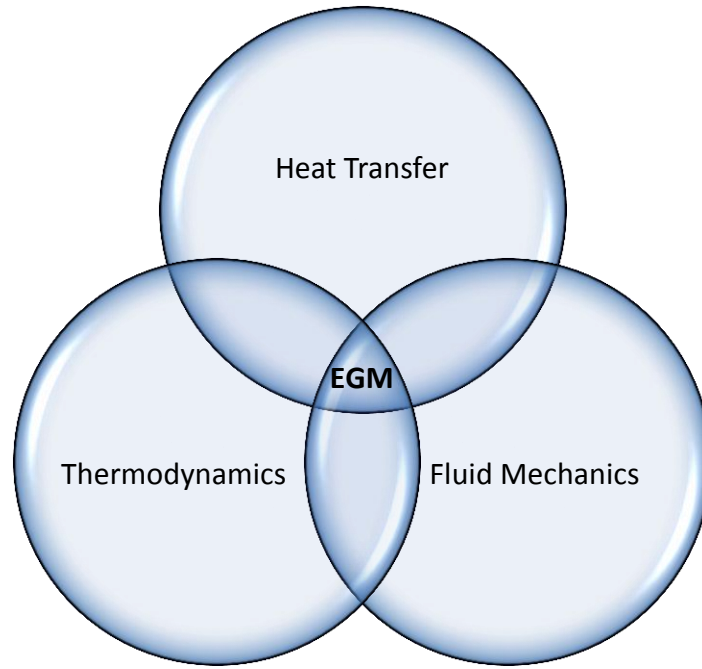
6.2. Energy and Exergy

Energy is conserved in every device or process and it cannot be destroyed. The first law of thermodynamic states that energy flows into and out of a system along paths of mass flow, heat transfer and work but is conserved. Unlike energy, exergy is not conserved and it represents quantitatively the 'useful energy' or, in other words, the ability to do or receive work. One can define exergy as the maximum theoretical work obtainable when a system is in equilibrium with its reference environment.

The destroyed exergy is proportional to the generated entropy. The destruction of exergy in a system is the cause of his departure from the ideal condition. By performing exergy analysis in a system or in a subsystem, it is possible to draw a map of how the destruction of exergy is distributed over the system considered. In this way, a designer can pinpoint the sources of high exergy destruction and concentrate efforts and resources for improving efficiency.

The method of thermodynamic optimization or EGM developed by Bejan [12,13] is a field of activity that implies the simultaneous application of different theories an relations afferent to three fields:

- Fluid mechanics
- Thermodynamics
- Heat transfer



Entropy Generation Minimization can be used in the preliminary stages of design and can be coupled with global cost minimization by using the method of thermo-economics.

6.3. Entropy Generation and Exergy Destruction

The thermodynamics of a system consists of accounting for the first law and the second law (Moran and Shapiro, 1995) [14]:

$$\frac{dE}{dt} = \sum_{i=0}^n \dot{Q}_i - \dot{W} + \sum_{in} \dot{m}h - \sum_{out} \dot{m}h \quad (6.1)$$

$$\dot{S}_{gen} = \frac{dS}{dt} - \sum_{i=0}^n \frac{\dot{Q}_i}{T_i} - \sum_{in} \dot{m}s + \sum_{out} \dot{m}s \geq 0 \quad (6.2)$$

Combining these two equations we obtain:

$$\dot{W} = -\frac{d}{dt}(E - T_0S) + \sum_{i=0}^n \left(1 - \frac{T_0}{T_i}\right) \dot{Q}_i + \sum_{in} \dot{m}(h - T_0S) - \sum_{out} \dot{m}(h - T_0S) - T_0\dot{S}_{gen} \quad (6.3)$$

The power output or input in the limit of reversible operation $\dot{S}_{gen} = 0$ is

$$\dot{W}_{rev} = -\frac{d}{dt}(E - T_0S) + \sum_{i=0}^n \left(1 - \frac{T_0}{T_i}\right) \dot{Q}_i + \sum_{in} \dot{m}(h - T_0S) - \sum_{out} \dot{m}(h - T_0S) \quad (6.4)$$

In engineering thermodynamics the terms on the right side of the previous equation are exergy contributes and the calculation of \dot{W}_{rev} is known as exergy analysis. Subtracting Eq. 6.3 from Eq. 6.4, one can arrive at the Gouy-Stodola theorem:

$$\dot{W}_{rev} = \dot{W} + T_0\dot{S}_{gen} \quad (6.5)$$

If we fix the power output in the limit of reversible operation since all the heat and mass flows (other than \dot{Q}_0) are fix the lost power $\dot{W}_{rev} - \dot{W}$ is always positive. An important statement can be pointed out: to minimize lost power when \dot{W}_{rev} is fixed is the same as maximizing power output in a power plant, and minimizing power input in a refrigeration plant. Consequently, this operation is also equivalent to minimizing the total rate of entropy generation [15]. To calculate the total entropy generation rate correctly, one must recognize that the optimization process (e.g., the variability of the heat input) requires "room to move," i.e., an additional, usually overlooked, contribution to the total entropy generation rate. This additional source of entropy generation on the outside of the visible confine of the system is what gives the design room to move.

The fact that the maximization of \dot{W} and the minimization of the total \dot{S}_{gen} lead to the same optimal design allows the designer to choose the method that fits better on the application considered. In the case of power plant it is easier to explain the optimization process in terms of power output whereas in the optimization of many basic components such as heat exchangers, fins or storage systems, the preferable method is the EGM.

Concluding, the entropy generation method can be used to:

- Optimize streams and components so that they destroy least exergy subjected to constraints;
- Make sure that the optimized entities match or can be fitted together into a new integrative design of the larger system.

6.4. Heat exchanger Design by Entropy Generation Minimization

In this work, the entropy generation method is used to optimize the design of heat exchangers. A heat exchanger can be modeled as an adiabatic control volume with two streams of mass as shown in Fig.6.1.

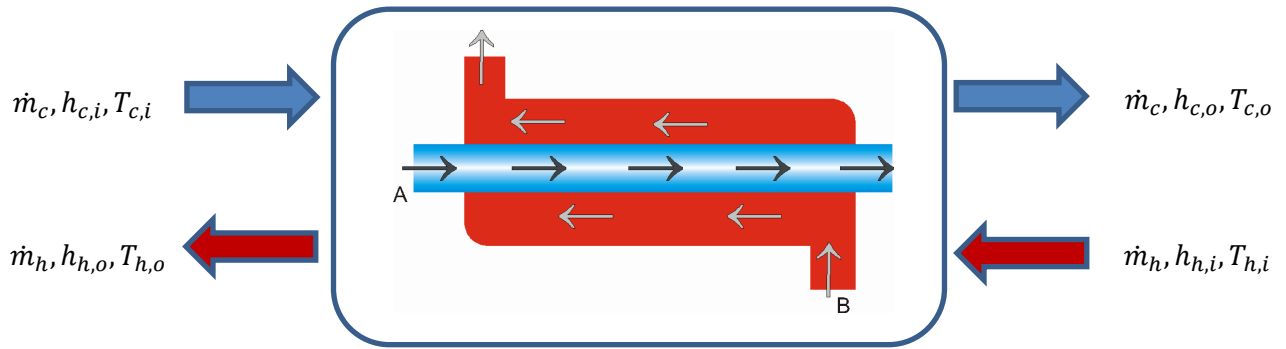


Figure 6.1. Control volume around heat exchanger

The degree of thermodynamic imperfection of the arrangements is measured by the entropy generation rate:

$$\dot{S}_{gen} = \dot{m}_h(s_{h,o} - s_{h,i}) + \dot{m}_c(s_{c,o} - s_{c,i}) \quad (6.6)$$

The previous expression can be expressed in terms of inlet and outlet temperature and pressures. In heat exchanger the heat conduction under finite temperature difference and fluid friction are two main irreversible factors to induce the entropy generation. Thus, we can split the previous expression of \dot{S}_{gen} in two terms:

$$\dot{S}_{gen} = \dot{S}_{gen,\Delta T} + \dot{S}_{gen,\Delta P} \quad (6.7)$$

Where

$$\dot{S}_{gen,\Delta T} = \int_i^o \left(\frac{\dot{m}c_p dT}{T} \right)_{h,c} = \dot{m}_h c_{p,h} \ln \frac{T_{h,o}}{T_{h,i}} + \dot{m}_c c_{p,c} \ln \frac{T_{c,o}}{T_{c,i}} \quad (6.8)$$

$$\dot{S}_{gen,\Delta P} = \frac{\Delta P_h}{\rho_h} \dot{m}_h \frac{\ln \frac{T_{h,o}}{T_{h,i}}}{T_{h,o} - T_{h,i}} + \frac{\Delta P_c}{\rho_c} \dot{m}_c \frac{\ln \frac{T_{c,o}}{T_{c,i}}}{T_{c,o} - T_{c,i}} \quad (6.9)$$

We can rewrite Eq. 6.7 in the following way:

$$\dot{S}_{gen} = \left[\dot{m}_h c_{p,h} \ln \frac{T_{h,o}}{T_{h,i}} + \frac{\Delta P_h}{\rho_h} \dot{m}_h \frac{\ln \frac{T_{h,o}}{T_{h,i}}}{T_{h,o} - T_{h,i}} \right] + \left[\dot{m}_c c_{p,c} \ln \frac{T_{c,o}}{T_{c,i}} + \frac{\Delta P_c}{\rho_c} \dot{m}_c \frac{\ln \frac{T_{c,o}}{T_{c,i}}}{T_{c,o} - T_{c,i}} \right] \quad (6.10)$$

For the case of ideal gas with constant specific heat, the entropy generation contributed by pressure drop can be written as:

$$\dot{S}_{gen,\Delta P} = \dot{m}_h R_h \ln \frac{P_{h,o}}{P_{h,i}} + \dot{m}_c R_c \ln \frac{P_{c,o}}{P_{c,i}} \quad (6.11)$$

When the heat exchanger works as evaporator the entropy generated is calculated as:

$$\dot{S}_{gen,\Delta T} = \frac{\dot{m}_c h_{fg}}{T_s} \quad (6.12)$$

Where h_{fg} is the latent heat and T_s is the saturation temperature.

Bejan [12,13] proposed to nondimensionalize the entropy generation with the following formula:

$$N_{s,\Delta T} = \frac{\dot{S}_{gen,\Delta T}}{\dot{m}c_p} \quad (6.13)$$

This expression leads to a paradox. In fact, with increasing the heat exchanger effectiveness, $N_{s,\Delta T}$ reaches a maximum but it does not correspond to the lowest value of ε . Therefore, we cannot say that the smaller the entropy generation, the better the heat exchanger performance is. To solve this phenomenon, Hesselgreaves [18] suggested another kind of nondimensionalizing method:

$$N_{s,\Delta T} = \frac{T_{c,i} \dot{S}_{gen,\Delta T}}{\dot{Q}} \quad (6.14)$$

$$N_{s,\Delta P} = \frac{T_{c,i} \dot{S}_{gen,\Delta P}}{\dot{Q}} \quad (6.15)$$

The previous expressions show that the entropy generation rate is related with the inlet and outlet conditions of the streams. The outlet conditions can be estimated using the correlations provided by thermodynamics and fluid mechanics so that the entropy generation is strictly related to the physical dimension of the system and the thermal properties of the fluids. The modified entropy generation number decreases monotonously with increasing the exchanger effectiveness as discussed by Hesselgreaves [18]. This method allow the designer to optimize the heat exchanger minimizing the entropy generation rate by varying the internal and external geometrical features of the system, subjected to constraints.

6.5. Minimization of the total entropy generation rate

The thermodynamic optimization described was concerned solely with the irreversibility of the counterflow heat exchanger. In some applications the hot stream is released to the environment so that it is necessary to take into account another source of irreversibility. This situation is sketched in *Fig.6.2* where the total entropy generation rate in the heat exchanger is:

$$\dot{S}_{gen} = \dot{m}_h(s_{h,o} - s_{h,i}) + \dot{m}_c(s_{c,o} - s_{c,i}) + \frac{\dot{Q}}{T_0} \quad (6.16)$$

The cooling rate experienced by the exhaust is:

$$\dot{Q} = \dot{m}_h c_{p,h}(T_{h,o} - T_0) \quad (6.17)$$

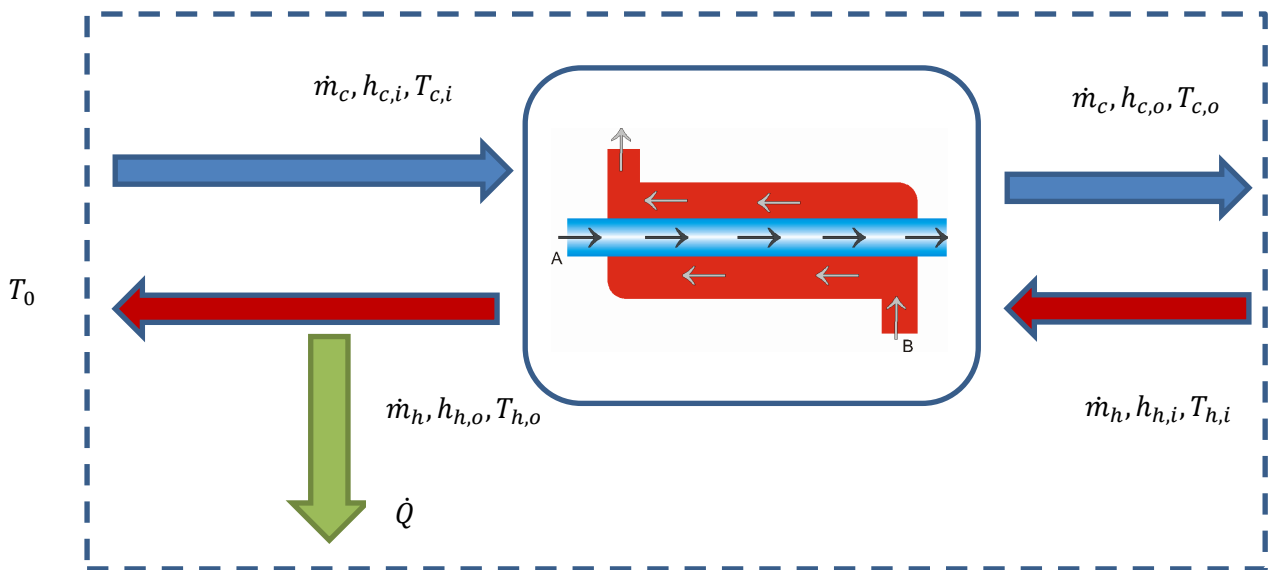


Figure 6.2. Control volume considering exergy released to the environment

7.1. Genetic algorithm

In recent years, some optimization methods that are conceptually different from the traditional mathematical programming techniques have been developed. Most of these modern methods are based on certain characteristics and behavior of biological, molecular, swarm of insects and neurobiological systems:

- a. Genetic algorithm
- b. Simulated annealing
- c. Particle swarm optimization
- d. Fuzzy optimization
- e. Neural-network-based methods

Particularly, genetic algorithm has attracted a lot of attention for the solution of complex engineering problems. In fact it requires only the function values (and not the derivate) and it can manage a lot of decision variables. The genetic algorithms are based on the principles of natural selection and are considered a stochastic method.

Many practical optimum design problems are characterized by mixed continuous-discrete variables that cannot be solved efficiently with standard nonlinear programming techniques. Genetic algorithms (GAs) are well suited for solving such problems and in most cases they can find the global optimum solution with a high probability. The base of the method is the Darwin's theory of the survival of the fittest.

Genetic algorithms are based on the principles of natural genetics and natural selection. The fundamental elements of natural genetics are:

- Reproduction
- Crossover
- Mutation

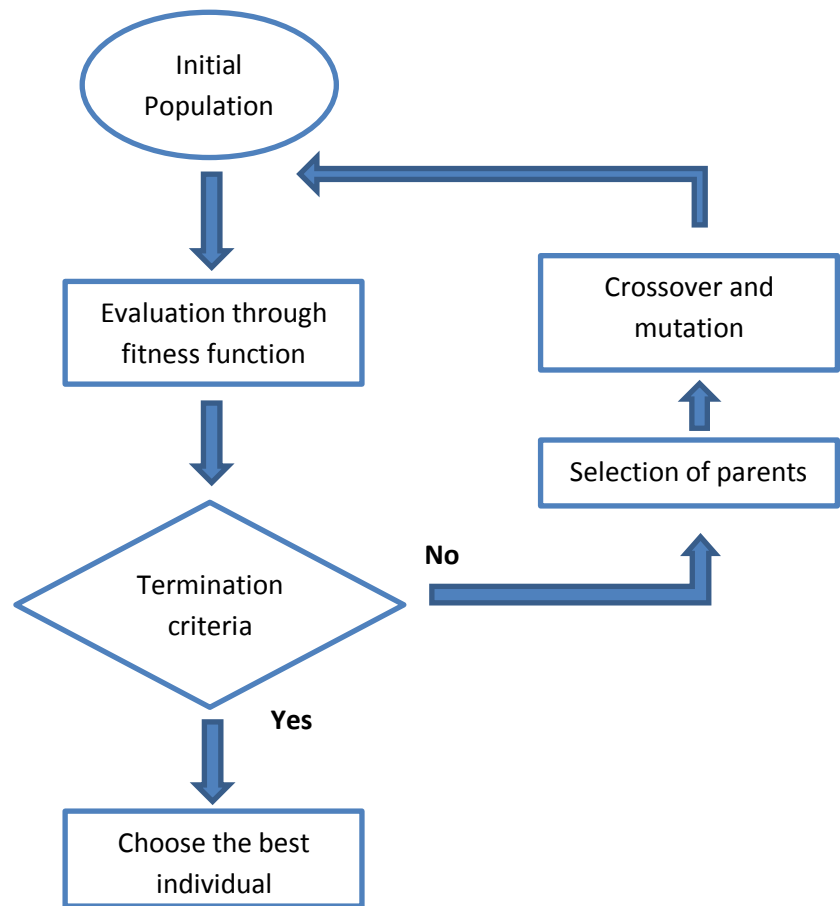


Figure 7.1. Flowchart of genetic algorithm procedure

7.2. Characteristics of GAs

Genetic algorithms have some important differences respect the traditional method of optimization:

- The starting point of genetic algorithms is a population of points instead of a single design point. Since several points are used as candidate solutions, GAs are less likely to get trapped at a local optimum.
- GAs use only the values of the objective function. The derivatives are not used in the search procedure.
- In GAs the design variables are represented as string of binary variables that correspond to the chromosomes in natural genetics.
- The objective function value corresponding to a design vector plays the role of fitness in natural genetics.
- In every new generation, a new set of string is produced by using randomized parents selection and crossover from the old generation. The research techniques is not merely random because GAs explore the new combinations with the available knowledge to find a new generation with better fitness or objective function value.

Table 7.1. Differences between genetic classical algorithms and genetic algorithms.

Classical Algorithms	Genetic Algorithms
Generates a single point at each iteration. The sequence of points approaches an optimal solution.	Generates a population of points at each iteration. The best point in the population approaches an optimal solution.
Selects the next point in the sequence by a deterministic computation.	Selects the next population by computation which uses random number generators.

As mentioned before, genetic algorithms are based on the survival of the fittest principle of nature so that they try to maximize (or minimize) a function called the fitness function. A general constrained minimization problem can be stated as:

$$\text{Minimize } f(\mathbf{x})$$

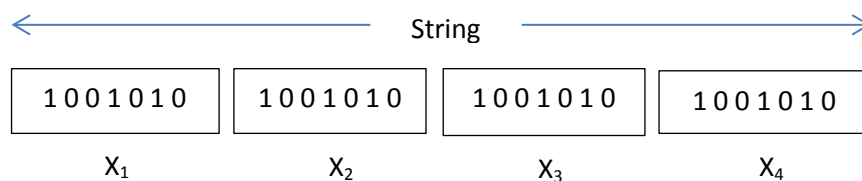
Subject to

$$g_i(\mathbf{x}) \leq 0, \quad i = 1, 2, \dots, m$$

$$h_j(\mathbf{x}) = 0, \quad j = 1, 2, \dots, n$$

The solution of an optimization problem by GAs starts with population of random strings denoting several design vectors. Each design vector is evaluated to find its fitness value. If the termination criteria are not satisfied the algorithm operates three operations: reproduction, crossover and mutation to produce a new population. The new population is further valuated to find the fitness values and tested for the convergence of the procedure. One cycle of reproduction, crossover, mutation and evaluation of the fitness function is called generation.

The vector that contains the design variable is represented by a string of binary digits:



7.3. Reproduction

Reproduction is the first operation applied to the population to select good design variable of the population to form a mating pool. It is a selection procedure that aims to select good elements of the population in order to achieve the optimum. The above-average individuals are picked up from the current population and they are inserted in the mating pool based on a probabilistic process.

7.4. Crossover

Crossover aims to create new strings of individuals by exchanging information among strings of the mating pool. In the commonly used process called single-point crossover operator, a crossover site is selected at random along the string length, and the binary digits (In genetic nature the alleles) lying on the right side of the crossover site are swapped between two strings. Following the nature principle, the two strings

selected for the crossover are called the parents and the strings generated by the crossover are known as a child. An example of crossover is presented below:

$$\text{Parent 1} \quad X_1 = \{0\ 1\ 0\ | \ 1\ 0\ 1\ 1\ 0\ 1\ 1\}$$

$$\text{Parent 2} \quad X_2 = \{1\ 0\ 0\ | \ 0\ 1\ 1\ 1\ 1\ 0\ 0\}$$

The results of crossover when the crossover site is 3, is given by

$$\text{Child 1} \quad X_3 = \{0\ 1\ 0\ | \ 0\ 1\ 1\ 1\ 1\ 0\ 0\}$$

$$\text{Child 2} \quad X_4 = \{1\ 0\ 0\ | \ 1\ 0\ 1\ 1\ 0\ 1\ 1\}$$

7.5. Mutation

Through crossover new strings with better fitness values are created for the new generations. The mutation operates changing of the binary digits (allele's value) in order to obtain new strings with a specific small mutation probability. The aims of the mutation operator are:

- To generate a string in the neighborhood of the current string, thereby accomplishing a local search around the current solution;
- To safeguard against a premature loss of important genetic material at a particular position
- To maintain diversity in the population

$$\text{Child 1} \quad X_3 = \{0\ 1\ 0\ | \ 0\ 1\ 1\ 1\ 1\ 0\ 0\}$$

$$\text{Child 1 with mutation} \quad X_3 = \{0\ 1\ 0\ | \ 0\ 1\ 1\ 0\ 1\ 0\ 0\}$$

The use of these three operators successively yields new generation with improved values of average fitness of the population. If any bad strings are created at any stage in the process, they will be eliminated by the reproduction operator in the next generation.

7.6. Multi-objective genetic algorithm

Multi-objective optimization problems have received interest from researchers since early 1960s. In a multi-objective optimization problem, multiple objective functions need to be optimized simultaneously. In the case of multiple objectives, there does not necessarily exist a solution that is best with respect to all objectives because of differentiation between objectives. A solution may be best in one objective but worst in another. Therefore, there usually exist a set of solutions for the multiple-objective case, which cannot simply be compared with each other. For such solutions, called Pareto optimal solutions or non-dominated solutions, no improvement is possible in any objective function without sacrificing at least one of the other objective functions.

Thus by using the concept of Pareto-optimality we can find a set of solutions that are all optimal compromises between the conflicting objectives. Pareto-optimality is a concept used economics, game theory, etc. A Pareto-optimal solution is one that is not dominated by any other solution i.e. it is one in which no objective can be improved without a deterioration in one or more of the other objectives. In the past few years, there has been a wide development in applying genetic algorithms to solve the multi-objective optimization problem, known as evolutionary multi-objective optimization or genetic multi-objective optimization. The basic features of genetic algorithms are the multiple directional and global searches, in which a population of potential solutions is maintained from generation to generation. The population-to-population approach is beneficial in the exploration of Pareto-optimal solutions. The main issue in solving multi-objective optimization problems by use of genetic algorithms is how to determine the fitness value of individuals according to multiple objectives.

8.1. Organic Rankine Cycle Optimization

Theoretical analysis described in Chapter 1 shows that ORC performance is very sensitive to the evaporating pressure (or temperature) and to the working fluid. Fluid selection plays an important role in the ORC design. Besides power performance, it is extremely important to take into consideration characteristics such as environmental impact, stability, safety and cost. This implies an accurate screening of the fluids and the evaporating temperature that provides the best trade-off between performance, environmental impact and safety.

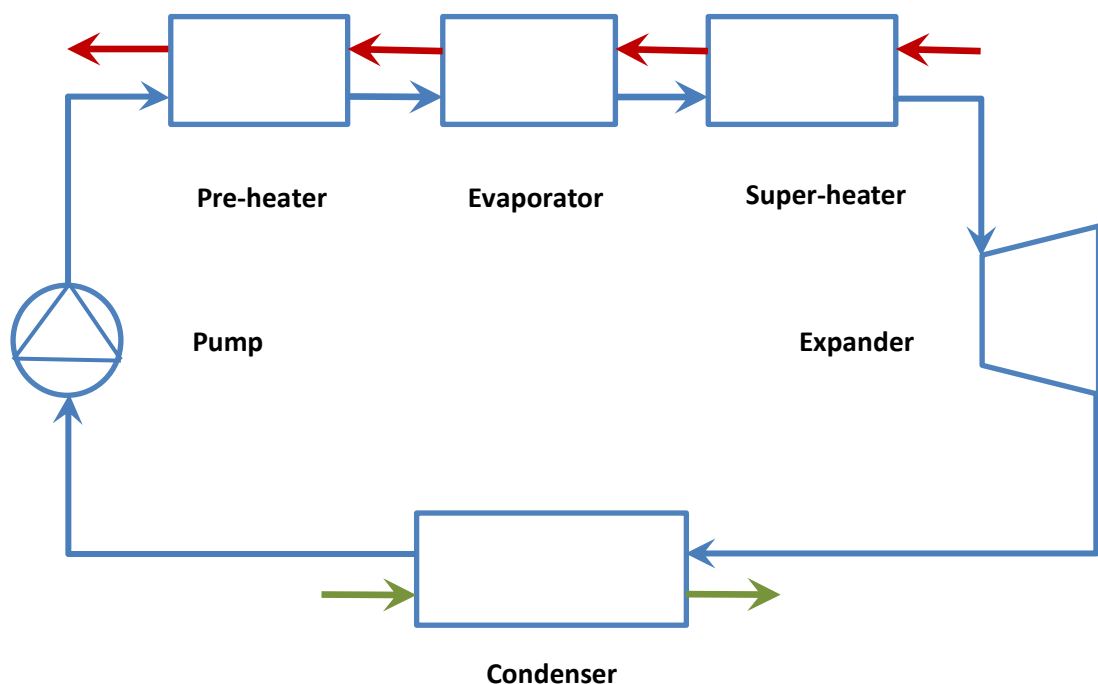


Fig. 8.1. ORC system

The objective of this work is to study the influence of the evaporating temperature and the working fluid on net power output, cycle efficiency and entropy generation of the system.

8.2. ORC analysis with fixed heat transfer rate

The first analysis considers an organic Rankine cycle with fixed heat transfer rate. The assumptions are the followings: the system is at the steady state, there is no pressure drop in the evaporator, pipes and condenser, the heat losses in the components are neglected and isentropic efficiencies of the pump and the expander are given. The working fluid at the inlet of the expander inlet and at the outlet of the condenser is superheated and subcooled respectively. The thermodynamic properties of working fluids and the ORC performance are calculated using REFPROP and MATLAB. The design point specification of the ORC is presented in *Table 8*. Since the exhaust gases from gas turbines have quite substantial oxygen content, in case of leakage, the mixing of oxygen and carbon based working fluids may cause explosion. To avoid this problem an intermediate loop is placed between the ORC and the heat source. The fluid selected for the intermediate loop is a glycol-based fluid named dowthermQ [19]. The properties of dowthermQ are shown in *Table 8.3*.

For sake of clarity, the following notation is used:

Table 8.1.

State	Number of node
Inlet of pump	1
Outlet of pump –inlet of pre-heater	2
Isentropic outlet of pump	2s
Outlet of pre-heater – inlet of evaporator	3
Outlet of evaporator – inlet of expander	4
Isentropic outlet of expander	5s
Outlet of expander – inlet condenser	5
Saturated vapor condition in the condenser	6
Outlet of condenser – inlet of pump	1
Heat source inlet	7
Pinch point – heat source side	8
Heat source outlet	9
Cooler inlet	10
Pinch point – cooler side	11
Cooler outlet	12

Table 8.2. ORC parameters

Parameter	Symbol	Value	Unit
Waste heat source temperature - inlet	T_7	180	°C
Waste heat source temperature - outlet	T_9	80	°C
Mass flow rate of waste heat source	\dot{m}_{hs}	0,25	Kg/s
Working fluid condensation temperature	T_6	30	°C
Water temperature at the inlet of condenser	T_{10}	15	°C
Pinch point on condenser	ΔPP_{cond}	10	°C
Environmental temperature	T_0	15	°C
Environmental pressure	P_0	100	kPa
Isentropic efficiency of the expander	η_{exp}	80%	
Isentropic efficiency of the pump	η_{pump}	60%	

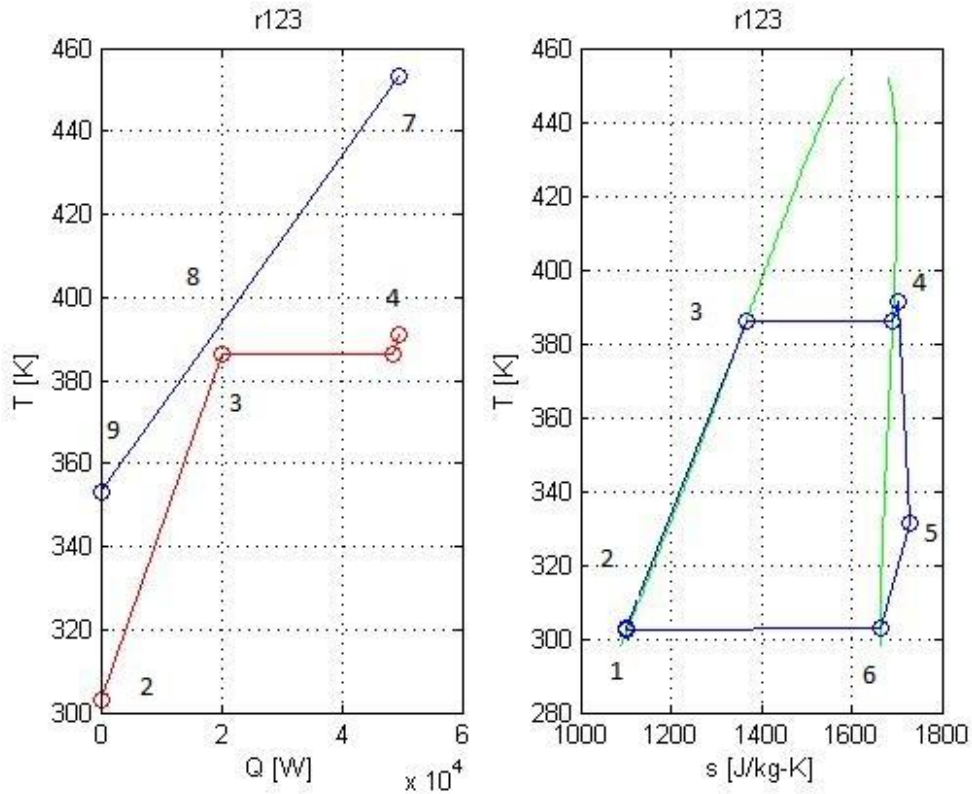


Fig. 8.2. State points

Table 8.3. dowthermQ properties correlations. $t_0 = 273,15$ K. Obtained by interpolation from data table provide by dowthermQ company [19].

Parameter	expression	Unit
Temperature	t	K
Enthalpy	$h_t = h_0 + (0.015t^2 + 0.7702t) - (0.015t_0^2 + 0.7702t_0)$	kJ
Heat capacity	$c_p = 0.003t + 0.7702$	kJ/kgK
Density	$\rho = 1187 - 0.756t$	kg/m ³
Entropy	$s = s_0 + 0.003(t - t_0) + 0.7702 \ln \frac{t}{t_0}$	kJ/K

The inlet and outlet temperatures and the mass flow rate of the heat source are given, thus, one can obtain the enthalpy using REFPROP and calculate the heat transfer rate:

$$h_7 = f(T_7) \quad (8.1)$$

$$h_9 = f(T_9) \quad (8.2)$$

$$\dot{Q}_{hs} = \dot{m}_{hs}(h_7 - h_9) \quad (8.3.)$$

The procedure to calculate net power output, efficiency and entropy generation rate is straightforward:

$$P_{eva} = f(T_3, \text{working fluid}) \quad (8.4)$$

$$T_4 = T_3 + \Delta_{sup} \quad (8.5)$$

$$[h_4, s_4] = f(T_4, P_{eva}, \text{working fluid}) \quad (8.6)$$

$$T_1 = T_6 - \Delta_{sub} \quad (8.7)$$

$$P_{cond} = f(T_6) \quad (8.8)$$

$$[h_1, s_1] = f(T_1, P_{cond}, \text{working fluid}) \quad (8.9)$$

$$s_1 = s_{2s} \quad (8.10)$$

$$h_{2s} = f(s_{2s}, P_{eva}, \text{working fluid}) \quad (8.11)$$

$$h_2 = h_1 + \frac{h_{2s} - h_2}{\eta_{pump}} \quad (8.12)$$

$$\dot{m}_{wf} = \dot{m}_{hs} \frac{h_7 - h_9}{h_4 - h_2} \quad (8.13)$$

$$s_{5s} = s_4 \quad (8.14)$$

$$h_{5s} = f(s_{5s}, P_{cond}, \text{working fluid}) \quad (8.15)$$

$$h_5 = h_4 - (h_4 - h_{5s})\eta_{exp} \quad (8.16)$$

$$[T_5, s_5] = f(h_5, P_{cond}, \text{working fluid}) \quad (8.17)$$

$$\dot{Q}_{out} = \dot{m}_{wf}(h_6 - h_9) \quad (8.18)$$

$$\dot{m}_{wtr} = \frac{\dot{m}_{wf}(h_6 - h_1)}{h_{11} - h_{10}} \quad (8.19)$$

$$T_{12} = T_{10} + \dot{m}_{wf} \frac{h_5 - h_1}{\dot{m}_{wtr} C_{p,wtr}} \quad (8.20)$$

$$[h_{12}, s_{12}] = f(T_{12}, P_{wtr}, \text{water}) \quad (8.21)$$

When all the thermodynamic states of the cycle are calculated, it is possible to compute the net power output, the efficiency and the total entropy generation rate:

$$\dot{W}_{net} = \dot{m}_{wf} [(h_4 - h_5) - (h_2 - h_1)] \quad (8.22)$$

$$\eta_{ORC} = \frac{\dot{W}_{net}}{\dot{Q}_{hs}} \quad (8.23)$$

$$\dot{S}_{tot} = \dot{S}_{eva} + \dot{S}_{exp} + \dot{S}_{cond} + \dot{S}_{pump} \quad (8.24)$$

Where:

$$\dot{S}_{eva} = \dot{m}_{wf} \left[(s_4 - s_2) - \frac{(h_4 - h_2)}{T_H} \right] = \dot{m}_{wf} [(s_4 - s_2) + (s_9 - s_7)] \quad (8.25)$$

$$\dot{S}_{exp} = \dot{m}_{wf} (s_5 - s_4) \quad (8.26)$$

$$\dot{S}_{cond} = \dot{m}_{wf} \left[(s_5 - s_1) + \frac{(h_5 - h_1)}{T_L} \right] = \dot{m}_{wf} [(s_5 - s_1) + (s_{12} - s_{10})] \quad (8.27)$$

$$\dot{S}_{pump} = \dot{m}_{wf} (s_2 - s_1) \quad (8.28)$$

The model implemented needs a control on the pinch point caused by the variation of the evaporating temperature. The lower the pinch point, the higher the heat transfer surface area of the heat exchanger. A lowest value 10°C is fixed. *Figure 8.3* shows the influence of the evaporating temperature to the pinch point. It can be see that the highest evaporating temperature in the cycle is the temperature where the pinch point is the minimum allowable.

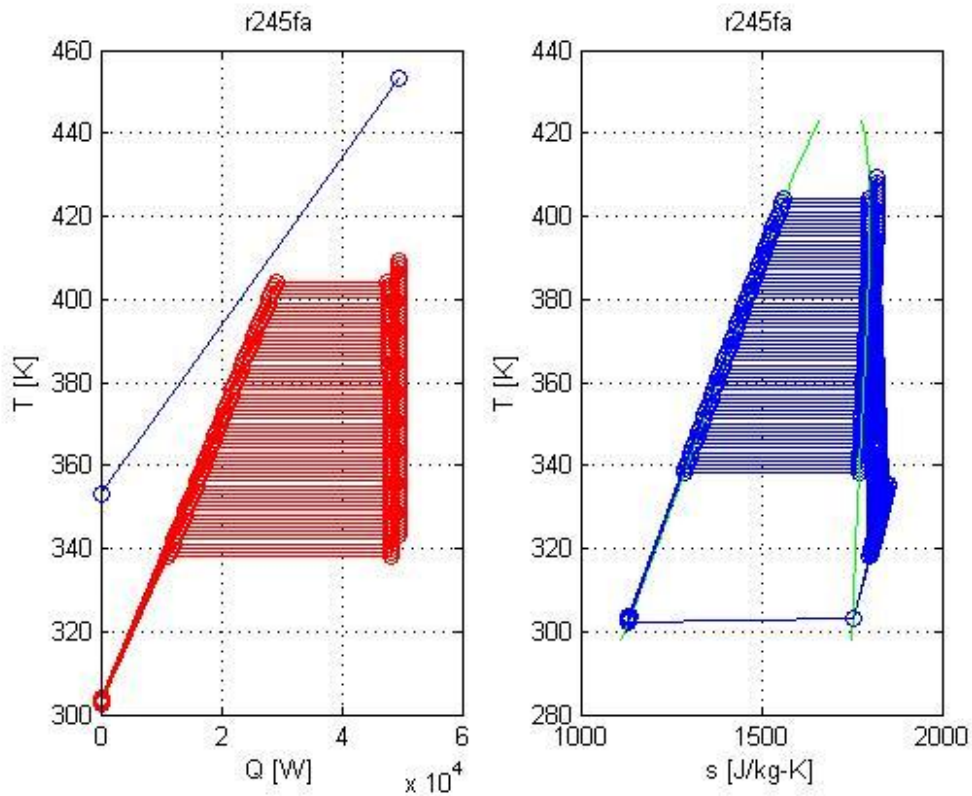


Fig. 8.3. a) T-Q diagram of pre-heater and evaporator with different evaporating temperature. b) T-s diagram of ORC with different evaporating temperature.

As expected, the highest value of net power output is obtained with the highest evaporating temperature. since the higher the evaporating temperature, the higher the enthalpy drop in the expander. This observation is valid because the enthalpy drop in the pump is much smaller than the enthalpy drop in the expander and it could be neglected. As a consequence the ORC thermal efficiency has the same trend.

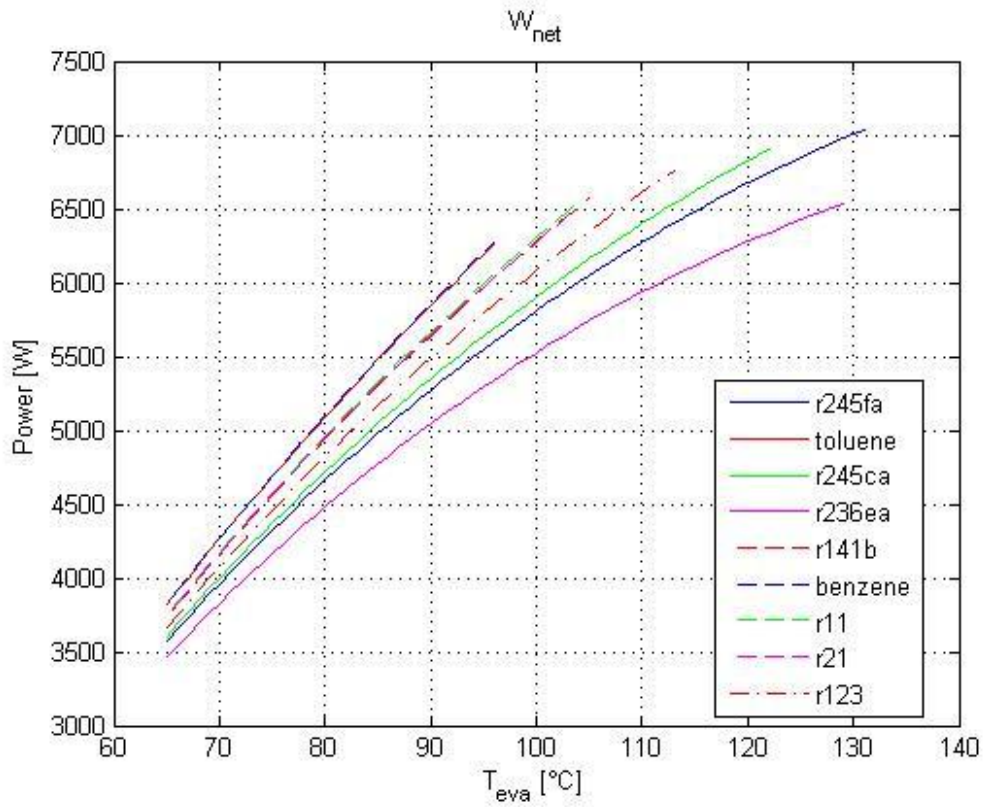


Fig. 8.4. Net Power Output vs. Evaporating temperature for different fluids with fixed heat load

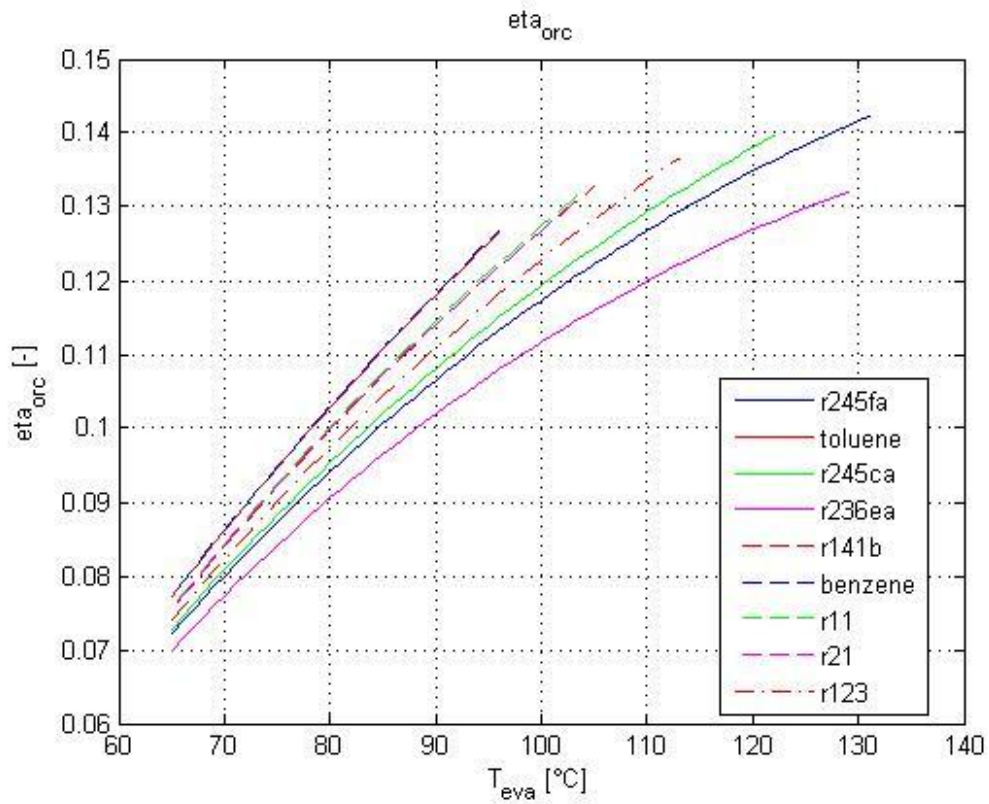


Fig. 8.5. ORC efficiency vs. Evaporating temperature for different fluids with fixed heat load

The effectiveness of the heat exchanger increases with the evaporating temperature since more heat is transmitted to the fluid as shown in Fig. 8.6. The entropy generated in the components of the cycle is shown in Fig. 8.7. It is evident that the lower the pinch point, the lower the entropy generation rate. In fact, the lowest value of entropy generated is related to the highest evaporating temperature. This is due to the fact that the entropy generated is caused by finite temperature difference and pressure drop. Because of the assumption of neglectable pressure drop, the only contribute is the finite temperature difference between the streams. The temperature that causes the highest power output is also the same that produces the lowest amount of entropy. This phenomenon is described by the Guoy-Stodola theorem:

$$W_{net} = W_{rev} - T_0 S_{gen} \quad (8.29)$$

Where W_{rev} is the maximum power that could be extracted if the cycle was reversible. W_{rev} can be extracted only if S_{gen} is equal to zero.

Finally, Fig. 8.8 shows the entropy generated by evaporator, condenser, expander and pump when r-236a is used as working fluid. It can be seen that evaporator has the greater entropy generation. This means that it is the main component that should be improved in order to reduce the total entropy generation rate. Furthermore, the influence of the pinch point on the entropy generated by the evaporator is evident. In fact the entropy generated decreases with the increase of the evaporating temperature and, as a consequence, the reduction of pinch point.

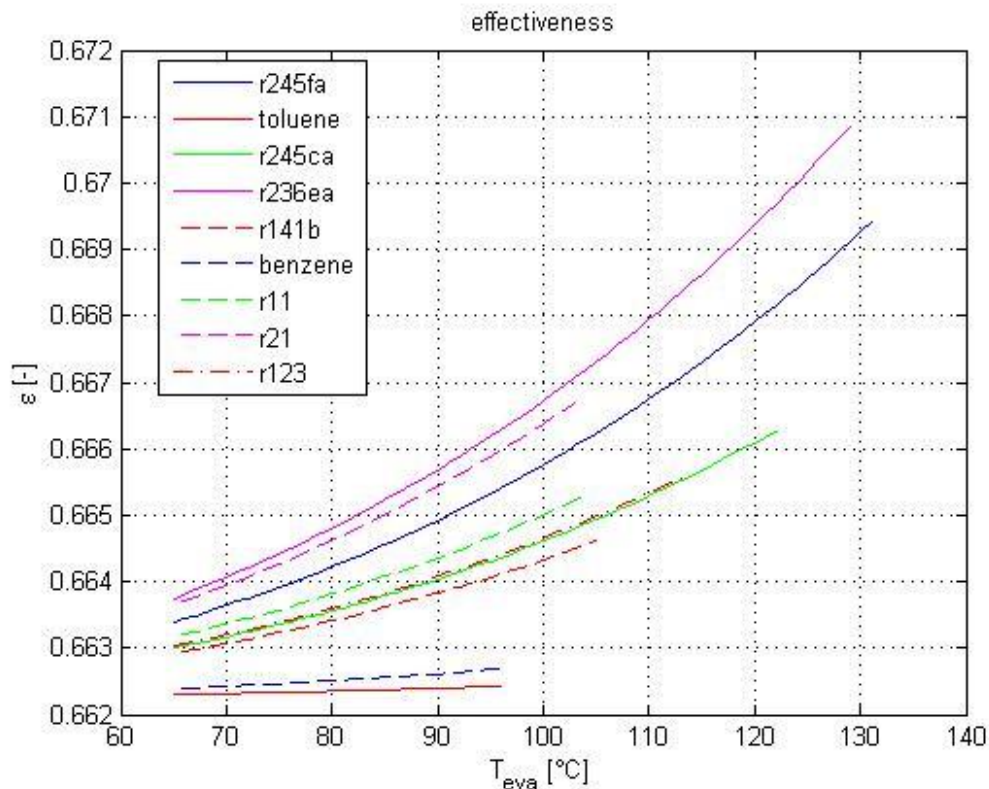


Fig. 8.6. Effectiveness vs. Evaporating temperature for different fluids with fixed heat load

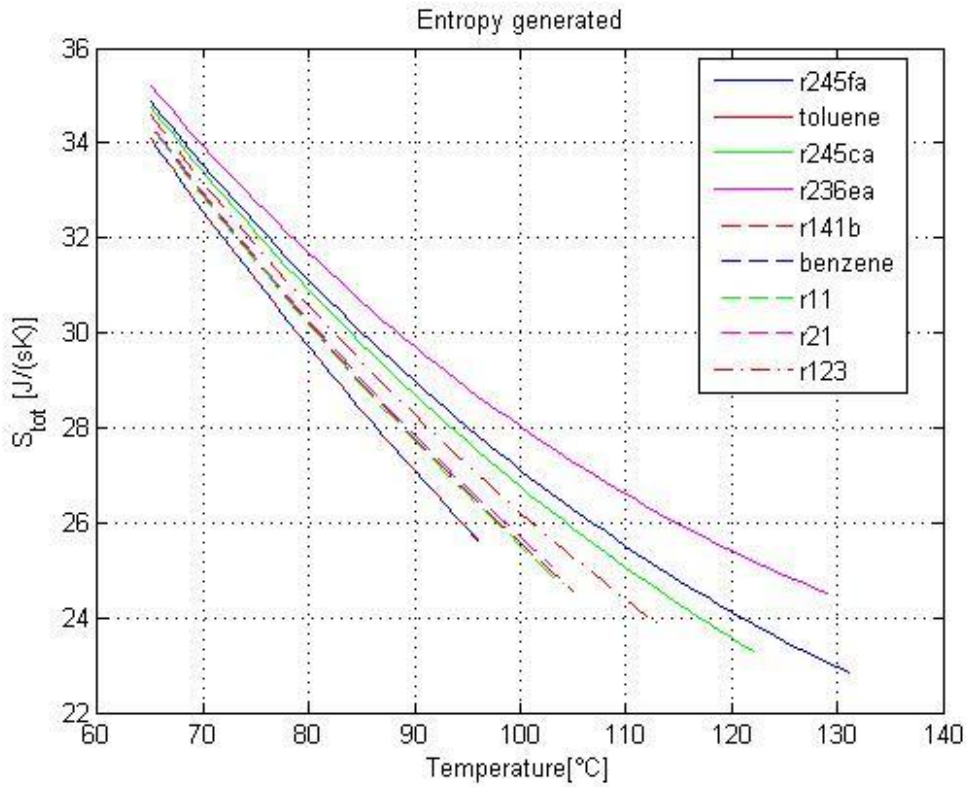


Fig. 8.7. Entropy generation rate vs. Evaporating temperature for different fluids with fixed heat load

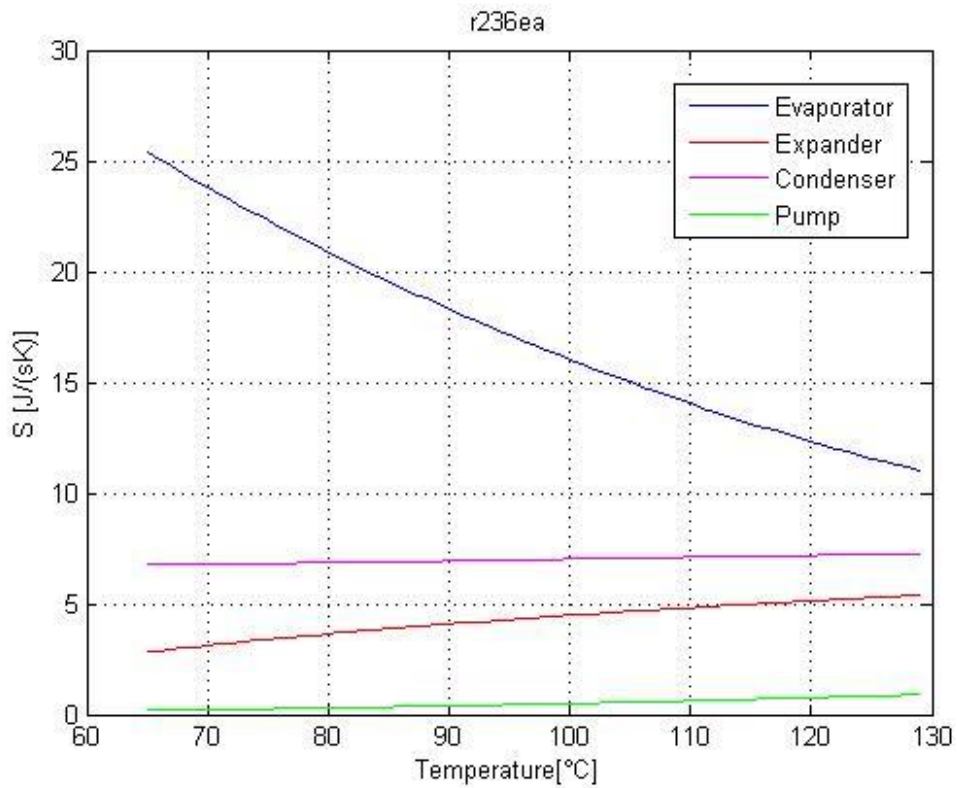


Fig. 8.8. Entropy generation rate vs. Evaporating temperature for evaporator, expander, condenser and pump. Fluid is r236ea.

8.3. ORC analysis with variable heat transfer rate

In the second model the assumption of fixed outlet temperature is removed, therefore the transfer rate is variable. For the purpose of this optimization, the minimum temperature difference between heat source and working fluid is imposed. A value of 10 K is selected at the inlet of the evaporator.

Table 8.4.

Parameter	Symbol	Value	Unit
Waste heat source temperature - inlet	T_7	180	°C
Mass flow rate of waste heat source	\dot{m}_{hs}	0,25	Kg/s
Working fluid condensation temperature	T_6	30	°C
Water temperature at the inlet of condenser	T_{10}	15	°C
Pinch point on condenser	ΔPP_{eva}	10	°C
Pinch point on condenser	ΔPP_{cond}	10	°C
Environmental temperature	T_0	15	°C
Environmental pressure	P_0	100	kPa
Isentropic efficiency of the expander	η_{exp}	80%	
Isentropic efficiency of the pump	η_{pump}	60%	

The optimal evaporation temperature results in the optimization of the net power output. Increase the evaporation temperature implies two antagonist effects:

- The heat recovery efficiency is decreased since the heat source is cooled down to a higher temperature. In fact, the higher is the evaporating temperature the higher is the exhaust outlet temperature.
- The expander specific work is increased since the pressure ratio is increased.

The approach is similar to the previous model:

$$h_7 = f(T_7) \quad (8.30)$$

$$P_{eva} = f(T_3, \text{working fluid}) \quad (8.31)$$

$$T_4 = T_3 + \Delta_{sup} \quad (8.32)$$

$$T_8 = T_3 + \Delta PP_{eva} \quad (8.33)$$

$$h_8 = f(T_8) \quad (8.34)$$

$$\dot{m}_{wf} = \dot{m}_{hs} \frac{h_7 - h_8}{h_4 - h_3} \quad (8.35)$$

$$[h_4, s_4] = f(T_4, P_{eva}, \text{working fluid}) \quad (8.36)$$

$$T_1 = T_6 - \Delta_{sub} \quad (8.37)$$

$$P_{cond} = f(T_6) \quad (8.38)$$

$$[h_1, s_1] = f(T_1, P_{cond}, \text{working fluid}) \quad (8.39)$$

$$s_1 = s_{2s} \quad (8.40)$$

$$h_{2s} = f(s_{2s}, P_{eva}, \text{working fluid}) \quad (8.41)$$

$$h_2 = h_1 + \frac{h_{2s} - h_2}{\eta_{pump}} \quad (8.42)$$

$$s_{5s} = s_4 \quad (8.43)$$

$$h_{5s} = f(s_{5s}, P_{cond}, \text{working fluid}) \quad (8.44)$$

$$h_5 = h_4 - (h_4 - h_{5s})\eta_{exp} \quad (8.45)$$

$$[T_5, s_5] = f(h_5, P_{cond}, \text{working fluid}) \quad (8.46)$$

$$\dot{Q}_{out} = \dot{m}_{wf}(h_6 - h_9) \quad (8.47)$$

$$\dot{m}_{wtr} = \frac{\dot{m}_{wf}(h_6 - h_1)}{h_{11} - h_{10}} \quad (8.48)$$

$$h_9 = h_7 - \frac{\dot{m}_{wf}(h_4 - h_2)}{\dot{m}_{hs}} \quad (8.49)$$

$$T_9 = f(h_9) \quad (8.50)$$

$$T_{12} = T_{10} + \dot{m}_{wf} \frac{h_5 - h_1}{\dot{m}_{wtr} C_{p,wtr}} \quad (8.51)$$

$$[h_{12}, s_{12}] = f(T_{12}, P_{wtr}, \text{water}) \quad (8.52)$$

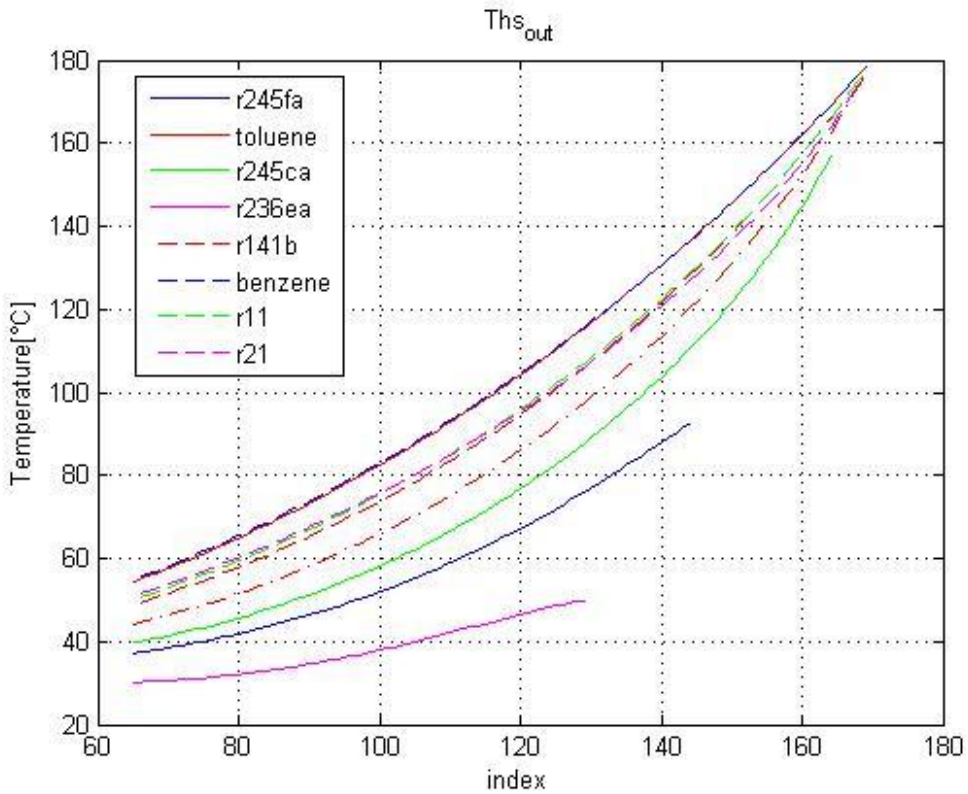


Fig. 8.9. Heat source Outlet Temperature vs. evaporating temperature for different fluids with variable heat load.

This analysis can be conducted for each candidate working fluid in order to define the optimum evaporation temperature. The results of this optimization are presented in *figure 8.10*. One can note the increase of the heat source outlet temperature with the increase of evaporation temperature and the consequent decrease of the heat transfer rate (*Fig. 8.10*). As a consequence, the lower the heat transfer rate, the lower the mass flow rate of the working fluid.

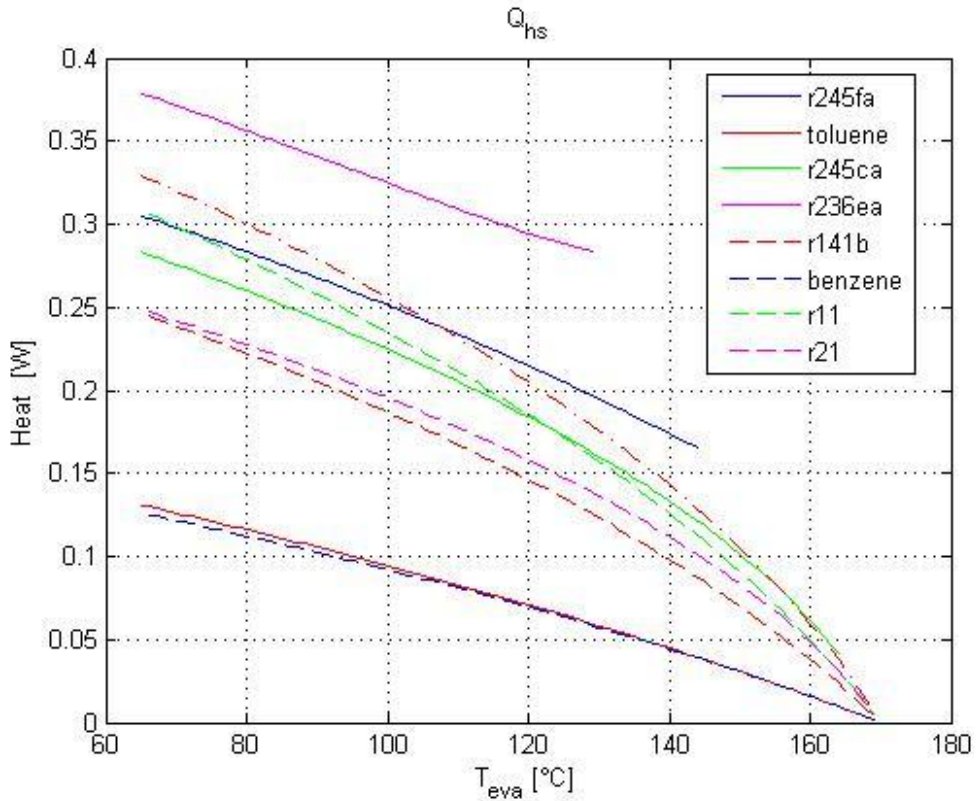


Fig. 8.10. Heat Transfer Rate vs. evaporating temperature for different fluids with variable heat load.

As described previously, pressure ratio and heat transfer rate have opposite effects on the maximum net power output. There is an optimal evaporating temperature (or pressure) that provides the maximum net power output for each fluid as shown in *Fig. 8.12*. In this case the ORC efficiency is not the best performance indicator since it does not consider the effect of the variable heat transfer rate (*Fig. 8.13*). The problem can be solved using the overall system efficiency that uses the maximum heat that can be extracted from the heat source as comparative value (*Fig. 8.1*). Contrary to the previous example, the effectiveness decreases with the increase of evaporating temperature since the outlet temperature of heat source increases as shown in *Fig. 8.15*. The lower the effectiveness the lower the heat extracted by the working fluid from the heat source and the higher the heat unused and released to the environment.

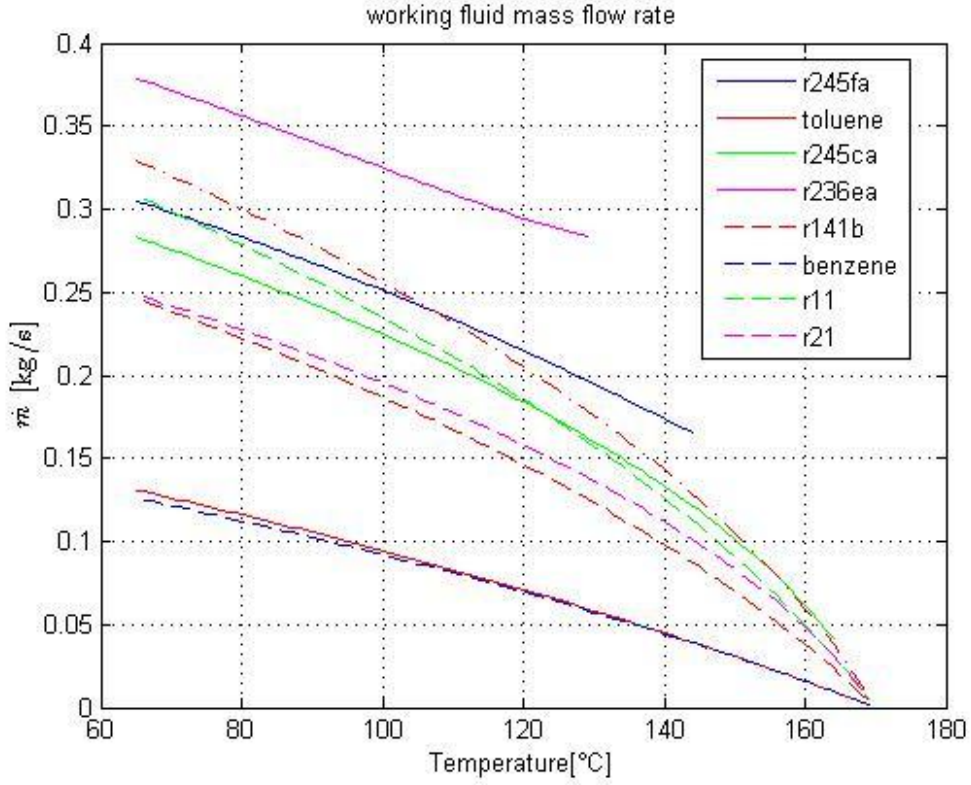


Fig. 8.11. Working fluid mass flow rate vs. evaporating temperature for different fluids with variable heat load.

Fig. 8.17 shows the entropy generated by evaporator, expander, condenser and pump. It can be noted the decreasing trend of total entropy generation rate that is due to the decreasing value of mass flow rate of the working fluid.

$$\dot{S}_{eva} = \dot{m}_{wf} \left[(s_4 - s_2) - \frac{(h_4 - h_2)}{T_H} \right] = \dot{m}_{wf} [(s_4 - s_2) + (s_9 - s_7)] \quad (8.53)$$

$$\dot{S}_{exp} = \dot{m}_{wf} (s_5 - s_4) \quad (8.54)$$

$$\dot{S}_{cond} = \dot{m}_{wf} \left[(s_5 - s_1) + \frac{(h_5 - h_1)}{T_L} \right] = \dot{m}_{wf} [(s_5 - s_1) + (s_{12} - s_{10})] \quad (8.55)$$

$$\dot{S}_{pump} = \dot{m}_{wf} (s_2 - s_1) \quad (8.56)$$

$$\dot{S}_{tot} = \dot{S}_{eva} + \dot{S}_{exp} + \dot{S}_{cond} + \dot{S}_{pump} \quad (8.57)$$

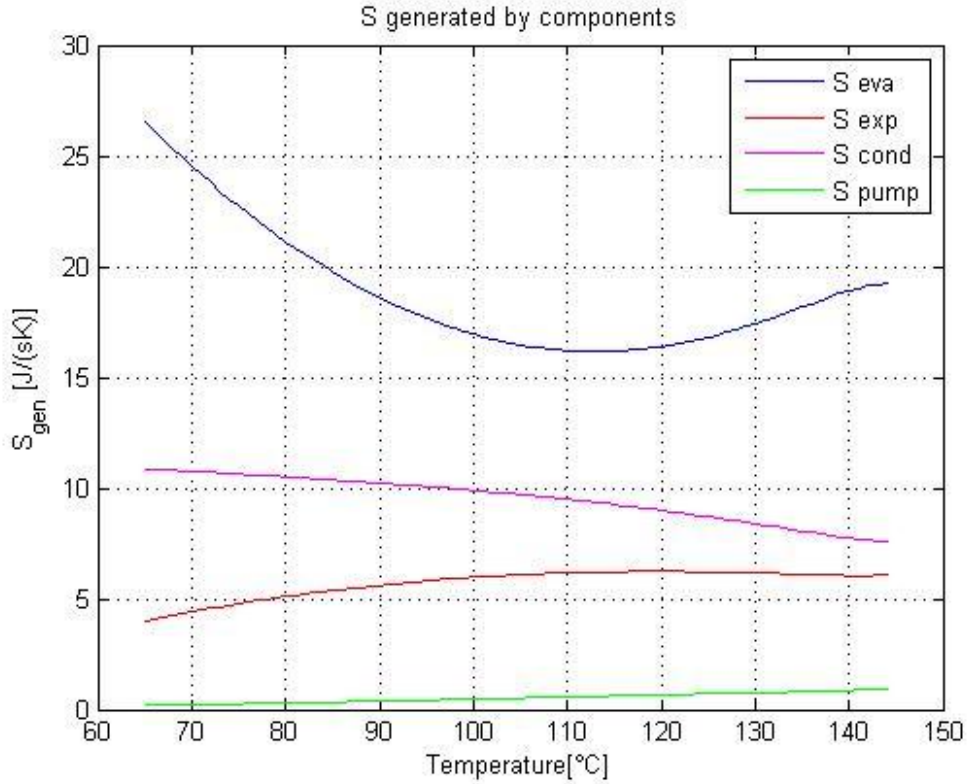


Fig. 8.12. Entropy generated by R-245fa in the evaporator, expander, condenser and pump.

This phenomenon would be in contradiction with the Gouy-Stodola theorem if we did not consider the exergy released into the environment. The contribution of the heat released into the environment is fundamental in order to perform the properly the exergetic analysis. If we consider the external irreversibility of ORC:

$$\dot{S}_{eva,ext} = \dot{m}_{hs} c_{p,hs} \left(\frac{T_9 - T_0}{T_0} + \ln \frac{T_0}{T_9} \right) \quad (8.58)$$

$$\dot{S}_{cond,ext} = \dot{m}_{wtr} c_{p,wtr} \left(\frac{T_{12} - T_0}{T_0} + \ln \frac{T_0}{T_{12}} \right) \quad (8.59)$$

We obtain the total entropy generated as follows:

$$\dot{S}_{gen} = \dot{S}_{tot} + \dot{S}_{eva,ext} + \dot{S}_{cond,ext} \quad (8.60)$$

As shown in Fig. 8.18, the total entropy generated has a minimum and that minimum is reached at the same evaporating temperature that produces the maximum net power output. Comparing Fig. 8.13 and Fig. 8.19, one can note that the optimal evaporating temperatures are the same in accordance with the Gouy-Stodola theorem.

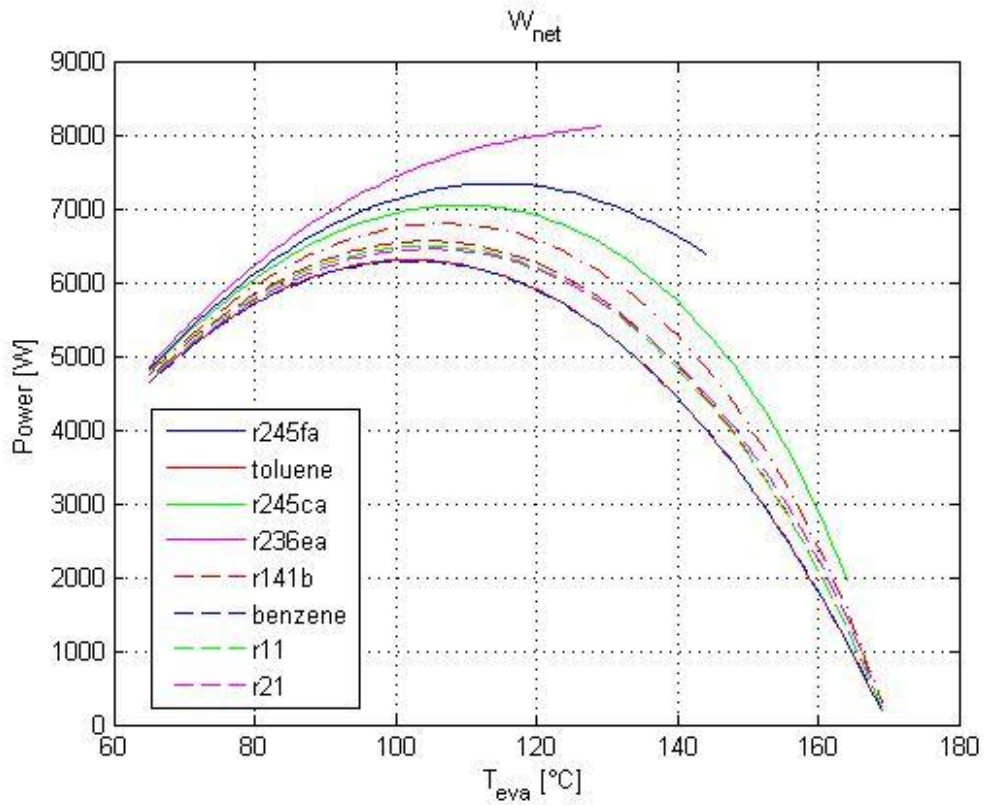


Fig. 8.13. Net Power Output vs. evaporating temperature for different fluids with variable heat load.

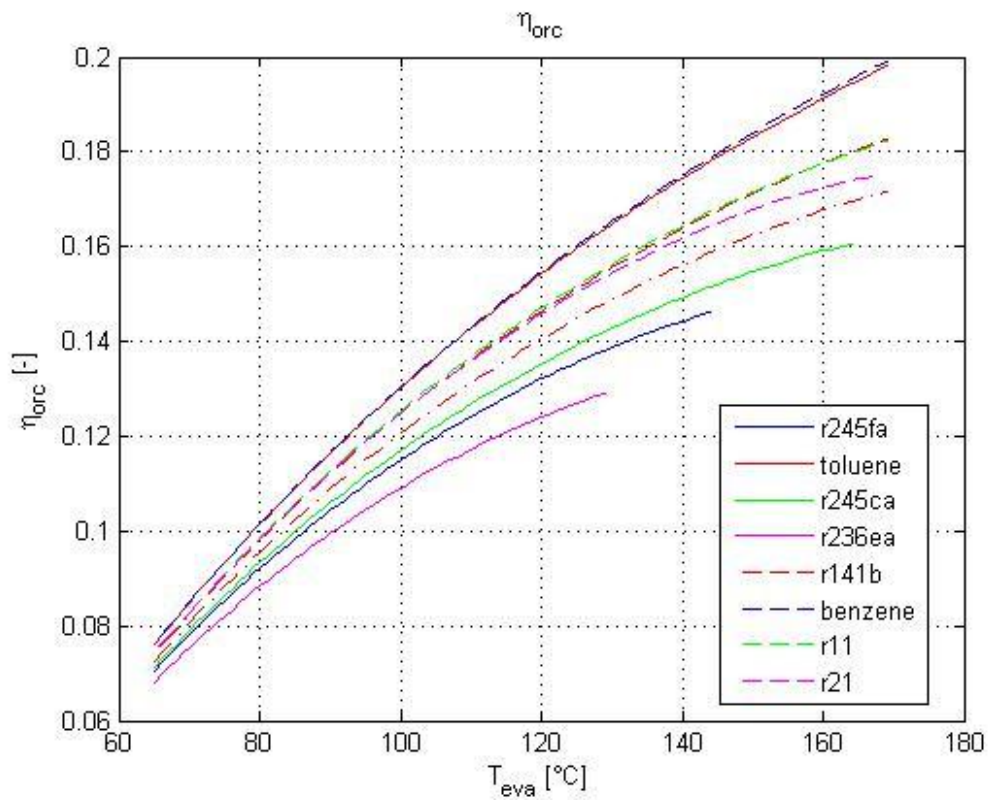


Fig.8.14. ORC efficiency vs. evaporating temperature for different fluids with variable heat load.

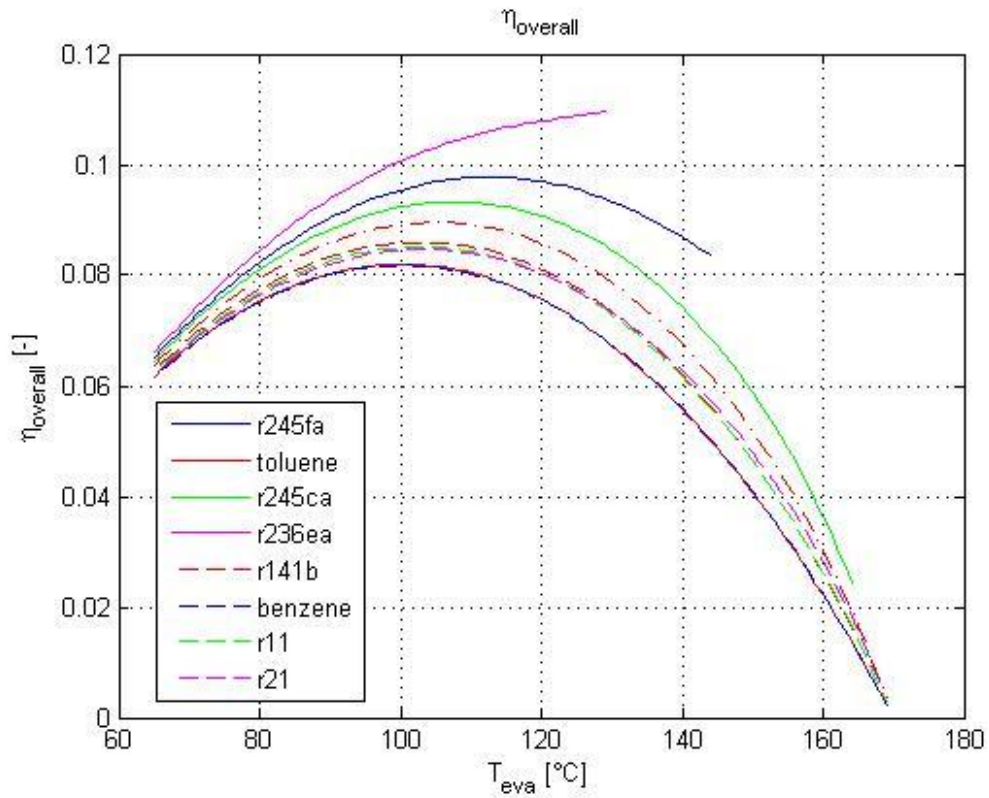


Fig. 8.15. System efficiency vs. evaporating temperature for different fluids with variable heat load.

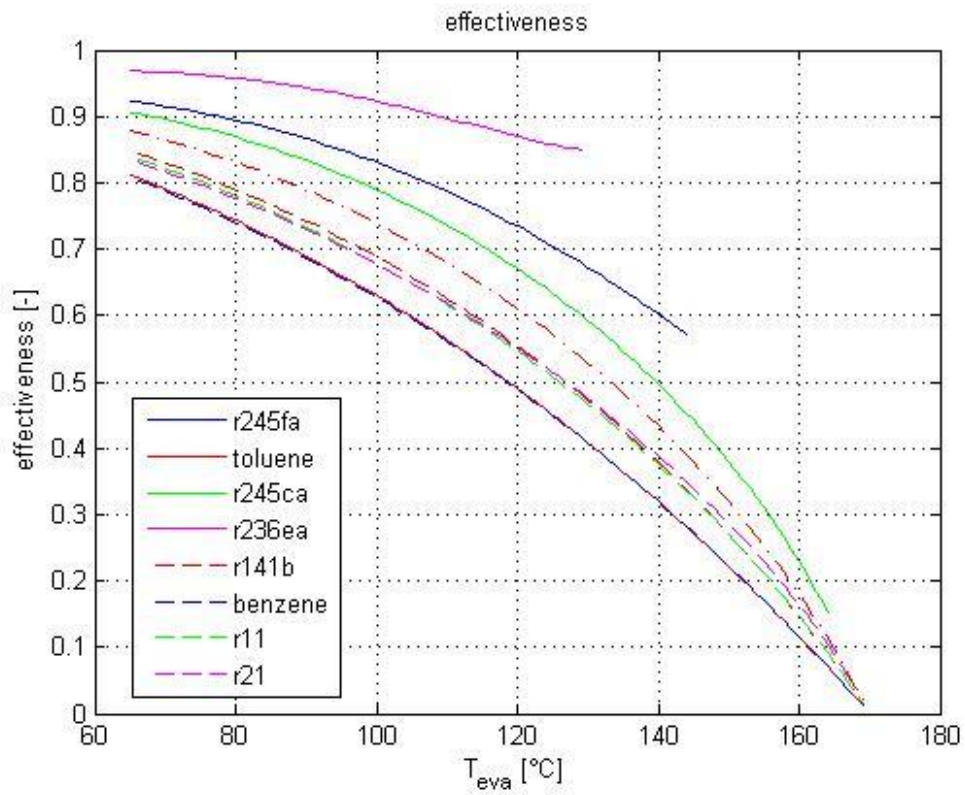


Fig. 8.16. Effectiveness vs. evaporating temperature for different fluids with variable heat load.

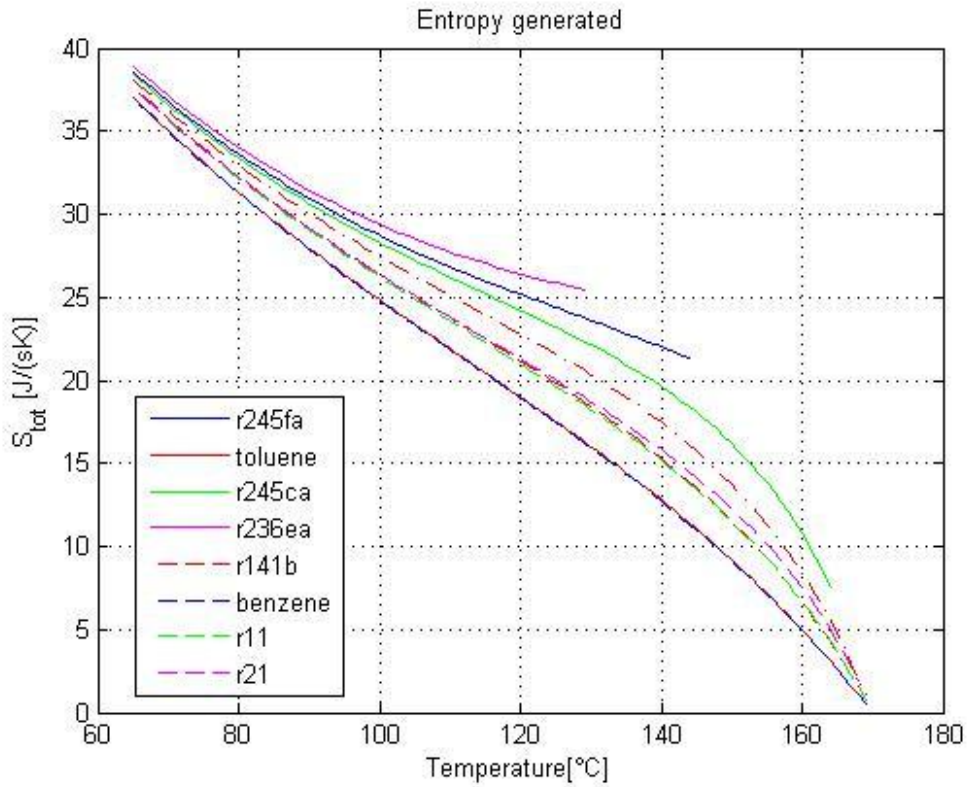


Fig. 8.17. Entropy generated in the cycle by evaporator, condenser, expander and pump vs. evaporating temperature. External irreversibility are not considered.

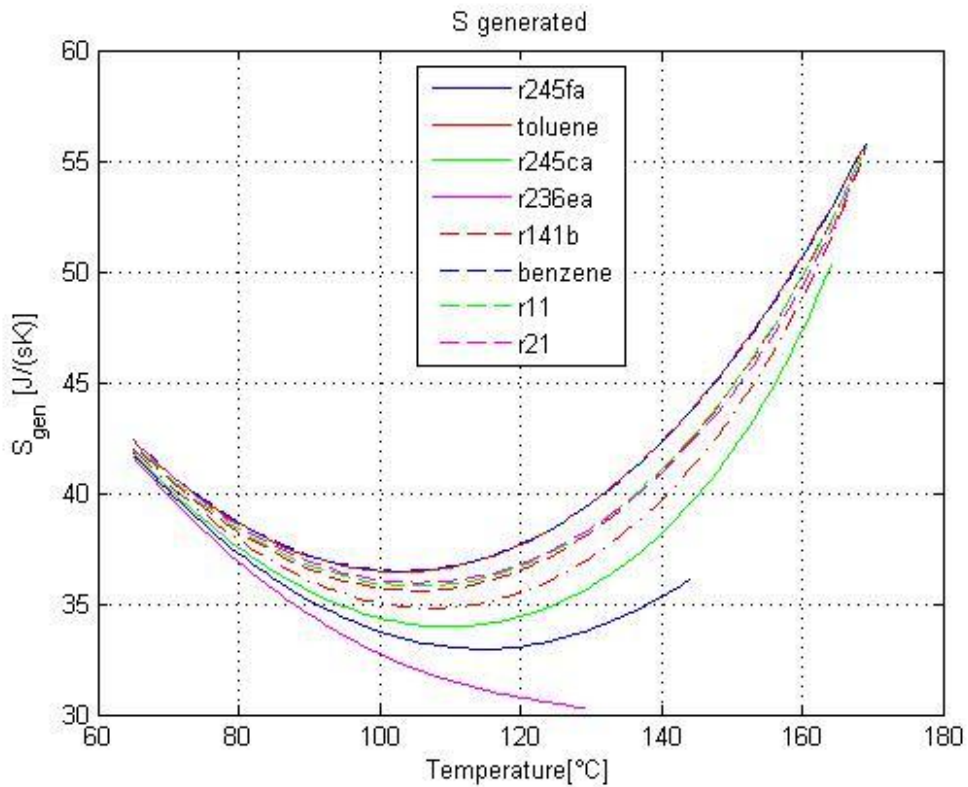


Fig. 8.18. Entropy generated in the cycle by evaporator, condenser, expander and pump vs. evaporating temperature. External irreversibility are considered.

Tab. 8.5. Optimal Temperatures (°C) obtained maximizing power and minimizing entropy.

Fluid	Teva_opt(°C)	Wnet_max[W]	Teva_opt(°C)	S min[W/K]	S released
r245fa	117.000	7545.391	118.000	32.250	7.153
toluene	102.000	6329.927	103.000	36.330	12.706
r245ca	110.000	7184.852	111.000	33.481	7.948
r236ea	129.000	8792.866	129.000	27.976	3.531
r141b	105.000	6602.297	106.000	35.435	10.995
benzene	102.000	6302.794	103.000	36.421	12.827
r11	105.000	6523.932	106.000	35.699	11.405
r21	105.000	6475.204	106.000	35.868	11.375
r123	107.000	6874.740	108.000	34.527	9.376

The minimum entropy generation is strictly influenced by fluid and boundary conditions. In fact the inlet temperature of heat source and its mass flow rate are fundamental in the optimization of the cycle. Wei et al.[20] explored the system performance analysis and optimization of ORC with r-245fa and found that it was a good way to improve the net power output of the system by maximizing the utilization of the waste heat as much as possible. In fact, the higher the exergy released into the environment, the lower the heat transferred to the working fluid. Each fluid has a different behavior and it is evident that boundary conditions are related to the exergy released into the environment. The higher the exergy (or the entropy) released into the environment the lower the power that can be extracted from the cycle. This consideration is demonstrated in *Table 8.5*. Toluene and Benzene give a higher entropy generation so that the net power output is lower than the other fluids. Particularly, r-236ea provides the lowest entropy released into the environment and the maximum power output. In fact, r-236ea matches very well with the boundary conditions defined instead of toluene and benzene that are usually employed with higher heat source temperature. In fact, exergetic losses are proportional to the area between the two curves in *figure 8.19-a and 8.20-a*; the higher the area, the lower the available work. The following figures show the optimal operating conditions of r-236ea and toluene.

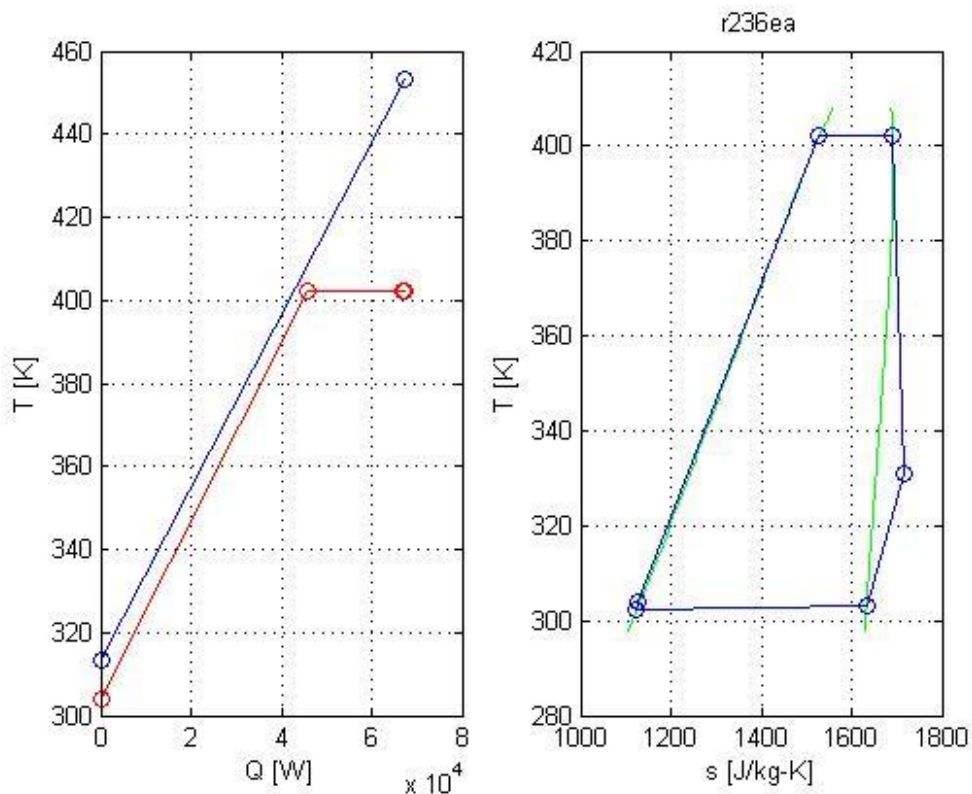


Fig. 8.19. T-Q diagram and T-s diagram of r-236ea.

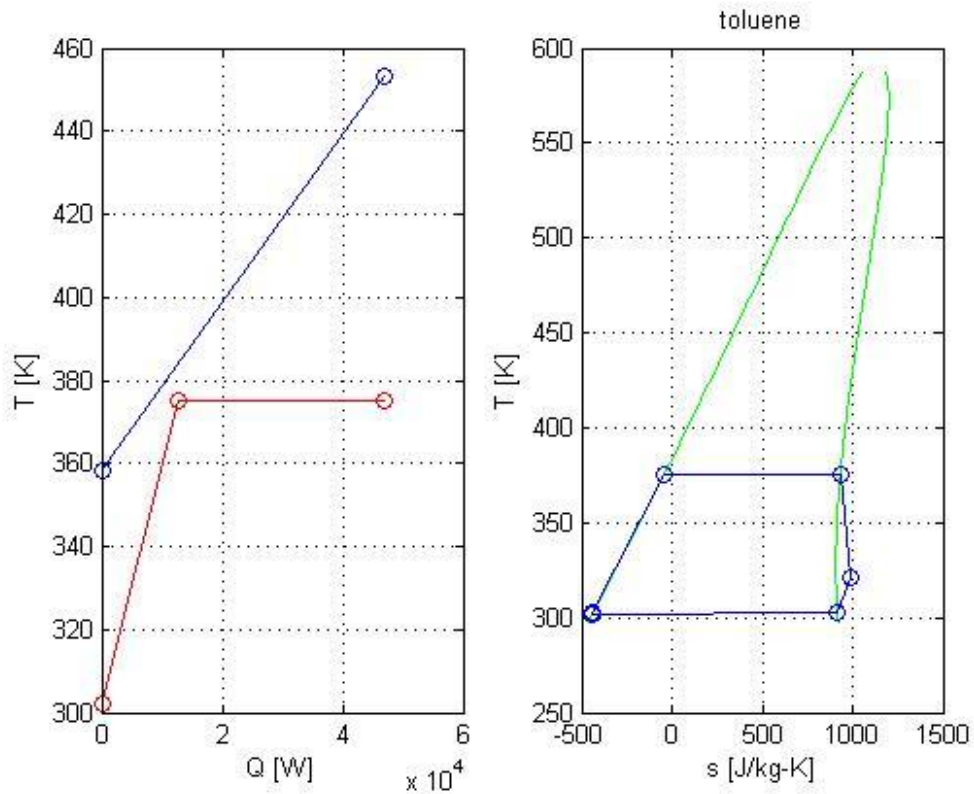
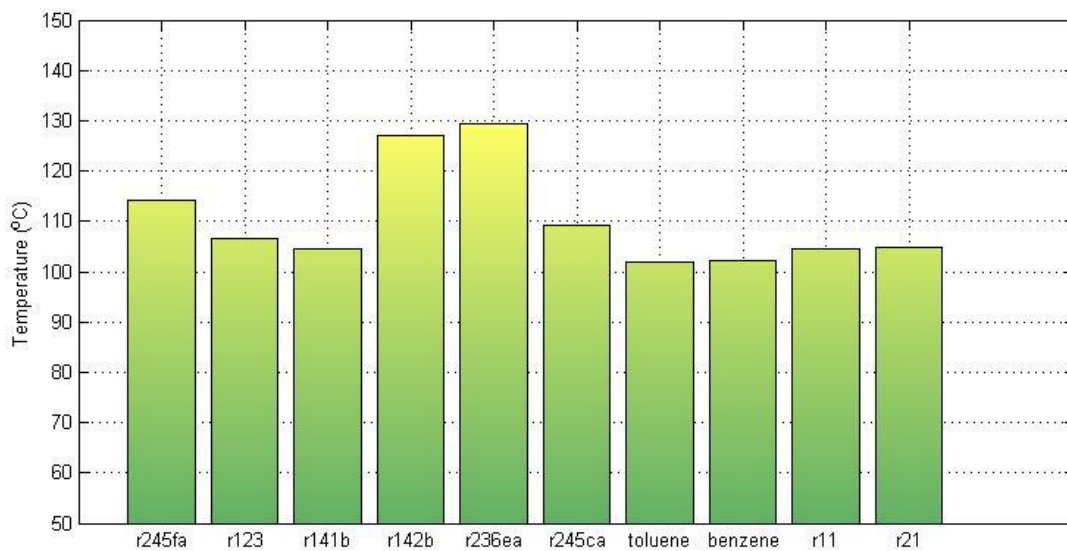


Fig. 8.20. T-Q diagram and T-s diagram of toluene.

8.4. Fluid selection

Operating temperatures and pressures are fundamental in the selection of working fluid. High evaporating pressure could be difficult to manage and influence the cost of pre-heater and evaporator. Fig. 8.21. shows the optimal evaporating pressure of each fluid. It can be noted the high pressure obtained by r-142b and r-236ea.



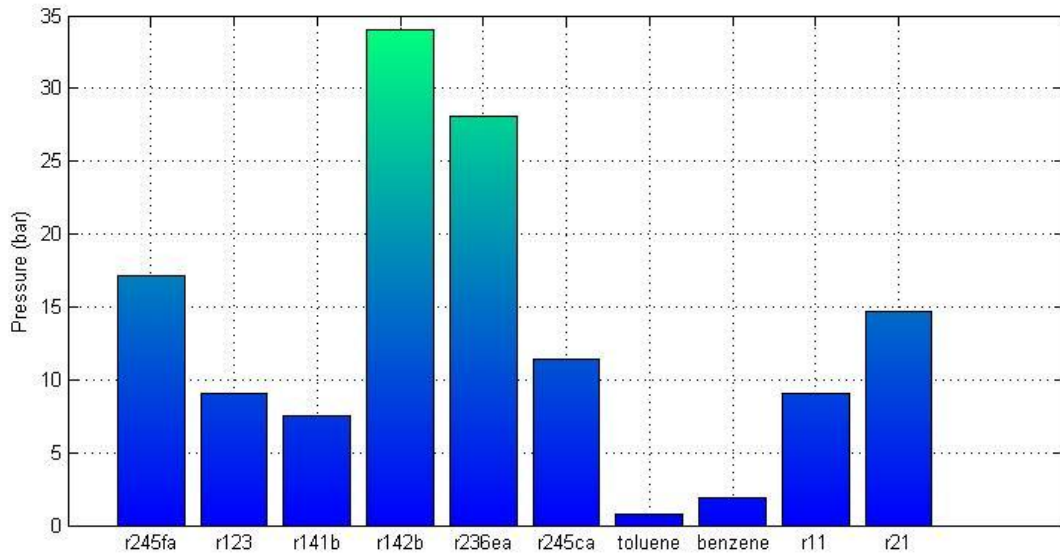
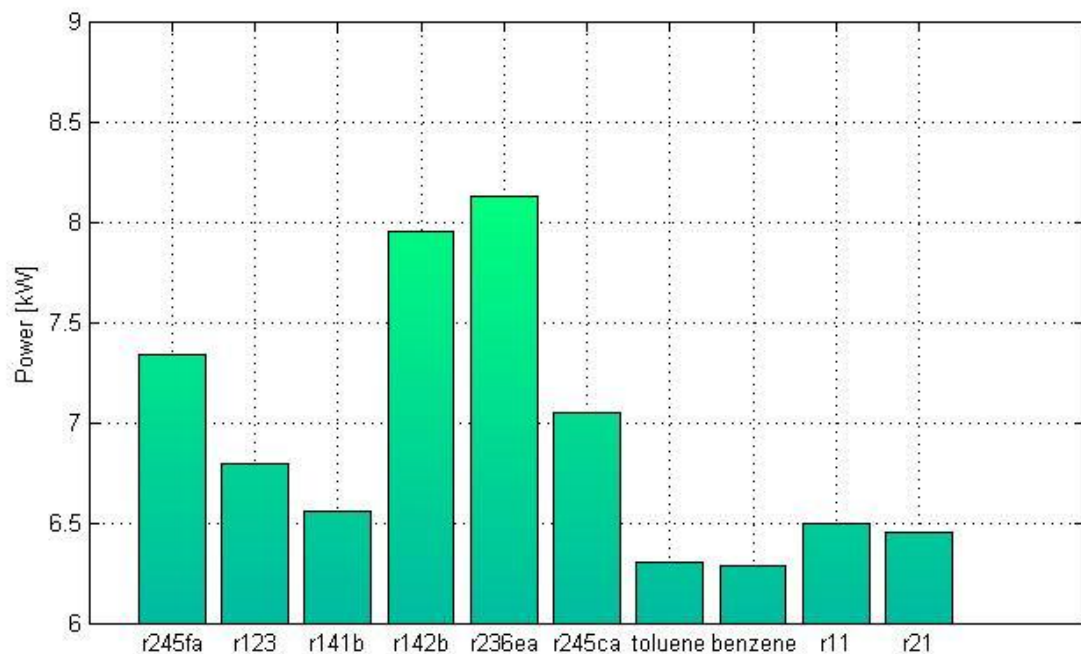


Fig. 8.21. Evaporating temperature and pressure for different fluids with variable heat load.

The operating pressure has an opposite effect on the net power output because the higher the pressure ratio the higher the enthalpy drop in the expander. As shown in Fig. 8.22 the fluids that provide the highest net power output are still r-142b and r-236ea.



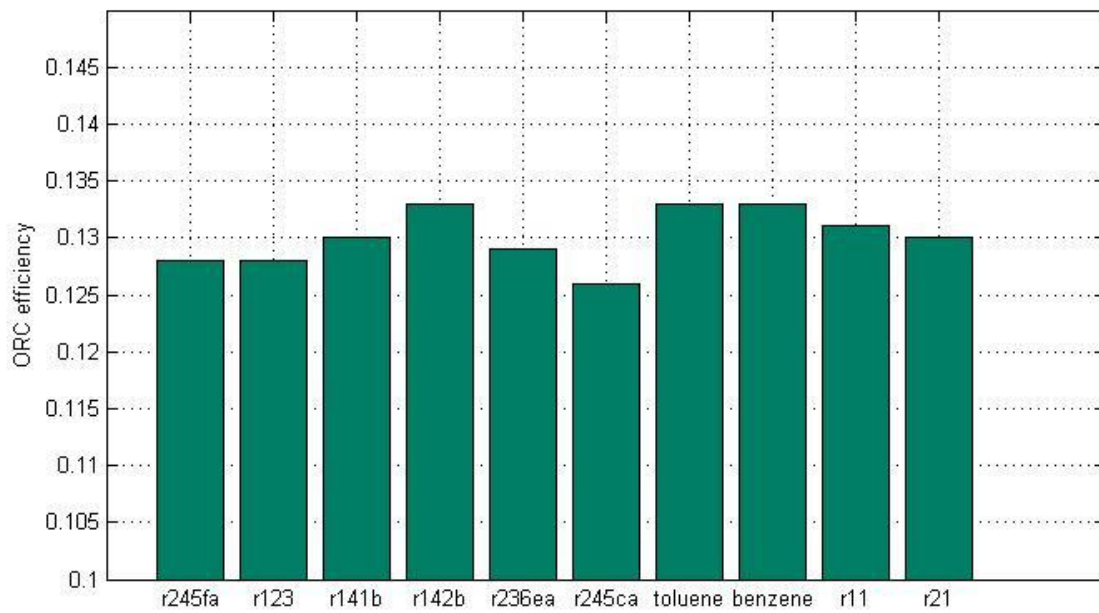
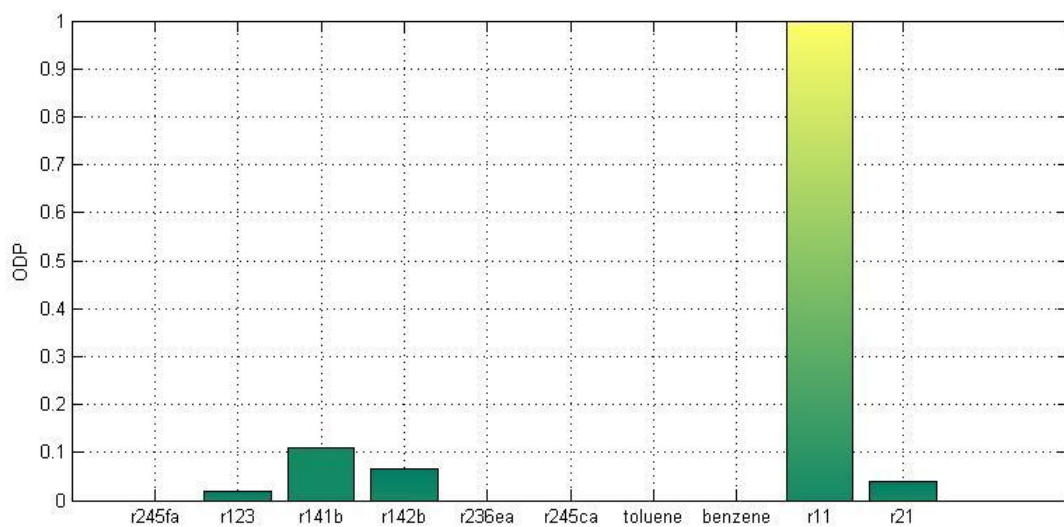


Fig. 8.22. Net power output and ORC efficiency for different fluids with variable heat load.

The Global-warming potential (GWP) is a relative measure of how much heat a greenhouse gas traps in the atmosphere. It compares the amount of heat trapped by a certain mass of a gas to the amount of heat trapped by a similar mass of carbon dioxide. A GWP is calculated over a specific time interval, commonly 20, 100 or 500 years. GWP is expressed as a factor of carbon dioxide (whose GWP is standardized to 1). Montreal and Kyoto protocol define the guideline to calculate these indexes. High values of ODP and GWP limit the choice of fluid. Fig. 8.23 shows ODP and GWP indexes of fluids considered. One can see the high values of ODP presented by r-141b and r142b. Regarding GWP(base 100 years) it is evident the high value of r142b that excludes it from the final selection.



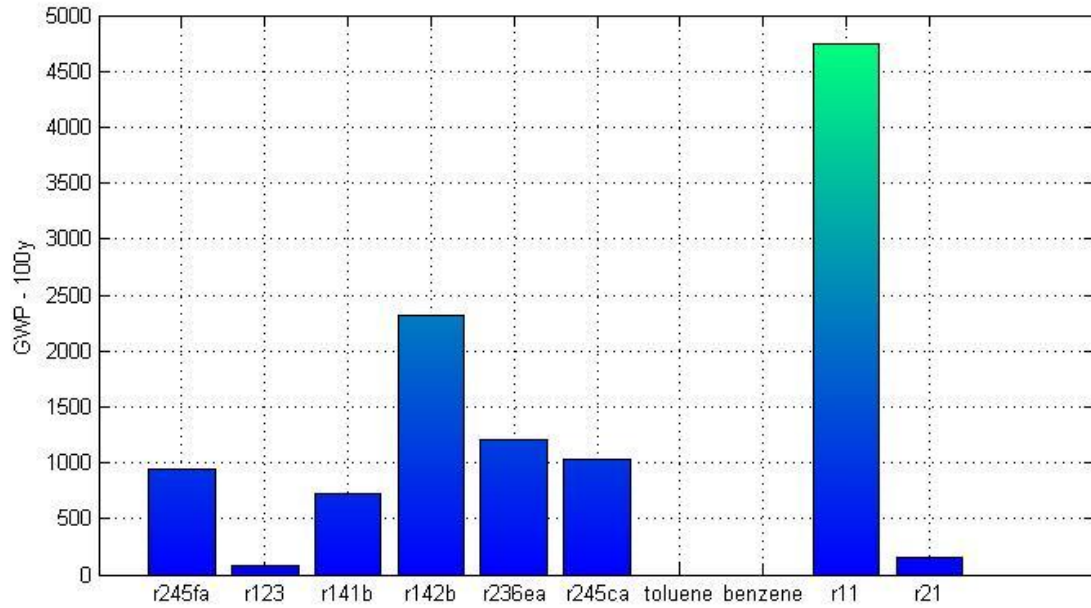


Fig. 8.23. ODP and GWP-100 for different fluids

Finally, a comparison between the entropy generation rates of each fluid is presented. The fluids with the lowest entropy generation rate are R-236ea, R-142b, R-245fa, R-245ca. These fluids have the lowest value of entropy generation rate in the evaporator. The entropy generation rate of the external process can strongly influence the total entropy generation rate. High external irreversibility occurs when high amount of hot source leaves the evaporator, as well as the cooling water leaves the condenser. One can note the high values of entropy generation rate in the expander and pump caused by the high pressure ratio.

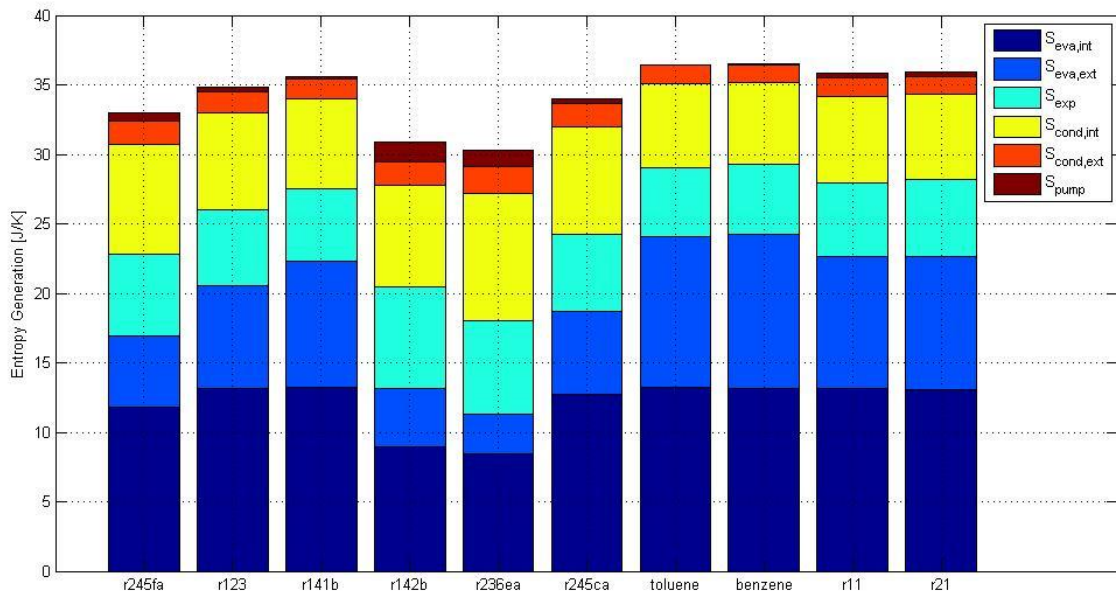


Fig. 8.24. Entropy generation for different fluids with variable heat load.

In order to perform the optimization of evaporator and economizer it is necessary to choose the fluids that fit better with the heat source boundary conditions. A trade-off between the previous considerations is required. Among all, the fluids that provide the best performance (in terms of power output and entropy generated) and the lowest environmental impact are:

- I. R-245fa
- II. R-236ea
- III. R-245ca

These fluids and their optimal operating conditions will be used as input of the second-level optimization. The results of the optimization are listed in *Table 8.6*.

Table 8.6. Optimal solutions for three fluids.

	R-245fa	R-236ea	R-245ca
Temperature			
T_eva [°C]	117.1	129.3	110.5
Tcond [°C]	30.0	30.0	30.0
Delta PP [°C]	10.0	10.0	10.0
T1 [°C]	25.0	25.0	25.0
T2s [°C]	25.5	25.9	25.3
T2 [°C]	26.2	26.9	25.7
T3 [°C]	117.1	129.3	110.4
T4 [°C]	117.1	129.3	110.4
T5 [°C]	44.4	49.7	48.1
T5s [°C]	53.2	57.8	57.0
T6 [°C]	30.0	30.0	30.0
T7 [°C]	180.0	180.0	180.0
T8 [°C]	127.1	139.3	120.4
T9 [°C]	60.3	35.8	64.3
T10 [°C]	15.0	15.0	15.0
T12 [°C]	20.6	20.8	20.6
Pressure			
Pcond [kPa]	177.78	244.36	121.66
Pcond [bar]	1.7778	2.4436	1.2166
Peva [kPa]	1819.32	2810.65	1172.40
Peva [bar]	18.1932	28.1065	11.7240
Mass flow rate			
Working fluid mass flow [kg/s]	0.235	0.325	0.213
Water mass flow [kg/s]	2.175	2.474	2.092
Heat transfer rate			
Heat flux H.E. total work. Fluid[W]	58370.61	68988.32	56564.90
Heat flux H.E. total HS[W]	58370.61	68988.32	56564.90
Heat flux ECO work. Fluid[W]	31273.47	47935.30	26190.96
Heat flux ECO heat[W]	31273.47	47935.30	26190.96
Heat flux EVA work. fluid[W]	27097.14	21053.02	30373.93
Heat flux EVA heat source[W]	27097.14	21053.02	30373.93
Heat flux cond. work. fluid[W]	50816.55	60150.94	49374.83
Heat flux condenser water[W]	50814.91	60147.72	49372.98
Power			

Pump power[W]	479.11	973.75	269.65
Expander power[W]	8033.18	9811.12	7459.72
Net power output[W]	7554.07	8837.37	7190.06
Performance index			
ORC efficiency	0.129	0.128	0.127
epsilon	0.778	0.942	0.749
System efficiency	0.101	0.120	0.095
Entropy generation rate			
S_eva_i sensible [J/(s/K)]	5.38	2.87	5.16
S_eva_i latent[J/(s/K)]	5.89	3.65	7.39
S_eva_i [J/(s/K)]	11.28	6.53	12.55
S_eva_e [J/(s/K)]	4.78	1.04	5.65
S_exp [J/(s/K)]	6.24	7.50	5.72
S_cond_i [J/(s/K)]	7.63	9.38	7.55
S_cond_e [J/(s/K)]	1.69	2.07	1.65
S_pump [J/(s/K)]	0.64	1.30	0.36
S_gen [J/(s/K)]	32.25	27.83	33.50

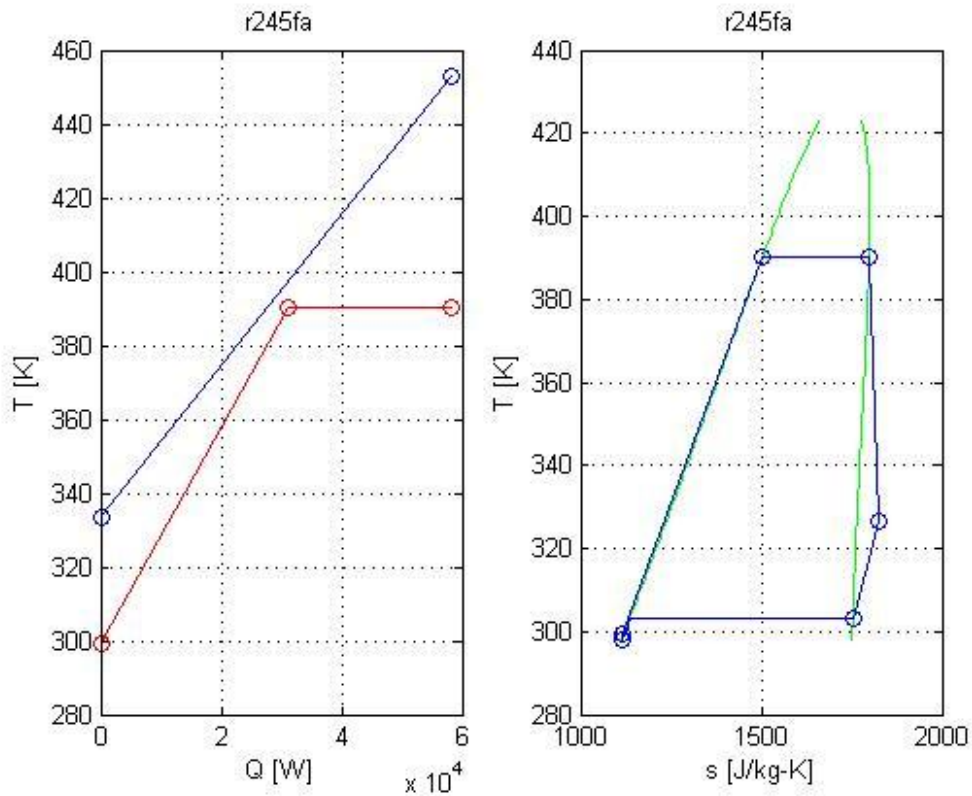


Fig. 8.25. Optimal cycle for r245fa

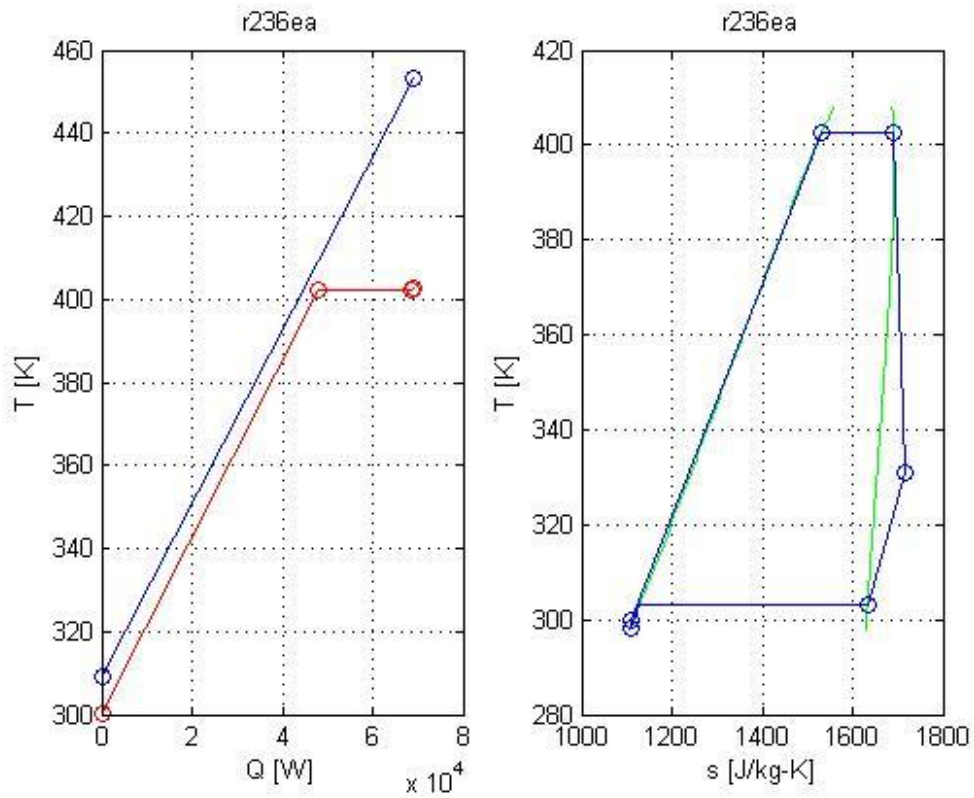


Fig. 8.26. Optimal cycle for r236ea

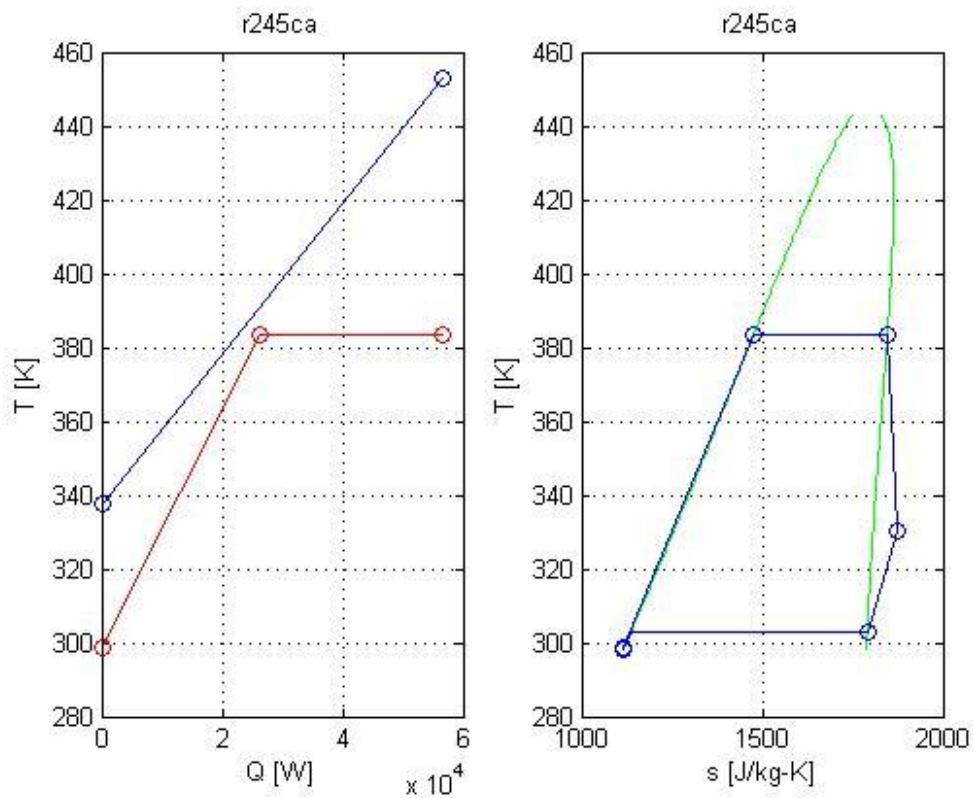


Fig. 8.27. Optimal cycle for r245ca

9 Multi Objective Optimization of STHE

9.1. Multi-Objective Optimization of Shell and tube Heat Exchanger

Shell and tube heat exchangers are the most widespread and commonly used heat exchanger configuration in the process industries. In fact, shell and tube heat exchangers provide large ratio of heat transfer area to volume and weight and they can be constructed in a wide range of sizes in order to satisfy a great variety of operating conditions. Furthermore, there are many modifications of the basic configuration, which can be used to solve special problems. The shell and tube heat exchanger can be easily cleaned, and the components most subjected to failure such as gasket and tubes can be easily replaced. Finally, an accurate design method exists and a multi-objective optimization may be applied to optimize the performance of the system.

9.2. Design problem formulation

The aim of the work is the optimization of shell and tube heat exchanger for ORC application. The optimization of the geometry of shell and tube heat exchangers is not trivial. There is a competition between the heat transfer and the pressure drop aspects. In fact, a geometry that minimizes the heat transfer surface could lead to a strong increase of the pressure drop, hence a higher pumping power. Furthermore, the working fluid and the operating conditions (temperatures and pressures) play a key role in the system performances. The procedure for the design problem can be summarized with the following steps:

- A. For given heat transfer duty (\dot{Q}) and fluid streams inlet temperatures, compute the outlet temperatures using overall energy balances and fluid mass flow rates specified. If outlet temperatures are given, the heat duty requirement can be computed.

$$\dot{Q} = \dot{m}_h c_{p,h} (T_{h,in} - T_{h,o}) = \dot{m}_c c_{p,c} (T_{c,o} - T_{c,in}) \quad (9.1)$$

- B. Select a shell inside diameter, tube diameter, tube pitch, layout, baffle spacing, baffle cut, number of passes and fluid arrangement. Calculate the number of tubes.

- C. Applying the Bell-Delaware method, the heat transfer coefficient on shell side can be calculated. Tube side heat transfer coefficient is computed with the Dittus-Boelter correlation (but other correlations could be used).

$$U = \left[\frac{1}{\alpha_s} + \frac{1}{h_s} + \frac{d_o \ln(d_o/d_i)}{2k_w} + \frac{1}{h_t} \frac{d_o}{d_i} + \frac{1}{\alpha_t} \frac{d_o}{d_i} \right]^{-1} \quad (9.2)$$

- D. For a shell and tube heat exchanger, the heat transfer area can be estimated by the following relation as described in chapter 5:

$$A = \frac{\dot{Q}}{U \Delta T_{lm} F_t} \quad (9.3)$$

$$\Delta T_{lm} = \frac{(T_{h,in} - T_{c,o}) - (T_{h,o} - T_{c,in})}{\ln \left(\frac{T_{h,in} - T_{c,o}}{T_{h,o} - T_{c,in}} \right)} \quad (9.4)$$

- E. The length of the tubes L is not known *a priori* because the total surface area A is not initially known. A value of L has to be guessed initially for estimating the heat transfer area and afterwards it is updated with the expression:

$$L = \frac{A}{\pi d_o N_t} \quad (9.5)$$

The new value of L is used to calculate heat transfer coefficient and pressure drop until convergence. Therefore, an iterative procedure is required to determine L and A .

In order to optimize the design procedure a multi-objective optimization has been carried out. Multi objective optimization minimizes several objective functions simultaneously, with a number of inequality or equality constraints. It can be mathematically expressed as follows:

$$\min f(x) = [f_1(x), f_2(x), \dots, f_n(x)], \quad x \in X \quad (9.6)$$

Subject to

$$g_j(x) = 0, \quad j = 1, 2, \dots, M \quad (9.7)$$

$$h_k(x) \leq 0, \quad k = 1, 2, \dots, K \quad (9.8)$$

Where x is a vector and is also called the decision vector because it contains the decision variables and X is the parameter space. If and only if, $f_i(x) \leq f_i(y)$ for $i = 1, 2, \dots, n$ and $f_j(x) < f_j(y)$ for least one objective function j , a feasible solution x is said to dominate another feasible solution y . A solution that is not dominated by another solution in the feasible region is called Pareto optimal solution. The set of all Pareto optimal solution forms the Pareto optimal set whereas the values of the objective functions related to the Pareto optimal set are called Pareto front. The performance evaluation criteria for heat exchanger are generally based on the first law of thermodynamics but, recently, the entropy generation minimization (EGM) suggested by Bejan has attracted a lot of attention. Furthermore, a cost optimization can be carried out in order to evaluate the influence of geometrical parameters, working fluid and operating conditions on total annual cost. The objective functions of the optimization design of a shell and tube heat exchanger can be several:

- Heat transfer area, volume or weight
- Pressure drop

- Entropy generation
- Total annual cost

In this work different case studies are proposed in order to achieve a good sensibility in the heat exchanger design. The algorithm used to perform multi-objective optimization is a genetic algorithm.

9.3. Test case and validation

In order to validate the model a test case is carried out. The starting point is the example 9.4 of Shah and Sekulic, Fundamentals of Heat Exchanger Design[8]. In order to demonstrate the usefulness of GA for determining the optimal design for a specified process, the geometry of a shell and tube heat exchanger was optimized under the process requirements found in *Table 9.1*.

Table 9.1.

	Hot Fluid	Cold Fluid
Fluid	Oil	Water
Inlet Temperature [°C]	65.6	37.4
Outlet Temperature [°C]	60.4	32.2
Mass Flow Rate [kg/s]	36.3	18.1
Fouling Resistance [m ² K/W]	0.000176	0.000088
Tube Material	Cu-Ni	
Type of shell and tube heat exchanger	TEMA E heat exchanger	

Table 9.2.

Fluid	Density ρ [kg/m ³]	Specific heat c_p [J/kg · K]	Dynamic viscosity μ [Pa · s]	Thermal conductivity k [W/m ² · K]	Prandtl Number Pr
Oil at 63°C	849	2094	64.6×10^{-3}	0.140	966
Water at 35°C	993	4187	0.723×10^{-3}	0.634	4.77

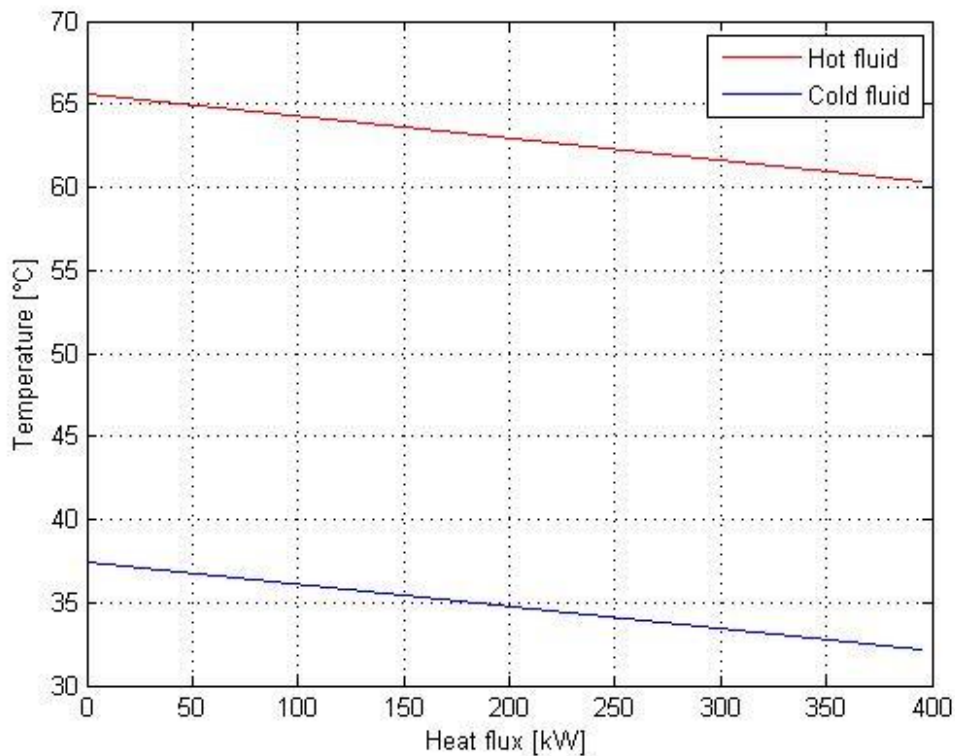


Fig. 9.1. Temperature profiles

The geometry of the heat exchanger proposed in the example is presented in Table 9.3.

Table 9.3.

Shell diameter D_s [m]	0.336
Tube outer diameter d_o [mm]	19.0
Baffle spacing at the center $L_{b,c}$ [mm]	0.279
Baffle spacing at the inlet and outlet $L_{b,o} = L_{b,o}$	0.318
Baffle cut l_c [mm]	86.7 or 25%
Tube pitch p_t [mm]	25.0
Layout of the tubes	45°
Fluid side	<i>Oil – shell side/ Water – tube side</i>
Tube material	<i>admiralty (70% Cu, 30% Ni)</i>
Thermal conductivity of tube wall [$W/m^2 \cdot K$]	111
Total number of tubes	102
Tube length [m]	4.3
Number of tube passes	2
Diameter of the outer tube limit [m]	0.321
Tube to baffle hole diametral clearance [mm]	0.794
Shell to baffle hole diametral clearance [mm]	2.946

Assuming the design parameters described above, it is possible to obtain the results listed in Table 9.4. The results obtained by the algorithm are closed to the results of the example presented. Table 9.4 and figure 9.2 show the results of the algorithm.

Table 9.4. Comparison between the solutions

	Example 9.4. Shah and Sekulic, Fundamentals of Heat Exchanger Design.	Model implemented	Relative error [%]
Heat flux [kW]	393.600	395.263	0.4225
Heat transfer coefficient – shell side [$W/m^2 \cdot K$]	698.80	699.24	0.0714
Pressure drop – shell side [kPa]	112.000	111.920	0.0630
Heat transfer coefficient – tube side [$W/m^2 \cdot K$]	7837.0	7803.0	0.4338
Pressure drop – tube side [kPa]	17.580	18.071	2.7929
Overall heat transfer coefficient [$W/m^2 \cdot K$]	536.10	536.16	0.0112
Heat transfer area [m^2]	26.180	25.910	1.0313
Total pressure drop [kPa]	129.58	129.21	0.2855
Tube length [m]	4.30	4.26	0.9302

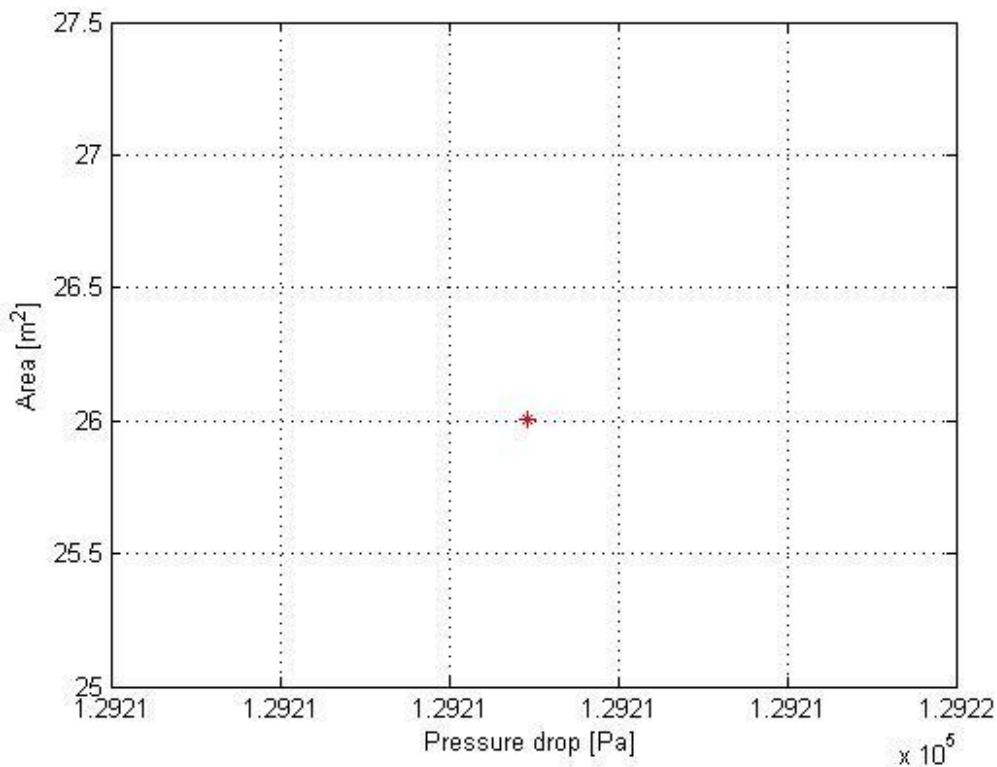


Fig. 9.2. Initial solution – A vs. Pressure drop

9.3.1. Optimal solutions

With an appropriate model in hand to assess the effect of the heat exchanger geometry on its performance, it is possible to optimize the heat exchanger. As the number of geometrical features taken into account increases, so does the total number of possible heat exchanger configuration to be considered. Therefore, only with a genetic algorithm it is possible to find rapidly the optimal solution.

The problem explained before can be solved using multi-objective genetic algorithm. The design variables are can vary as described in *Table 9.5*.

Table 9.5.

Decision Variable	Range of values
D_s [mm]	300 ÷ 500
d_o [mm]	15,87 ÷ 63,5
$L_{b,c}$	$0,7D_s ÷ 0,9D_s$
$L_{b,i}$	$1,0B_c ÷ 1,2B_c$
Baffle cut – l_c	25% ÷ 45%
p_t [mm]	$1,25d_o ÷ 1,5d_o$
Layout	30°, 45°, 60°, 90°

As shown in *Fig. 9.3*, the total region is divided into two regions by the Pareto optimal set. The design points with heat transfer area and pressure drop located above the PF are feasible, but not optimal. The ones in the region II are infeasible. Therefore, the solution in Pareto set is optimal in the sense that its heat transfer area and pressure drop achieves the minimum values under the design requirements and constraints. It is important to note that normally the optimal solution for the multi-objective optimization design is not unique. The designer can select one from the Pareto set according to the specific design requirements. Therefore, the multi-objective optimization design of heat exchanger is more flexible than a single objective optimization design. It can be seen the location of the initial solution indicated by the blue star. The effect of the optimization technique is evident. In fact, in order to achieve the same area of 26 m², the pressure drop is reduced to 40 kPa.

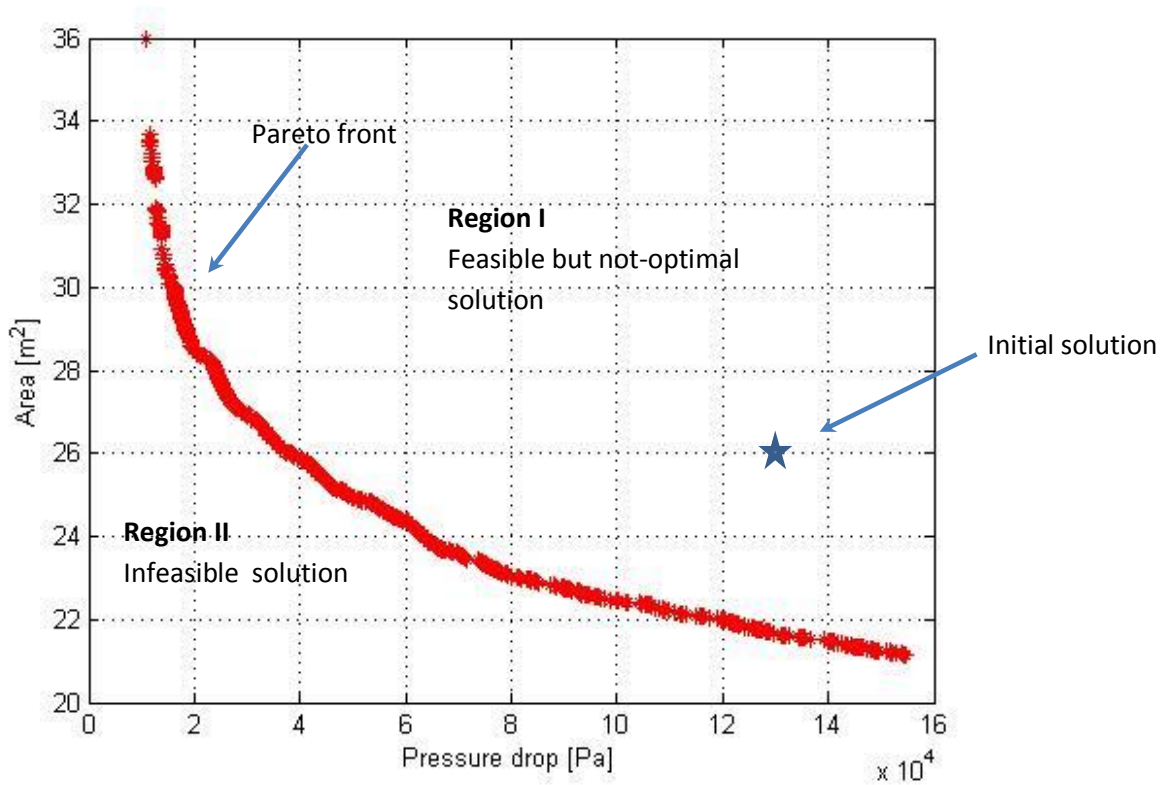
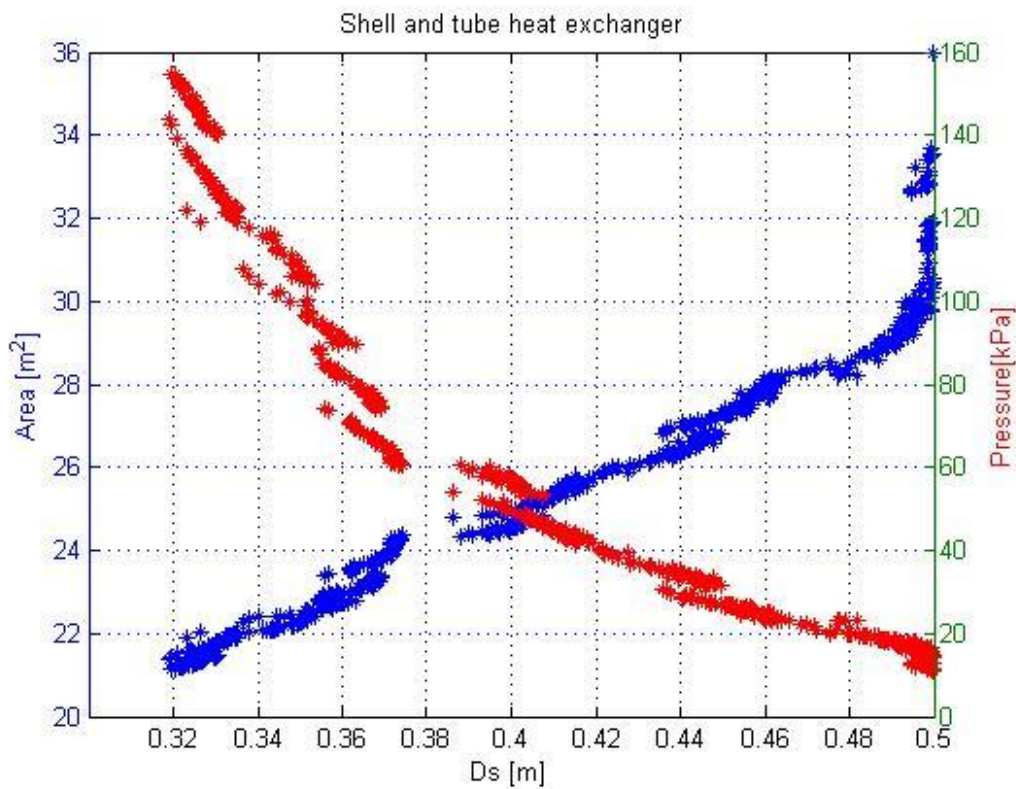


Fig. 9.3. Pareto front – Area vs. Pressure drop

The influence of the design variables on heat transfer area and pressure drop are shown in *figure 9.4*. It can be seen in *Fig. 9.4* that the higher the shell diameter the lower the pressure drop. On the other hand, the higher the shell diameter, the higher the heat transfer area. Furthermore, it can be noted that the design point with heat transfer area equals to 24 m^2 and pressure drop of 60 kPa corresponds to the intersection of the trends in *figure 9.4*. This is one of the closest points of Pareto optimal set to the ideal solution (heat transfer area=0, pressure drop=0). The behavior of the baffle spacing and baffle cut are similar. In fact, as shown in *Fig 9.5*. and *9.6*, the larger the baffle spacing, the lower the fluid velocity, hence the lower the heat transfer coefficient. Further, the smaller the heat transfer coefficient, the higher the heat transfer area. Similarly, the higher the baffle spacing, the lower the fluid velocity, hence the lower the pressure drop. Similar considerations can be done in order to describe the effect of baffle cut.

The effect of baffle spacing at inlet and outlet does not seem to have influence on heat transfer area and pressure drop. Even if it is not shown, tube pitch influences the number of tubes inside the shell. The selection of tube pitch is a compromise between a close pitch and an open pitch. Close pitch (small values of p_t/d_o) increases shell-side heat transfer and surface compactness. On the other hand, open pitch (large values of p_t/d_o) decreases shell-side plugging and ease in shell-side cleaning. Usually, Tube pitch p_t is chosen so that the pitch ratio is $1.25 < p_t/d_o < 1.5$.



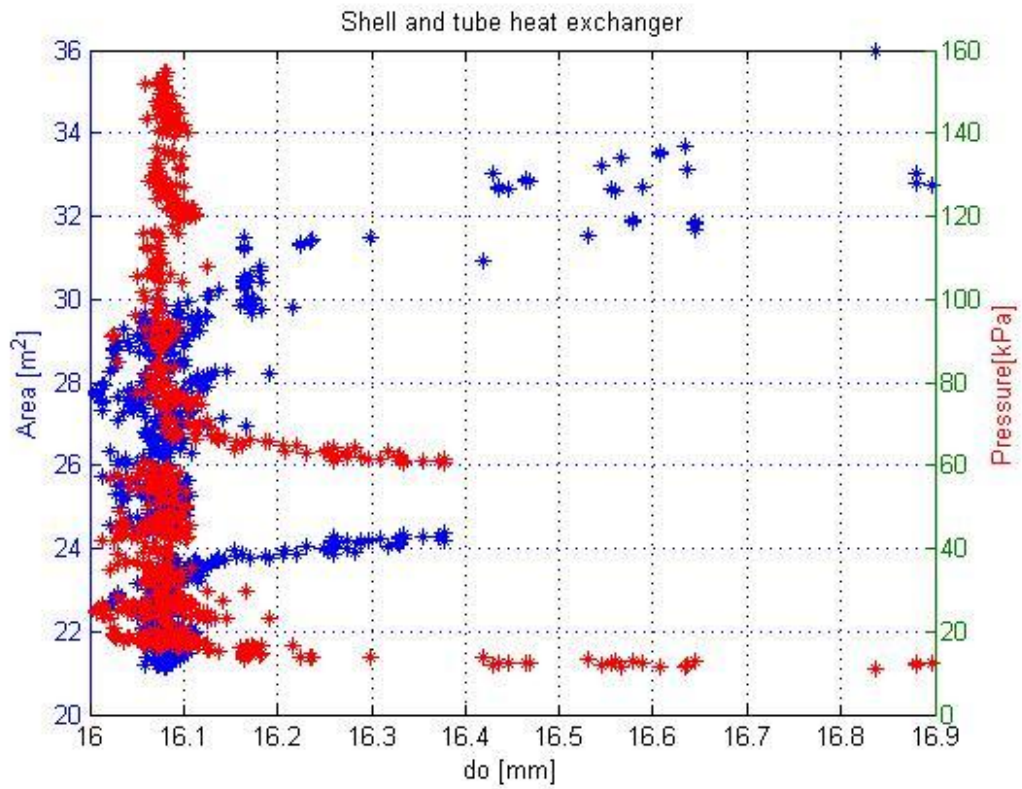
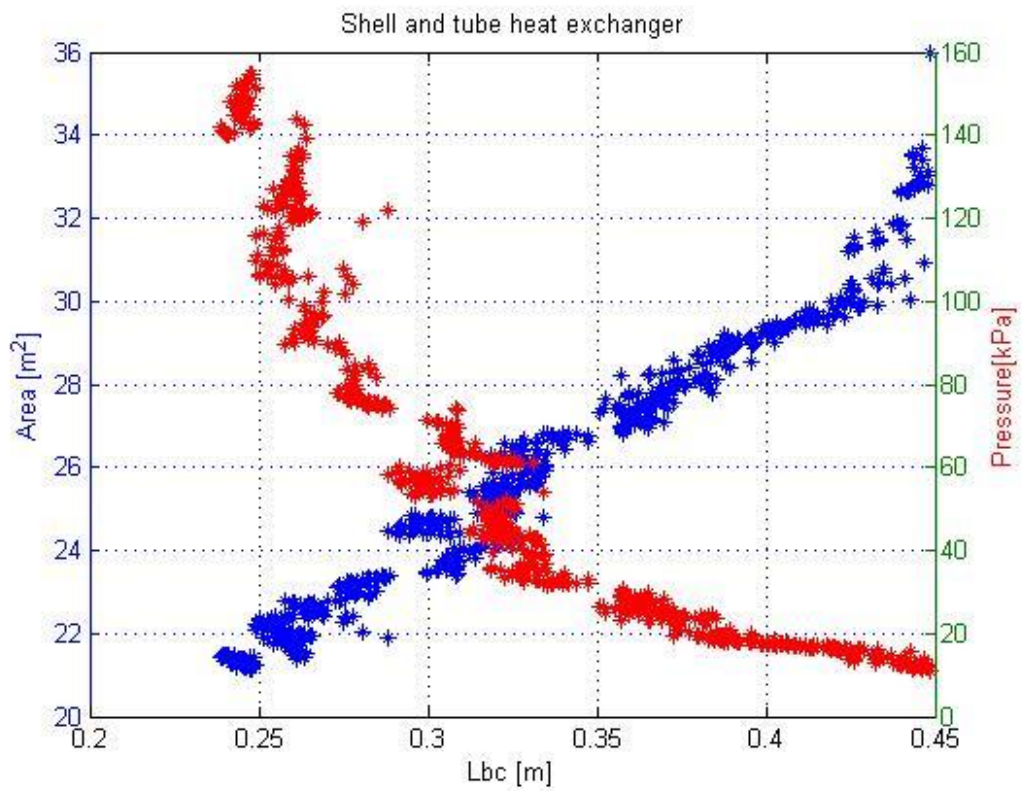


Fig. 9.4. Influence of D_s and d_o on objective functions



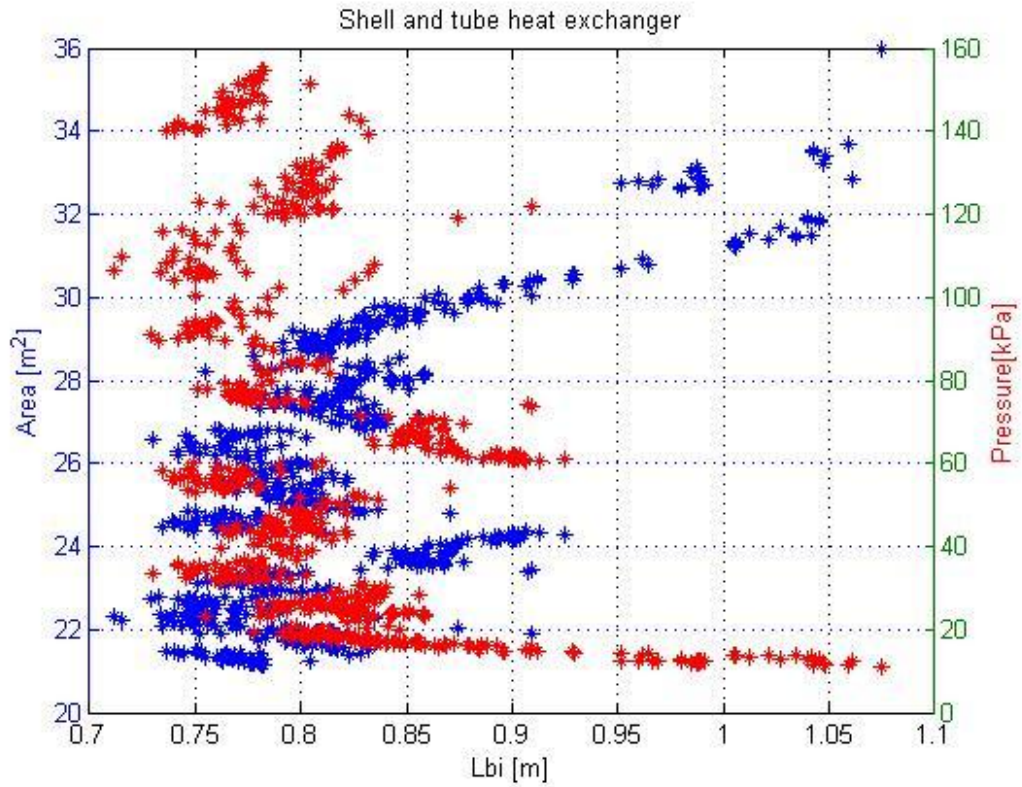
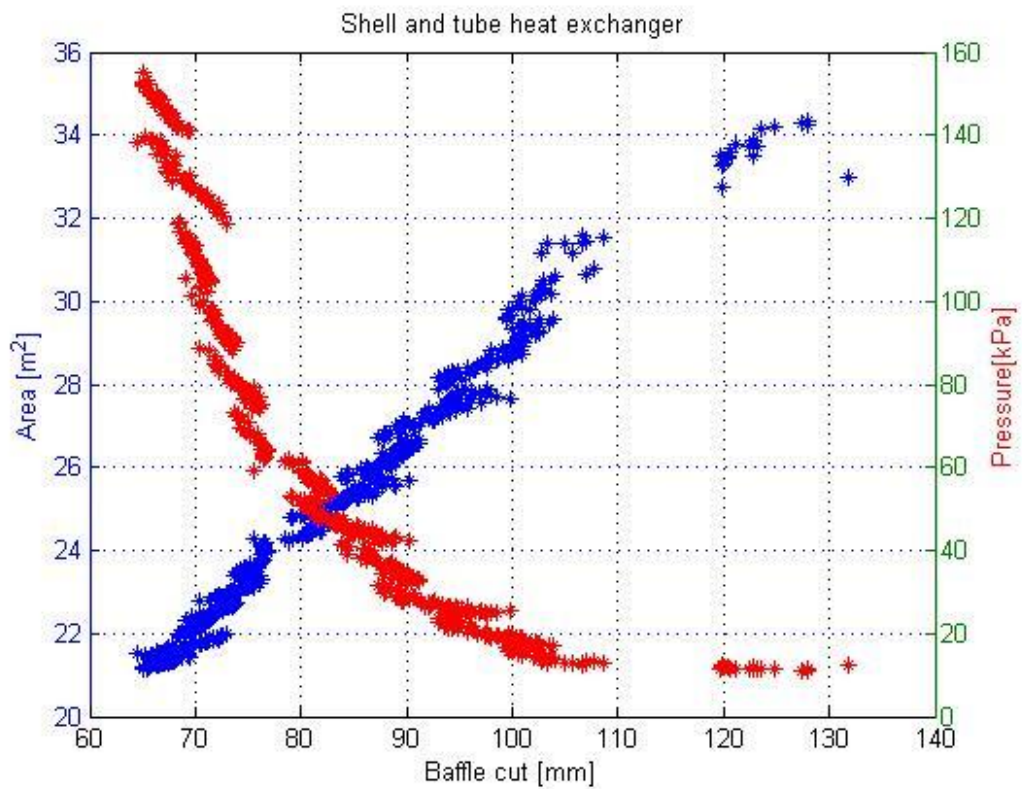


Fig. 9.5. Influence of Lbc and Lbi on objective functions



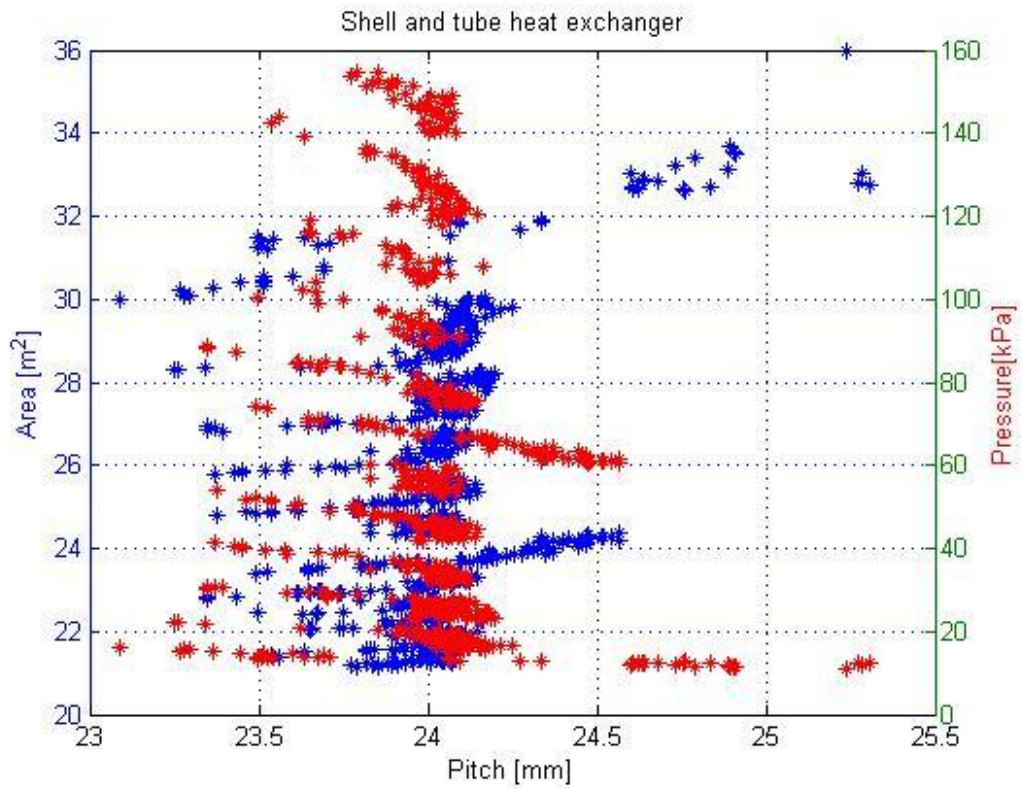


Fig. 9.6. Influence of Baffle cut and pitch on objective functions

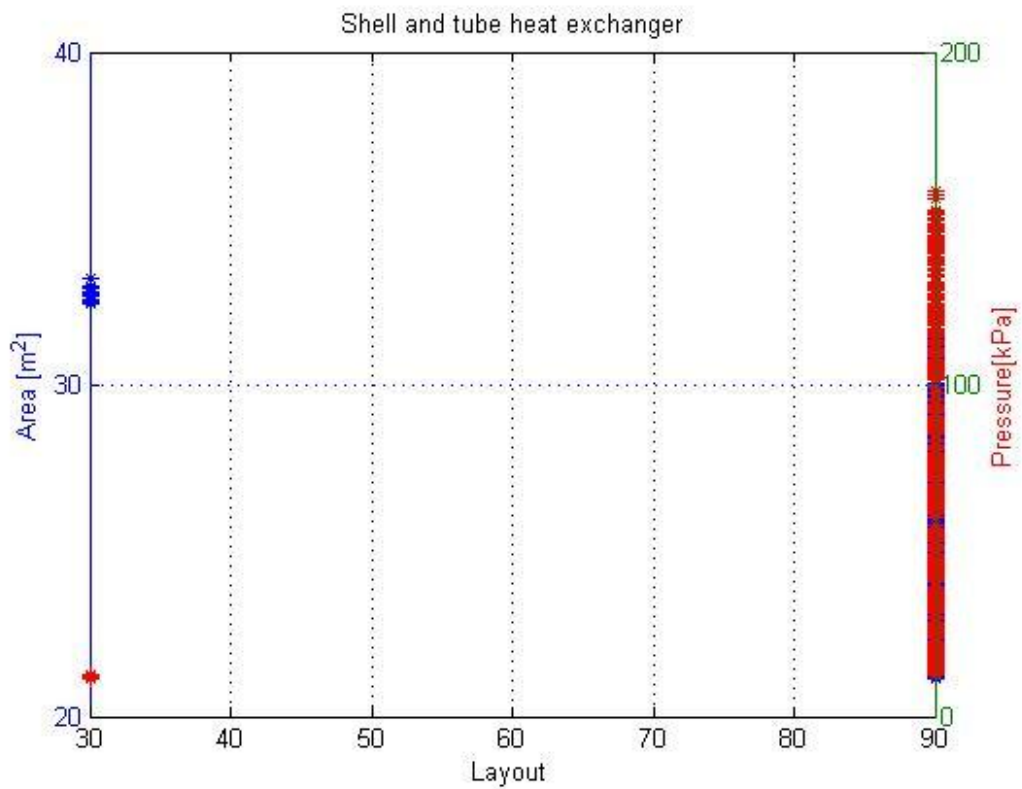


Fig. 9.7. Influence of tube layout on objective functions

The number of tubes can be calculated as a consequence of shell diameter, tube pitch and outer tubes diameter. The influence of this number is shown in *Fig 9.8*. Because tube diameter and pitch length have small range of variability, the effect on heat transfer area and pressure drop is similar to the one of shell diameter. One of the most important parameters to consider is the fluid velocity that must be inside a specific range. The velocity must be high enough to prevent any suspended solids settling, but not so high as to cause erosion. Furthermore, high velocities will reduce fouling. High velocities will give high heat-transfer coefficients but also high-pressure drop. Generally, shell side velocity must be greater than 0.2 and lesser than 1.2 m/s. Tube side velocity must be greater than 1 m/s and lesser than 2 m/s.

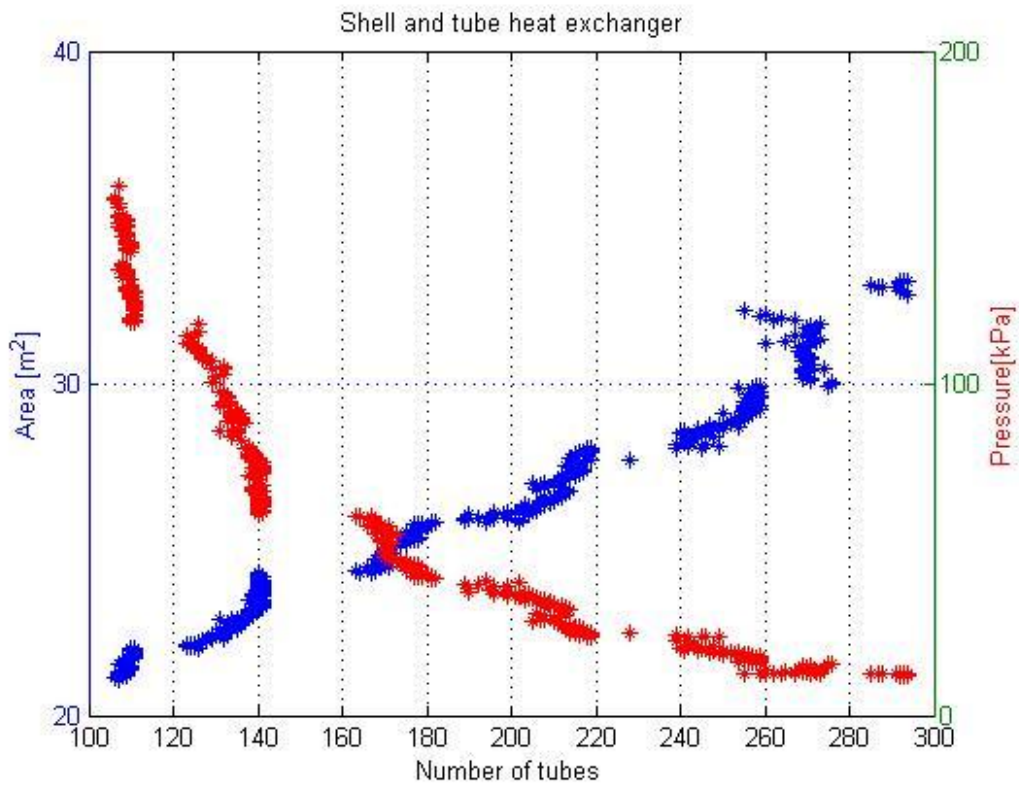


Fig. 9.8. Influence of number of tubes on objective functions.

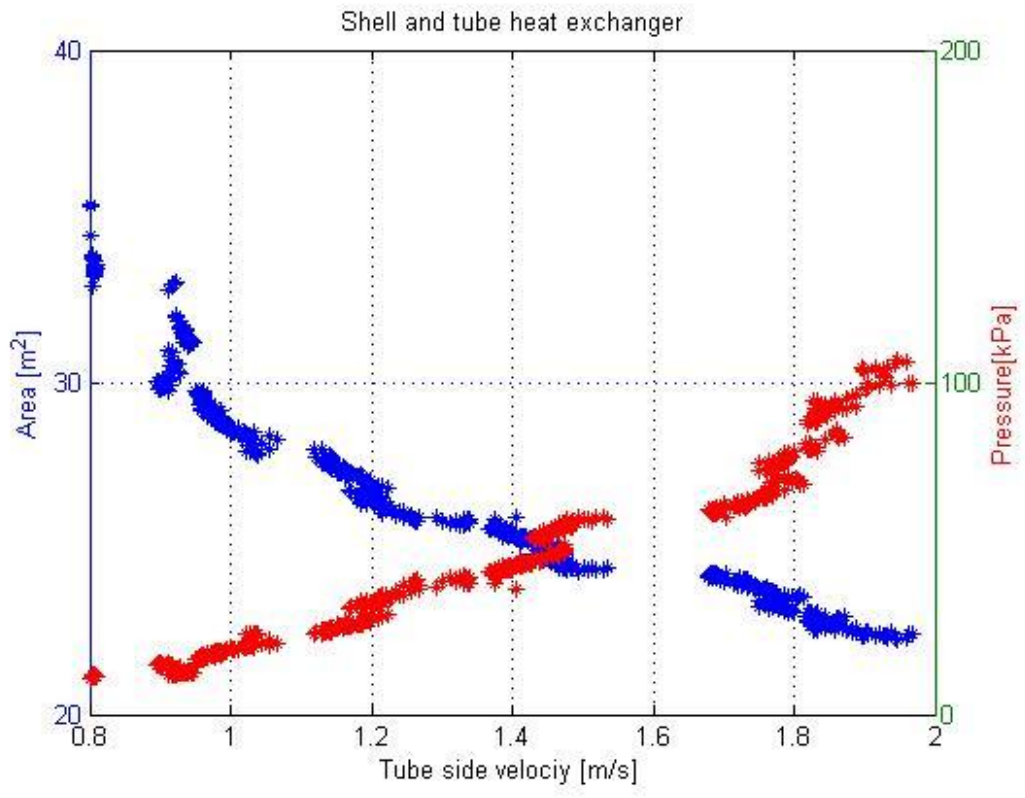


Fig. 9.9. Fluid velocity on tube side.

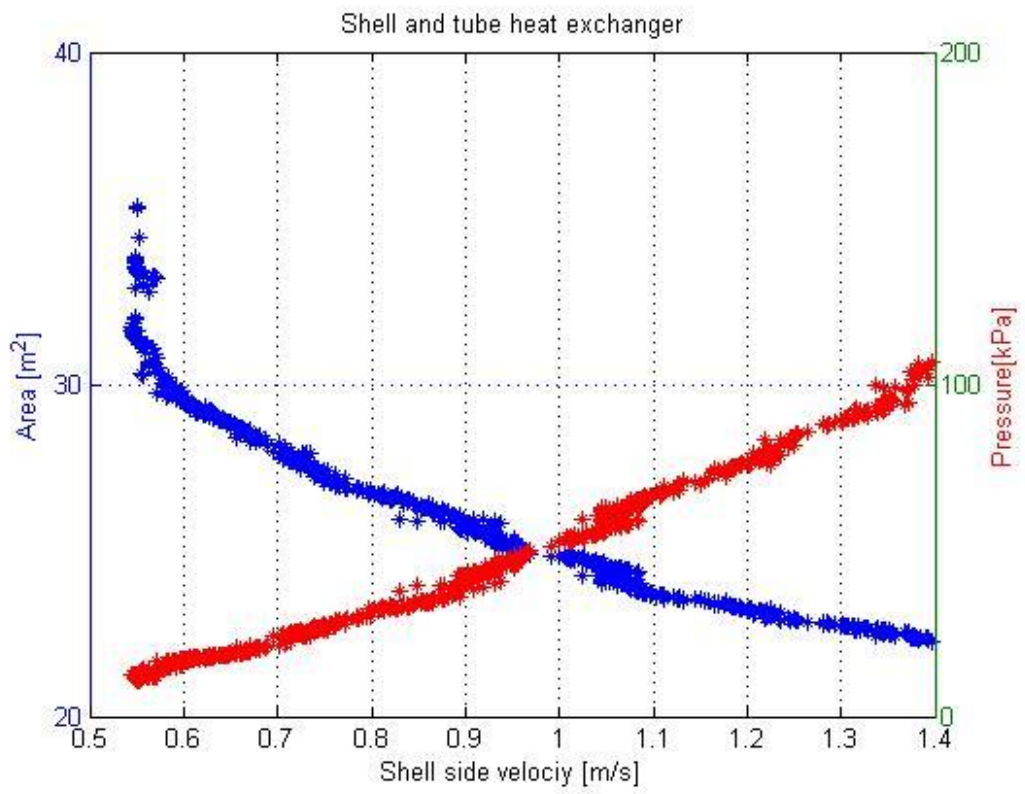


Fig. 9.10. Fluid velocity on shell side.

9.4. Multi objective optimization of economizers for organic Rankine cycle

In this section a real case of study [23] is considered. The aim of the problem is to design a shell and tube heat exchanger for an organic Rankine cycle. The heat exchanger is an economizer with the following requirements:

Table 9.6.

	Hot Fluid	Cold Fluid
Fluid	Dowtherm Q	Cyclopenthane
Inlet Temperature T_{in} [°C]	193.01	115.14
Outlet Temperature T_{out} [°C]	129.96	178.01
Mass Flow Rate [kg/s]	49.26	39.77
Fouling Resistance [m^2K/W]	0.0002	0.0002
Tube Material	Stainless Steel	
Heat Flux [kW]	6441.845	-6441.845
Stream side	Tube	Shell

The first consideration regards the general arrangement of the heat exchanger. The first screening takes into account the number of tube and shell passes, the tube layout and the hot fluid side. The screening can be done using the correction factor for the logarithmic mean temperature method based on *equations 9.3 and 9.4*.

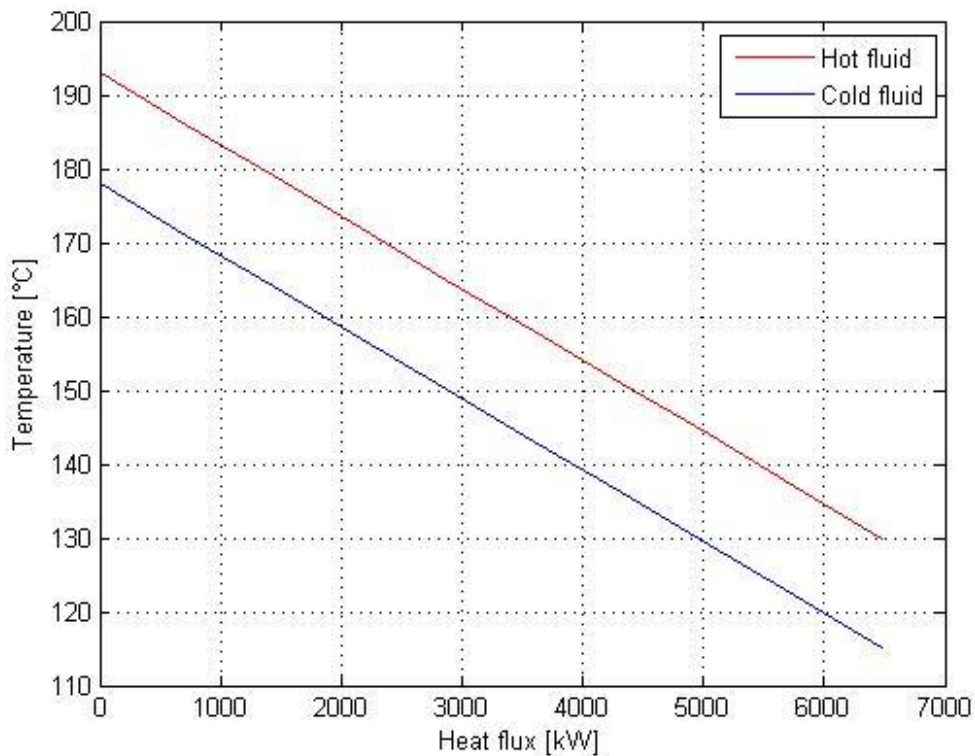


Fig. 9.11. Temperature profiles of the economizer

The following assumptions are made in the derivation of the temperature correction factor F_t , in addition to those made for the calculation of the log mean temperature difference:

1. Equal heat transfer areas in each pass.
2. A constant overall heat-transfer coefficient in each pass.

3. The temperature of the shell-side fluid in any pass is constant across any cross section.
4. There is no leakage of fluid between shell passes.

An economic exchanger design cannot normally be achieved if the correction factor F_t falls below 0.75. In these cases an alternative type of exchanger should be considered which gives a closer approach to true counter-current flow. The use of two or more shells in series, or multiple shell-side passes, will give a closer approach to true counter-current flow, and should be considered where a temperature cross is likely to occur. Temperature cross is the difference between the outlet temperatures of fluids. In this case the temperature cross is very high and several shell passes are expected.

Different solutions are considered varying the number of heat exchangers used to provide the heat flux and the number of shell passes. The heat transfer rate requested can be obtained connecting two or more heat exchangers in series.

Table 9.7. Correction factor for different arrangements

NHE	N Shell Pass	Heat flux [W]	FT	Th _{out} [°C]	Tc _{in} [°C]
1.0	1.0	6441844.50	0.4018	129.96	115.14
1.0	2.0	6441844.50	0.3873	129.96	115.14
1.0	4.0	6441844.50	0.7736	129.96	115.14
2.0	1.0	3220922.25	0.3872	162.20	148.39
2.0	2.0	3220922.25	0.7772	162.20	148.39
2.0	4.0	3220922.25	0.9523	162.20	148.39
3.0	1.0	2147281.50	0.4614	172.62	158.68
3.0	2.0	2147281.50	0.9159	172.62	158.68
3.0	4.0	2147281.50	0.9801	172.62	158.68
4.0	1.0	1610461.12	0.7943	177.77	163.68
4.0	2.0	1610461.12	0.9554	177.77	163.68
4.0	4.0	1610461.12	0.9892	177.77	163.68
5.0	1.0	1288368.90	0.8804	180.85	166.62
5.0	2.0	1288368.90	0.9724	180.85	166.62
5.0	4.0	1288368.90	0.9932	180.85	166.62



The preferable solutions are indicated in table 9.7. One shell side (TEMA E) is preferable because is simpler and cheaper than one with two shell passes (TEMA F). Thus, the following solution is proposed:

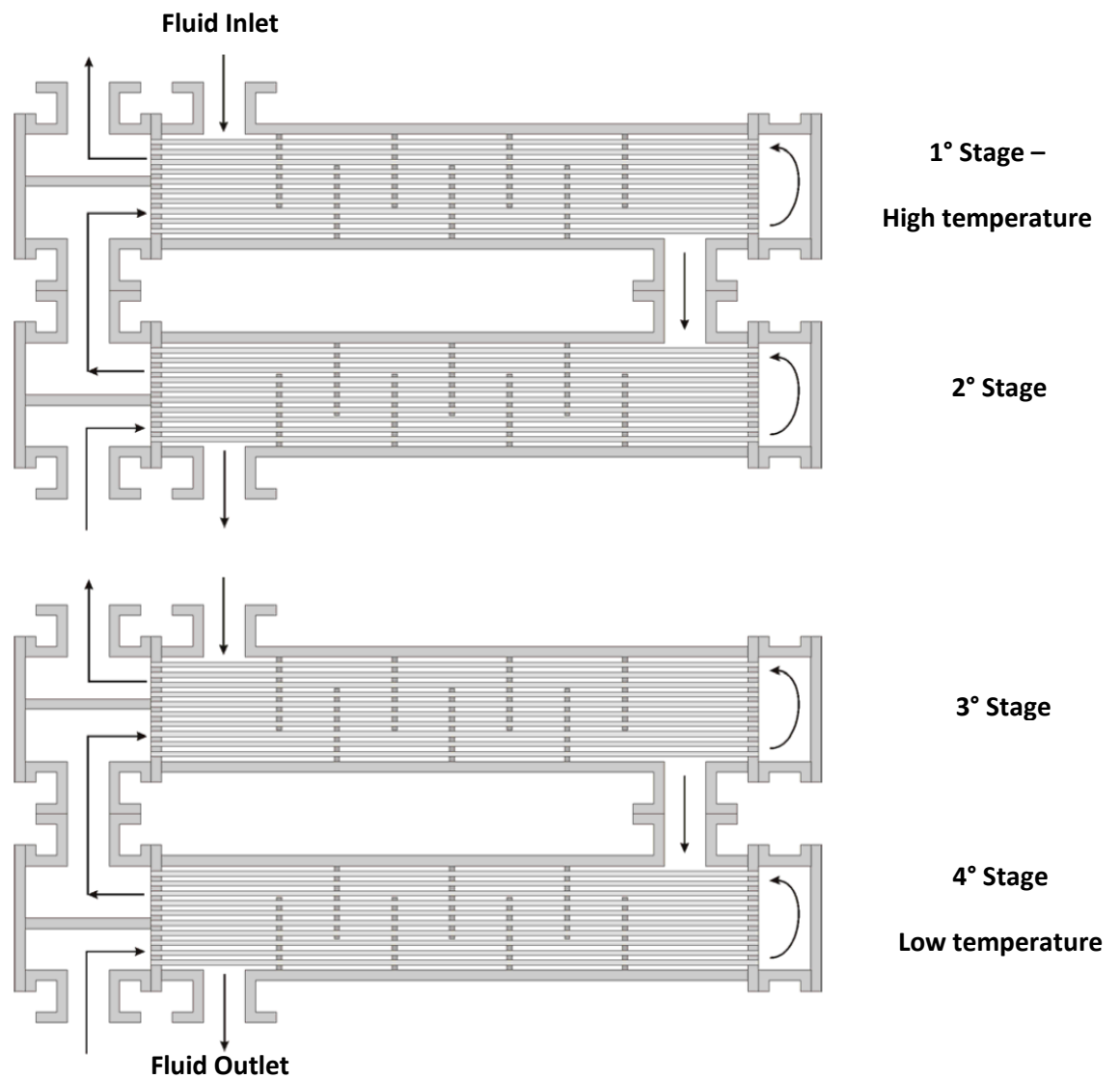


Fig.9.12 Flow arrangement. Four heat exchangers in series.

The aim of the work is to design and optimize the first stage of the series (with the highest temperatures). The other stages follow the same procedure. Different objective functions are used in order to compare the results. The requirements of the heat exchanger are listed in *table 9.8*.

Table 9.8.

	Hot Fluid	Cold Fluid
Fluid	Dowtherm Q	Cyclopenthane
Inlet Temperature T_{in} [$^{\circ}C$]	193.01	115.14
Outlet Temperature T_{out} [$^{\circ}C$]	177.77	163.68
Mass Flow Rate [kg/s]	49.26	39.77
Fouling Resistance [m^2K/W]	0.0002	0.0002
Tube Material	Stainless Steel	
Heat Flux [kW]	1610.461	1610.461
Stream side	Tube	Shell

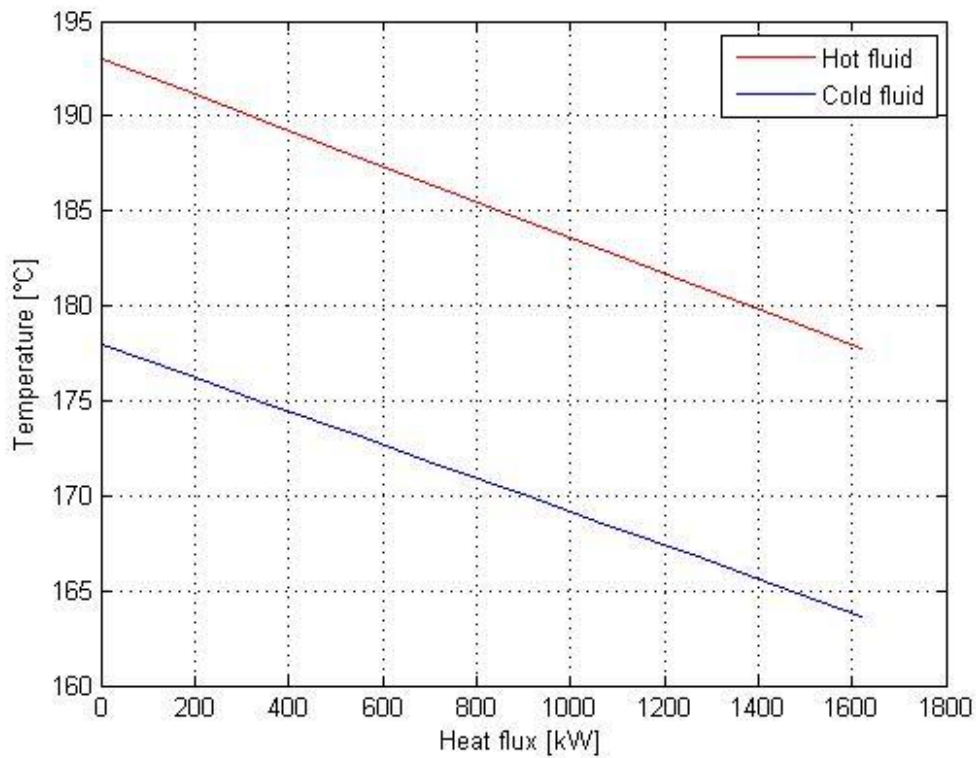


Fig. 9.13. Temperature profiles

9.4.1. Volume and pressure drop minimization

The decision variables considered in this case study are:

1. The shell diameter D_s
2. The tube outer diameter d_o
3. The baffle spacing at the center $L_{b,c}$
4. The baffle spacing at the inlet and outlet $L_{b,i} = L_{b,o}$
5. The baffle cut l_c
6. The tube pitch p_t
7. The layout of the tubes
8. Side of cold fluid

Table 9.9. Design variables and range of values.

Decision Variable	Range of values
D_s [mm]	300 ÷ 1000
d_o [mm]	15,87 ÷ 63,5
$L_{b,c}$	$0,1D_s ÷ 0,4D_s$
$L_{b,i} = L_{b,o}$	$1B_c ÷ 1,6B_c$
Baffle cut	0,25 ÷ 0,45
p_t	$1,25d_o ÷ 1,5d_o$
Layout	30°, 45°, 60°, 90°
side of cold fluid	Shell side, tube side

The objective functions are the volume and the total pressure drop:

$$f_1(x) = \frac{\pi D_s^2}{4} L_{tubes} \tag{9.10}$$

$$f_2(x) = \Delta P_{shell} + \Delta P_{tube} \tag{9.11}$$

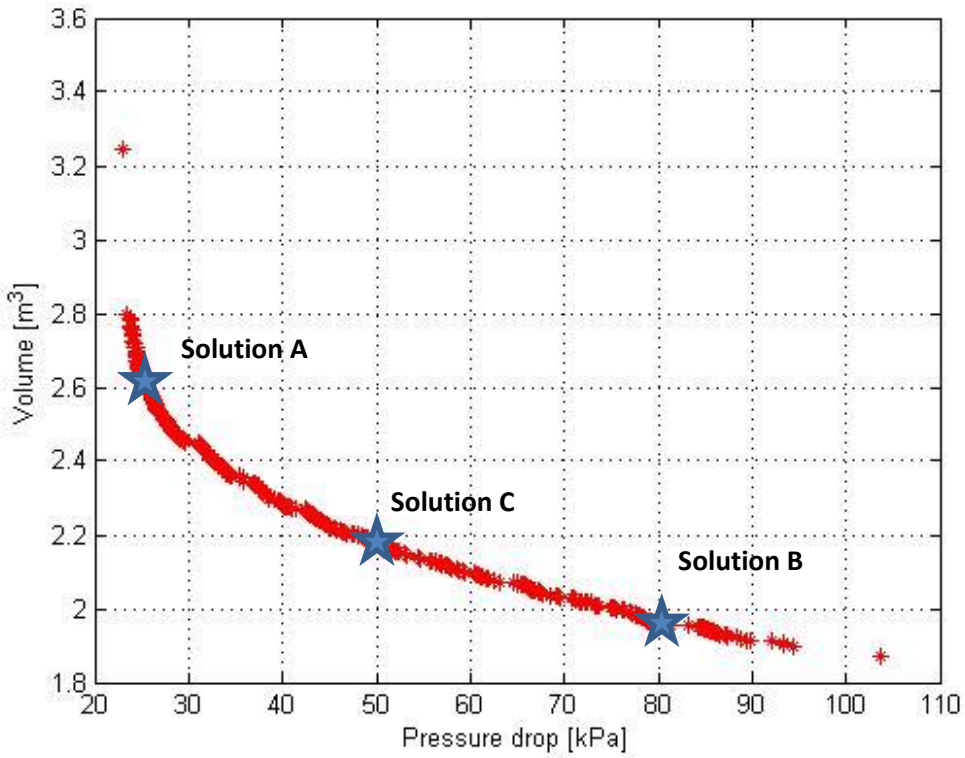


Fig. 9.14. Pareto front – Volume vs. Pressure drop

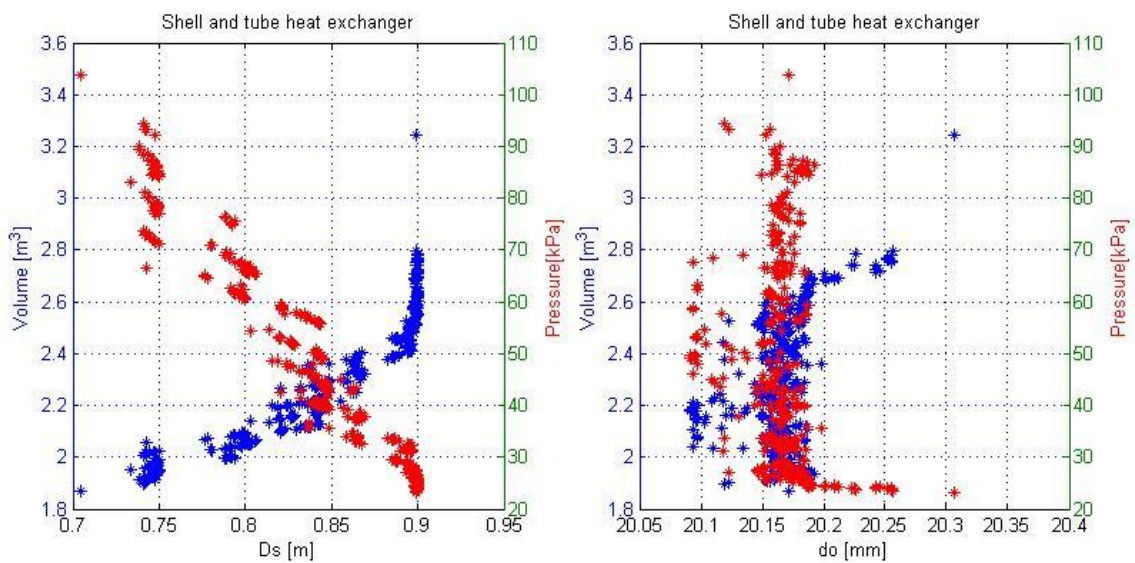


Fig. 9.15. Influence of design variables on volume and pressure drop

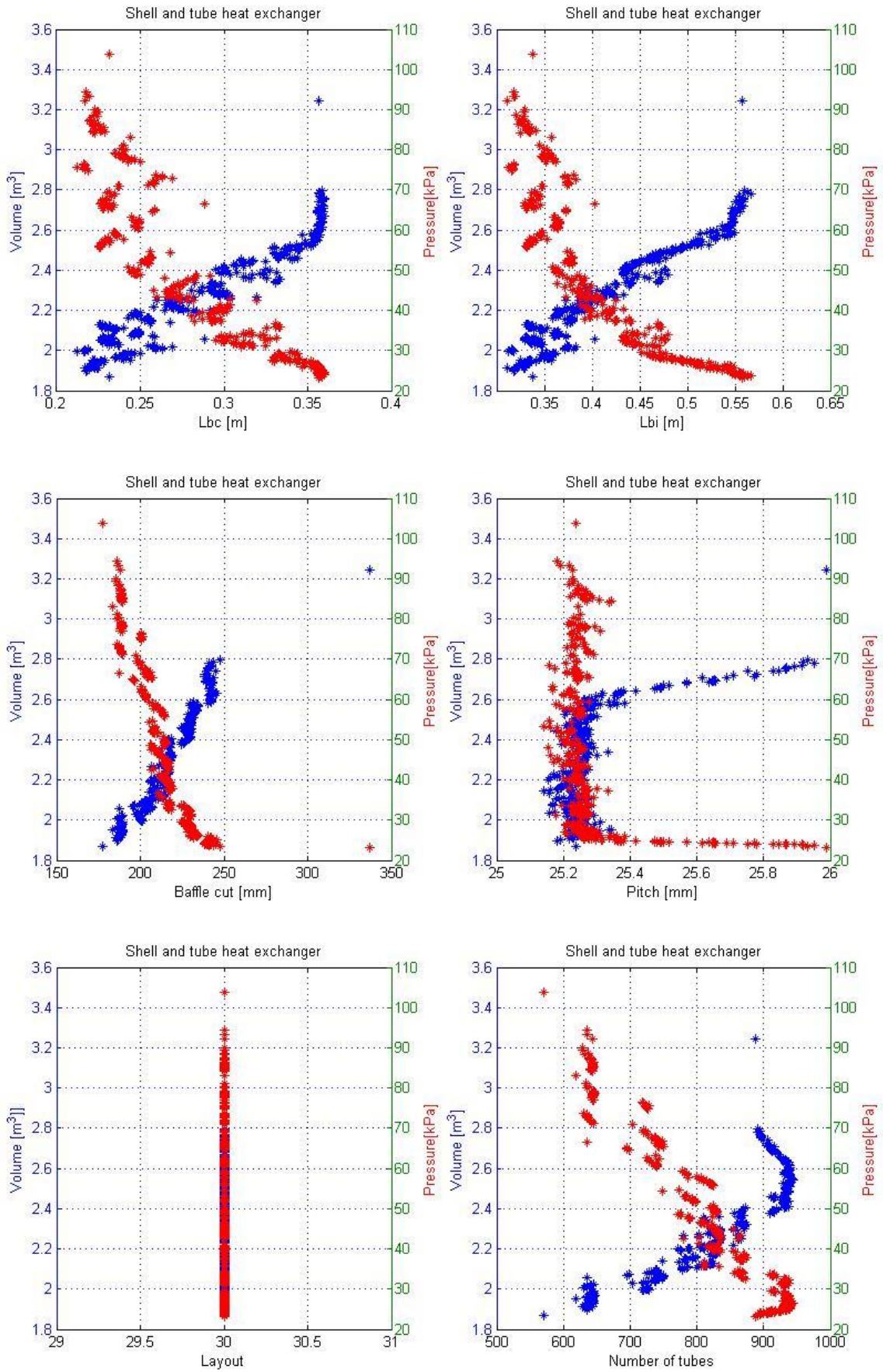


Fig. 9.16. Influence of design variables on volume and pressure drop

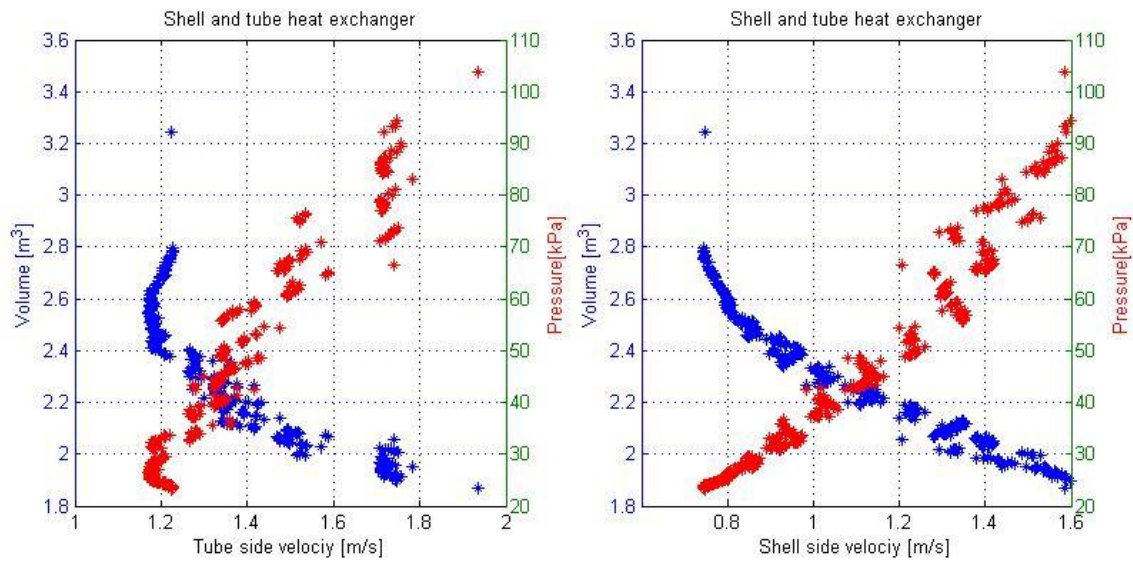


Fig. 9.17. Influence of fluid velocities on volume and pressure drop

Three possible solutions are displayed in Table 9.10.

Table 9.10. Three possible solutions

	Solution A	Solution B	Solution C
Volume [m ³]	2.685	1.976	2.161
Pressure drop[kPa]	24.507	78.415	51.475
Shell Diameter[m]	0.899	0.748	0.829
Tube outer diameter[m]	0.020	0.020	0.020
Baffle spacing at center	0.396*Ds	0.322*Ds	0.308*Ds
Baffle spacing at inlet/outlet	1.542*Lbc	1.465*Lbc	1.487*Lbc
Baffle cut [%]	26.6	25.3	25.1
Tube pitch	1.27*do	1.252*do	1.252*do
Layout	30°	30°	30°
Number of tubes	912	644	790
Number of tube passes	4	4	4
Number of shell passes	1	1	1
Hot fluid side	shell	shell	shell
Cold fluid side	tube	tube	tube
Tube length [m]	4.234	4.500	4.007
Total surface area [m ²]	244.939	183.577	202.427
Fluid velocity on shell side [m/s]	0.768	1.429	1.217
Fluid velocity on tube side [m/s]	1.208	1.715	1.386
Type of heat exchanger	TEMA E	TEMA E	TEMA E

The designer can select one solution from the Pareto set in accordance with the specific design requirements. If the most important requirement is the volume, solution B is preferable. If a low value of pressure drop is required, solution A leads the design. A trade-off is represented by solution C.

Using an algorithm, it is possible to draw the tube layout in order to have the exact number of tubes. As shown in figure 9.18, the number of tube of solution C is 769. This number is close to the value of 790 calculated using an approximate expression.

Usually, the higher pressure stream should be allocated to the tube-side because the high-pressure tubes will be cheaper than a high-pressure shell. Furthermore, the stream in the tubes produces lower pressure drop and in an ORC the higher the pressure drop the lower the net power output. These considerations lead to allocate the cold fluid to the tube and the hot fluid in the shell.

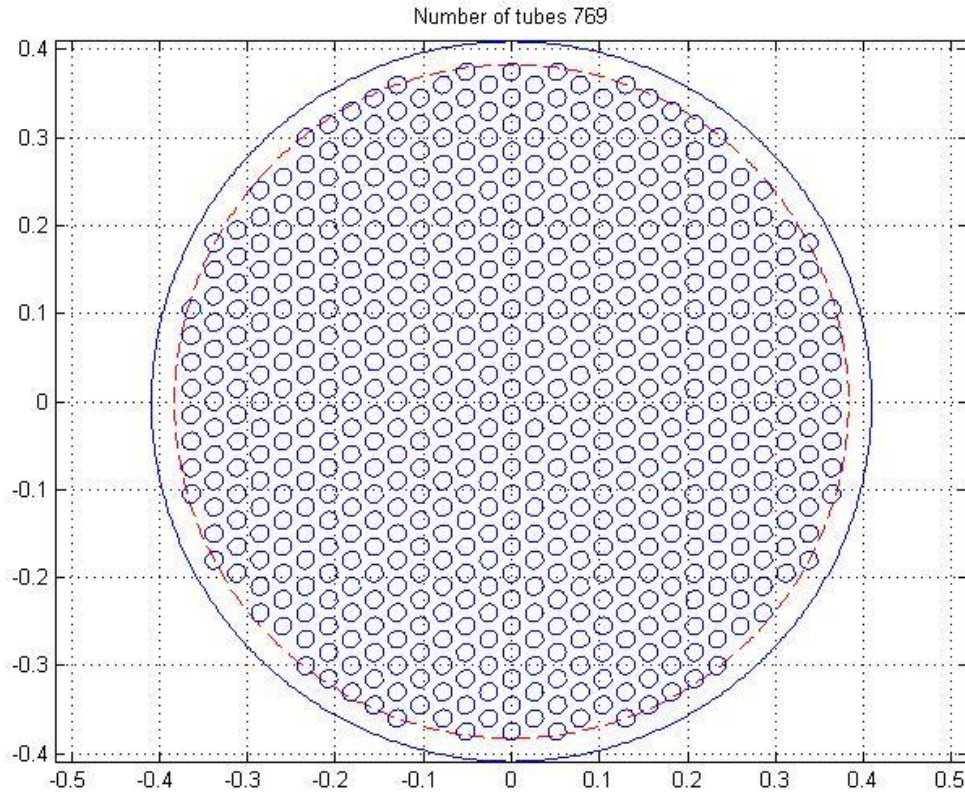


Fig.9.18. Tube layout of solution C

In order to increase the heat transfer coefficient on shell side, finned tube can be considered. On the other hand, finned surfaces cause high pressure drop and high fouling factors.

9.4.2. Volume, pressure drop and cost minimization

The evaluation of heat exchanger performance must be coupled with the cost estimation in order to achieve the best performance with the lowest expenses. The total cost of a heat exchanger can be seen as the combination of two major costs: the initial cost and the operating cost.

The initial cost (or capital cost) is the purchase cost of the heat exchanger. The estimation of the cost of purchase is usually based on the estimation of the heat transfer surface and on earlier knowledge and experience of exchanger manufacturing. The following correlation can be used for a carbon steel heat exchanger as suggested by Wild and Gosselin [25]:

$$C_{in} = 3.28 \cdot 10^4 \left(\frac{A}{80} \right)^{0.68} \quad (9.12)$$

Where the purchase cost is expressed in \$ and the heat transfer area is in m^2 . Because the purchase cost also depends on the operating pressure and temperature as well as the material of construction, some correction factors are necessary:

$$C_{in} = k_M k_P k_T \cdot 3.28 \cdot 10^4 \left(\frac{A}{80} \right)^{0.68} \quad (9.13)$$

Where k_M, k_P and k_T are correction factors that takes into account the material of construction, the operating pressure and temperature respectively.

The operating cost is governed by the pumping power that is required for driving the hot and cold fluids through the exchanger. The operating cost can be determined from:

$$C_{op} = (E_s + E_t) \cdot op \cdot ec \quad (9.14)$$

Where E_s and E_t are the required pumping powers (in W) for the shell and tube sides respectively, op is the annual operating period (in hours) and ec is the electricity cost:

$$E_s = \frac{\Delta P_s \cdot \dot{m}_s}{\rho_s \eta_s} \quad (9.15)$$

$$E_t = \frac{\Delta P_t \cdot \dot{m}_t}{\rho_t \eta_t} \quad (9.16)$$

The total cost of heat exchanger is expressed in annuities:

$$C_{tot} = C_{init} \frac{i(1+i)^n}{(1+i)^n - 1} + C_{op} \quad (9.17)$$

Where i is the fractional interest rate per year and n is the expected lifetime of the heat exchanger.

Table 9.11.

Parameter	Value
<i>op</i>	5000 hours/year
<i>ec</i>	0.1 \$/kWh
<i>lifetime</i>	20 years
<i>Interest rate</i>	5%

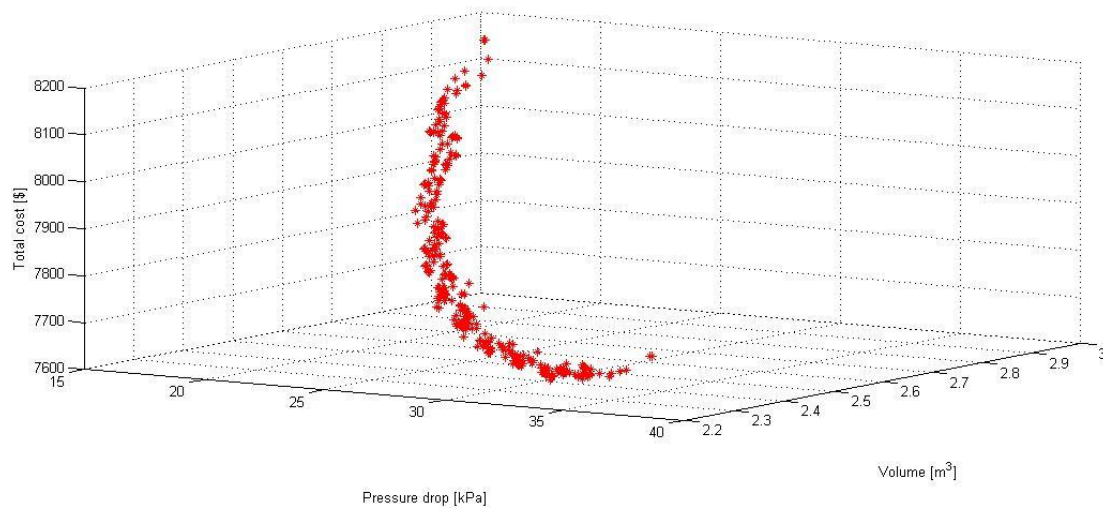


Fig. 9.19. Pareto front – Total annual cost vs. Volume vs. Pressure drop

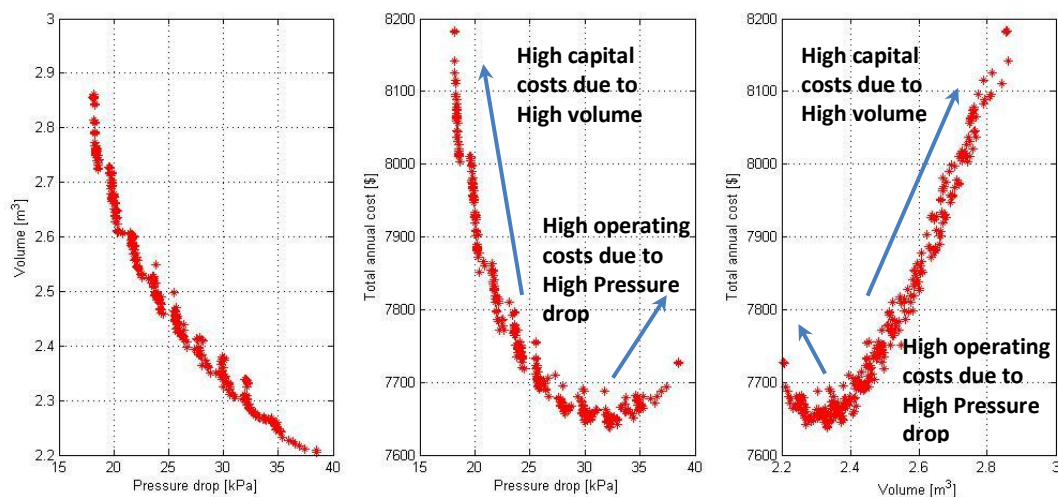


Fig. 9.20. Pareto front. A) Volume vs. Pressure drop B) Total cost vs. Pressure drop C) Total cost vs. Volume

Using three objective functions the optimal Pareto set can be represented in a three dimensional plot. It can be seen the opposite influence of volume and pressure drop on total cost. In fact, capital cost is related to the heat transfer area (thus the volume) as expressed in equation 9.20. On the other hand, operating cost is proportional to the pressure drop. Figure 9.21-a shows the inverse relation between volume and pressure drop as widely described in the previous section. Figure 9.21-c shows the Pareto optimal set highlighting the relation between total annual cost and volume. As expected, the higher the volume the higher the total annual cost. However, when the volume is too low, pressure drop increases rapidly. This causes high operating cost. Therefore, a minimum is defined. It is important to say that total annual cost is only a rough estimation and more accurate research are necessary to validate this model.

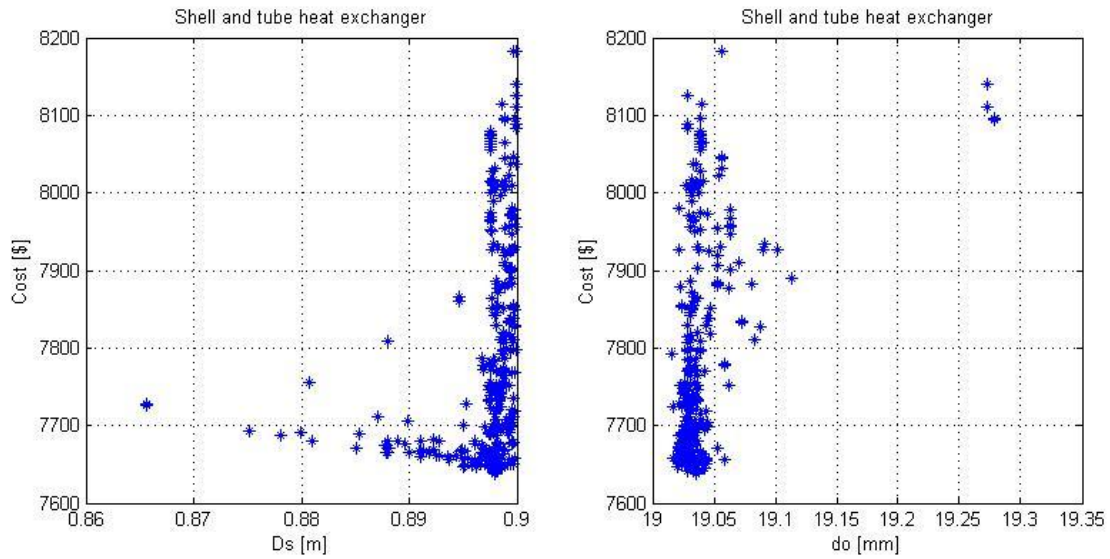


Fig. 9.21. Influence of D_s and d_o on total annual cost.

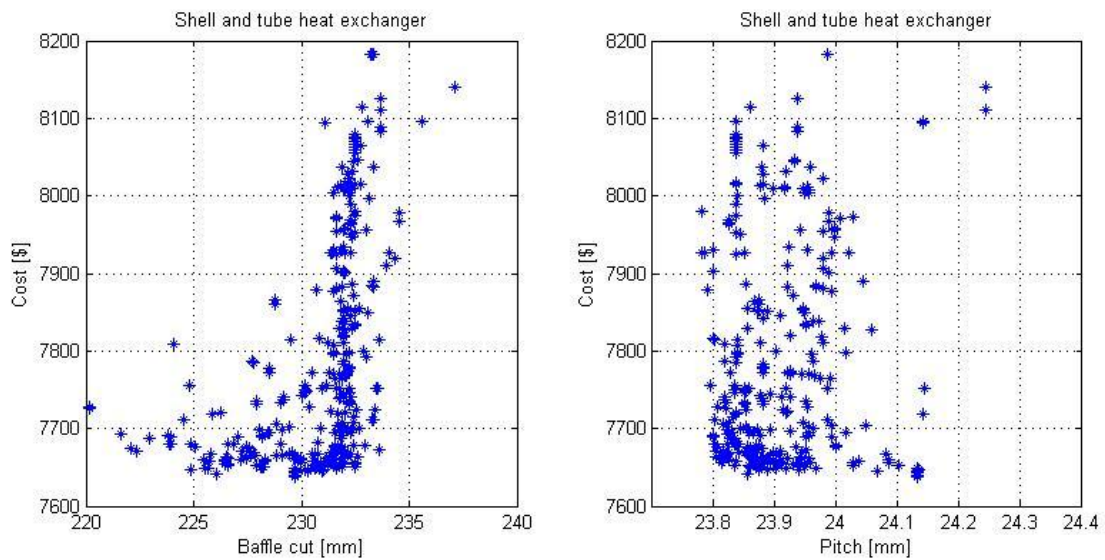


Fig. 9.22. Influence of L_{bc} , L_{bi} , Baffle cut and pitch on total annual cost.

Optimized solution is obtained by means of the following design variables:

Table 9.12. Solution of minimum total annual cost

	Solution
Volume [m ³]	2.337
Pressure drop [kPa]	32.147
Total annual cost [\$]	7643.667
Shell Diameter[m]	0.898
Tube outer diameter [m]	0.019
Baffle spacing at center [m]	0.218* D_s
Baffle spacing at inlet/outlet [m]	1.017* L_{bc}

Baffle cut [%]	25.6
Tube pitch	1.268*do
Layout	30°
Number of tubes	1030
Number of tube passes	4
Number of shell passes	1
Hot fluid side	shell
Cold fluid side	tube
Tube length	3.690
Total surface area	227.275
Fluid velocity on shell side	1.219
Fluid velocity on tube side	1.401
Type of heat exchanger	TEMA E
Material of construction	CS shell, aluminum tubes
Expected lifetime	20
Annual operating period [hours]	5000
Electricity cost [\$/kWh]	0.1
Fractional interest rate[%]	5

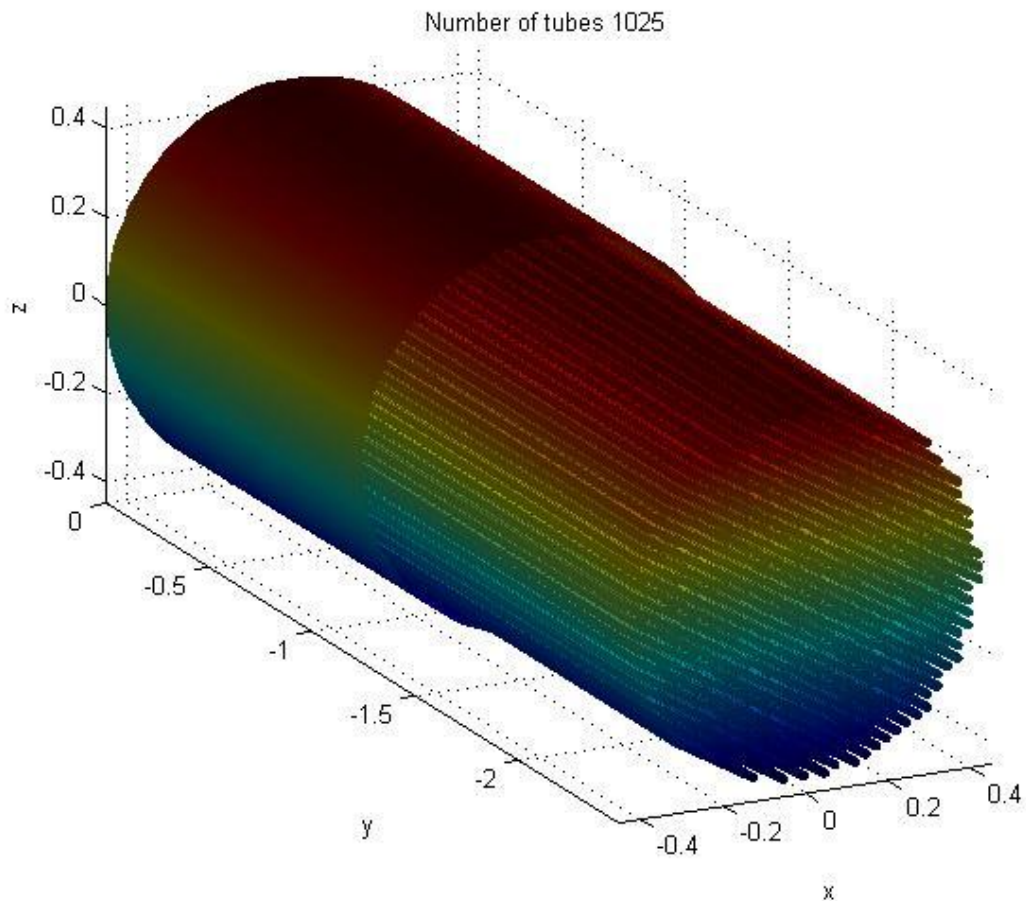


Fig. 9.19.3D view of shell and tube geometry – solution C

10

Multi Objective Optimization of PHE

10.1. Multi-objective optimization of plate heat exchangers

Compact heat exchangers like plate heat exchangers are the best solutions for small scale organic Rankine cycles. In fact, the diffusion of the brazing technology has allowed the construction of high temperature and high pressure plate heat exchangers. The possibility to manage fluids with high temperature and high pressure is fundamental in the design of organic Rankine cycles. Thanks to the brazing process, plate heat exchangers are pressure resistant up to 45 bar and temperature resistant up to 200°C. Furthermore, carefully designed plate pattern of the corrugated plates easily achieves high thermal transfer rate in either counter flow or parallel flow arrangement. Finally, brazed Plate Heat Exchanger is much lighter in weight and smaller in size, if compared to shell tube exchangers and easier to install and replace.

A brazed plate heat exchanger consists of multiple corrugated steel plates stacked one on top of the other and vacuum brazed together. This design creates a series of parallel, non-intersecting channels through which the two liquids can flow without ever coming in contact with each other. Being separated only by a steel plate, the liquids move in close proximity to each other allowing for thermal energy exchange to occur.

In the following work, a thermal modeling is conducted for optimal design of compact heat exchanger in order to maximize performance and minimize cost.

10.2. Plate heat exchanger design

The design of plate heat exchanger is very difficult because a lot of different plate configurations are available in the market and manufacturers do not provide correlations to calculate heat transfer coefficient and pressure drop. Information on the performance of the various patterns of plate used are not generally available. Furthermore, only few research about two phase heat transfer are available in literature [4,5,6,7].

The design procedure is the following:

1. Define the duty, the rate of the heat transfer required \dot{Q} .
2. If the specification of the problem is incomplete, determine the unknown fluid temperature or fluid mass flow rate from a heat balance.

$$\dot{Q} = \dot{m}_h c_{p,h} (T_{h,in} - T_{h,o}) = \dot{m}_c c_{p,c} (T_{c,o} - T_{c,in}) \quad (10.1)$$

- Calculate the fluid parameters at the mean temperature such as density, viscosity, thermal conductivity and heat capacity.

$$[\rho, \mu, k, c_p] = f(T) \quad (10.2)$$

- Calculate the mean log temperature difference

$$\Delta T_{lm} = \frac{(T_{h,in} - T_{c,o}) - (T_{h,o} - T_{c,in})}{\ln\left(\frac{T_{h,in} - T_{c,o}}{T_{h,o} - T_{c,in}}\right)} \quad (10.3)$$

- Evaluate the log mean temperature correction factor F_t

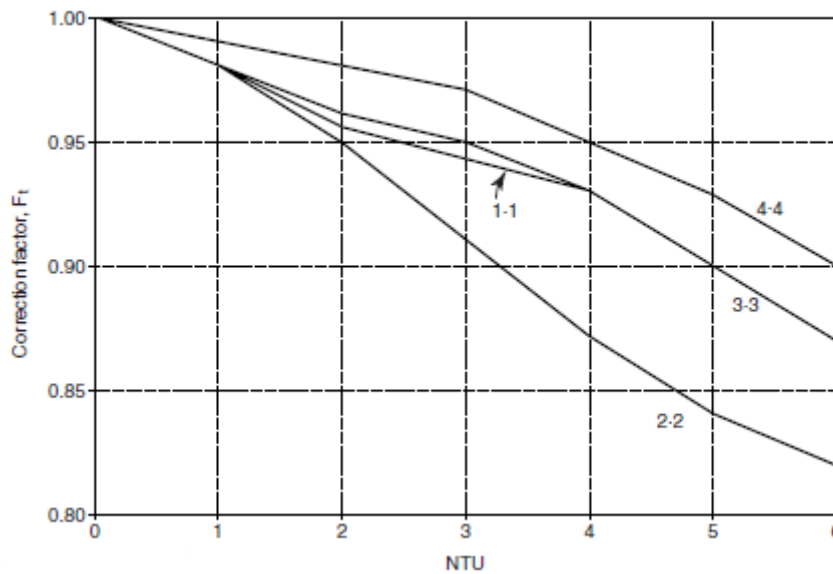


Figure 10.

Log mean temperature correction factor for plate heat exchangers. Taken from Coulson and Richardson.

- Calculate the corrected mean temperature difference $\Delta T_m = F_t \Delta T_{lm}$
- Propose a geometry for the plate heat exchanger and calculate the specific mass flow rate

$$G = \frac{\dot{m}}{N_{channel} \times pass \times bL_w} \quad (10.4)$$

- Calculate the heat transfer coefficient using Martin's correlation (chapter 4) for single phase flow and Kim correlation for two phase flow.
- Calculate the overall heat transfer coefficient

$$U = \left[\frac{1}{\alpha_c} + R_c + \frac{t}{k_w} + R_h + \frac{1}{\alpha_t} \right]^{-1} \quad (10.5)$$

- Calculate the heat transfer area necessary to the heat transfer rate required

$$A = \frac{\dot{Q}}{U \Delta T_{lm} F_t} \quad (10.6)$$

- Compare the heat transfer area calculated at point 10 with the heat transfer area proposed at point 7. If the relative error is less than 10%, proceed. If unsatisfactory return to step 7 and modify the geometry
- Check the pressure drop for each stream.

10.3. Test case and validation

In order to validate the model a test case has been carried out. The starting point is the example 12.13 of the book “Coulson & Richardson, Chemical Engineering”. The aim of the problem is to design a plate heat exchanger with the following requirements:

Table 10.1.

	Hot Fluid	Cold Fluid
Fluid	Methanol	Water
Inlet Temperature [°C]	95	25
Outlet Temperature [°C]	40	40
Mass Flow Rate [kg/s]	27.8	68.9
Fouling factor [m ² K/W]	1/10 000	1/6 000
Tube Material	Titanium	
Thickness [mm]	0.75	

Table 10.2.

Fluid	Density ρ [kg/m ³]	Specific heat c_p [J/kg · K]	Dynamic viscosity μ [Pa · s]	Thermal conductivity k [W/m ² · K]	Prandtl Number Pr
Methanol at 67.5°C	750	2840	3.4×10^{-3}	0.190	5.1
Water at 32.5°C	995	4187	0.8×10^{-3}	0.59	5.7

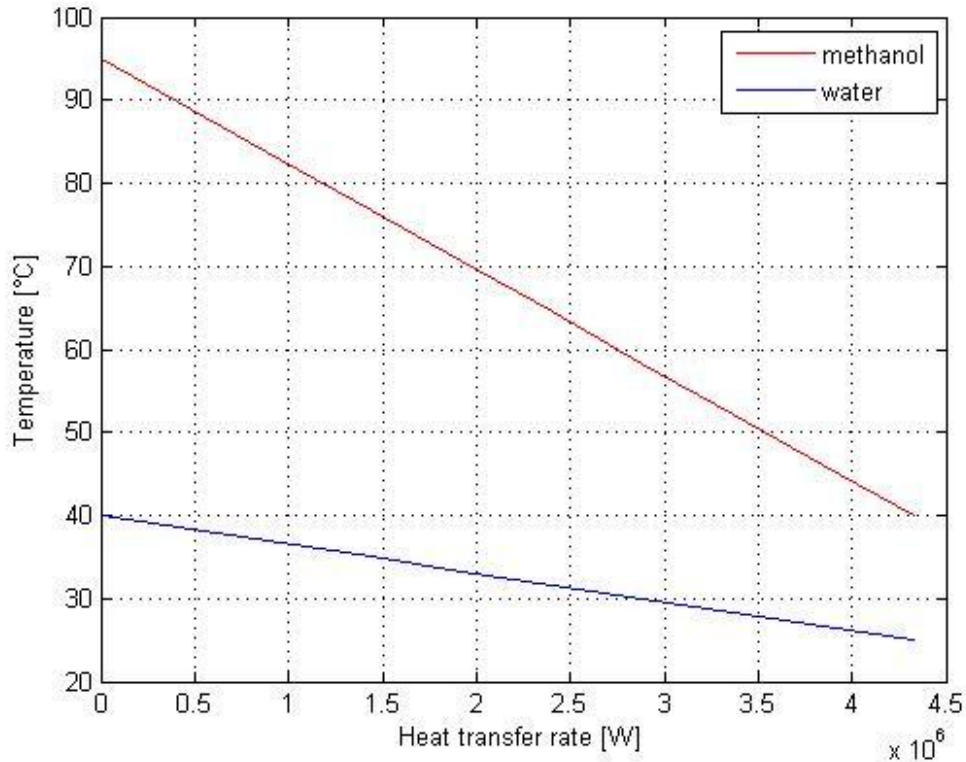


Fig. 10.1. Temperature profiles

The solution proposed in the book is shown in table 10.3:

Table 10.3.

Plate width L_w [m]	0.5
Plate length L_v [m]	1.5
Plate spacing b [mm]	3.0
Number of plates N_p	97
Number channel per pass N_{cp}	48

Table 10.4.

	Solution of "Coulson & Richardson"	Solution of the thermal model implemented	Relative error [%]
Channel velocity – Hot fluid [m/s]	0.51	0.5148	0.94
Channel velocity – cold fluid [m/s]	0.96	0.9619	0.20
Reynolds number – Hot fluid	6750	6813	0.93
Reynolds number – Cold fluid	6896	7589	10.0
Nusselt number – Hot fluid	153.2	143.8	6.13
Nusselt number – Cold fluid	162.8	155.7	4.36
Heat transfer coefficient – Hot fluid [W/m ² · K]	4870	4555	6.46
Heat transfer coefficient – cold fluid [W/m ² · K]	16009	16071	0.38
Overall heat transfer coefficient [W/m ² · K]	1754	1766	0.01
Pressure drop – Hot fluid [kPa]	16.659	20.414	22.54
Pressure drop – Cold fluid [kPa]	77.546	94.033	21.26
Total pressure drop [kPa]	94,205	114,447	21.48

As shown in table 10.4, the results are closed even though different correlations are used. The correlations adopted in the example are the following:

$$\frac{h_f d_h}{k_f} = 0.26 Re^{0.65} Pr^{0.4} \left(\frac{\mu}{\mu_w} \right)^{0.14} \quad (10.7)$$

$$\Delta P = 8 J_f \frac{L_p \mu u^2}{d_h^2} \quad (10.8)$$

Where

h_f is the heat transfer coefficient of the fluid

$Re = \frac{\rho u d_h}{\mu}$ is the Reynolds number

$u = \frac{\dot{m}}{A_{cr} \rho}$ is the channel velocity

$A_{cr} = \left(\frac{N_p - 1}{2} \right) L_w b$ is the cross sectional area for flow

d_h is the hydraulic diameter

L_p is the path length

$J_f = 0.6 Re^{-0.3}$ is the friction factor

The corrugations on the plates will increase the projected plate area, and reduce the effective gap between the plates. For rough sizing, where the actual plate design is not known, this increase can be neglected. The channel width equals the plate pitch minus the plate thickness. There is no heat transfer across the end plates, so the number of effective plates will be the total number of plates less two.

More accurate is the Martin's correlation used in the model that takes into account chevron angle:

$$Nu = \frac{\alpha d_h}{\lambda} = 0.205 Pr^{1/3} \left(\frac{\mu}{\mu_p} \right)^{1/6} (f Re^2 \sin 2\beta)^{0.374} \quad (10.9)$$

$$\frac{1}{\sqrt{f}} = \frac{\cos \beta}{(0.045 \tan \beta + 0.09 \sin \beta + f_0 / \cos \beta)^{0.5}} + \frac{1 - \cos \beta}{\sqrt{3.8 f_1}} \quad (10.10)$$

If $Re < 2000$

$$f_0 = \frac{16}{Re} \quad (10.11)$$

$$f_1 = \frac{149.25}{Re} + 0.9625 \quad (10.12)$$

If $Re > 2000$

$$f_0 = (1.56 \ln Re - 3)^{-2} \quad (10.13)$$

$$f_1 = \frac{9.75}{Re^{0.289}} \quad (10.14)$$

10.4. Sensitivity analysis

In order to increase the sensibility in the design of plate heat exchangers a sensitivity analysis is carried out. The aim off this section is to evaluate the influence of each geometric parameter on heat transfer area (or volume) and pressure drop. The procedure is to set all variables except one and observe the influence that this variable has on total heat transfer area (or volume) and pressure drop.

10.4.1. Width of the plate, Channel spacing and number of plates

As expected, the higher the plate width, the higher the volume and the lower the pressure drop. In fact it influences the cross section area, hence the fluid velocity through the channel. High velocity means low heat transfer area but also high pressure drop. Channel spacing and number of plates have the same behavior.

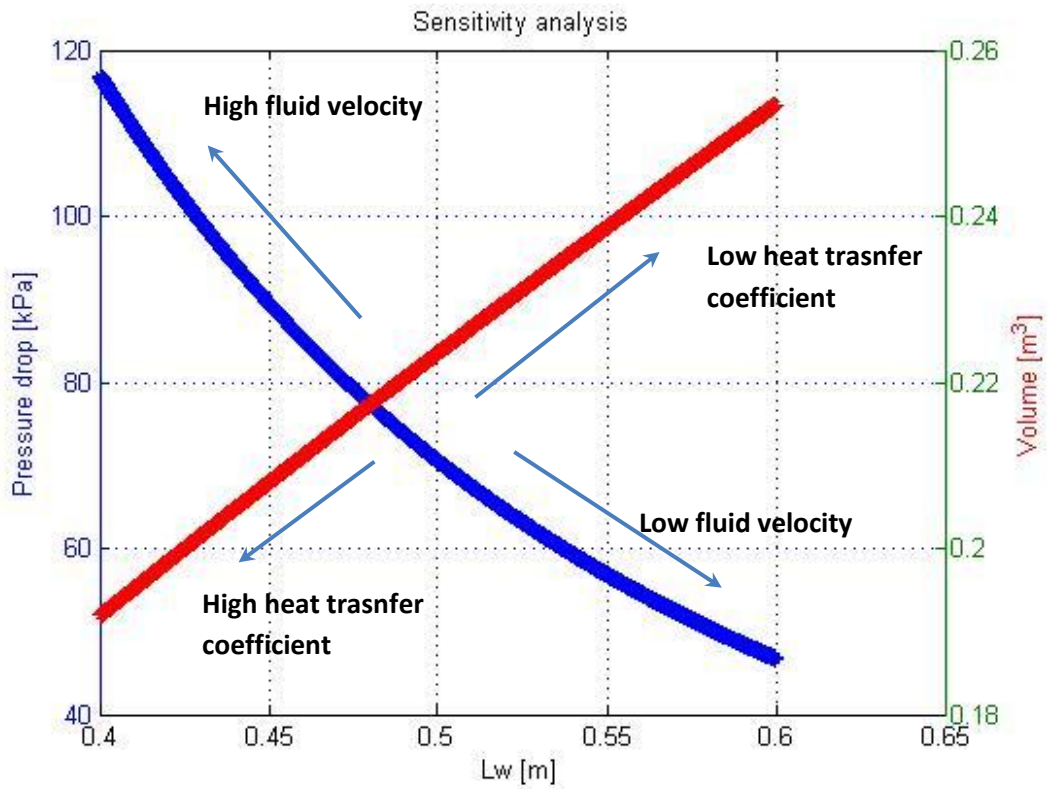


Fig. 10.2. Influence of plate width on pressure drop and volume

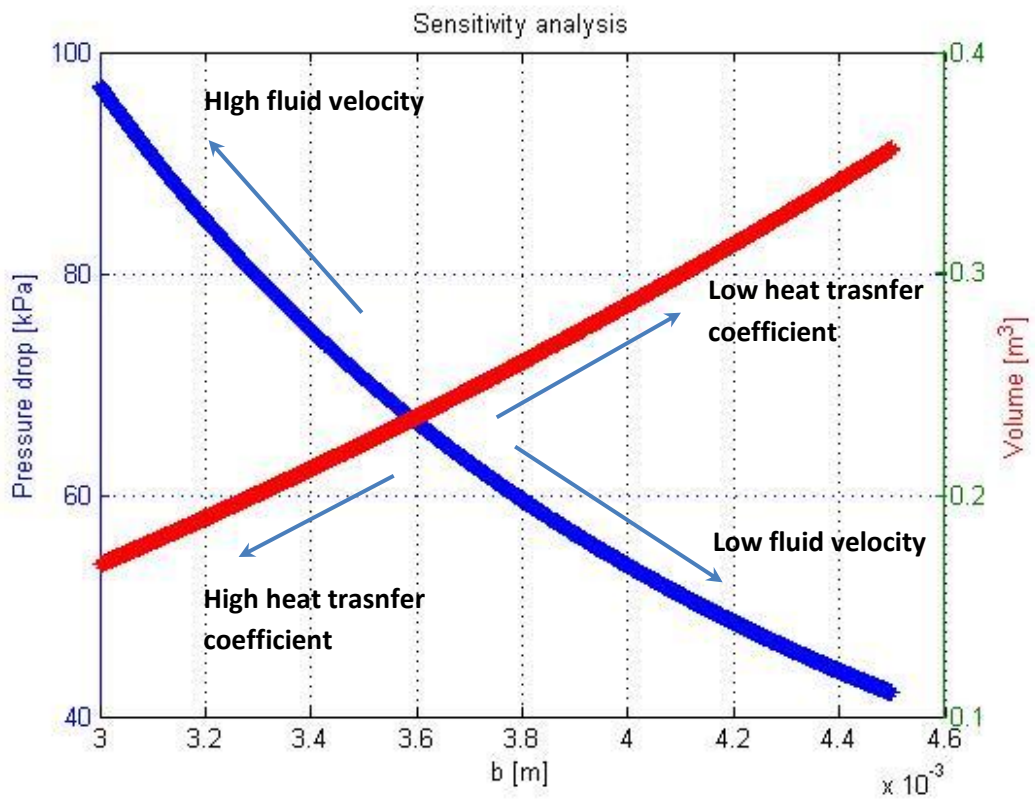


Fig. 10.3. Influence of plate channel spacing on pressure drop and volume

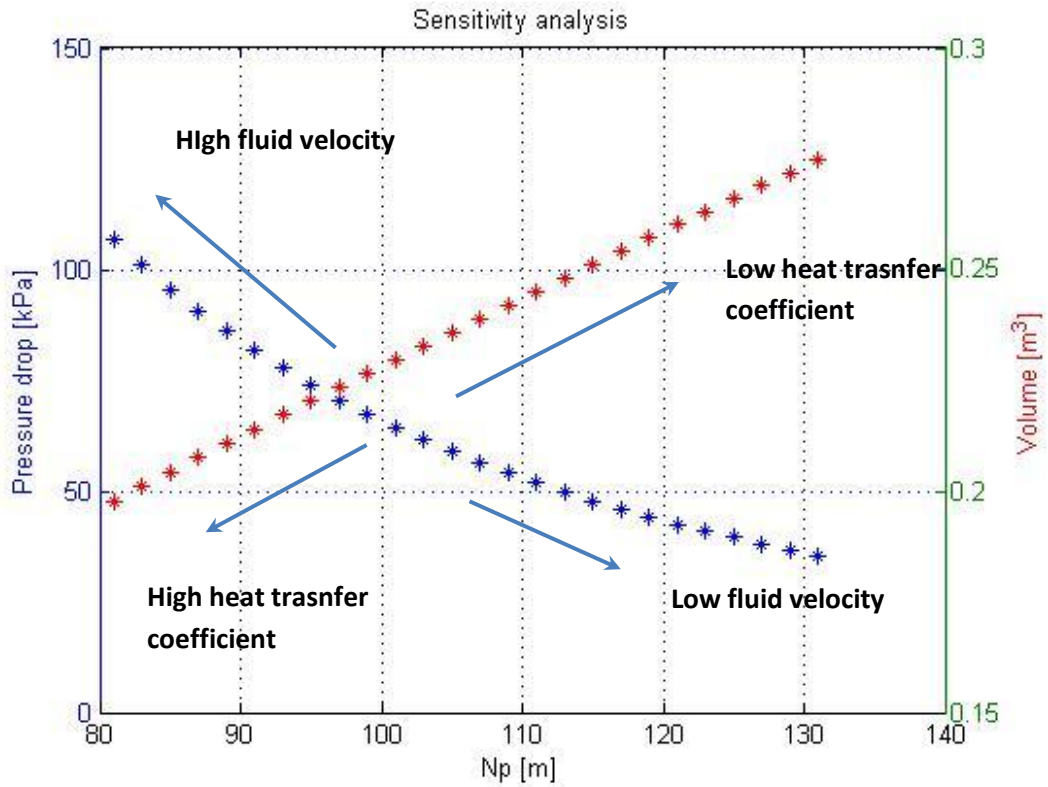


Fig. 10.4. Influence of number of plate on pressure drop and volume

10.4.2. Chevron angle

As shown in figure 10.5, the chevron angle β has different influence on heat transfer coefficient and pressure drop respect the previous parameters. The higher β , the higher the heat transfer coefficient α since more turbulence is created. On the other hand, the higher β , the higher the pressure drop.

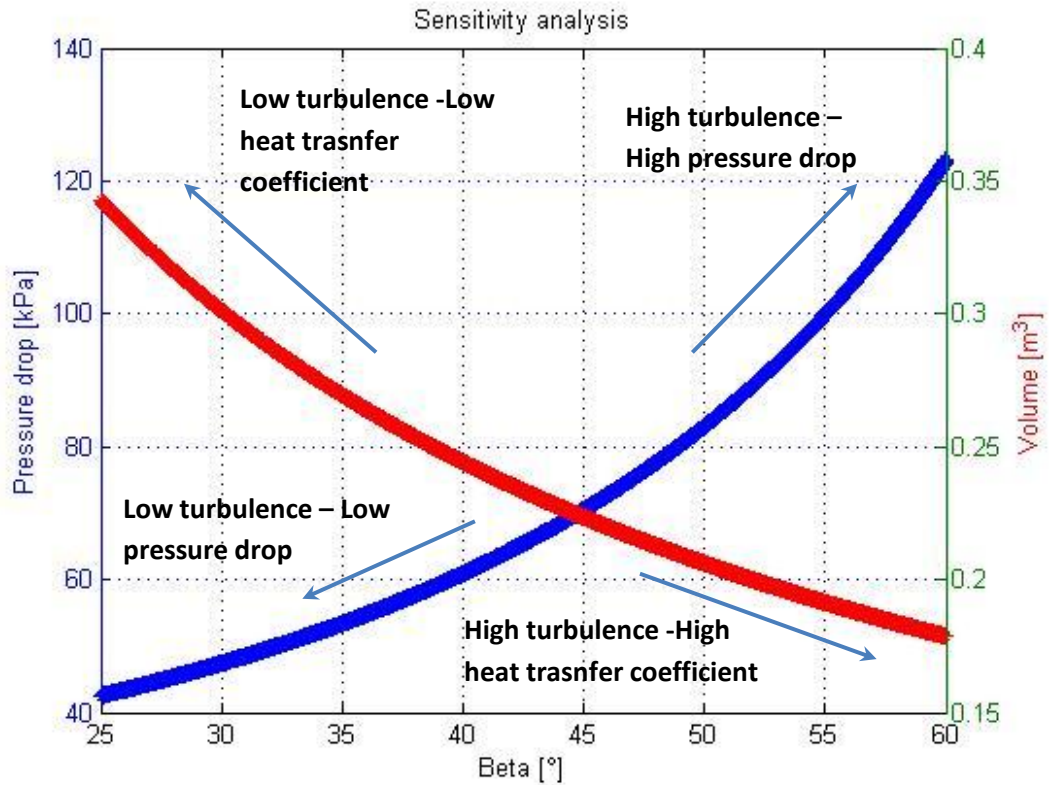


Fig. 10.5. Influence of chevron angle on pressure drop and volume

10.4.3. Channel aspect ratio

The channel aspect ratio is related to the enlargement factor ϕ . The enlargement factor is the ratio between the developed length and the projected length. As described in chapter 5, the channel aspect ratio is the ratio between the mean channel spacing b and the corrugation pitch p_c :

$$X = \frac{2b}{p_c} \quad (10.15)$$

$$\phi = \frac{1}{6} \left(1 + \sqrt{1 + X^2} + 4 \sqrt{1 + \frac{X^2}{2}} \right) \quad (10.16)$$

The value of X is normally between 0.84 and 1.17 and describes the corrugation pattern. Corrugated plates induce turbulence and increase heat transfer area till 15%. The higher the channel aspect ratio, the higher the heat transfer since the developed area increases.

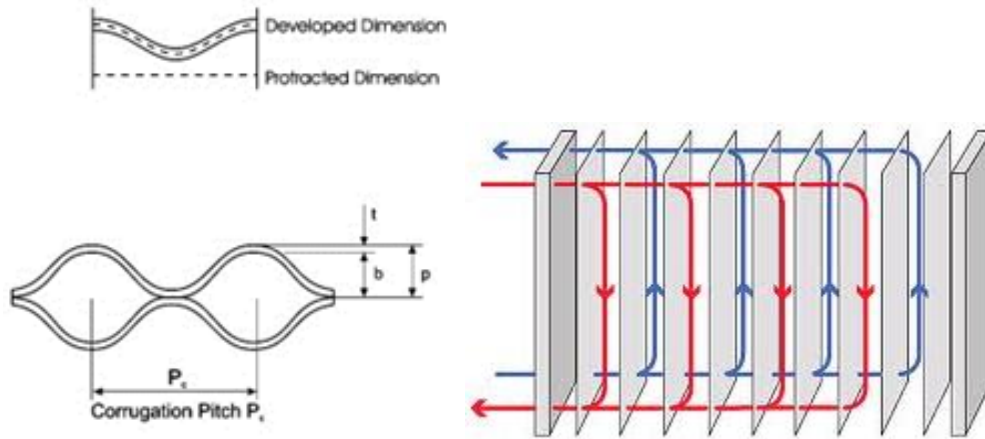


Fig. 10.6. A) Projected length vs. developed length. B) 1/1 floe arrangements

10.5. Optimization

In order to optimize the design procedure a multi-objective optimization is carried out. Multi objective optimization minimizes several objective functions simultaneously, with a number of inequality or equality constraints. It can be mathematically expressed as follows:

$$\min f(x) = [f_1(x), f_2(x), \dots, f_n(x)], \quad x \in X \quad (10.17)$$

Subject to

$$g_j(x) = 0, \quad j = 1, 2, \dots, M \quad (10.18)$$

$$h_k(x) \leq 0, \quad k = 1, 2, \dots, K \quad (10.19)$$

Where x is a vector and is also called the decision vector because it contains the decision variables and X is the parameter space. If and only if, $f_i(x) \leq f_i(y)$ for $i = 1, 2, \dots, n$ and $f_j(x) < f_j(y)$ for least one objective function j , a feasible solution x is said to dominate another feasible solution y . A solution that is not dominated by another solution in the feasible region is called Pareto optimal solution. The set of all Pareto optimal solution forms the Pareto optimal set whereas the values of the objective functions related to the Pareto optimal set are called Pareto front. The objective functions considered in this case study are volume and total pressure drop:

$$f_1(x) = V \quad (10.20)$$

$$f_2(x) = \Delta P_h + \Delta P_c \quad (10.21)$$

The design variables are:

Table 10.5.

Design variable	Range
Plate width L_w [m]	0.2 – 0.6
Plate spacing b [mm]	2.5 – 4.5
Number pass N_{plates}	80 – 140
Chevron angle β [°]	25° – 65°
Channel aspect ratio [–]	0.84 – 1.12

Volume is calculated as follows:

$$V = [(N_p - 1)b + N_p t]L_v L_w \quad (10.22)$$

Where t is the plate thickness and is assumed constant: $t = 0.4\text{mm}$. The arrangement considered is 1/1. This means that each fluid does only one passage as shown in figure 10.6-b.

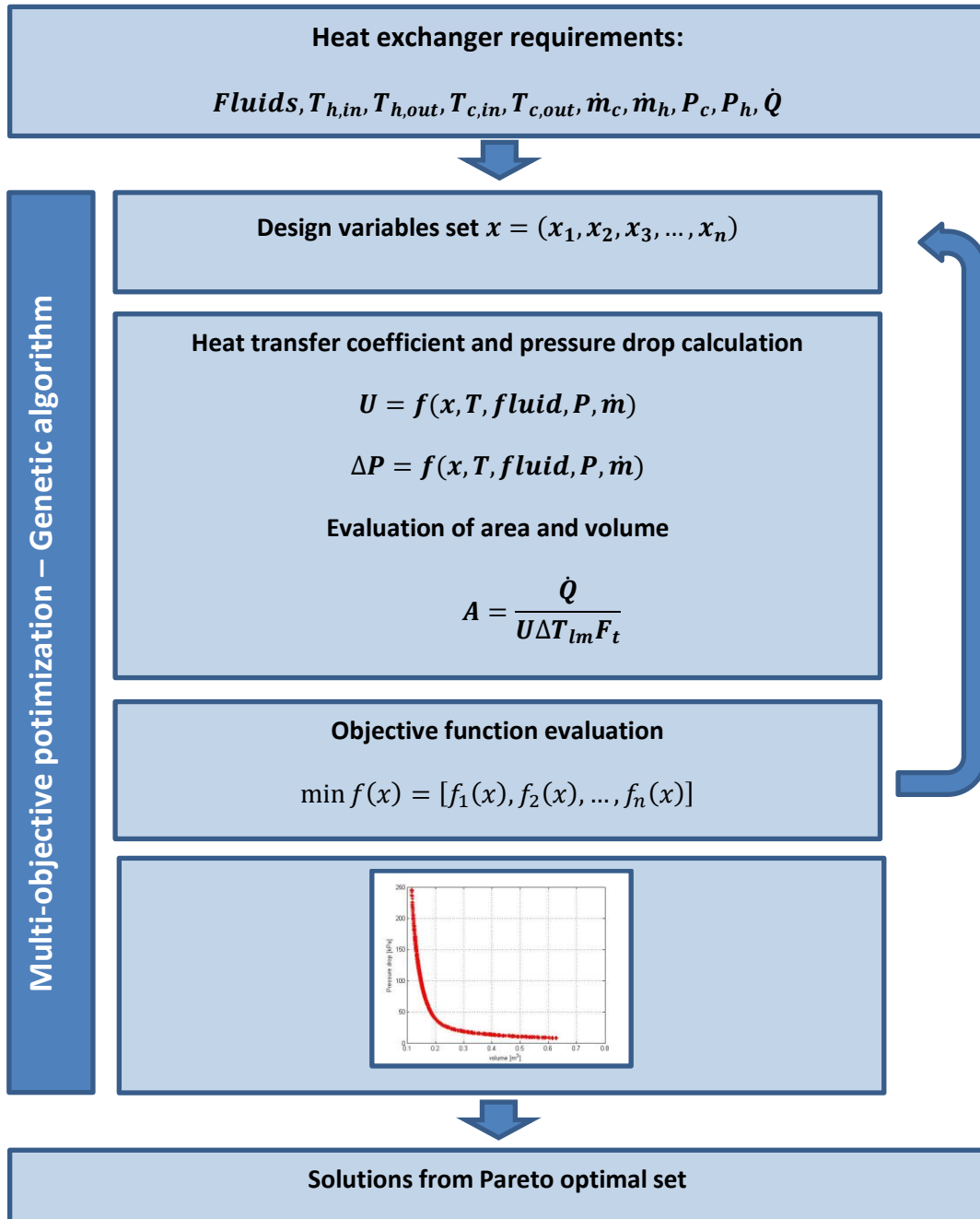


Fig. 10.7. Scheme of multi-objective optimization with genetic algorithm.

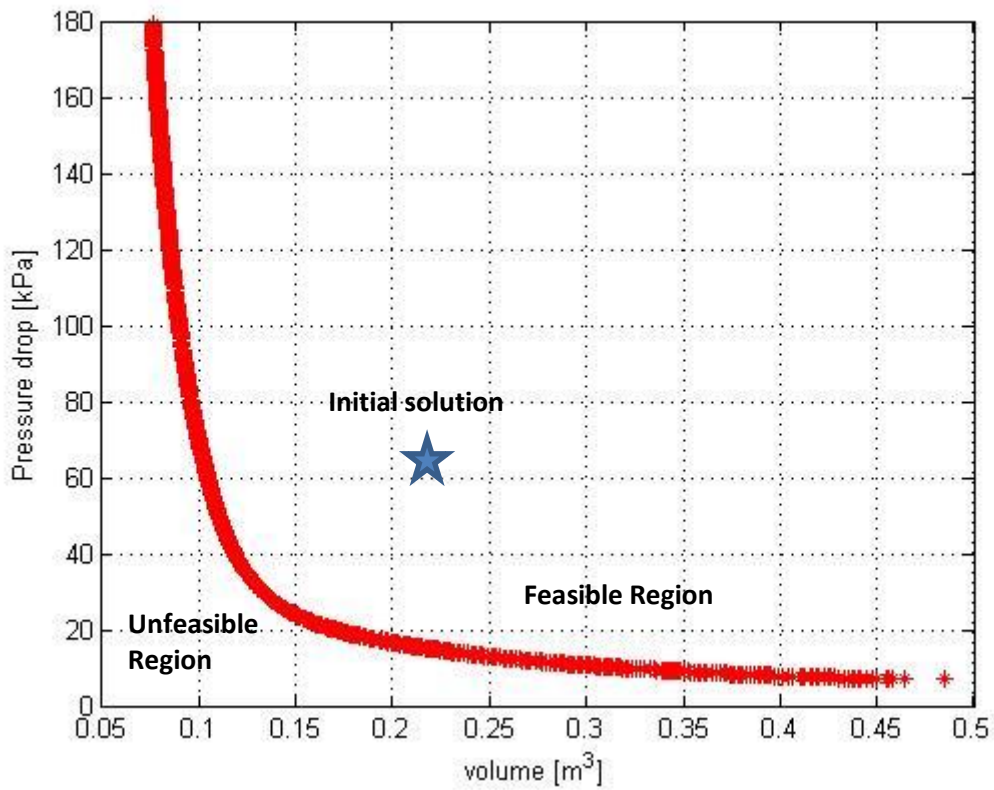


Fig. 10.8. Pareto front. Initial solution is displayed in the feasible region.

As shown in Fig. 10.8, the initial solution proposed in the example is in the feasible region. The Pareto optimal set describe all the optimal solutions obtained varying the geometric parameters of the heat exchanger. The influence of the design variables on volume and pressure drop is shown in figure 10.9-10-11. It can be noted that the trends follow the considerations pointed out in the sensitivity analysis.

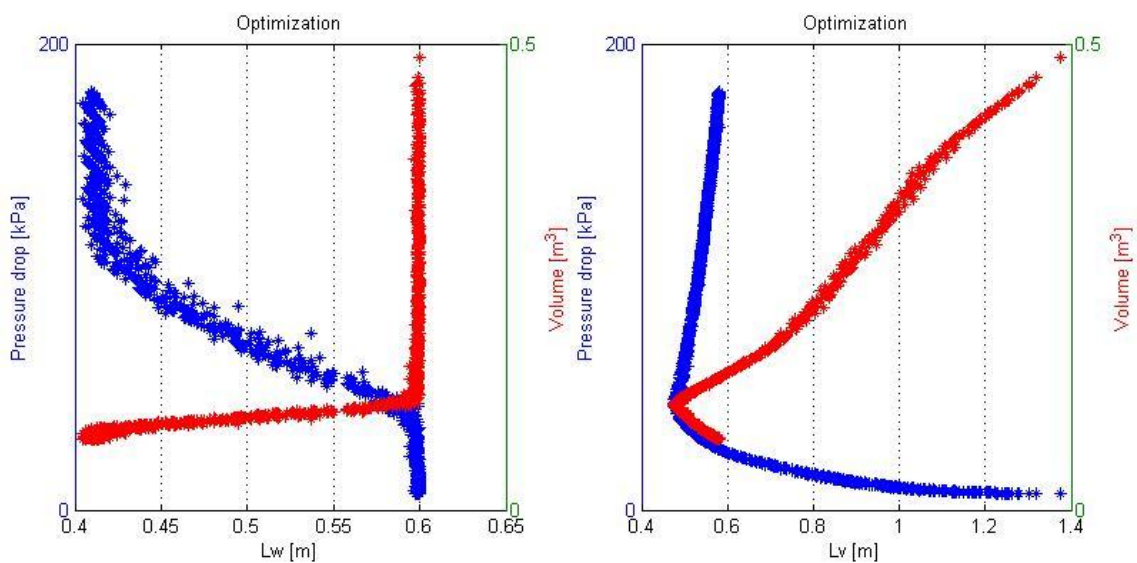


Fig. 10.9. Influence of design variables on pressure drop and volume

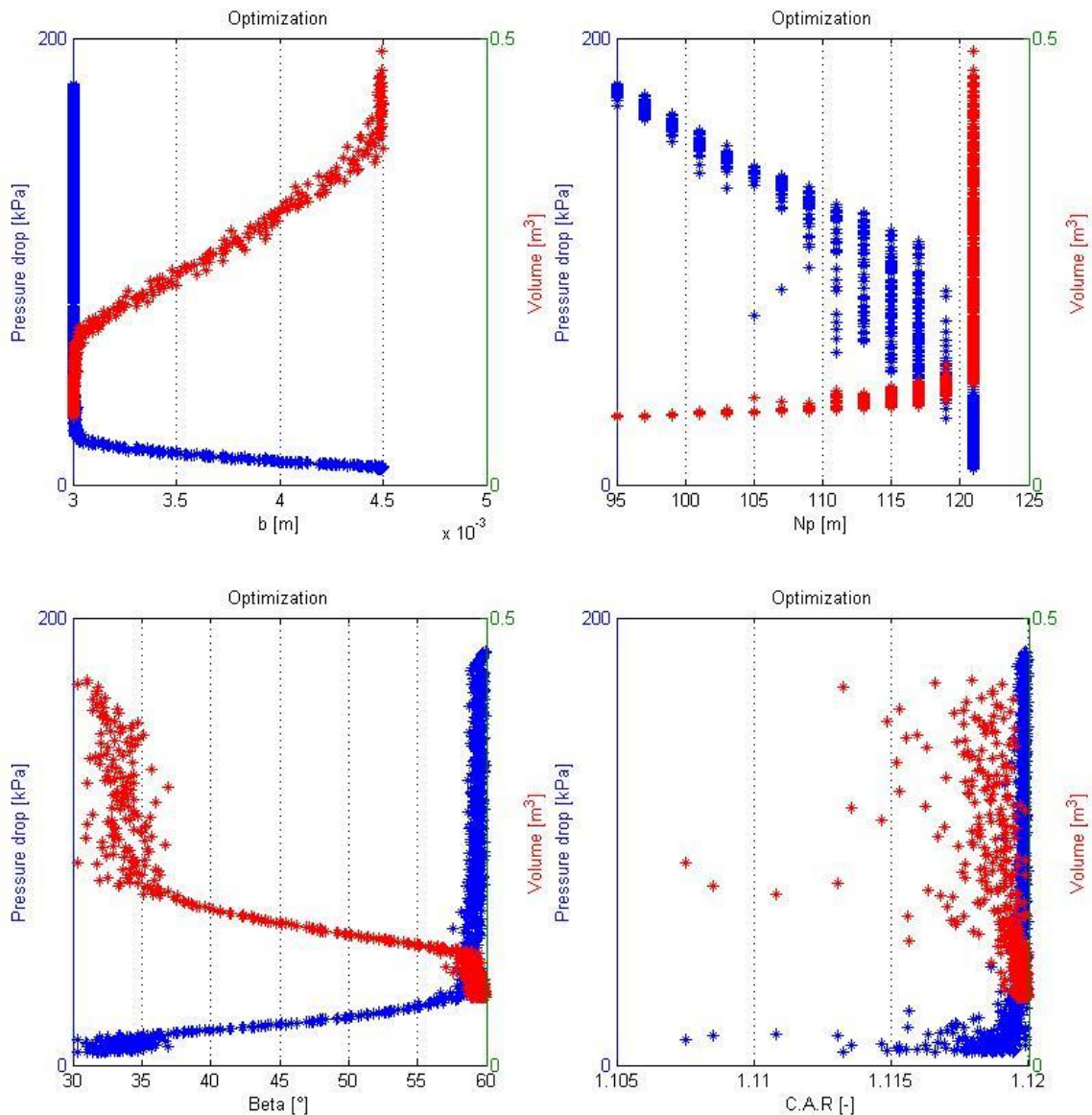


Fig. 10.10. Influence of design variables on pressure drop and volume

10.6. Optimization of plate heat exchangers for organic Rankine cycles

The optimization of heat exchangers for organic Rankine cycles follows the guidelines described previously but a real design procedure must consider the operating conditions of the heat exchanger. In order to consider the operating conditions of the heat exchanger, the results of the cycle optimization reported in chapter 8 are taken as starting point. The aim of the work is the design and optimization of the heat exchangers (economizer and evaporator) for the three solutions proposed in *table 10.6*.

Table 10.6.

	R-245fa	R-236ea	R-245ca
Temperature			
T _{eva} [°C]	117.1	129.3	110.5
Delta PP [°C]	10.0	10.0	10.0
T ₁ [°C]	25.0	25.0	25.0

	T2s [°C]	25.5	25.9	25.3
	T2 [°C]	26.2	26.9	25.7
	T3 [°C]	117.1	129.3	110.4
	T4 [°C]	117.1	129.3	110.4
	T5 [°C]	44.4	49.7	48.1
	T5s [°C]	53.2	57.8	57.0
	T6 [°C]	30.0	30.0	30.0
	T7 [°C]	180.0	180.0	180.0
	T8 [°C]	127.1	139.3	120.4
	T9 [°C]	60.3	35.8	64.3
Pressure				
	Peva [kPa]	1819.32	2810.65	1172.40
	Peva [bar]	18.1932	28.1065	11.7240
Mass flow rate				
	Working fluid mass flow [kg/s]	0.235	0.325	0.213
Heat transfer rate				
	Heat flux H.E. total work. Fluid[W]	58370.61	68988.32	56564.90
	Heat flux ECO work. Fluid[W]	31273.47	47935.30	26190.96
	Heat flux EVA work. fluid[W]	27097.14	21053.02	30373.93
Power				
	Net power output[W]	7554.07	8837.37	7190.06
Performance index				
	epsilon	0.778	0.942	0.749
Entropy generation rate				
	S_eva_i sensible [J/(s/K)]	5.38	2.87	5.16
	S_eva_i latent[J/(s/K)]	5.89	3.65	7.39
	S_eva_i [J/(s/K)]	11.28	6.53	12.55
	S_eva_e [J/(s/K)]	4.78	1.04	5.65
	S_gen [J/(s/K)]	32.25	27.83	33.50

The operating requirements for the heat exchanger design are displayed in *Table 10.6*. In order to obtain a set of optimal solutions, six design variables are selected and their ranges are listed in *Table 10.7*:

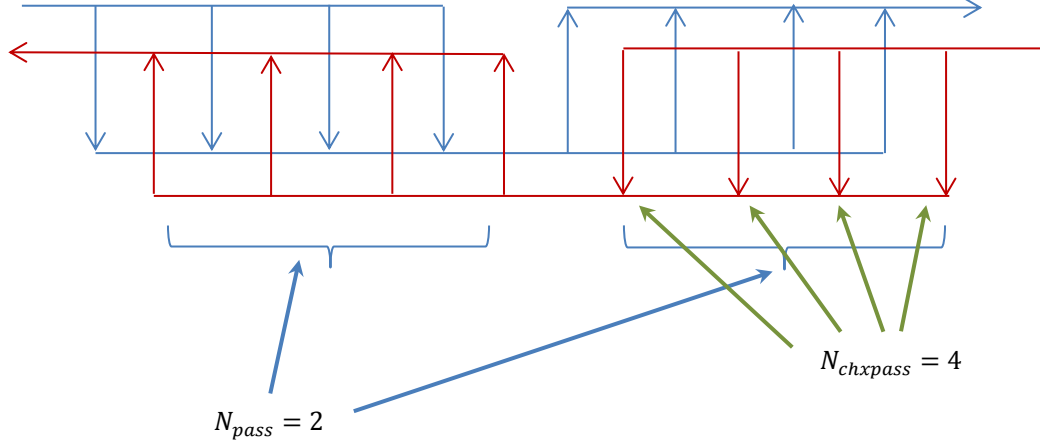
Table 10.7.

Design variable	Range
Plate width L_w [m]	0.2 – 0.6
Plate spacing b [mm]	2.5 – 4.5
Number pass N_{pass}	1 – 8
Number of channel for pass N_{chpass}	1 – 20
Chevron angle β [°]	25° – 65°
Channel aspect ratio [–]	0.84 – 1.12

The plate length, L_p , is the geometric parameter used to achieve the right heat transfer area, hence it depends from the other design variables. The number of plates is obtained with the following expression:

$$N_p = 2(N_{pass} \cdot N_{chxpass}) + 1 \quad (10.23)$$

Where N_{pass} is the number of passages through the heat exchanger of one fluid whereas $N_{chxpass}$ is the number of channels for each passage. With a fixed value of total channel, the higher N_{pass} the higher the velocity of the fluid. High velocity means high heat transfer coefficient and low heat transfer area.



On the other hand, high velocity implies high friction losses and high number of passages increase the length of the path to calculate the pressure drop.

The objective functions considered are:

$$f_1(x) = V \quad (10.24)$$

$$f_2(x) = \Delta P_h + \Delta P_{ch} \quad (10.25)$$

$$f_3(x) = S_{gen,dt} + S_{gen,dp} \quad (10.26)$$

Where the thickness of the plate is assumed constant: $t = 0.4 \text{ mm}$. Entropy is computed as follows:

$$\dot{S}_{gen,\Delta T} = \int_i^o \left(\frac{\dot{m}c_p dT}{T} \right)_{h,c} = \dot{m}_h c_{p,h} \ln \frac{T_{h,o}}{T_{h,i}} + \dot{m}_c c_{p,c} \ln \frac{T_{c,o}}{T_{c,i}} \quad (10.27)$$

$$\dot{S}_{gen,\Delta P} = \frac{\Delta P_h}{\rho_h} \dot{m}_h \frac{\ln \frac{T_{h,o}}{T_{h,i}}}{T_{h,o} - T_{h,i}} + \frac{\Delta P_c}{\rho_c} \dot{m}_c \frac{\ln \frac{T_{c,o}}{T_{c,i}}}{T_{c,o} - T_{c,i}} \quad (10.28)$$

The entropy generation caused by the heat transfer is constant since the operating temperatures are fixed. Thus, the entropy generation rate is influenced only by pressure drop.

The Pareto front obtained by the multi-objective optimization design is shown in Fig 10.11-12-13-14-15. As expected, the optimal set for r236ea is shifted to higher volumes than r245fa and 245ca. This is due to the higher effectiveness of r236ea compared to the other fluids that causes higher heat transfer area. It can be seen that the value of entropy generation rate is higher than the value reported in *table 10.6*. In fact, in the optimization of the cycle presented in chapter 9 the pressure drop was neglected. The design of the heat exchanger allows the designer to consider the pressure drop and improve the model of the organic Rankine cycle. As shown in Fig. 10.11, 10.12, 10.13 the higher the pressure drop the higher the entropy generation rate in the heat exchanger. Obviously, the higher is the entropy generation rate, the lower is the net power

output of the cycle. On the contrary, the lower the pressure drop the higher the volume. These considerations lead the designer to select the optimal geometry of the heat exchanger.

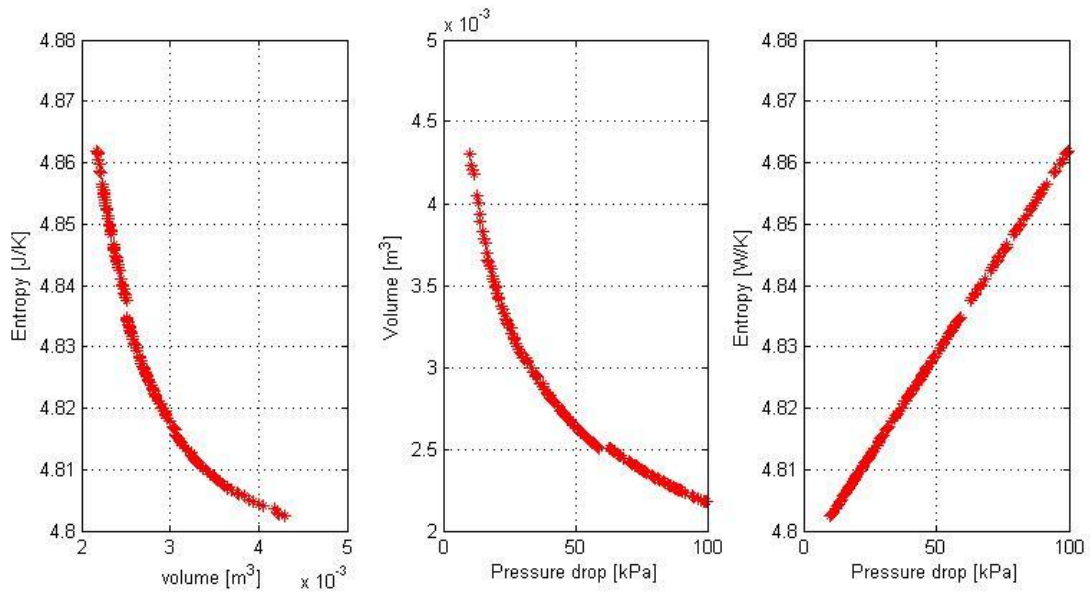


Fig. 10.11. Pareto front of r245ca

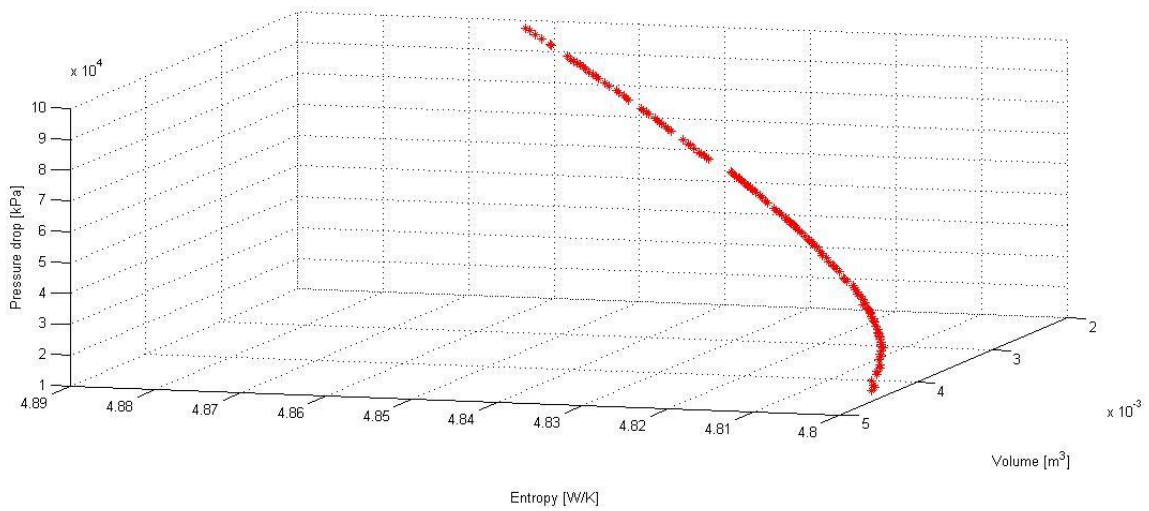


Fig. 10.12. Pareto front of r245ca

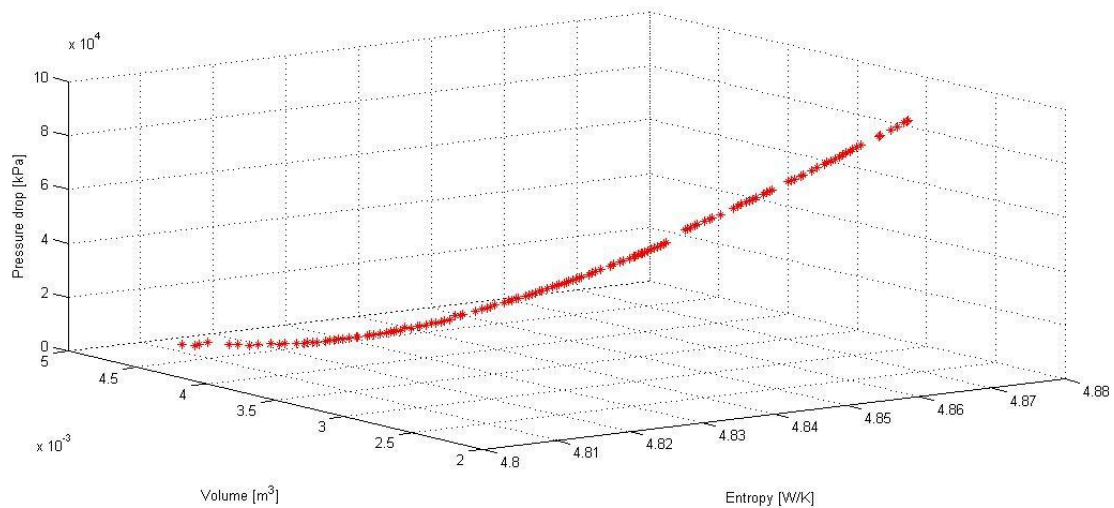


Fig. 10.13. Pareto front of r245ca

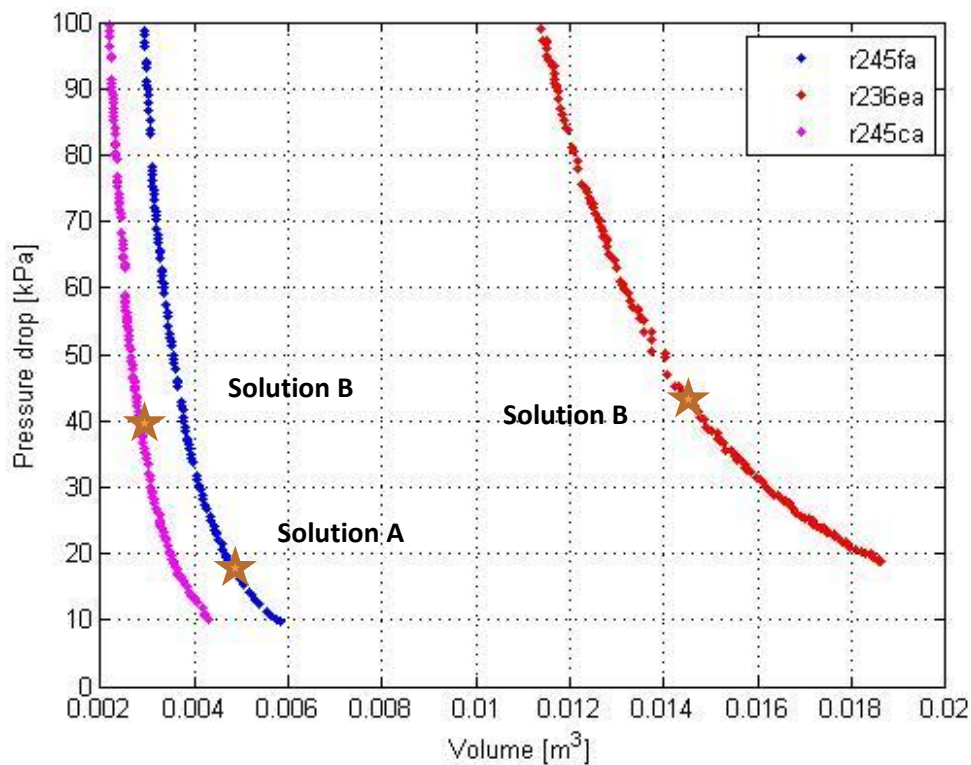


Fig. 10.14

Three solutions are selected from the Pareto front in order to show the design variables associated:

Table 10.8.

Design variable	Solution A	Solution B	Solution C
Fluid	R245fa	R236ea	R245ca
Plate width L_w [m]	0.116	0.111	0.114
Plate length L_v [m]	0.209	0.476	0.231
Plate spacing b [mm]	2.5	2.22	2.50
Number pass N_{pass}	7	7	6

Number of channel for pass $N_{chxpass}$	5	8	3
Number of plates	71	113	37
Chevron angle β [°]	56.7	57.3	58.0
Channel aspect ratio [-]	1.12	1.103	1.118
Volume [m^3]	0.004752	0.015540	0.008815
Pressure drop [kPa]	18.544	34.054	42.976
Entropy generation rate [J/(Ks)]	4.941018	2.856452	4.824193
Heat transfer area	2.040	7.405	1.171
Hot fluid velocity [m/s]	0.190	0.132	0.195
Cold fluid velocity [m/s]	0.135	0.138	0.320

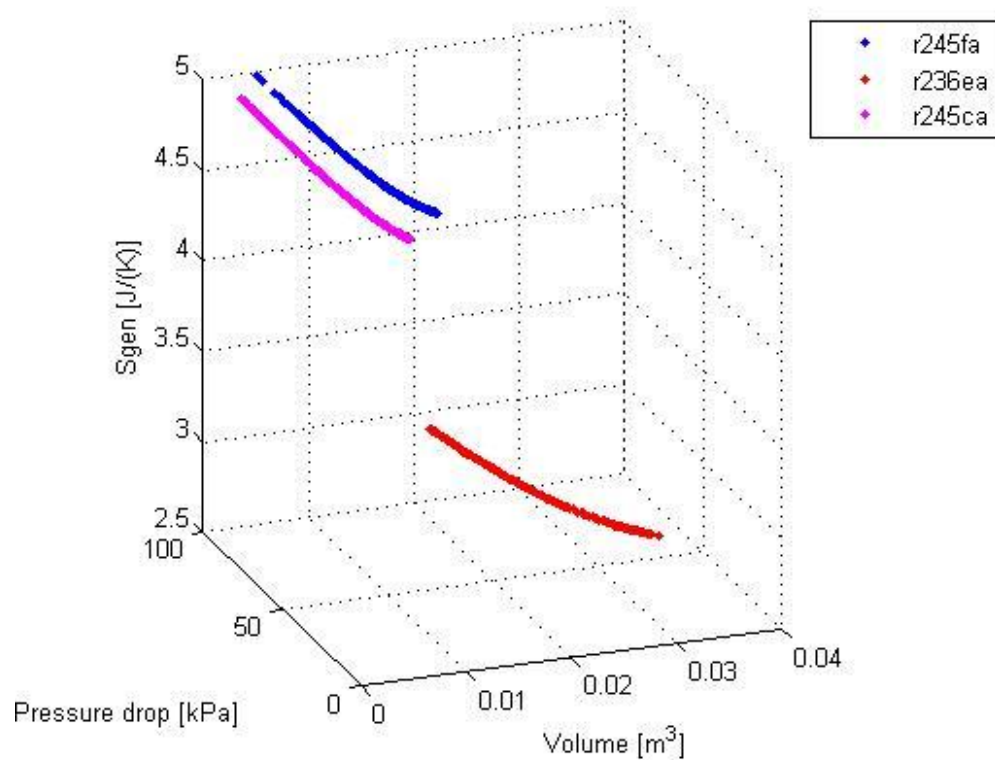


Fig. 10.15. Comparison of Pareto front for three fluids

Generally, heat exchangers with pressure drop higher than 50 kPa are considered. When sizing a PHE, we have very little choice in the selection of plate dimensions, unlike plate-fin and tube-in heat exchanger designs, because we cannot arbitrarily select a plate width L_w or plate length L_v . Instead, we should select from a relatively small pool of available plate sizes from any manufacturer.

I propose the following solutions available in the market:

Table 10.9

	Solution A	Solution B	Solution C
Company	Swep	Swep	Swep
Product name	B12	B25T	B12
Plate width L_w [m]	0.117	0.119	0.117
Plate length L_v [m]	0.234	0.479	0.234
Plate spacing b [mm]	2.24	2.34	2.24
Number pass N_{pass}	7	7	6
Number of channel for pass N_{chpass}	5	8	3
Number of plates	71	113	37
Chevron angle β [°]	60	60	60



Swep – model B25T



Swep – model B35

10.7. Optimization of evaporator

The same approach can be adopted to design the evaporator. As shown in *figure 10.17*, two cases are taken into consideration: one pass and two pass arrangements. Generally, two-phase heat transfer coefficient is higher than single-phase heat transfer coefficient. Therefore, the evaporator requires less area than the economizer.

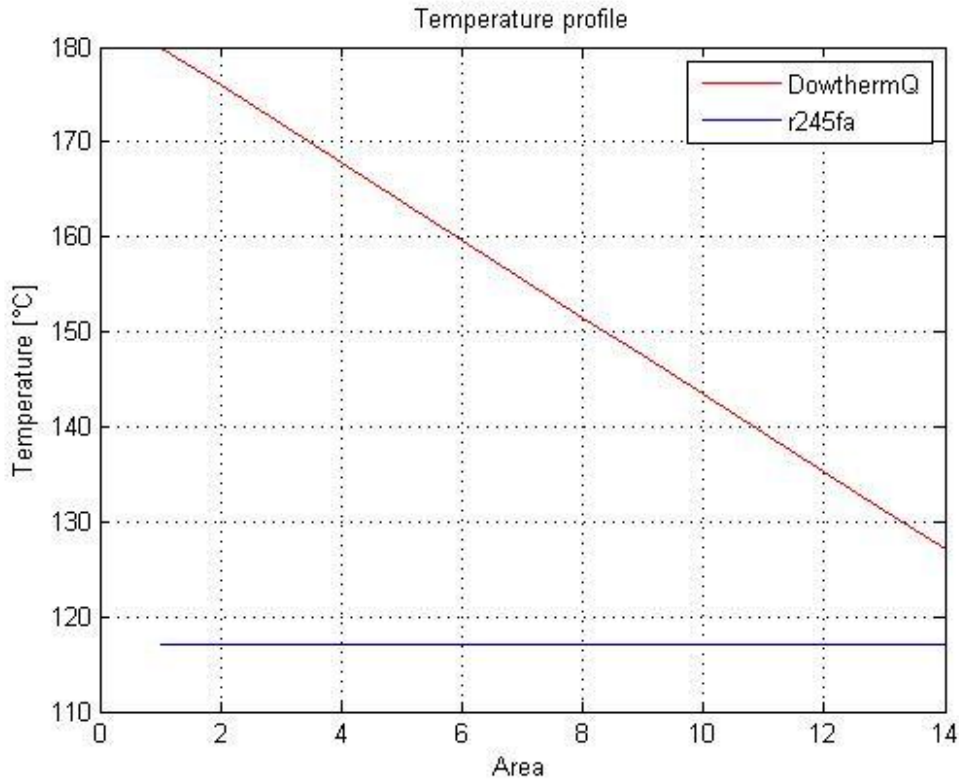


Fig. 10.16. Temperature profiles of evaporator.

Table 10.10.

Design variable	Range
Plate width L_w [m]	0.1 – 0.6
Plate spacing b [mm]	2.0 – 2.5
Number pass N_{pass}	1 – 2
Number of channel for pass N_{chpass}	1 – 20
Chevron angle β [°]	25° – 60°
Channel aspect ratio [–]	0.84 – 1.12

The objective functions considered are the same of the previous case:

$$f_1(x) = V \quad (10.29)$$

$$f_2(x) = \Delta P_h + \Delta P_{ch} \quad (10.30)$$

$$f_3(x) = S_{gen,dt} + S_{gen,dp} \quad (10.31)$$

It can be noted that r245ca is the fluid that has the highest heat transfer rate in the evaporator. This means that r245ca needs more heat transfer area than the other fluids.

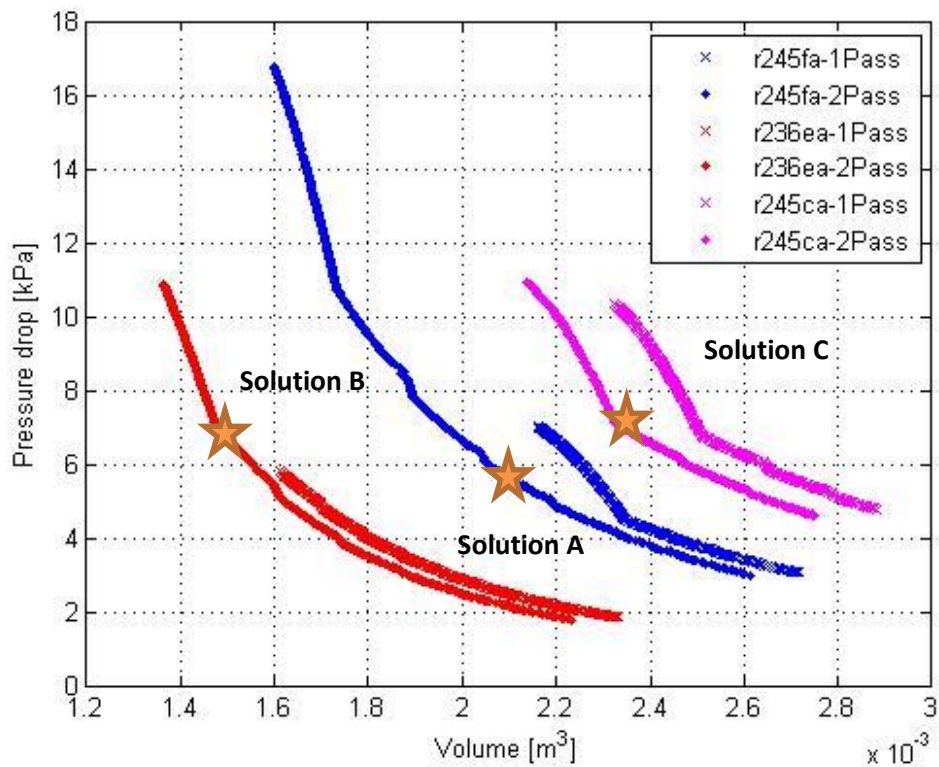


Fig. 10.17.

Table 10.11.

Design variable	Solution A	Solution B	Solution C
Fluid	R245fa	R236ea	R245ca
Plate width L_w [m]	0.119	0.119	0.117
Plate length L_v [m]	0.239	0.232	0.234
Plate spacing b [mm]	2.24	2.24	2.24
Number pass N_{pass}	7	5	8
Number of channel for pass N_{chpass}	2	2	2
Number of plates	29	21	33
Chevron angle β [°]	59.9	59.9	59.9
Channel aspect ratio [-]	0.843	0.841	0.86
Volume [m ³]	0.002060	0.001490	0.002316
Pressure drop [kPa]	5.707	6.882	7.410
Entropy generation rate [J/(Ks)]	5.512376	3.375084	6.942971
Heat transfer area	0.869	0.617	0.986
Hot fluid velocity [m/s]	0.159	0.219	0.138

There are three products in the catalog of *Swep* that meet the requirements:

Table 10.12.

	Solution A	Solution B	Solution C
Company	Swep	Swep	Swep
Product name	B10T	B12	B12
Plate width L_w [m]	0.119	0.117	0.117
Plate length L_v [m]	0.243	0.234	0.234
Plate spacing b [mm]	2.24	2.24	2.24

Number pass N_{pass}	7	6	6
Number of channel for pass N_{chpass}	2	2	2
Number of plates	31	21	33
Chevron angle β [°]	60	60	60

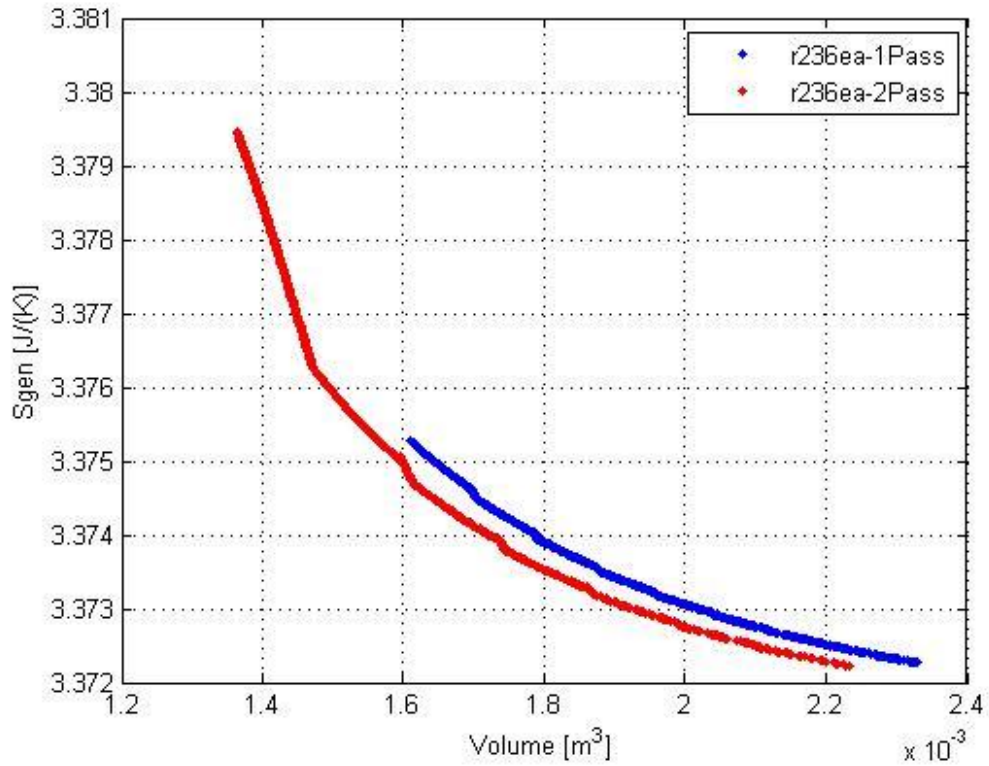


Fig. 10.18 Entropy generation rate for r-236ea



Swep model B12

10.8. Techno-economic optimization

For a complete optimal design of a heat exchanger the total annual cost must be considered. In fact, when the capital cost of a heat exchanger is high and the operating cost is low, the use of large pressure drops for a design may be beneficial. On the other hand, the same design may have to assume much lower pressure drops if the operating cost is high compared to the capital cost. In order to compare the total annual costs of different optimal solutions, a thermo-economic optimization is carried out.

The total annual cost of a heat exchanger system is represented by:

$$C_{tot} = C_{init} \frac{i(1+i)^n}{(1+i)^n - 1} + C_{op} \quad (10.32)$$

The capital cost, C_{init} , is the purchase cost of the heat exchanger. L. Wang and B. Sundèn [22] suggested a rough model to calculate the capital cost of plate heat exchangers:

$$C_{init} = 418 \cdot A^{0.85} \quad (10.33)$$

Where the Initial cost is expressed in \$ whereas the area is in m^2 .

The operating cost C_{op} , is governed by the pumping power that is required for driving the hot and cold fluids through the exchanger. The operating cost can be determined from:

$$C_{op} = (E_c + E_h) \cdot op \cdot ec \quad (10.34)$$

Where E_h and E_c are the required pumping powers (in kW) for hot and cold sides respectively, op is the annual operating period (in hours) and ec is the electricity cost:

$$E_h = \frac{\Delta P_h \cdot \dot{m}_h}{\rho_h \eta_p} \quad (10.35)$$

$$E_c = \frac{\Delta P_c \cdot \dot{m}_c}{\rho_c \eta_p} \quad (10.36)$$

The pressure drop influences in opposite way operating cost and capital cost. In fact, low pressure drop means low operational cost but, also, high volume and high initial cost.

Table 10.13.

Design variable	Range
Plate width L_w [m]	0.1 – 0.6
Plate spacing b [mm]	2.0 – 2.5
Number pass N_{pass}	1 – 2
Number of channel for pass N_{chpass}	1 – 20
Chevron angle β [°]	25° – 60°
Channel aspect ratio [-]	0.84 – 1.12
Parameters	
Material	<i>stainless steel</i>
Operating hours	5000 hours/year
Lifetime	10 years
Electricity cost	0.15 \$/kWh

The objective functions are:

$$f_1(x) = V \tag{10.37}$$

$$f_2(x) = \Delta P_h + \Delta P_{ch} \tag{10.38}$$

$$f_3(x) = C_{tot} \tag{10.39}$$

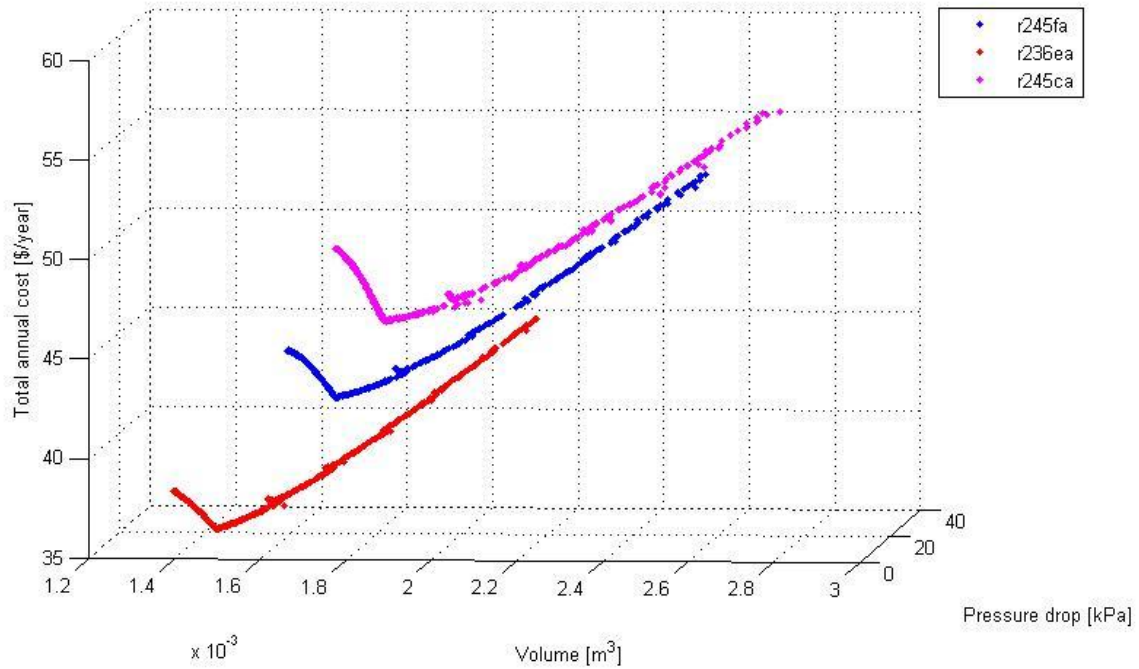


Fig. 10.19. Pareto optimal set for the fluids selected.

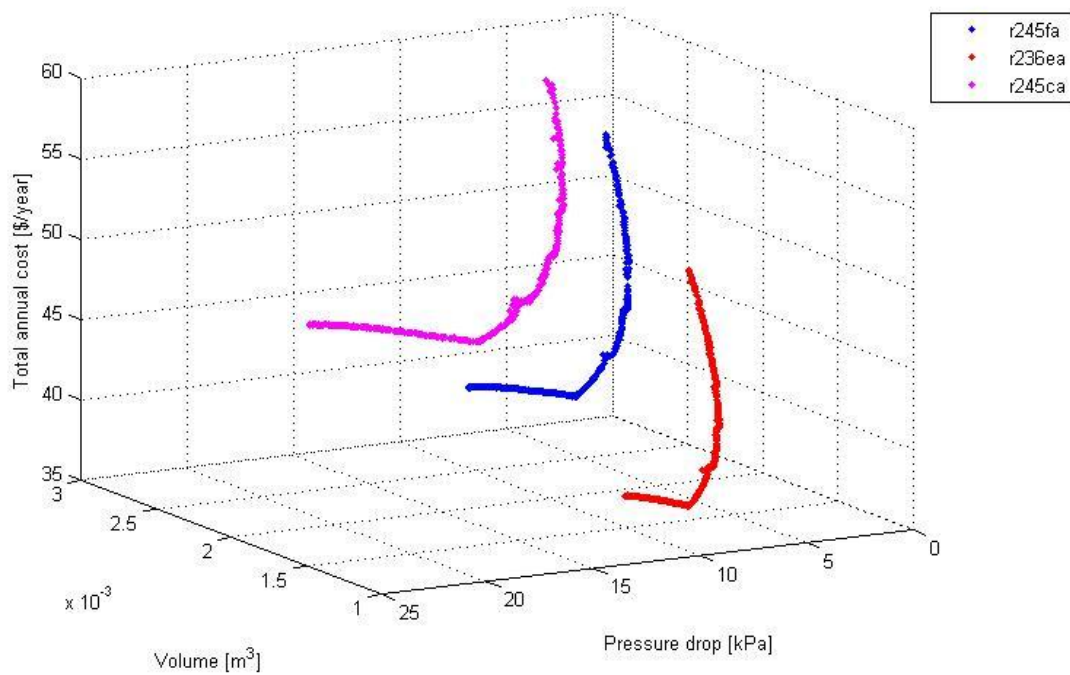


Fig. 10.20. Pareto optimal set for the fluids selected.

As expected, pressure drop and volume influence total annual cost. Since, three objective functions are set, Pareto front could be shown in three dimensions. The optimal point can be found as a trade-off between costs related to volume and costs related to pressure drop as shown in figure 10.22-23. It can be noted the linear trend of the cost related to the pressure drop as defined in the operating cost equation (Eq. 10.34). On the other hand, volume (or area) is related to the cost with a polynomial expression (Eq. 10.33).

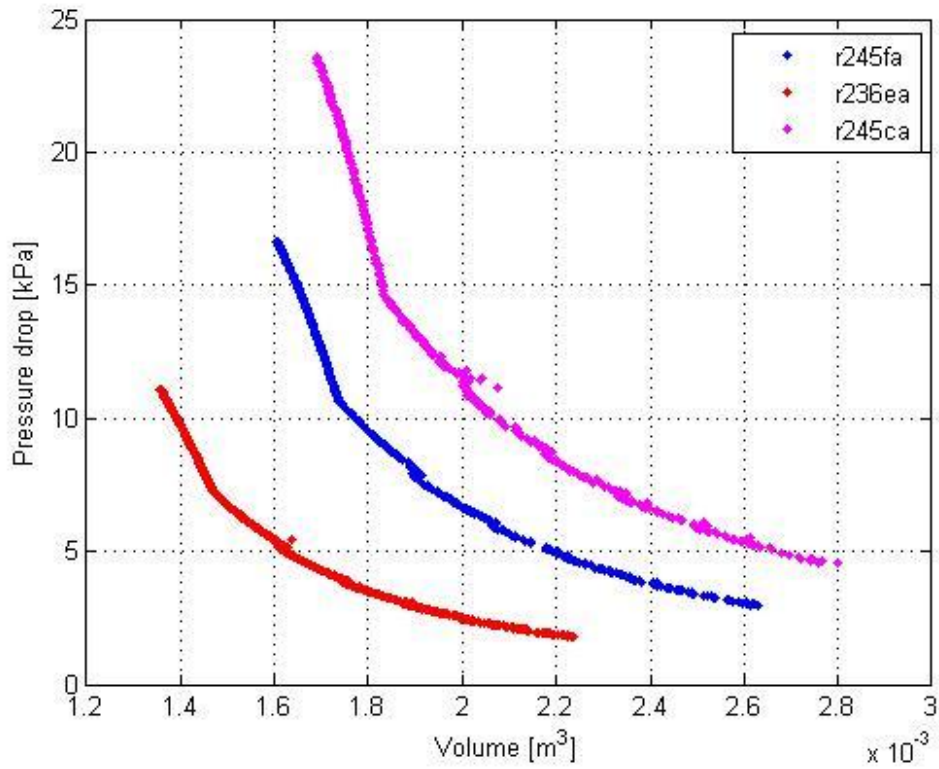


Fig. 10.21. Pressure drops vs. volume

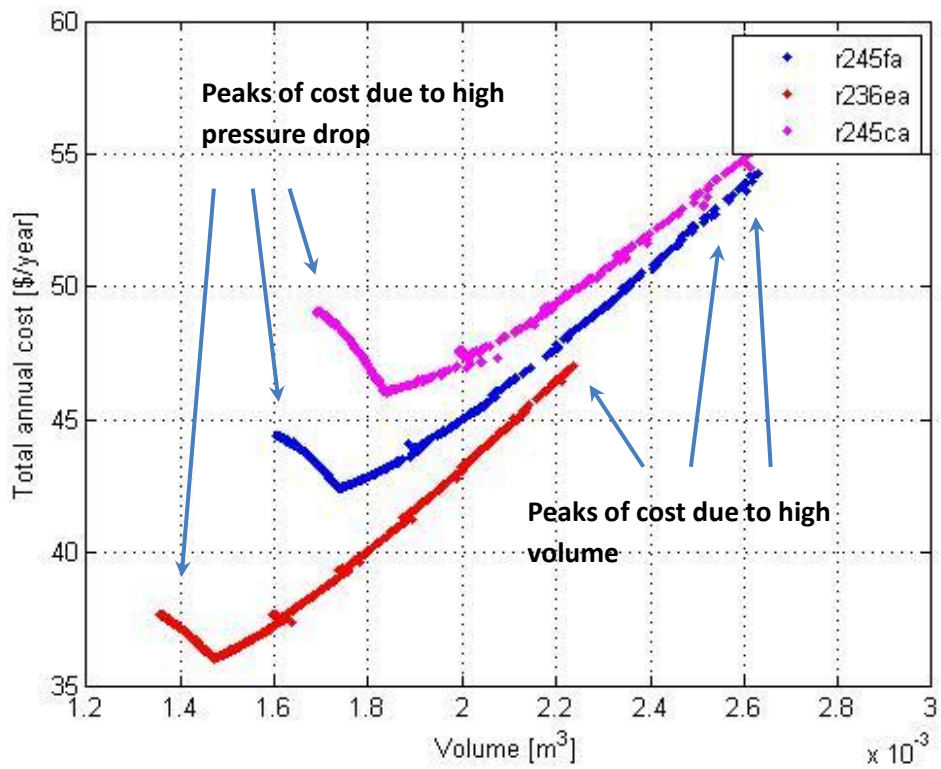


Fig. 10.22. Total annual cost vs. volume

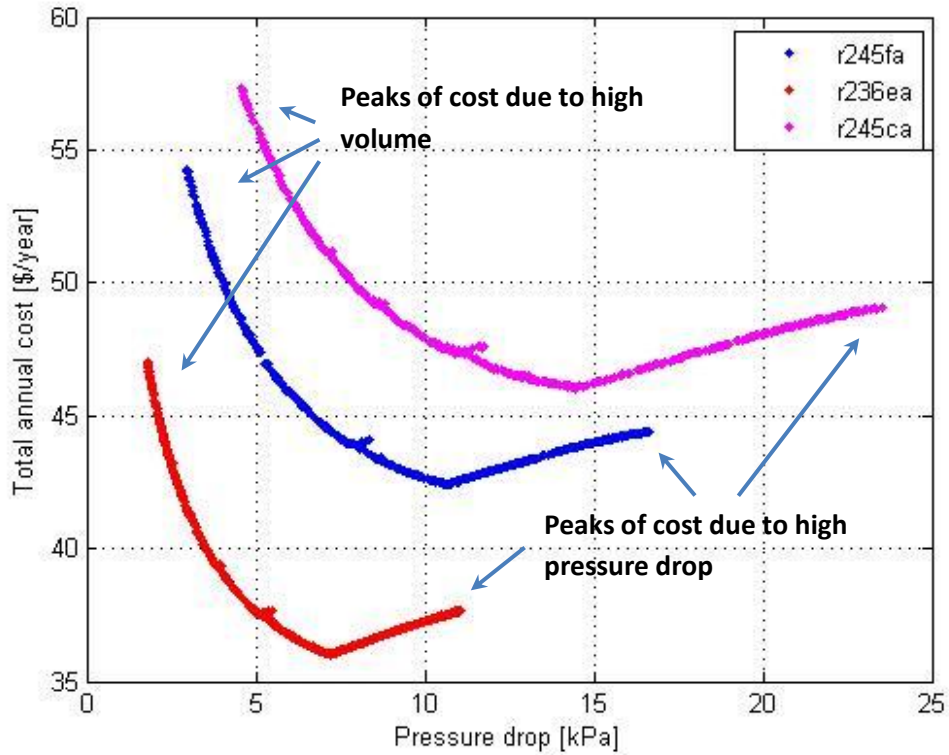


Fig. 10.23. Total annual cost vs. Pressure drop.

Conclusions

In this study the influence of heat exchanger design on organic Rankine cycles is analyzed. In order to enhance the performance of the cycle a first screening of working fluids and operating conditions is carried out. The fluid plays a key role on power output, efficiency, effectiveness and entropy generation rate. Furthermore, environmental impact and safety are important factors that lead the designer to select the working fluid.

Shell and tube heat exchangers are the most commonly used heat exchanger configuration in the process industries when high heat transfer rate is required. In fact, the configuration gives a large surface area in a small volume.

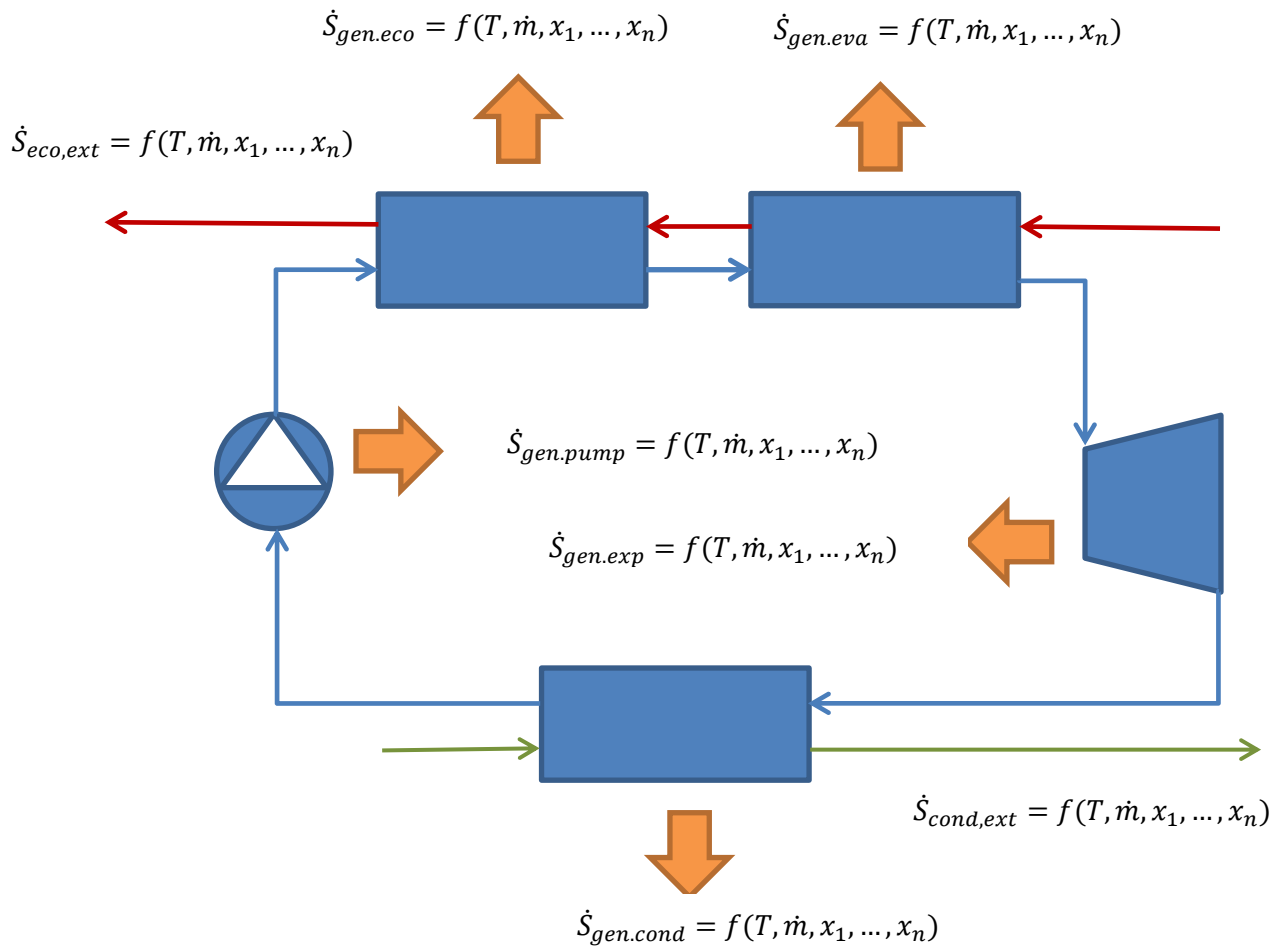
In my work, I present an integrated model to evaluate the pressure drop and the heat transfer surface area required for a shell and tube heat exchanger. I consider nine design variables regarding the geometry of the heat exchanger and the side where the working fluid flows (i.e. shell or tube). The optimization is performed using multi-objective genetic algorithm. Volume, pressure drop and total annual cost are the fitness functions used to obtain the Pareto optimal set. Theoretically, the optimal solutions in the Pareto optimal set obtained from the multi-objective genetic algorithm are the best trade-off between the objectives functions considered. The results of heat exchanger optimization show that low volume means high pressure drop and vice versa. Total annual cost depends on the initial cost to purchase the heat exchanger and the operating cost. Initial cost is related to the heat transfer area whereas operating cost is proportional to the pressure drop. A trade-off between them leads to a minimum of total annual cost.

For low heat source temperatures, plate heat exchangers are the best solution. Therefore, compact heat exchangers are proposed for economizer and evaporator. The optimization was performed using multi-objective genetic algorithm. I consider six design variables to define the optimal geometry of plate heat exchanger. Volume, pressure drop, total annual cost and entropy generation rate are used as fitness functions. Three test cases are analyzed in order to compare volume, pressure drop and total annual cost. The results show that operating conditions and working fluid strongly affect the total annual cost of economizer and evaporator.

Future work could exploit entropy generation minimization to optimize cycle performance and total annual cost of each component of the cycle. It is demonstrated that maximize net power output leads to the same results of minimize entropy generation rate. The cycle performance and the total annual cost can be optimized considering evaporating temperature, working fluid and geometric characteristics of each component as design variables.

Total entropy generation rate can be minimized considering all the sources of irreversibility (including exergy released to the environment).

The following scheme shows the entropy generation rate of each component. Entropy generation rate depends on operating conditions (working fluid, evaporating temperature, condensing temperature, heat source temperature) and geometric characteristics of each component that affect pressure drop and isentropic efficiency (x_1, \dots, x_n).



References

- [1] B. Saleh, G. Koglbauer, M. Wendland, J. Fischer, Working fluids for low-temperature organic Rankine cycles, *Energy*, (2005).
- [2] Z.Q. Wang, N.J. Zhou, J. Guo, X.Y. Wang, Fluid selection and parametric optimization of organic Rankine cycle using low temperature waste heat, *Energy*, (2011).
- [3] H. Chen, D.Y. Goswami, E.K. Stefanakos, A review of thermodynamic cycles and working fluids for the conversion of low-grade heat, *Renewable and Sustainable Energy Reviews*, (2011).
- [4] Zahid.H. Ayub, Plate heat exchanger literature survey and new heat transfer and pressure drop correlations for refrigerant evaporators, *Taylor & Francis, Heat Transfer Engineering* (2003).
- [5] Y. Yan, T.F. Lin, Evaporation Heat Transfer and Pressure drop of refrigerant R-134a in a plate heat exchanger, *Journal of Heat Transfer*, (1999)
- [6] Y.Y. Hsieh, T.F. Lin, Saturated Flow Boiling Heat Transfer and Pressure Drop of refrigerant R-410A in a Vertical Plate Heat Exchanger, *Heat and Mass Transfer*, (2001)
- [7] D.H. Han, K.J. Lee, Y.H. Kim, Experiments on the Characteristics of Evaporation of R410A in Brazed Plate Heat Exchanger with Different Geometric Configurations, *Applied Thermal Energy*, (2003)
- [8] R.K. Shah, D.P. Sekulic, *Fundamentals of Heat Exchanger Design*, John Wiley & Sons, Hoboken, New Jersey, (2003).
- [9] J. M. Coulson and J. F. Richardson, *Chemical Engineering, Volume 1, Sixth edition Fluid Flow, Heat Transfer and Mass Transfer*.
- [10] R.B. Serth, *Process Heat Transfer- Principles and applications*, Elsevier Science & Technology Books, (2007).
- [11] I. Prigogine, *Introduction to Thermodynamics of Irreversible Processes*, Wiley, New York (1967).
- [12] A. Bejan, *Advanced Engineering Thermodynamics*, Wiley (1988).
- [13] A. Bejan, *Entropy Generation Minimization*, Wiley (1982).
- [14] M.J. Moran, H.N. Shapiro, *Fundamentals of engineering thermodynamics*, Wiley, New York.

- [15] A. Bejan, The Equivalence of Maximum Power and Minimum Entropy Generation Rate in the Optimization of Power Plants.
- [16] A. Bejan, J.C. Ordònez, Entropy Generation Minimization in parallel-plates counterflow heat exchangers, International Journal of Energy Research,(2000).
- [17] J.Guo, L.Cheng, M,Xu, Multi-Objective Optimization of heat Exchanger design by Entropy Generation Minimization, Journal of Heat Transfer,(2010).
- [18] J.Hesselgreaves, Rationalisation of Second Law Analysis of Heat Exchangers, International Journal of Heat Transfer, 2000.
- [19] dowthermQ properties, <http://www.dow.com>
- [20] D.H. Wei, X.S. Lu, Z. Lu, J.M. Gu, Performance Analysis and Optimization of Organic Rankine Cycle (ORC) for Waste Heat Recovery, Energy Conversion and Management, 2009.
- [21] A. Franco, N. Giannini, A General Method for the Optimum Design of Heat Recovery Steam Generators, Energy, 2006.
- [22] L.Wang, B.Sudèn, Optimal design of plate heat exchangers with and without pressure drop specifications, Applied Thermal Engineering, 2003.
- [23] L.Pierobon, F. Haglind, Waste heat recovery for off-shore application, Proceedings of the ASME 2012 International Mechanical Engineering Congress & ExpositionIMECE2012.
- [24] B.Allen, L. Gosselin, Optimal geometry and flow arrangement for minimizing the cost of shell and tube condensers, International Journal of energy research, 2008.
- [25] P. Wildi-Tremblay, L. Gosselin, Minimizing shell and tube heat exchanger cost with genetic algorithms and considering maintenance, International Journal of energy research, 2006.
- [26] Z. Guo-Yan, W. En, T. Shan-Tung, Techno-economic study on compact heat exchangers, International Journal of energy research, 2008.
- [27] P.Ahamdi, H. Hajabdollahi, I.Dincer, Cost and entropy generation minimization of a cross-flow plate fin heat exchanger using multi-objective algorithm, Journal of heat transfer, 2011.
- [28] A. Bejan, Fundamentals of exergy analysis, entropy generation minimization, and the generation of flow architecture, International Journal of energy research, 2002.
- [29] C. Kuo, S. Hsu, K. Chang, C. Wang, Analysis of a 50 kW organic Rankine cycle system, Energy, 2011.
- [30] J. Huang, T. Sheer, M. Bailey-McEwan, Heat transfer and pressure drop in plate heat exchanger refrigerant evaporators, Refrigeration, 2011.
- [31] A. Durmus, H. Benli, I. Kurtbas, H. Gul, Investigation of heat transfer and pressure drop in plate heat exchangers having different surface profiles, International Journal of Heat and Mass Transfer, 2008.
- [32] B. Palm, J.Claesson, Plate heat exchangers: Calculation Methods for single- and two phase flow, Heat transfer engineering, 2006.

- [33] P.K. Nag, S. De, Design and operation of a heat recovery steam generator with minimum irreversibility, Applied thermal Engineering, 1997.
- [34] F.V. Garcia, J.R. Garcia-Cascales, A simplified model for shell and tubes heat exchangers: Practical application, Applied thermal engineering, 2010.
- [35] P. J. Mago, Exergetic evaluation of an organic Rankine cycle Using Medium-grade waste heat, Energy sources, 2012.
- [36] W. Gu, Y. Wang, B. Zheng, Theoretical and experimental investigation of an organic Rankine cycle for a waste heat recovery system, Journal of Power and Energy, 2009.
- [37] D. Wang, X. Ling, H. Peng, Performance analysis of double organic Rankine cycle for discontinuous low temperature waste heat recovery, Applied thermal engineering, 2011.
- [38] J. Ponce-Ortega, M.S. Gonzalez, A. J. Gutierrez, Use of genetic algorithms for the optimal design of shell and tube heat exchangers, Applied thermal engineering, 2018.
- [39] C.J. Butcher, B.V. Reddy, Second law analysis of a waste heat recovery based power generation system, Heat and mass transfer, 2007.
- [40] A.A. Lakew, O. Bolland, Working fluids for low-temperature heat source, Applied thermal engineering, 2010.
- [41] J.P. Roy, A. Misra, Parametric optimization and performance analysis of a regenerative organic Rankine cycle using R-123 for waste heat recovery, Energy, 2012.
- [42] F. Al-Sulaiman, I. Dincer, F. Hamdullahpur, Energy and exergy analyses of biomass trigeneration system using organic Rankine Cycle, Energy, 2012.
- [43] P.J. Mago, K.K. Srinivasan, L.M. Chamra, C. Somayaji, An examination of exergy destruction in organic Rankine cycles, International Journal of Energy Research, 2008.
- [44] S. Quoilin, S. Declaye, B. F. Tchanche, V. Lemort, Thermo-economic optimization of waste heat recovery Organic Rankine Cycles
- [45] C. He, C. Liu, H. Gao, H. Xie, Y. Li, S. Wu, J. Xu, The optimal evaporation temperature and working fluids for subcritical organic Rankine cycle, Energy, 2012.
- [46] A. Fakheri, A General Expression for the Determination of the Log Mean Temperature Correction Factor for Shell and Tube Heat Exchangers, Journal of Heat Transfer, 2003.